

13. SITE 833¹

Shipboard Scientific Party²

HOLE 833A

Date occupied: 2 December 1990
Date departed: 3 December 1990
Time on hole: 1 day, 17.5 hr
Position: 14°52.57'S, 167°52.78'E
Bottom felt (rig floor; m, drill-pipe measurement): 2640.5
Distance between rig floor and sea level (m): 11.5
Water depth (drill-pipe measurement from sea level; m): 2628.5
Total depth (rig floor; m): 2840.0
Penetration (m): 199.5
Number of cores (including cores with no recovery): 26
Total length of cored section (m): 199.5
Total core recovered (m): 97.75
Core recovery (%): 49.0
Oldest sediment cored:
Depth below seafloor (m): 199.5
Nature: calcareous clayey volcanic siltstone
Age: Pleistocene
Measured velocity (km/s): 1.855

HOLE 833B

Date occupied: 3 December 1990
Date departed: 14 December 1990
Time on hole: 13 days, 19.5 hr
Position: 14°52.56'S, 167°52.78'E
Bottom felt (rig floor; m, drill-pipe measurement): 2640.0
Distance between rig floor and sea level (m): 11.5
Water depth (drill-pipe measurement from sea level (m): 2629.0
Total depth (rig floor; m): 3641.1
Penetration: 1001.1
Number of cores (including cores with no recovery): 99
Total length of cored section (m): 923.7
Total core recovered (m): 519.54
Core recovery (%): 56.2
Oldest sediment cored:
Depth below seafloor (m): 952.9
Nature: calcareous volcanic siltstone and sandstone
Age: early Pliocene
Measured velocity (km/s): 4.902
Principal results: We arrived at Site 833 on 2 December 1990 at 0500 Universal Time Coordinated (UTC). While on site we drilled two

holes (Holes 833A and 833B). We departed Site 833 at 0030 UTC 14 December 1990.

Site 833 (proposed site IAB-2) is located on the lower east-central flank of the North Aoba Basin (NAB), along the northwestern flank of Maewo Island, approximately 24 km northwest of the northern tip of Maewo Island and about 72 km southeast of the active volcanic island of Santa Maria, which was observed on 4–5 December 1990 to be emitting whitish-gray smoke from a vent near Mount Garat. The NAB lies between uplifted bedrock masses of Espiritu Santo and Maewo islands and is separated from the northern Vanikolo Basin to the north by Santa Maria Island and from the South Aoba Basin (SAB) to the south by the volcanic island of Aoba.

After a seismic reflection transect across the NAB connecting Site 832 with Site 833 and a brief survey around Site 833, we began drilling without any problems. In Hole 833A we cored 199.5 meters below seafloor (mbsf) and recovered 97.75 m of core for a recovery rate of 49.0%. Hole 833B was drilled to a total depth of 1001.1 mbsf, coring 923.7 m and recovering 519.54 m for a recovery rate of 56.2%.

Five lithostratigraphic units were identified in the cores collected at Site 833. Lithostratigraphic Unit I (0–84.0 mbsf, Hole 833A) consists of numerous interbedded unlithified volcanic ashes and volcanic silt; ash layers are thinner and more numerous in the upper part of the unit and the carbonate content increases to about 15% near the seafloor. Lithostratigraphic Unit II (84.0–199.5 mbsf in Hole 833A and 77.4–375.8 mbsf in Hole 833B) contains calcareous siltstones and claystones that are highly bioturbated; the unit is more lithified and finer grained than Unit I. Volcanic ash and volcanic sand are negligible, suggesting a period of fairly slow sedimentation and minimal volcanic activity. Lithostratigraphic Unit III (375.8–577.8 mbsf) is composed of black volcanic sand and fine-grained basaltic breccia with low carbonate content. Sediment accumulation rates average 313 m/m.y. Lithostratigraphic Unit IV (577.8–830.3 mbsf) comprises black volcanic sandstones and siltstones interbedded with sandstones, siltstones, and claystones that are both finer grained and more calcareous than the volcanoclastic sedimentary rocks. Packages (30 cm to several meters in thickness) of fining-upward sequences of volcanic sediment with coarser-grained basal layers and sharp top and bottom boundaries characterize this unit. Lithostratigraphic Unit V (830.3–1001.1 mbsf) is characterized by sediments similar to those in Unit IV except that the sediments in Unit V are interbedded with basaltic sills with thicknesses of 65 m or more. Sedimentary rocks in Unit V show minimal structural deformation; minor evidence of contact metamorphism is exhibited primarily by an increase in the chlorite content of calcareous volcanic siltstone adjacent to the sills.

The keys to the divisions within the lithostratigraphic units include the grain size of volcanic ash and epiclastic volcanic sediments, carbonate content, and bioturbation. These characteristics are closely related. When the sediment accumulation rates of volcanic ash and sand are high, carbonate content is low and bioturbation is suppressed in response to enhanced influxed volcanic sediments. When the volcanic ash input decreases, sediment accumulation rates are low (97 m/m.y.) and volcanic silt and clay dominate. Carbonate sediments then form a significant proportion of the total sediment accumulation, and burrowing organisms have sufficient time to rework the sediments.

Four structural units were defined at Site 833. Structural Unit A (0–376 mbsf) includes lithostratigraphic Units I, II, and the very top of III, and contains only a few structures resulting from tectonic deformation. Structural Unit B (376–616 mbsf) includes

¹ Collot, J.-Y., Greene, H. G., Stokking, L. B., et al., 1992. *Proc. ODP, Init. Repts.*, 134: College Station, TX (Ocean Drilling Program).

² Shipboard Scientific Party is as given in the list of participants preceding the contents.

lithostratigraphic Units III and the upper part of IV and is defined by slump features and some normal faults. Structural Unit C (616–830 mbsf) correlates with lithostratigraphic Unit IV and is characterized by slumps and numerous normal faults with well-developed slickensides, some overprinted with faults indicating sinistral strike-slip. Structural Unit D (830–1001 mbsf) correlates with lithostratigraphic Unit V defined by 10°–30° dipping beds entrapped by the intruding sill and by the presence of several reverse and strike-slip faults.

Volcanic ash layers are abundant in the upper 150 m of Site 833, becoming increasingly sporadic downhole. These are potassium-rich pyroclastic sediments similar to those found at Site 832 and are attributed to eruptions from the Central Chain of volcanoes. Deeper in Hole 833B, occasional basaltic tuffs were recovered from between 308 and 317 mbsf: these are of a different type, having low-potassium, island-arc tholeiite affinity. Volcanic clasts from the coarse sandstones and breccias at about 400 mbsf include ankaramitic basalts, resembling those of Site 832, and these are also of island-arc tholeiite type. At 830 mbsf calcareous volcanic siltstones are cut by a highly plagioclase-phyric high potassium calc-alkaline basaltic sill with a distinctly chilled upper contact. Basaltic sills of similar composition make up much of the succession below this and are interstratified with calcareous volcanic siltstones and bioturbated mixed sedimentary rocks. There is sufficient evidence of chilling to establish the intrusive nature of the basalt. Although the sills could be interpreted as a series of separate intrusions, their compositional uniformity suggests that a large body of magma may have invaded the un lithified sediments simultaneously at a number of stratigraphic levels.

Foraminifers and nannofossils were again the best source for age information. An age of late Pleistocene to Holocene is assigned to the interval from 0 to 183.5 mbsf (in both Holes 833A and 833B), early Pleistocene for the interval from 193.1 to 375.8 mbsf, late Pliocene for the interval from 385.5 to 635.6 mbsf, and early Pliocene for the interval from 635.6 to 945 mbsf. The Pliocene-Pleistocene boundary lies in the interval from 250 to 375.8 mbsf, but the exact location is uncertain. Further uncertainty arises from the assignment of the lowermost part of Hole 833B to Zone N19 (foraminifers), which is included in the early Pliocene.

For the overall sedimentary sequence above the sill a very high sediment accumulation rate of 97–322 m/m.y. was determined, using mainly the first appearance datums of foraminifers and nannofossils in sequences where reworking is common. Analyses of benthic foraminifers indicate that most of the sediments found at Site 833 were deposited in the lower bathyal zone, although some shallow-water fauna were found sporadically throughout Hole 833B.

All undisturbed cores from Hole 833A and most consolidated sediments in Hole 833B were measured with the cryogenic magnetometer and alternating-field (AF) demagnetized at 10 mT. Paleomagnetic results at Site 833 show normal polarity from 0 to 80 mbsf. Because of poor core recovery few magnetic measurements could be obtained from 80 to 200 mbsf and no evidence for reversed polarity exists in this interval. The first interval of reverse magnetic polarity was found between 220 and 250 mbsf and the transition from the Matuyama Chron to Brunhes Chron (0.73 Ma) may occur between 210 and 220 mbsf.

Magnetic susceptibility in the volcanic sandstone at Site 833 is high (0.02 SI) and this nearly normal magnetization may have been acquired during diagenesis and consolidation (viscous magnetization of these rocks appears to be quite strong as well). The sills at the bottom of Hole 833B also have high magnetic susceptibility (0.04–0.08 SI) and a high intensity (100 A/m) of magnetization. However, this magnetization is very soft and easily removed with low AF magnetization. Results from the most stable samples indicate a shallow positive inclination that may correspond to a reversed polarity.

Fluid geochemistry at Site 833 revealed extremely wide-ranging values in chloride (568–1241 mM), sodium (150–534 mM), potassium (0.4–14.9 mM), magnesium (0–39.7 mM), and calcium (2.6–548.5 mM) concentrations in the pore fluids. Each of these solutes is characterized by either its maximum (chloride and

calcium) or minimum (sodium, potassium, and magnesium) value at depths between 490 and 630 mbsf. These depths correspond to the location of the well-cemented volcanic sandstone and sedimentary rocks. Diagenesis and cementation of the volcanogenic sediment presumably causes the variations in solute concentrations. These are similar to the diagenesis observed at Site 832, but the most altered calcium, chloride, and sodium concentrations are nearly two times more extreme at Site 833. The maximum concentrations of alkalinity (19.9 mM), phosphate (55.2 μ M), and ammonia (1794 μ M) occur between depths of 20 and 40 mbsf. The concentrations are not extremely high, probably reflecting the low (generally <0.5%) organic carbon content of the sediments and slightly lower sediment accumulation rate at this site.

In general, physical properties correspond to lithostratigraphic units at Site 833. Unlike Site 832, physical properties do not remain constant to significant depths. They display a normal pattern of decreased porosity and increased density from 0 to 84 mbsf. This is probably a result of the location of Site 833 on the flank of the Aoba Basin, away from the depocenter at Site 832. Physical properties exhibit a distinct correlation between index properties and velocities, particularly in lithostratigraphic Units III (375.8–577.8 mbsf) and V (830–1000 mbsf), which are zones of low porosity and water content, and high bulk density and sonic velocity. The transition at 375.8 mbsf from Pleistocene siltstones with ash layers to more well-cemented Pliocene sandstones and basaltic breccias is very obvious in the physical properties data.

Because of partial hole collapse and filling problems after drilling ceased, not all of the hole could be logged and constraints on time prevented us from using the complete complement of logging tools. However, good results were obtained from the geophysical and geochemical tools between 250 and 900 mbsf, with distinct increases in resistivity and velocities taking place between 380 and 430 mbsf, which correlates with volcanic sandstones and breccia at these depths. The contact with the basaltic sill and the overlying sedimentary rocks is easily distinguished in the logs with sharp increases in resistivity, velocities, thorium, and potassium at 830 mbsf.

Initial interpretations of the drilling data at Site 833 indicate that a thick (nearly 400 m) Pleistocene volcanic sandstone and ash sequence exists. Although not as thick as that found at Site 832 (<600 m), this sequence represents a rapid accumulation of Pleistocene volcanic material emitted from the active Central Chain volcanoes. The existence of volcanic breccia at about 400 to 560 mbsf suggests uplift and erosion of volcanic rocks on Maewo Island. A much thicker (>350 m) Pliocene sequence exists at Site 833, compared to only about 70 m recovered at Site 832; however, nearly half of this sequence is composed of basaltic sills that may have been intruded into the Pliocene sedimentary rocks as late as the Pleistocene. Initial evaluation of this sill complex indicates the rocks are highly potassic and share similar petrology with the Central Chain.

BACKGROUND AND OBJECTIVES

Site 833 is the second of two sites (Sites 832 and 833) located within the intra-arc basin of the central New Hebrides Island Arc (Vanuatu). The site is located on lower east-central flank of the North Aoba Basin (NAB), the northwestern flank of Maewo Island, at 2629.0 meters below sea level (mbsl), approximately 24 km northwest of the northern tip of Maewo Island about 72 km due southeast of the active volcanic island of Santa Maria (Figs. 1 and 2). The background for drilling at Site 833 is similar to that at Site 832 (see "Background and Objectives" section, "Site 832" chapter, this volume). The principal objectives of drilling at Site 833 are also the same as at Site 833, namely:

1. To establish if the central New Hebrides Island Arc is a product of cyclic arc volcanism and tectonism since the Oligocene, and to refine the relationship of the volcanism to changing subduction direction and angles.

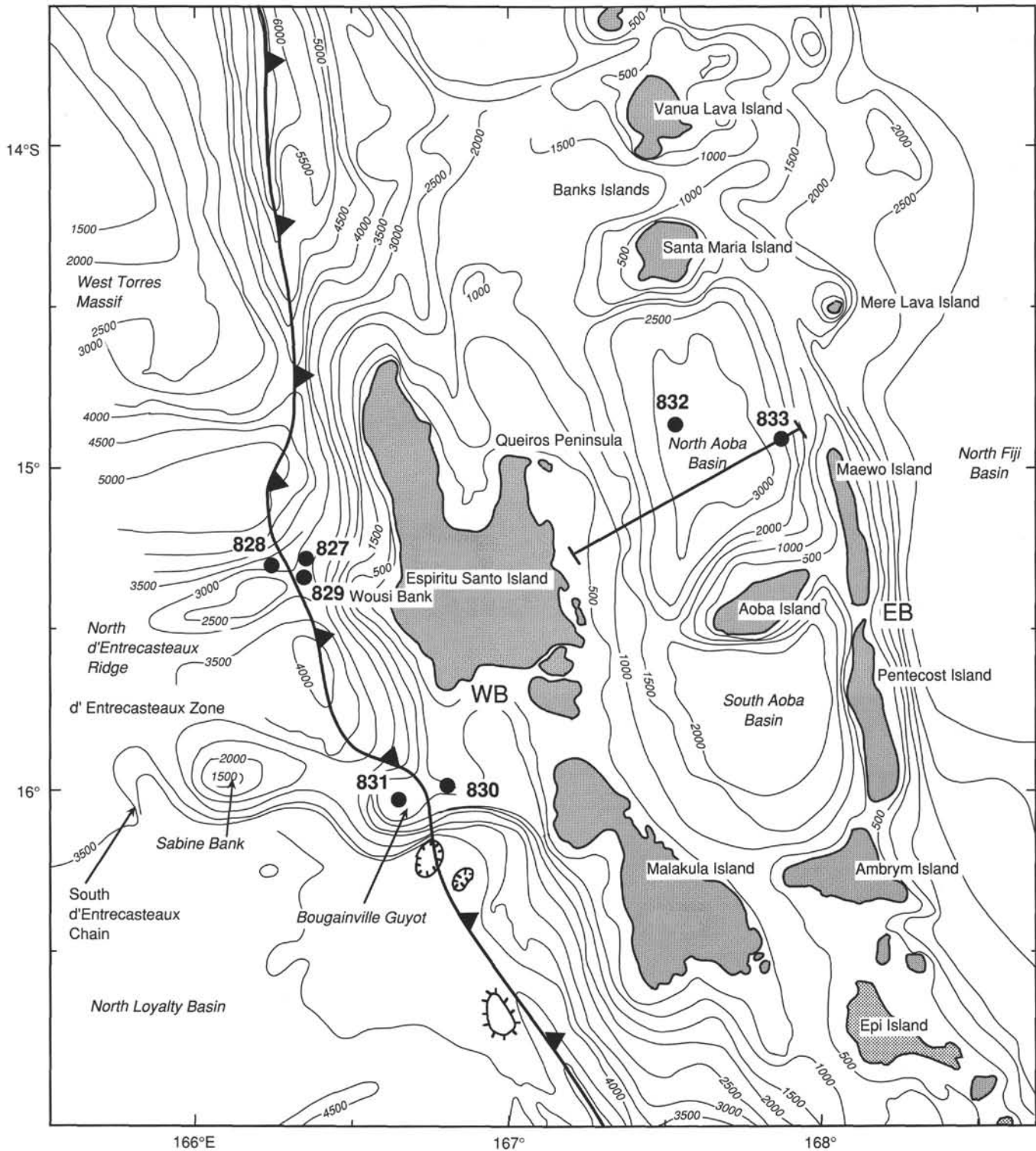


Figure 1. Bathymetric map of intra-arc basin (Central Basins) area of the central New Hebrides Island Arc showing location of drill sites of Leg 134. Solid line in North Aoba Basin is location of seismic reflection profile shown in Figure 4 (in "Site 832" chapter, this volume). Bold line with teeth indicates approximate position of subduction zone; teeth are on upper plate. EB = Eastern Belt, WB = Western Belt. Bathymetry (in meters) modified after Chase and Seekins (1988).

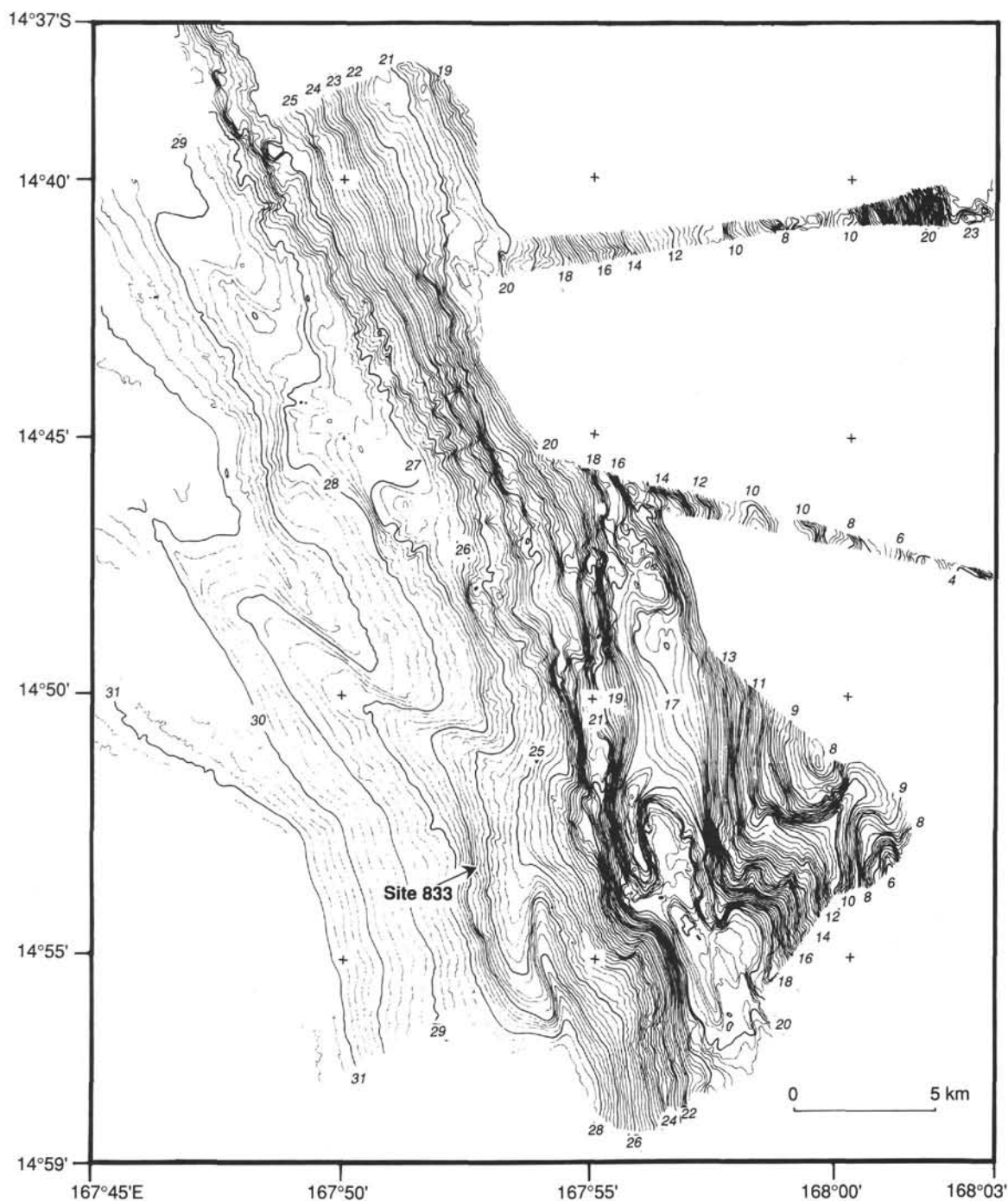


Figure 2. Detailed Seabeam bathymetric map of the eastern flank of the North Aoba Basin (after Daniel et al., 1989) showing the location of Site 833; contours are in hundreds of meters; contour interval is 20 m.

2. To determine if the thick sedimentary sequence of the intra-arc basin formed as a result of uplift of the western margin by the middle Miocene and uplift of the eastern margin starting from the middle Pliocene, and to establish whether the basin floor was a sloping platform for most of its history or whether it evolved rapidly into its deep downbowed (graben) form during the Quaternary.

3. To evaluate the role of extraneous events, such as arc polarity reversals and collision with ridges, in the formation of the intra-arc basin in light of the major differences between this arc-platform complex and other, volcanic arcs such as Tonga, Kermadec, and the Marianas.

SEISMIC STRATIGRAPHY

Multichannel Seismic Data

Multichannel seismic line 20 (Figs. 3 and 4) crosses eastward over both the NAB and the large submarine ridge that supports the islands of Pentecost and Maewo. The unconformity drilled at Site 832 is also present below Site 833, and below the latter site, nearly all thinning of rocks onto the eastern flank of the basin occurs above the unconformity, indicating that uplift of this flank is very young. In fact, high-resolution seismic records obtained by the 3.5-kHz system aboard ship

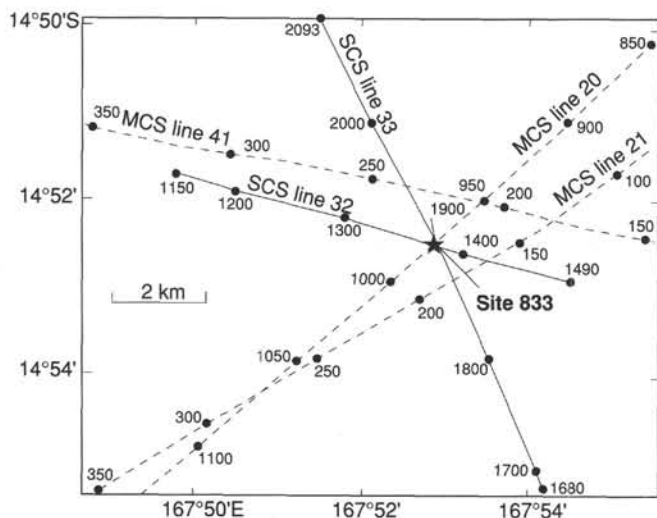


Figure 3. Trackline map showing the locations of Site 833, single-channel seismic lines 32 and 33, as well as migrated multichannel seismic lines 20 and 21 (USGS, L5-82-SP) and 41 (French Multipso, CI-86-SP).

indicate that anticlines that deform the eastern flank involve all rocks and sediment as shallow as the seafloor, suggesting that deformation continues today.

The main objective at Site 833 is the rock section that underlies the unconformity, below a depth of about 300 mbsf. Comparison of multichannel seismic section 19 (Fig. 6 in "Site 832" chapter, this volume) with section 20 (Fig. 4) shows that below Sites 832 and 833, the unconformity produces a strong, continuous reflection. Below Site 833, however, rocks under the unconformity are more highly reflective to a greater sub-bottom depth than are rocks under Site 832. Although part of this difference might result from attenuation of high-frequency acoustic energy within the poorly consolidated, shallow sediment below Site 832, drilling at Site 833 shows that the rocks penetrated at depth are actually different from those below Site 832, suggesting marked facies changes between the two sites.

Single-Channel Seismic Data

Single-channel seismic reflection data were collected over Site 833, using two 80-in.³ water guns for the source and a streamer that has a 100-m-long active section. Aboard-ship processing included predictive deconvolution, bandpass filtering, and automatic gain control. Velocity data used to convert depth in the hole to traveltime come from the measurement of physical properties (see "Physical Properties" section, this chapter).

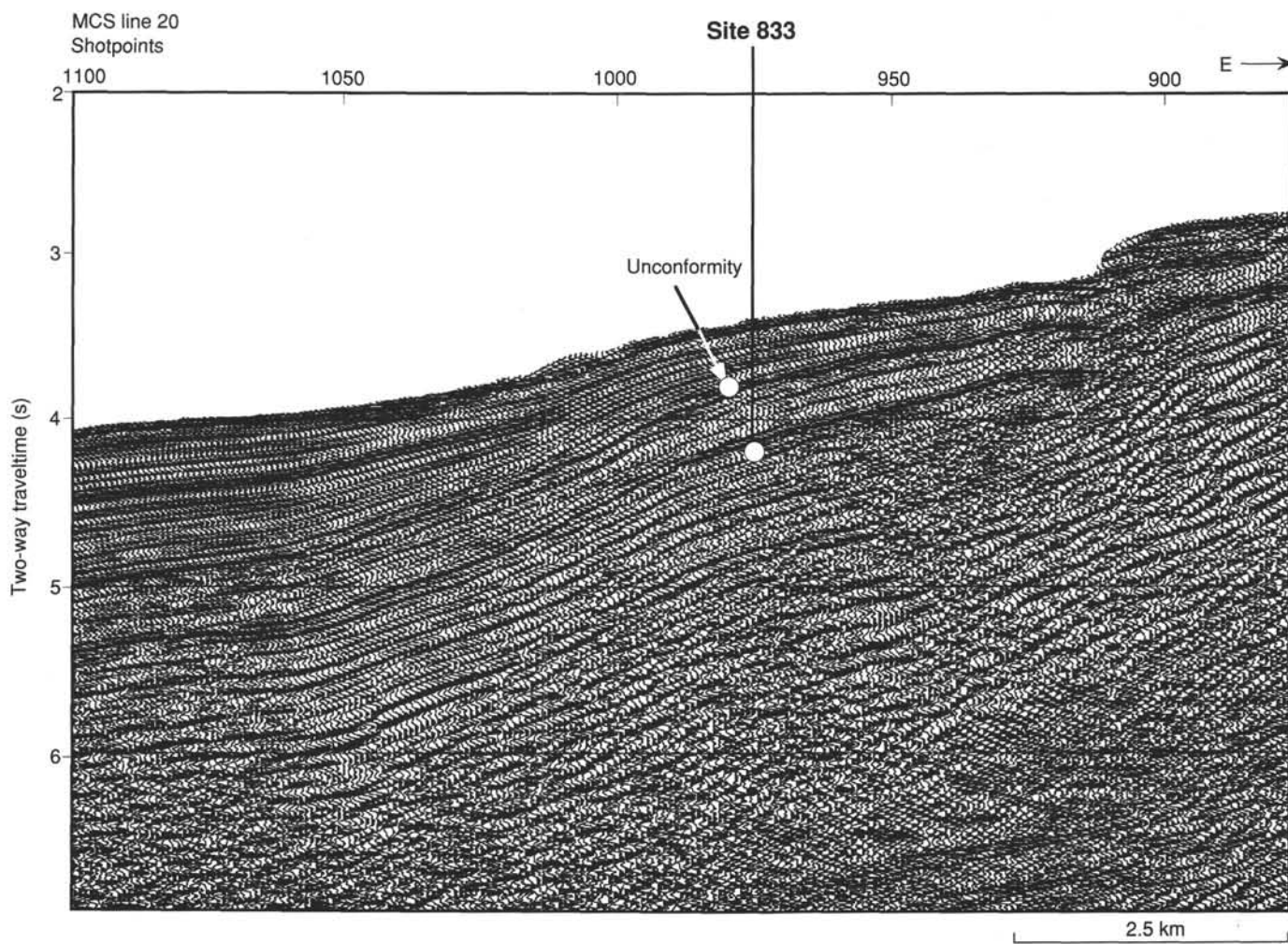


Figure 4. Part of migrated multichannel seismic line 20 (USGS, L5-82-SP) that crosses the eastern flank of the North Aoba Basin, over Site 833. White dot at end of line represents the total depth of the hole.

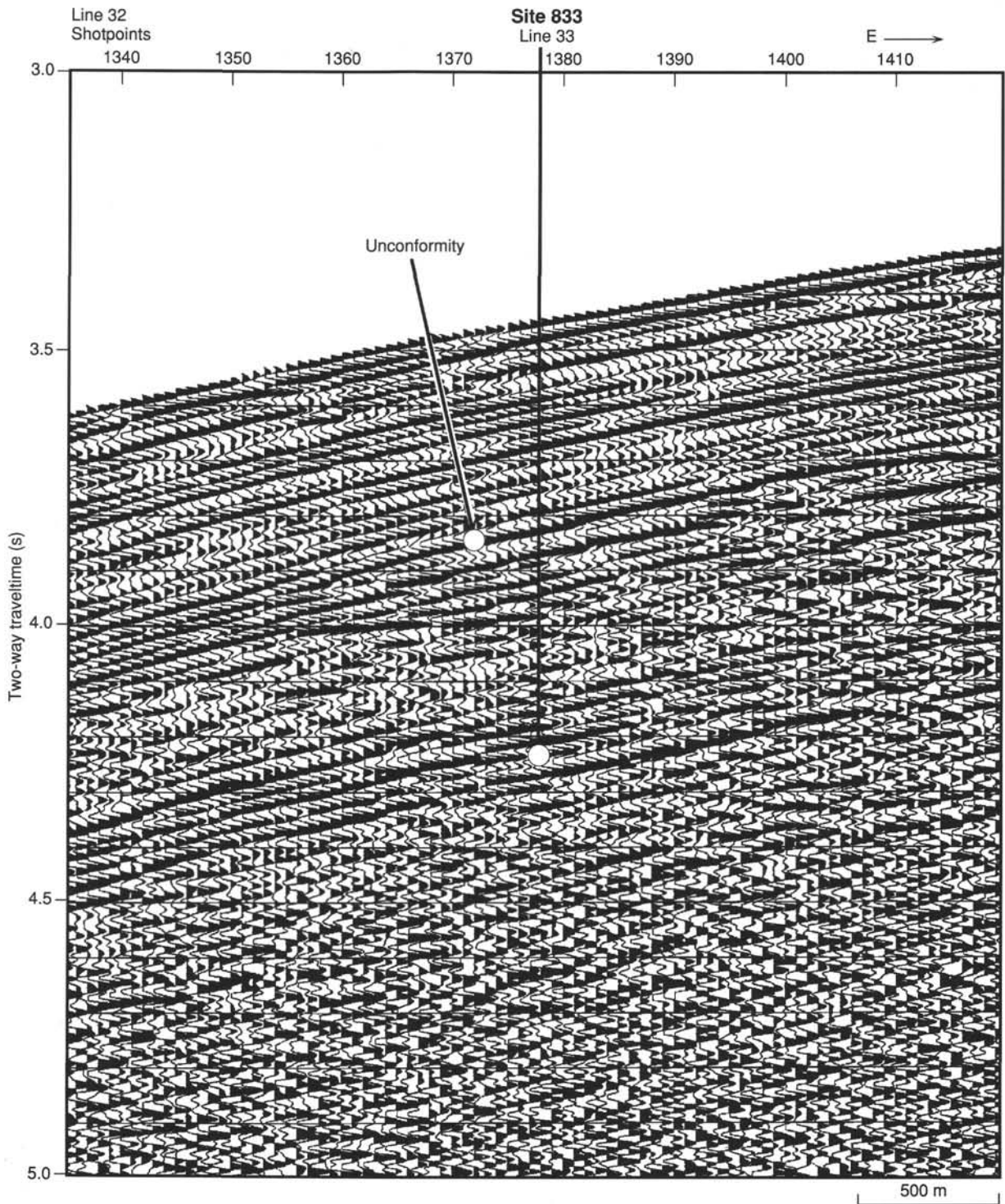


Figure 5. Part of single-channel seismic line 32 that crosses east-west over Site 833.

Site 833 lies at the intersection of single-channel seismic lines 32 and 33 that were collected aboard ship (Figs. 3, 5, and 6). The even, horizontally continuous acoustic layering of the shallow basin fill is evident in both seismic sections. These sections have been deconvolved, so the likelihood that this layering results as an artifact of an oscillatory source pulse has been reduced. Furthermore, the multichannel and single-channel images of the subsurface appear similar. Along seismic section 32, rocks between the traveltimes of the sea-

bottom reflection and 4.0 seconds (s) produce strong, continuous events, but reflections later than 4.0 s are fainter and discontinuous. This faintly reflective layer is succeeded downward by another layer that returns strong, parallel, continuous reflections.

Seismic section 33 was collected obliquely across small anticlines that strike nearly north-south; this obliquity may explain why rock layering below this line appears different from layering below crossing line 32. The main differences are

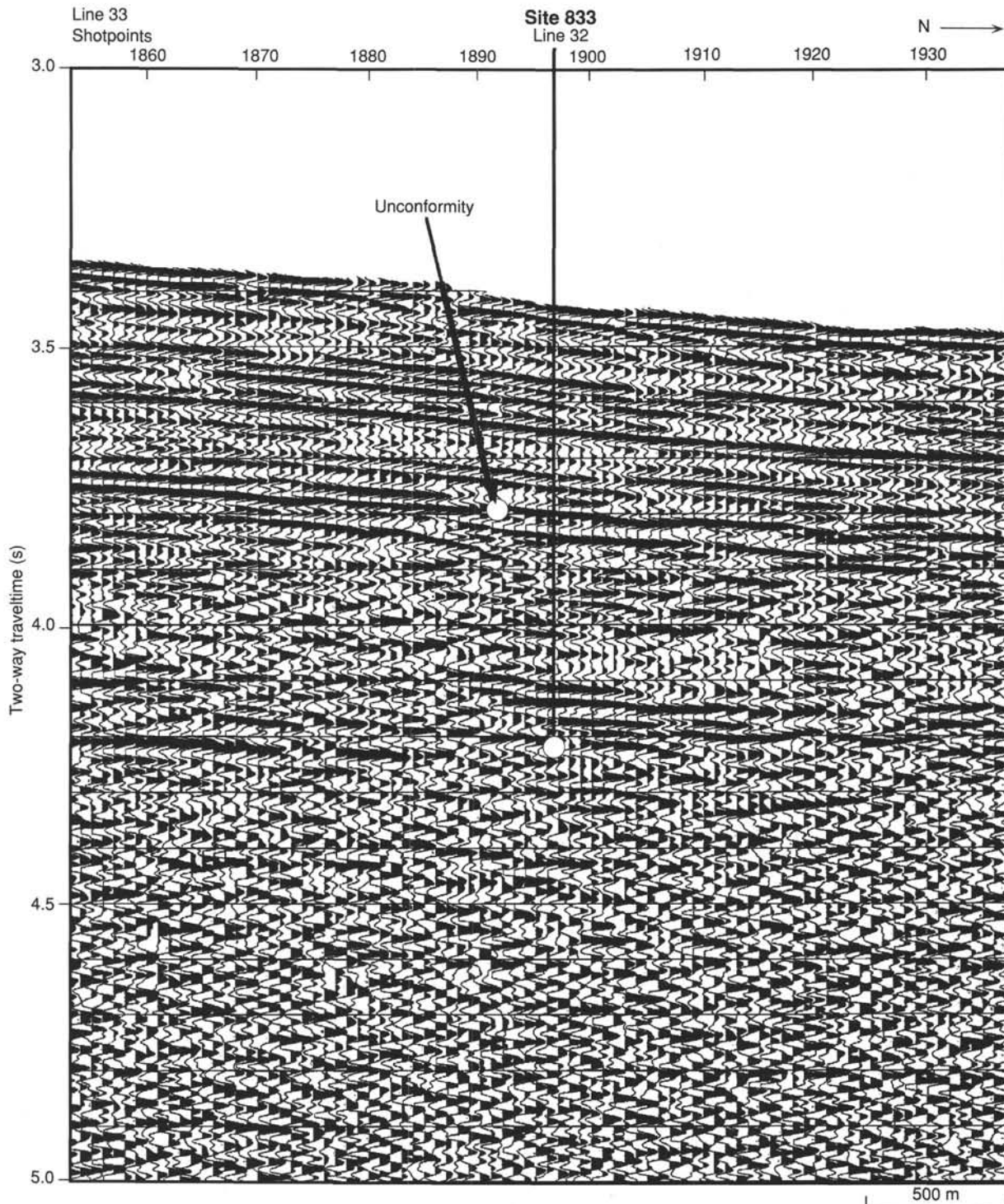


Figure 6. Part of single-channel seismic line 33 that trends north-south over Site 833.

that along section 33 the upper part of the basin fill seems to be more sharply divided into layers than does the equivalent fill below line 32. Furthermore, along section 33, the deepest layer at 4.2 s is discontinuous.

A preliminary correlation between seismic data and lithostratigraphy (Fig. 7) indicates that strong, parallel reflections are returned by lithostratigraphic Units I and II, which near the bottom are upper Pliocene to Pleistocene nanofossil chalk and volcanic silt and near the top are Pleistocene to

Holocene volcanic silts and ash (see "Lithostratigraphy" section, this chapter). Lithostratigraphic Unit III is a coarse volcanic sandstone with fine-grained basaltic breccia. This unit correlates on the seismic sections with a band of strong, and in part, low-frequency reflections. Unit IV includes volcanic sandstone and siltstone near its top, with an increase of calcareous material downunit, and its base is composed of limestone. This calcareous rock section correlates with a part of the seismic data that includes primarily

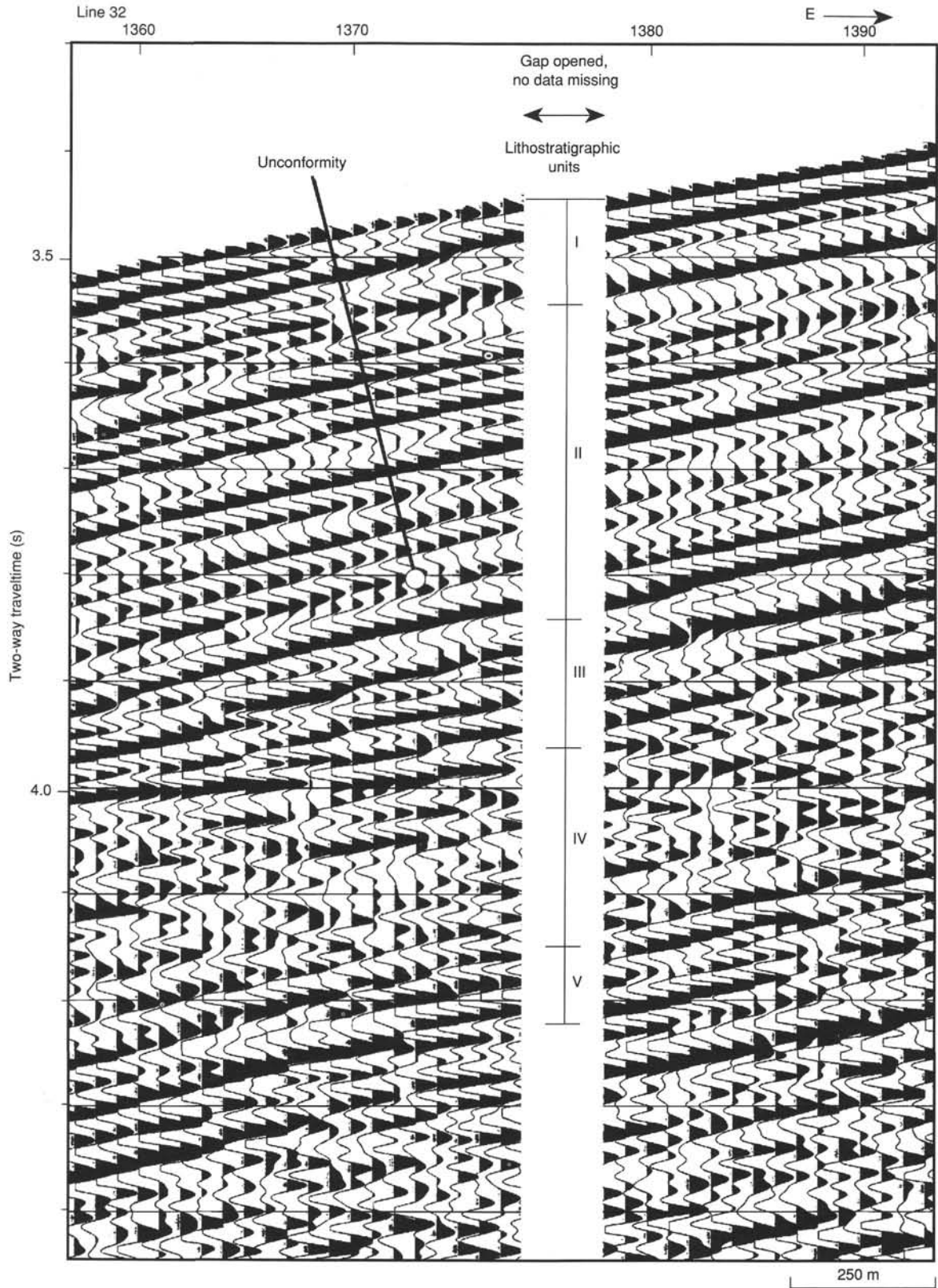


Figure 7. Detailed part of single-channel seismic line 32. Lithostratigraphic units, indicated in the center of the figure, are explained in the "Lithostratigraphy" section (this chapter).

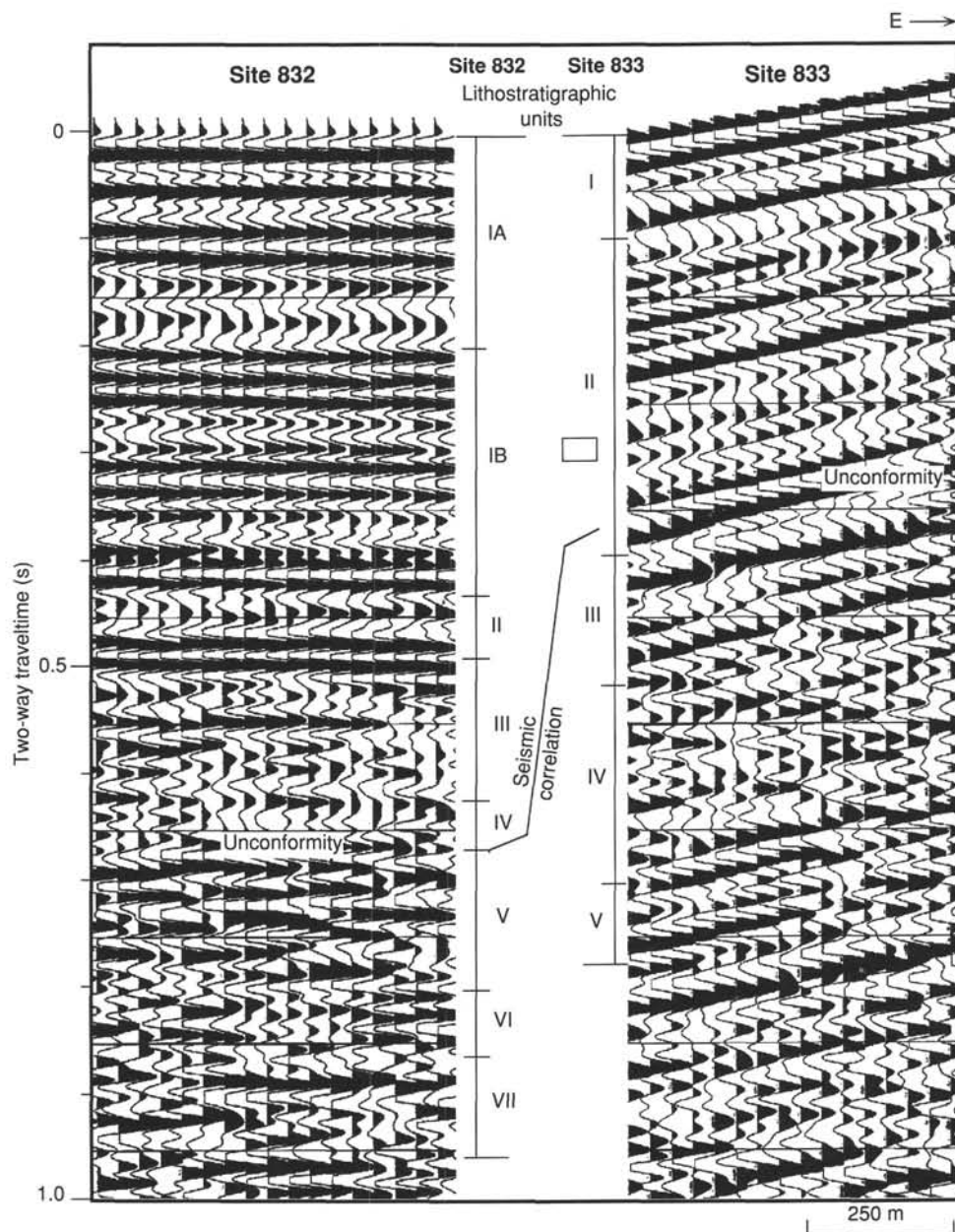


Figure 8. Detailed parts of single-channel seismic lines from Sites 832 and 833. The lithostratigraphic units are explained in the "Lithostratigraphy" sections in this chapter and the "Site 832" chapter. The line in the center of the figure labeled "seismic correlation" shows where the unconformity lies in both holes as correlated using multichannel seismic reflection data.

discontinuous, low-amplitude events. Lithostratigraphic Unit V encompasses interbedded basalt sills and fine-grained sediment. Surprisingly, this rock alternation produces parallel reflections that are continuous over long distances and can easily be confused with events from interbedded sandstone and siltstone.

The lithostratigraphy of the North Aoba Basin shows that below Site 832, the unconformity coincides with the contact between the breccia of lithostratigraphic Unit IV and the limestone of Unit V, and that the equivalent stratigraphic horizon below Site 833 lies between the sandstone and breccia of lithostratigraphic Unit III and the calcareous sediment and limestone of Unit IV (Fig. 8). Seismic reflection data, however, suggest an alternative equivalence: the correlation of reflections from across the basin indicates that the breccia/

limestone contact between lithostratigraphic Units IV and V below Site 832 is acoustically equivalent to the contact below Site 833 that lies between lithostratigraphic Units II and III. This contact separates volcanoclastic sediments of Unit II from the sandstone and breccia of Unit III. Consequently, the reflection that was once presumed to be from the unconformity not only follows some time-transgressive feature, but also does not reveal by the spatial variations in its attributes the substantial facies changes that must lie within the basin fill.

OPERATIONS

Site 833 is located about 19 nautical miles (nmi) east-southeast of Site 832 and only about 9 nmi west of the northern tip of Maewo Island. A seismic reflection profile was

Table 1. Coring summary, Holes 833A and 833B.

Core	Date (1990)	Time (UTC)	Depth (mbsf)	Length cored (m)	Length recovered (m)	Recovery (%)	Age
134-833A-							
1H	2 December	1250	0.0–9.5	9.5	9.60	101.0	Pleistocene
2H	2 December	1345	9.5–19.0	9.5	10.09	106.2	Pleistocene
3H	2 December	1500	19.0–28.5	9.5	9.97	105.0	Pleistocene
4H	2 December	1715	28.5–32.6	4.1	4.11	100.0	Pleistocene
5H	2 December	1800	32.6–39.2	6.6	6.60	100.0	Pleistocene
6H	2 December	1915	39.2–45.2	6.0	6.04	100.0	Pleistocene
7H	2 December	2000	45.2–54.0	8.8	8.83	100.0	Pleistocene
8H	2 December	2100	54.0–58.1	4.1	4.11	100.0	Pleistocene
9H	2 December	2245	58.1–62.9	4.8	4.87	101.0	Pleistocene
10H	2 December	2320	62.9–69.7	6.8	6.83	100.0	Pleistocene
11H	3 December	0015	69.7–76.0	6.3	6.37	101.0	Pleistocene
12H	3 December	0100	76.0–78.0	2.0	0.79	39.5	Pleistocene
13H	3 December	0200	78.0–81.1	3.1	4.19	135.0	Pleistocene
14X	3 December	0245	81.1–84.0	2.9	0.03	1.0	Pleistocene
15X	3 December	0320	84.0–93.7	9.7	0.19	2.0	Pleistocene
16X	3 December	0410	93.7–103.3	9.6	3.39	35.3	Pleistocene
17X	3 December	0500	103.3–113.0	9.7	0.47	4.8	Pleistocene
18X	3 December	0545	113.0–122.6	9.6	0.34	3.5	Pleistocene
19X	3 December	0725	122.6–132.3	9.7	0.00	0.0	Pleistocene
20X	3 December	0800	132.3–142.0	9.7	0.00	0.0	Pleistocene
21X	3 December	0850	142.0–151.7	9.7	4.11	42.4	Pleistocene
22X	3 December	1000	151.7–161.3	9.6	0.52	5.4	Pleistocene
23X	3 December	1125	161.3–170.9	9.6	2.29	23.8	Pleistocene
24X	3 December	1400	170.9–180.6	9.7	1.65	17.0	Pleistocene
25X	3 December	1510	180.6–190.3	9.7	0.57	5.9	Pleistocene
26X	3 December	1625	190.3–199.5	9.2	1.79	19.4	Pleistocene
Coring totals				199.5	97.75	49.0	
134-833B-							
1R	4 December	0550	77.4–86.9	9.5	2.32	24.4	Pleistocene
2R	4 December	0630	86.9–96.6	9.7	3.49	36.0	Pleistocene
3R	4 December	0730	96.6–106.2	9.6	1.00	10.4	Pleistocene
4R	4 December	0815	106.2–115.8	9.6	3.28	34.1	Pleistocene
5R	4 December	0850	115.8–125.5	9.7	3.70	38.1	Pleistocene
6R	4 December	0925	125.5–135.2	9.7	0.62	6.4	Pleistocene
7R	4 December	1005	135.2–144.8	9.6	0.34	3.5	Pleistocene
8R	4 December	1110	144.8–154.5	9.7	1.47	15.1	Pleistocene
9R	4 December	1220	154.5–164.1	9.6	4.11	42.8	Pleistocene
10R	4 December	1335	164.1–173.8	9.7	2.42	24.9	Pleistocene
11R	4 December	1440	173.8–183.5	9.7	2.53	26.1	Pleistocene
12R	4 December	1540	183.5–193.1	9.6	3.80	39.6	Pleistocene
13R	4 December	1640	193.1–202.8	9.7	2.89	29.8	Pleistocene
14R	4 December	1745	202.8–212.4	9.6	5.28	55.0	Pleistocene
15R	4 December	1850	212.4–222.1	9.7	1.84	18.9	Pleistocene
16R	4 December	2000	222.1–231.7	9.6	3.96	41.2	Pleistocene
17R	4 December	2100	231.7–240.9	9.2	3.13	34.0	Pleistocene
18R	4 December	2300	240.9–250.5	9.6	2.76	28.7	Pleistocene
19R	5 December	0000	250.5–260.0	9.5	6.25	65.8	Pleistocene
20R	5 December	0100	260.0–269.7	9.7	4.49	46.3	Pleistocene
21R	5 December	0200	269.7–279.3	9.6	5.13	53.4	Pleistocene
22R	5 December	0310	279.3–288.9	9.6	5.50	57.3	Pleistocene
23R	5 December	0415	288.9–298.6	9.7	3.76	38.7	Pleistocene
24R	5 December	0520	298.6–308.2	9.6	1.83	19.0	Pleistocene
25R	5 December	0630	308.2–317.9	9.7	3.03	31.2	Pliocene-Pleistocene
26R	5 December	0735	317.9–327.5	9.6	5.36	55.8	Pliocene-Pleistocene
27R	5 December	0845	327.5–337.2	9.7	4.28	44.1	Pliocene-Pleistocene
28R	5 December	0950	337.2–346.9	9.7	3.61	37.2	Pliocene-Pleistocene
29R	5 December	1100	346.9–356.5	9.6	3.84	40.0	Pliocene-Pleistocene
30R	5 December	1200	356.5–366.2	9.7	0.88	9.1	Pliocene-Pleistocene
31R	5 December	1350	366.2–375.8	9.6	5.38	56.0	Pliocene-Pleistocene
32R	5 December	1545	375.8–385.5	9.7	4.70	48.4	Pliocene
33R	5 December	1745	385.5–395.2	9.7	2.10	21.6	?
34R	5 December	2000	395.2–404.9	9.7	2.98	30.7	?
35R	5 December	2200	404.9–414.5	9.6	5.94	61.9	?
36R	6 December	0000	414.5–424.2	9.7	5.48	56.5	?
37R	6 December	0215	424.2–433.8	9.6	2.50	26.0	?
38R	6 December	0330	433.8–443.2	9.4	9.82	104.0	
39R	6 December	0540	443.2–452.5	9.3	7.49	80.5	
40R	6 December	0700	452.5–462.1	9.6	0.00	0.0	
41R	6 December	0930	462.1–464.1	2.0	0.00	0.0	
42R	6 December	1505	464.1–467.5	3.4	0.00	0.0	
43R	6 December	1615	467.5–471.5	4.0	0.00	0.0	
44R	6 December	1810	471.5–481.1	9.6	0.02	0.2	
45R	6 December	2015	481.1–490.3	9.2	3.51	38.1	late Pliocene
46R	6 December	2200	490.3–500.0	9.7	6.77	69.8	Pliocene

Table 1 (continued).

Core	Date (1990)	Time (UTC)	Depth (mbsf)	Length cored (m)	Length recovered (m)	Recovery (%)	Age
47R	6 December	2340	500.0–509.6	9.6	9.15	95.3	Pliocene
48R	7 December	0120	509.6–519.3	9.7	9.61	99.1	Pliocene
49R	7 December	0320	519.3–528.9	9.6	9.31	97.0	Pliocene
50R	7 December	0515	528.9–538.6	9.7	7.27	74.9	Pliocene
51R	7 December	0700	538.6–548.2	9.6	9.47	98.6	Pliocene
52R	7 December	0910	548.2–557.9	9.7	9.85	101.0	
53R	7 December	1100	557.9–567.8	9.9	8.61	86.9	late Pliocene
54R	7 December	1300	567.8–577.7	9.9	9.69	97.9	
55R	7 December	1445	577.7–587.4	9.7	8.36	86.2	
56R	7 December	1625	587.4–597.0	9.6	6.74	70.2	late Pliocene
57R	7 December	1800	597.0–606.7	9.7	3.93	40.5	
58R	7 December	1800	606.7–616.3	9.6	7.06	73.5	late Pliocene
59R	7 December	2100	616.3–625.9	9.6	7.28	75.8	late Pliocene
60R	7 December	2245	625.9–635.6	9.7	8.35	86.1	late Pliocene
61R	8 December	0000	635.6–645.2	9.6	7.82	81.4	late Pliocene
62R	8 December	0120	645.2–654.9	9.7	7.15	73.7	late Pliocene
63R	8 December	0240	654.9–664.6	9.7	8.87	91.4	late Pliocene
64R	8 December	0350	664.6–674.2	9.6	9.67	101.0	early Pliocene
65R	8 December	0520	674.2–683.8	9.6	8.82	91.9	early Pliocene
66R	8 December	0645	683.8–693.5	9.7	8.76	90.3	early Pliocene
67R	8 December	0750	693.5–703.1	9.6	8.63	89.9	early Pliocene
68R	8 December	0910	703.1–712.8	9.7	7.86	81.0	early Pliocene
69R	8 December	1050	712.8–722.5	9.7	10.03	103.4	early Pliocene
70R	8 December	1235	722.5–732.2	9.7	8.26	85.1	early Pliocene
71R	8 December	1415	732.2–741.9	9.7	8.96	92.4	early Pliocene
72R	8 December	1540	741.9–751.5	9.6	9.81	102.0	early Pliocene
73R	8 December	1700	751.5–760.8	9.3	6.97	74.9	early Pliocene
74R	8 December	1845	760.8–770.4	9.6	8.08	84.1	early Pliocene
75R	8 December	2000	770.4–779.7	9.3	7.55	81.2	early Pliocene
76R	8 December	2140	779.7–789.3	9.6	9.84	102.0	early Pliocene
77R	8 December	2250	789.3–799.0	9.7	7.42	76.5	
78R	9 December	0015	799.0–808.7	9.7	5.32	54.8	early Pliocene
79R	9 December	0220	808.7–818.3	9.6	9.97	104.0	early Pliocene
80R	9 December	0400	818.3–828.0	9.7	9.53	98.2	?
81R	9 December	0650	828.0–834.0	6.0	4.60	76.6	
82R	9 December	1030	834.0–844.1	10.1	4.59	45.4	
83R	9 December	1430	844.1–851.2	7.1	4.45	62.7	
84R	9 December	1615	851.2–856.2	5.0	1.16	23.2	
85R	10 December	1930	856.2–865.9	9.7	3.05	31.4	
86R	9 December	2215	865.9–875.4	9.5	3.93	41.3	
87R	10 December	0300	875.4–885.2	9.8	1.08	11.0	
88R	10 December	0315	885.2–894.8	9.6	2.02	21.0	early Pliocene
89R	10 December	0500	894.8–904.5	9.7	6.65	68.5	early Pliocene
90R	10 December	0750	904.5–914.2	9.7	7.00	72.1	
91R	10 December	1200	914.2–923.9	9.7	7.53	77.6	
92R	10 December	1505	923.9–933.6	9.7	3.78	38.9	
93R	10 December	1805	933.6–943.3	9.7	5.20	53.6	early Pliocene
94R	10 December	2100	943.3–952.9	9.6	2.57	26.8	early Pliocene
95R	11 December	0030	952.9–962.6	9.7	2.10	21.6	
96R	11 December	0530	962.6–972.2	9.6	4.41	45.9	
97R	11 December	0850	972.2–981.9	9.7	4.87	50.2	
98R	11 December	1235	981.9–991.5	9.6	5.31	55.3	
99R	11 December	1705	991.5–1001.1	9.6	7.65	79.7	
Coring totals				923.7	519.54	56.2	

conducted between the two sites and a brief preliminary survey was performed prior to launching the beacon at 0500 UTC on 2 December 1990.

Hole 833A

The first core, recovered with the advanced piston corer (APC), penetrated the seafloor at 2629.0 mbsf. Oriented APC cores were attempted starting with Core 134-833A-2H. Although only the first three attempts achieved a full 9.5-m stroke, the APC was employed successfully to 81 mbsf using the advance-by-recovery method. Some cores consisted mainly of fluidized ash and volcanic sand (see "Lithostratigraphy" section, this chapter); however, this was less of a problem than at Site 832.

The extended core barrel system (XCB) was used when sufficient APC stroke was no longer possible (below 81 mbsf).

Again the volcanic silt and ash were difficult to recover and core recovery averaged 13% for the interval 81–200 mbsf (see Table 1). The downhole temperature measurement program was more successful than at Site 832 and obtained five usable data points, including one at total depth (see "Downhole Measurements" section, this chapter). At 199.5 mbsf, XCB coring was halted in favor of the rotary core barrel system (RCB). A total of 199.5 m were cored and 97.75 m recovered using the APC/XCB in Hole 833A for a recovery rate of 49% (see Table 1).

Hole 833B

Continuous RCB coring began after the hole had been drilled to 77.4 mbsf. Core recovery gradually increased with depth and degree of induration of the sediment to about 320 mbsf (see "Lithostratigraphy" section, this chapter). Core recovery and hole conditions were generally good to 1001

mbsf (total depth), although drilling slowed drastically when basaltic sills were encountered at 831 mbsf (see "Igneous Petrology" section, this chapter). With the exception of about 40 m of intercalated sediments, the basalt persisted to total depth. Hole conditions remained good, but torque increased for the final three or four cores. At 1001 mbsf, coring operations were terminated because of lack of time and diminished prospects of penetrating Miocene sediments. A total of 923.7 m were cored and 519.54 m recovered with the RCB for a recovery rate of 56.2% (Table 1).

The upper portion of the hole was somewhat unstable during the wiper trip to prepare it for logging. Fine volcanic silt flowed into the hole, causing the drill string to stick and bridges to form in the hole after the first log.

The geophysical tool string, consisting of the dual induction tool, the sonic tool, the lithodensity tool, and the Lamont-Doherty Geological Observatory (LDGO) temperature tool, was recorded over most of the open-hole interval. After considerable difficulty, the lower half of the hole was logged using the formation microscanner. The geochemistry combination surveyed the same open-hole interval as well as the remainder of the hole through the drill pipe (see "Downhole Measurements" section, this chapter).

When operating time expired, the drill string and beacon were recovered and the *JOIDES Resolution* departed for the port call in Fiji at 2330 UTC on 13 December. Leg 134 came to its official end with the first mooring line in the port of Suva at 1900 UTC on 16 December 1990.

LITHOSTRATIGRAPHY

Two holes were drilled at Site 833: Hole 833A penetrated 199.5 m of sediments and Hole 833B penetrated 752.9 m of sedimentary rocks and 169.8 m of interbedded sedimentary and basaltic rocks, after washing down to 77.4 mbsf. The stratigraphic succession at Site 833 is divided into five lithostratigraphic units primarily on the basis of lithological characteristics from visual core descriptions and smear-slide data, but percentages of carbonate from coulometer analyses and biostratigraphic ages also are taken into consideration (Figs. 9 and 10). Lithostratigraphic Unit I, which occurs only in Hole 833A, is divided into two subunits and Unit II is subdivided into four subunits (Table 2).

Lithostratigraphic Unit I

Depth: 0–84.0 mbsf (Hole 833A)
Interval: Sections 134-833A-1H-1, 0 cm, to 134-833A-15X-1, 0 cm
Thickness: 84.0 m
Age: late Pleistocene to Holocene

Unit I consists of unlithified volcanic silts and clayey silts interbedded with numerous fine- to coarse-grained vitric volcanic ashes (Fig. 11). It is divided into two subunits: Subunit IB has a lower carbonate content and ash beds that are thicker and coarser than in Subunit IA. Many of the coarser and thicker volcanic ash units were recovered as soupy sediments that were severely disturbed by coring (e.g., Core 134-833A-9H). There is a near-absence of bioturbation or other evidence of bottom fauna. Total carbonate decreases with depth in lithostratigraphic Unit I (Fig. 10).

Subunit IA

Depth: 0–40.8 mbsf (Hole 833A)
Interval: Sections 134-833A-1H-1, 0 cm, to 134-833A-6H-2, 12 cm
Thickness: 40.8 m
Age: late Pleistocene to Holocene

Subunit IA primarily consists of unlithified, dark greenish gray to very dark gray (10Y 4/1 to 5Y 3/1), clayey to sandy

volcanic silt interbedded with numerous layers of black (5Y 2.5/1), fine vitric volcanic ash with some coarse vitric volcanic ash layers. Horizons containing more than 10% foraminifers or nannofossils commonly occur within the volcanic silt. Vitric ash layers are usually 0.5 to 3 cm thick, but some ash layers as thick as 12 cm occur. Many of the volcanic ash layers have sharp bases and exhibit normally graded bedding, and at their upper limits they commonly grade into volcanic silt. The presence of large numbers of foraminifers in some ashes indicates that the ash may have been transported by turbidity currents to Site 833 after mixing with foraminifers on the seafloor, rather than by settling directly through the water column. In some cores there are dozens of thin vitric volcanic ash layers (e.g., Cores 134-833A-3H and -5H). The volcanic silts often contain an abundance of volcanic glass (Fig. 10), suggesting a high background level of volcanic ash deposition.

Subunit IB

Depth: 40.8–84.0 mbsf (Hole 833A)
Interval: Sections 134-833A-6H-2, 12 cm, to 134-833A-15X-1, 0 cm
Thickness: 43.2 m
Age: late Pleistocene to Holocene

Subunit IB is distinguished from Subunit IA by thick, soupy beds of vitric volcanic ash that are much thicker and coarser than the ash layers of Subunit IA. Six soupy ash layers, 23–45 m thick, in which no sedimentary structures can be recognized, occur in the subunit. In addition, total carbonate content of Subunit IB is less than that of Subunit IA (Fig. 10). The second major lithology in Subunit IB is dark gray (5Y 4/1) clayey volcanic silt. Interbedded with the volcanic silt are thin, fine vitric volcanic ash layers.

Lithostratigraphic Unit II

Depth: 84.0–199.5 mbsf (Hole 833A) and 77.4–375.8 mbsf (Hole 833B)
Interval: Sections 134-833A-15X-1, 0 cm, to 134-833A-26X-CC, 17 cm, and Sections 134-833B-1R-1, 0 cm, to 134-833B-31R-CC, 30 cm
Thickness: 298.4 m (115.5 m in Hole 833A; 298.4 m in Hole 833B)
Age: late Pliocene or early to late Pleistocene to Holocene

Several major lithologies comprise lithostratigraphic Unit II, including gray (5Y 5/1) clayey (or silty) nannofossil (or calcareous) mixed sedimentary rock; gray to very dark gray (5Y 5/1 to 3/1) to dark greenish gray (10Y 4/1) calcareous clayey volcanic siltstone; and dark gray to very dark gray (5Y 4/1 to 3/1) clayey volcanic siltstone. Other combinations of textures occur as well, but most sediments are fine-grained. The entire unit is subject to intense bioturbation, particularly the carbonate-rich lithologies (Fig. 12).

Some subunits are distinguished by having a greater proportion of very dark gray to black (5Y 3/1 to 2.5/1) fine to coarse vitric volcanic tuff; although tuffs or similar vitric volcanic sandstones or siltstones, which may be tuffs, occur in all subunits. Vitric volcanic ash or black vitric volcanic sandstones commonly have a sharp basal contact with underlying sediment and the upper contact is usually gradational (Fig. 12). The lower parts of the sandstone layers are often thinly laminated (~1–3 mm).

The preceding general description illustrates that sedimentary rocks composing lithostratigraphic Unit II are variable in character and composition, but the unit is quite distinct from lithostratigraphic Unit I in at least four respects. First, sediments in lithostratigraphic Unit II are usually bioturbated to heavily bioturbated with abundant

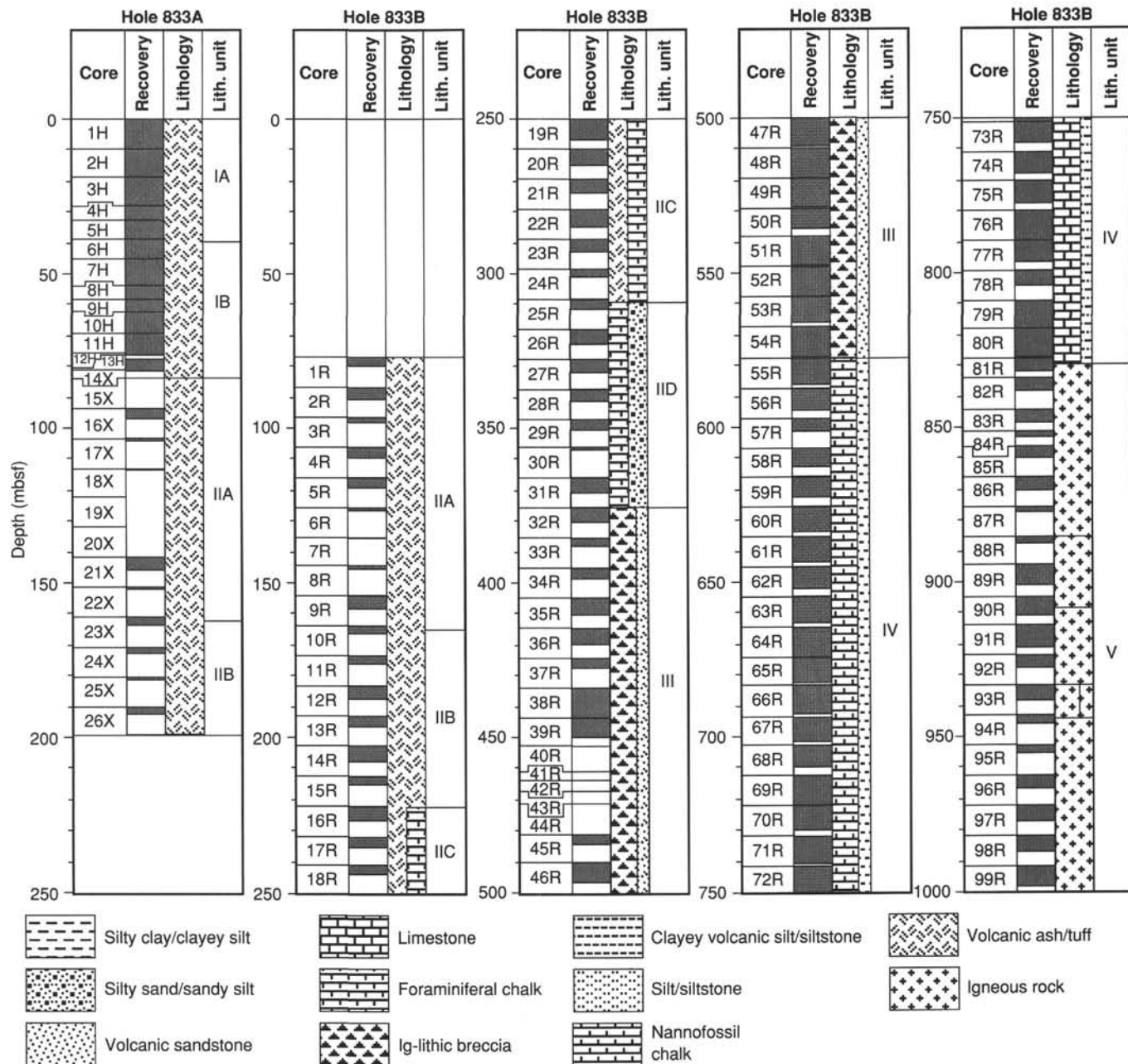


Figure 9. Lithostratigraphy of Site 833.

burrows, pellets, and mottling. Second, sediments in Unit II are much more lithified than the plastically deformable sediment of Unit I. Third, Unit II contains a significantly higher proportion of carbonate. Finally, the proportion of volcanic ash as either discrete beds, or mixed into the major lithologies, is much lower than in Unit I (see percentage of volcanic glass, Fig. 10). Deformation features in Unit II include contorted beds, folds, and minor faults and fractures (Fig. 13). Another interesting feature of this unit is a layer of gypsum that crystallized along a horizontal bedding plane or fracture (Fig. 14).

Subunit IIA

Depth: 84.0–161.95 mbsf (Hole 833A) and 77.4–164.4 mbsf (Hole 833B)

Interval: Sections 134-833A-15X-1, 0 cm, to 134-833A-23X-1, 65 cm, and Sections 134-833B-1R-1, 0 cm, to 134-833B-10R-1, 30 cm

Thickness: 87.0 m (78.0 m in Hole 833A; 87.0 m in Hole 833B)
Age: early to late Pleistocene or Holocene

An abrupt end to abundant vitric volcanic ashes marks the transition from Subunit IB to Subunit IA (Fig. 10), and total carbonate content is greater in the deeper subunit (Fig. 10). The dominant lithology of Subunit IIA is a gray (5Y 4/1), clayey nannofossil mixed sedimentary rock with subordinate amounts of sandy volcanic siltstone and calcareous clayey siltstone. Except for the few volcanic tuffs in Subunit IIA, most of the sediments are slightly to heavily bioturbated.

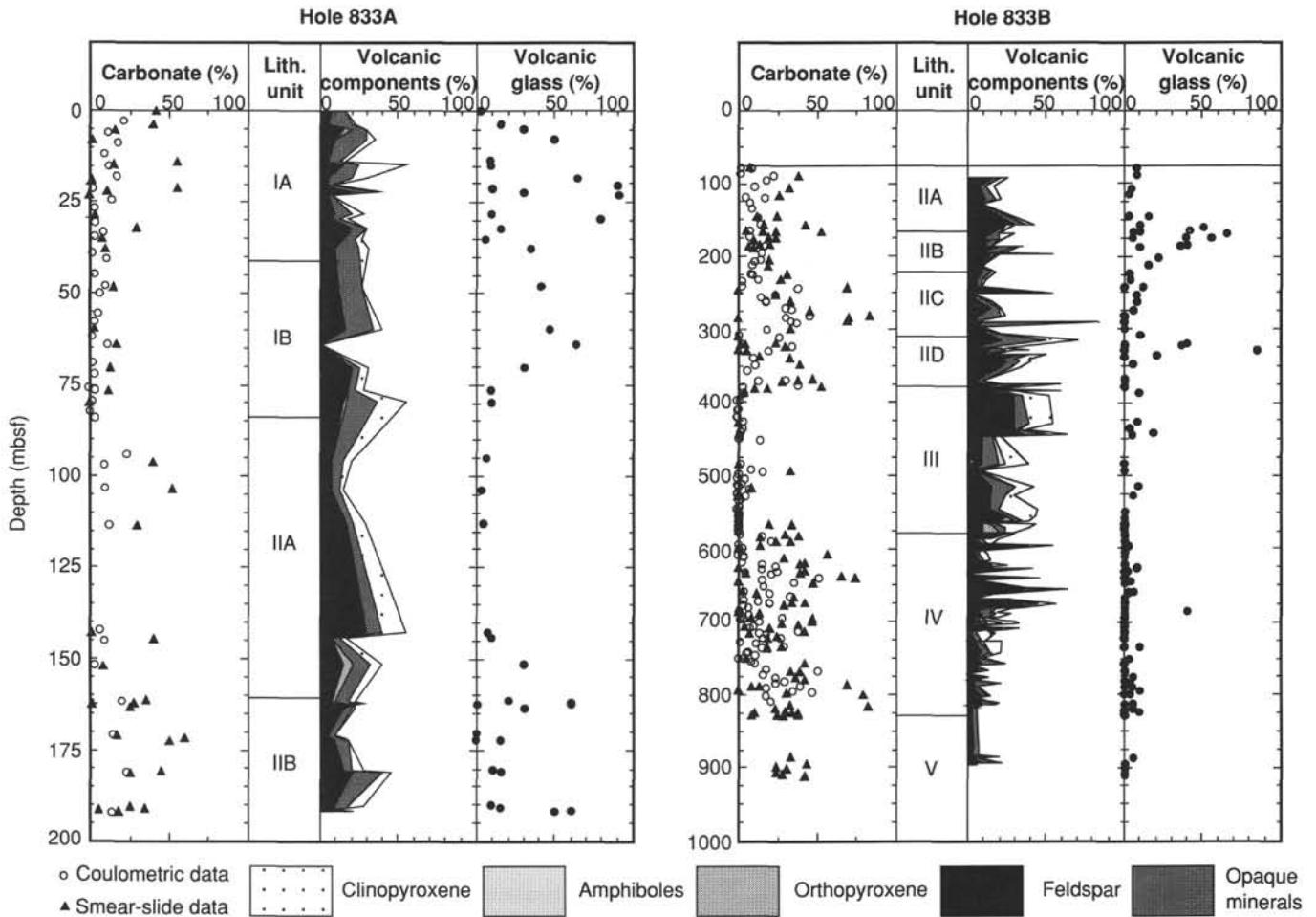


Figure 10. Variation in percentages of carbonate and volcanic components with depth in Holes 833A and 833B. Carbonate content was determined by both coulometric and smear-slide analyses; volcanogenic mineral content was estimated from smear slides.

Subunit IIB

Depth: 161.95–199.5 mbsf (Hole 833A) and 164.4–222.1 mbsf (Hole 833B)
 Interval: Sections 134-833A-23X-1, 65 cm, to 134-833A-26X-CC, 17 cm, and Sections 134-833B-10R-1, 30 cm, to 134-833B-16R-1, 0 cm
 Thickness: 57.7 m (37.5 m in Hole 833A; 57.7 m in Hole 833B)
 Age: early to late Pleistocene or Holocene

Subunit IIB is similar to Subunit IIA, but contains more black to very dark gray (5Y 2.5/1 to 3/1) volcanic tuff layers (Fig. 15). Typical lithologies include gray to greenish gray (5Y 5/1 to 10Y 4/1) calcareous clayey volcanic siltstone; greenish gray (10Y 5/1) sandy volcanic siltstone with foraminifers, nanofossils, and calcareous grains; gray to very dark gray (5Y 5/1 to 3/1), clayey silty mixed sedimentary rock with nanofossils, foraminifers, and calcareous grains; and dark gray (5Y 4/1) vitric sandy volcanic siltstone with clay and foraminifers. The vitric tuff beds range in thickness from 5 to 25 cm (commonly the tuff beds are laminated and their upper parts grade into the overlying bioturbated lithologies). Core-breaks often occur near the base of coarse tuff beds where the coarse, friable sands have been washed away (e.g., Fig. 15). The high glass content of the nonpyroclastic sediments (e.g., Core 134-833B-13R) indicates that vitric ash has mixed with the other sediments in Subunit IIB.

Subunit IIC

Depth: 222.1–308.37 mbsf (Hole 833B)
 Interval: Sections 134-833B-16R-1, 0 cm, to 134-833B-25R-1, 17 cm
 Thickness: 86.3 m
 Age: early Pleistocene

The major lithologies in Subunit IIC are silty volcanic claystones and clayey volcanic siltstones that contain more carbonate than other subunits of Unit II (Fig. 10). Beds of foraminiferal chalk and mixed sediments occur as major lithologies in Cores 134-833B-21R to -23R (274–299 mbsf). Cores 134-833B-22R to -24R, at 280–299 mbsf, contain neritic grains including light gray (5Y 7/1) mollusc-algal floatstone and rudstone. A distinguishing feature of this subunit, relative to the rest of lithostratigraphic Unit II, is the presence of contorted, slump-folded and faulted beds in Cores 134-833B-19R, -22R, and -23R (250–260 mbsf and 280–299 mbsf; Fig. 13). Core 134-833B-19R contains dendritic water-escape structures, also called vein structures.

Subunit IID

Depth: 308.4–375.8 mbsf (Hole 833B)
 Interval: Sections 134-833B-25R-1, 17 cm, to 134-833B-31R-CC, 30 cm
 Thickness: 67.4 m
 Age: early Pleistocene

Table 2. Lithostratigraphic units, Site 833.

Interval	Unit	Subunit	Depth (mbsf)	Thickness (m)	Age
Sections 134-833A-1H-1, 0 cm, to 134-833A-15X-1, 0 cm	I		0–84.0	84.0	late Pleistocene to Holocene
Sections 134-833A-1H-1, 0 cm, to 134-833A-6H-2, 12 cm		IA	0–40.8	40.8	late Pleistocene to Holocene
Sections 134-833A-6H-2, 12 cm, to 134-833A-15X-1, 0 cm		IB	40.8–84.0	43.2	late Pleistocene to Holocene
Sections 134-833A-15X-1, 0 cm, to 134-833A-26X-CC, 17 cm, and	II		84.0–199.5	115.5	
Sections 134-833B-1R-1, 0 cm, to 134-833B-31R-CC, 30 cm	II		77.4–375.8	298.4	early Pleistocene to late Pleistocene or Holocene
Sections 134-833A-15X-1, 0 cm, to 134-833A-23X-1, 65 cm, and		IIA	84.0–162.0	78.0	
Sections 134-833B-1R-1, 0 cm, to 134-833B-10R-1, 30 cm		IIA	77.4–164.4	87.0	late Pleistocene to Holocene
Sections 134-833A-23X-1, 65 cm, to 134-833A-26X-CC, 17 cm, and		IIB	162.0–199.5	37.5	
Sections 134-833B-10R-1, 30 cm, to 134-833B-16R-1, 0 cm		IIB	164.4–222.1	57.7	early Pleistocene to late Pleistocene or Holocene
Sections 134-833B-16R-1, 0 cm, to 134-833B-25R-1, 17 cm		IIC	222.1–308.4	86.3	early Pleistocene
Sections 134-833B-25R-1, 17 cm, to 134-833B-31R-CC, 30 cm		IID	308.4–375.8	67.4	early Pleistocene
Sections 134-833B-32R-1, 0 cm, to 134-833B-55R-1, 8 cm	III		375.8–577.8	202.0	late Pliocene
Sections 134-833B-55R-1, at 8 cm, to 134-833B-81R-2, 80 cm	IV		577.8–830.3	252.5	early Pliocene to late Pliocene
Sections 134-833B-81R-2, at 80 cm, to 134-833B-99-6, 136 cm	V		830.3–1001.1	170.8	early Pliocene

Subunit IID is marked by a major increase in the occurrence and thickness of black (5Y 2.5/1) vitric volcanic sandstone or coarse tuff interbedded with volcanic siltstones and claystones. These major lithologies, except for the black volcanic sands, continue to be highly bioturbated and carbonate-rich (Fig. 12). The sandstones often are laminated and rarely bioturbated except in their upper parts. Above sharply defined bases, the sandstones grade upward into the bioturbated lithologies. The vitric component is usually partially devitrified. Load casts at the bases of the black volcanic sand layers indicate episodic deposition (Fig. 12).

Lithostratigraphic Unit III

Depth: 375.8–577.8 mbsf (Hole 833B)
 Interval: Sections 134-833B-32R-1, 0 cm, to 134-833B-55R-1, 8 cm
 Thickness: 202.0 m
 Age: late Pliocene to possible early Pleistocene

Unit III is characterized by black (5Y 2.5/1), coarse-grained volcanic sandstones (Fig. 16) and black (5Y 2.5/1), fine-grained basaltic breccias. Above and below this unit the rocks are often calcareous and much finer grained. The basaltic breccias are the dominant lithology only in Cores 134-833B-35R, -36R, -37R, -46R, and -47R (405–434 mbsf and 490–510 mbsf; Fig. 17), but they represent the relative coarseness of this unit. Even in cores where basaltic breccia does not occur, the volcanic sandstone is quite coarse-grained and basaltic clasts may occur (e.g., in Section 134-833B-34R-CC). Only three cores in this entire lithostratigraphic unit contain a significant proportion of carbonate-rich interbeds: Cores 134-

833B-37R, -47R, and -48R (424–433 mbsf and 500–520 mbsf) contain very dark gray (5Y 3/1), calcareous silty volcanic claystone.

The rocks in Core 134-833B-39R (443–453 mbsf) are unusually fine-grained volcanic siltstone and heavily bioturbated, dark greenish gray (5GY 4/1) chloritic claystone. Zeolitic grains occur throughout the core and are concentrated with clasts of the chloritic claystone in Section 134-833B-39R-2, 20–50 cm. No similar lithology exists in any other core at Site 833.

Lithostratigraphic Unit IV

Depth: 577.8–830.3 mbsf (Hole 833B)
 Interval: Sections 134-833B-55R-1, 8 cm, to 134-833B-81R-2, 80 cm
 Thickness: 252.5 m
 Age: early to late Pliocene

Lithostratigraphic Unit IV begins with the appearance of foraminiferal sandy volcanic siltstone and the disappearance of basaltic breccias and very coarse-grained volcanic sandstones. Planktonic foraminifers are abundant; benthic foraminifers occur as well. Significant quantities of very dark gray to black (5Y 3/1 to 2.5/1), silty volcanic sandstones and sandy siltstones continue as important lithologies in the upper part of Unit IV. In general, these volcanic sandstones are laminated and are rarely bioturbated. The more carbonate-rich lithologies, particularly the mixed sedimentary rocks, are usually intensely bioturbated, although examples of laminated carbonate-rich intervals do occur. The rest of Unit IV consists of calcareous volcanic siltstones, calcareous silty mixed sedi-

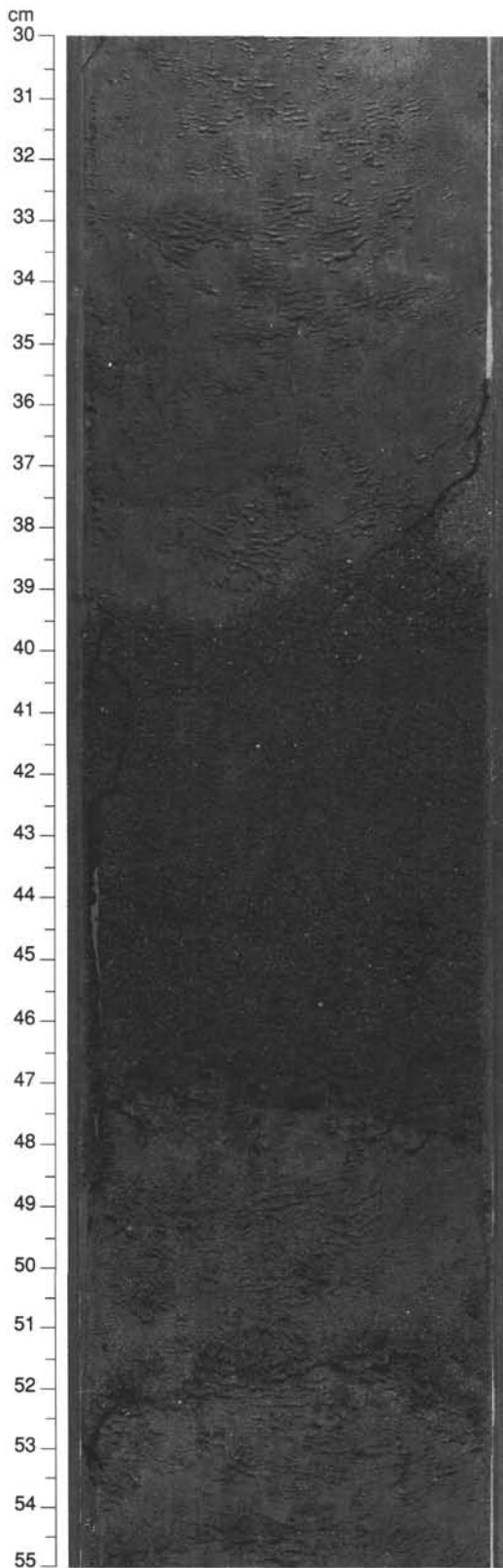


Figure 11. Interval 134-833A-1H-6, 30-55 cm, is a black vitric volcanic ash layer interbedded with volcanic silt.

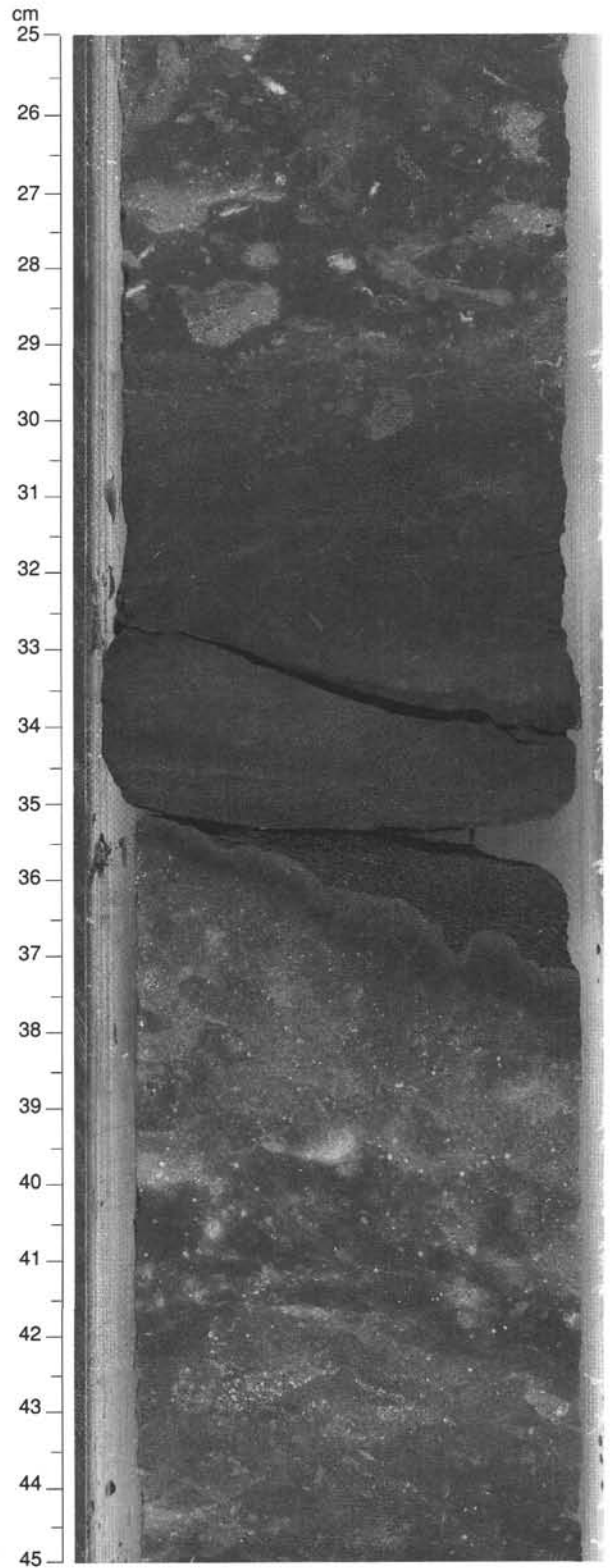


Figure 12. Interval 134-833B-27R-1, 25-45 cm, from Subunit IID shows a laminated, silty vitric volcanic sandstone (34-36 cm) above a sharp basal contact with load casts. The upward gradation to a bioturbated calcareous volcanic siltstone is transitional. This calcareous bioturbated sediment above 29 cm and below 37 cm is a typical lithology in lithostratigraphic Unit II.

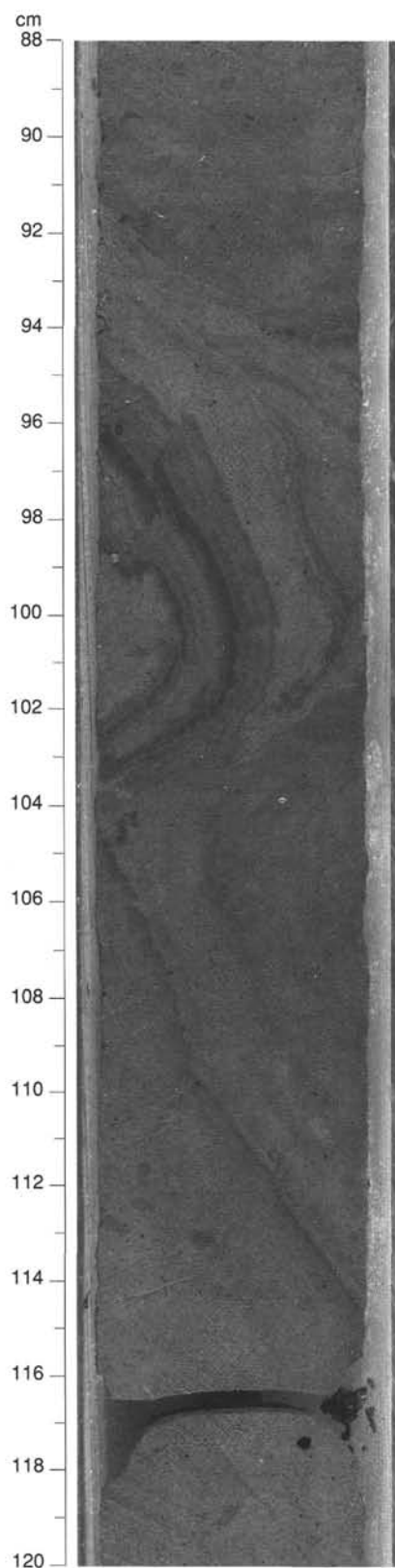


Figure 13. Interval 134-833B-22R-2, 88–120 cm, contains a faulted slump fold in foraminiferal chalk from Subunit IIC.

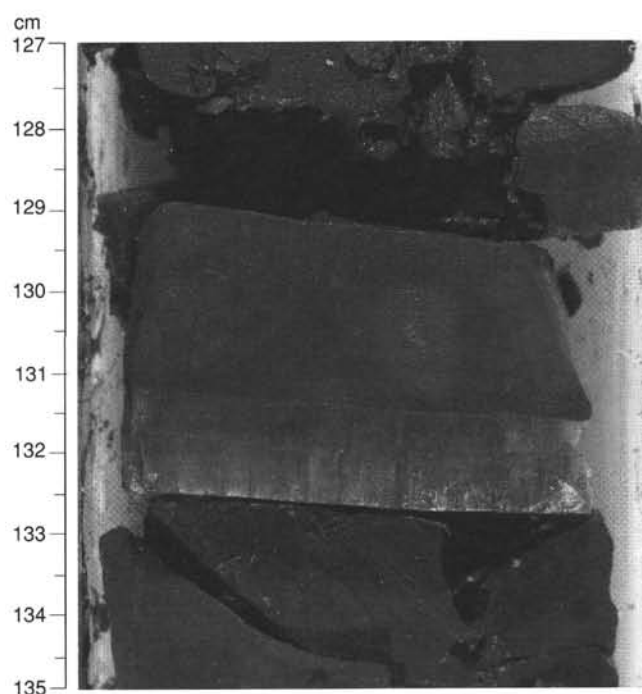


Figure 14. Interval 134-833B-27R-2, 127–135 cm, contains a layer of gypsum about 1 cm thick that crystallized in a horizontal fracture or bedding plane.

mentary rock, foraminiferal nannofossil chalk, sed-lithic breccia, and silty limestone.

Numerous fining-upward sequences occur in Unit IV. These sequences range from approximately 25 cm to several meters in thickness, but are most commonly about 75 cm thick. The fining upward sequences commonly begin at a sharp basal contact, sometimes exhibiting load casts, overlying a carbonate-rich, heavily bioturbated lithology (Fig. 18). Basal sediments are often laminated volcanic siltstones or sandstones with white laminae of carbonate grains, some of which are large benthic foraminifers (e.g., Fig. 19). The volcanic sediment becomes finer grained upsection, evidence of bioturbation begins and increases rapidly as the carbonate content increases concomitantly (e.g., Fig. 19). The tops of the sequences consist of very fine-grained, carbonate-rich sediments that are very heavily bioturbated and mottled. Occurrences of possible *Zoophycos* trace fossils are common in the bioturbated intervals.

Lithostratigraphic Unit V

Depth: 830.3–1001.1 mbsf (Hole 833B)

Interval: Sections 134-833B-81R-2, 82 cm, to 134-833B-99R-6, 136 cm

Thickness: 170.8 m

Age: early Pliocene (sediments only)

Unit V consists of interbedded sedimentary rocks and basaltic sills. Basalt occurs at the top of this unit (Fig. 20) and continues for 21.6 m to 851.9 mbsf, where 42 cm of sedimentary rock were recovered (Section 134-833B-84R-1, 65–107 cm). Additional intervals of sedimentary rock occur at 885.2–886.2 mbsf, 886.7–910.1 mbsf, and 935.1–946.0 mbsf (in Cores 134-833B-88R, -89R, -93R, and -94R).

Most of the sedimentary rocks of lithostratigraphic Unit V are gray to very dark gray (5Y 5/1 to 3/1), calcareous silty volcanic claystones or siltstones and clayey or silty mixed sedimentary rocks. Fining-upward sequences often begin at

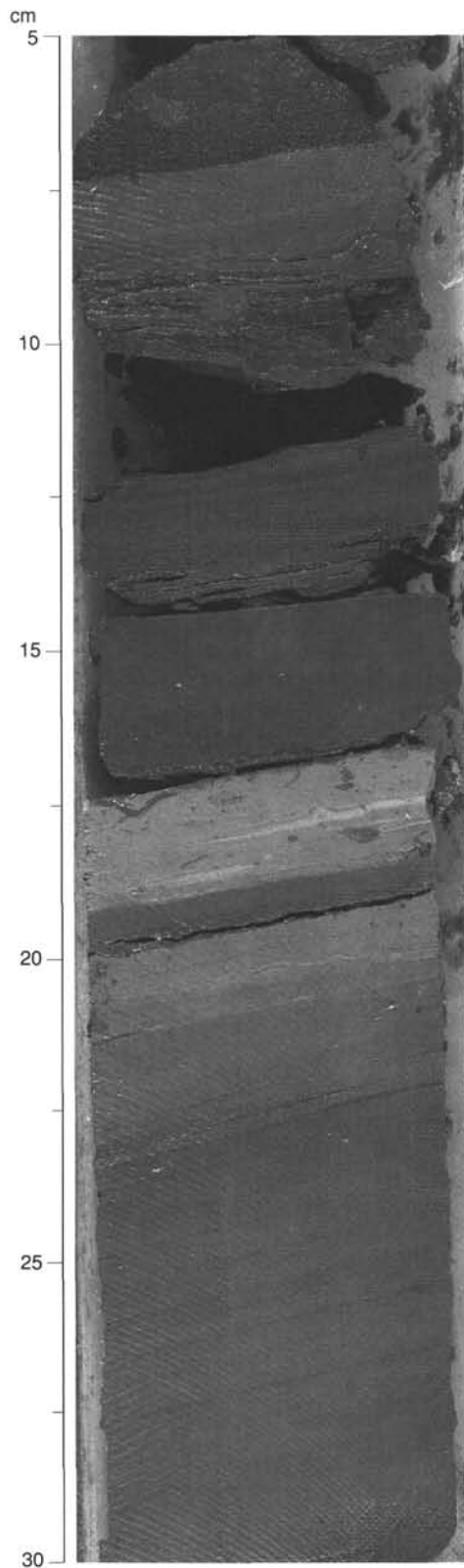


Figure 15. Interval 134-833B-13R-1, 5–30 cm, from Subunit IIB shows a laminated black vitric volcanic siltstone overlying laminated clayey calcareous chalk. The core broke at the contact between these two units and some of the friable volcanic sandstone was washed out of the core from the three breaks between 10 and 17 cm. Significant amounts of this lithology may have been lost in this fashion.

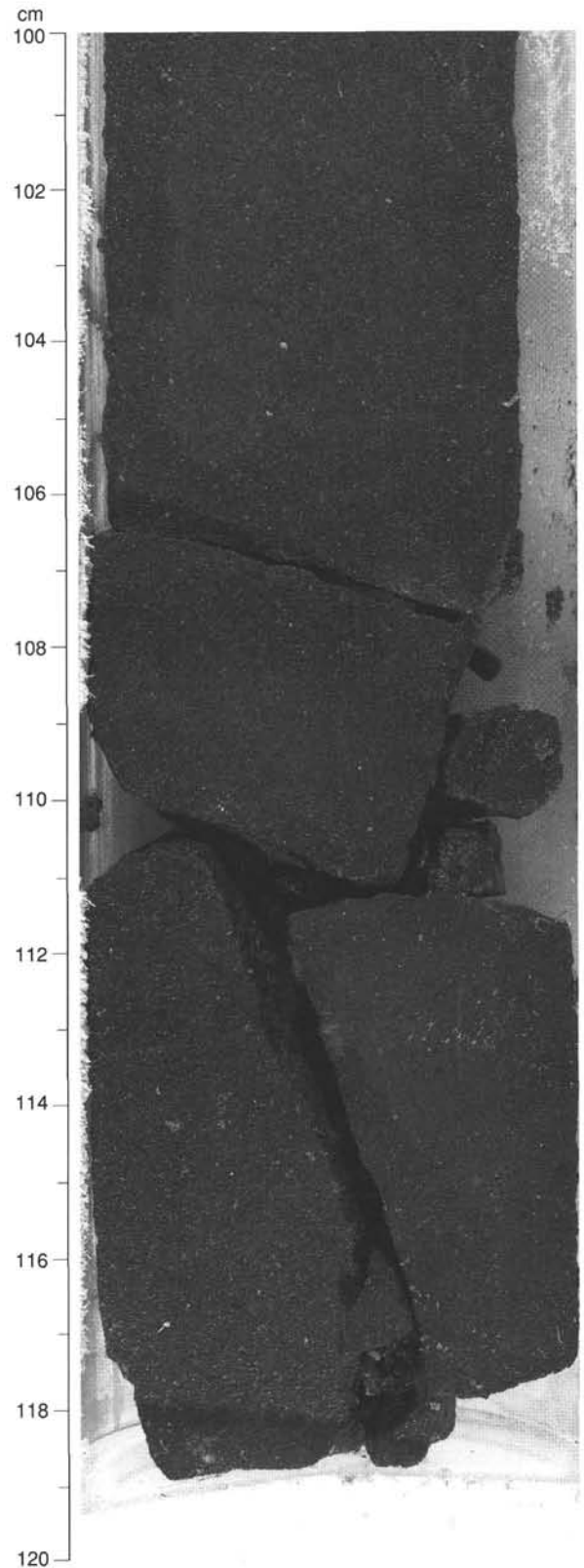


Figure 16. Interval 134-833B-32R-2, 100–120 cm, contains typical coarse-grained volcanic sandstone of lithostratigraphic Unit III.

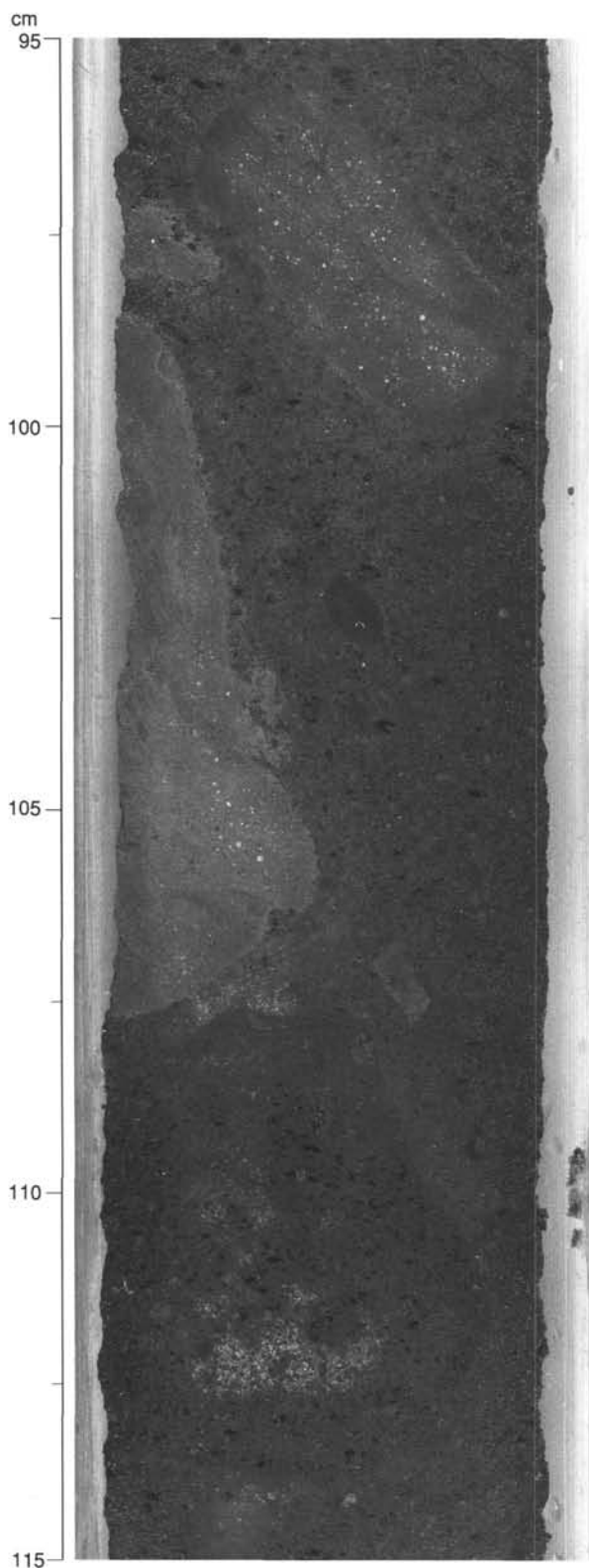


Figure 17. Interval 134-833B-47R-3, 95–115 cm, shows rounded clasts of calcareous silty claystone (96–99.5 cm and 98.5–107.5 cm) and vesicular basalt (108–113 cm) in a breccia from Unit III.

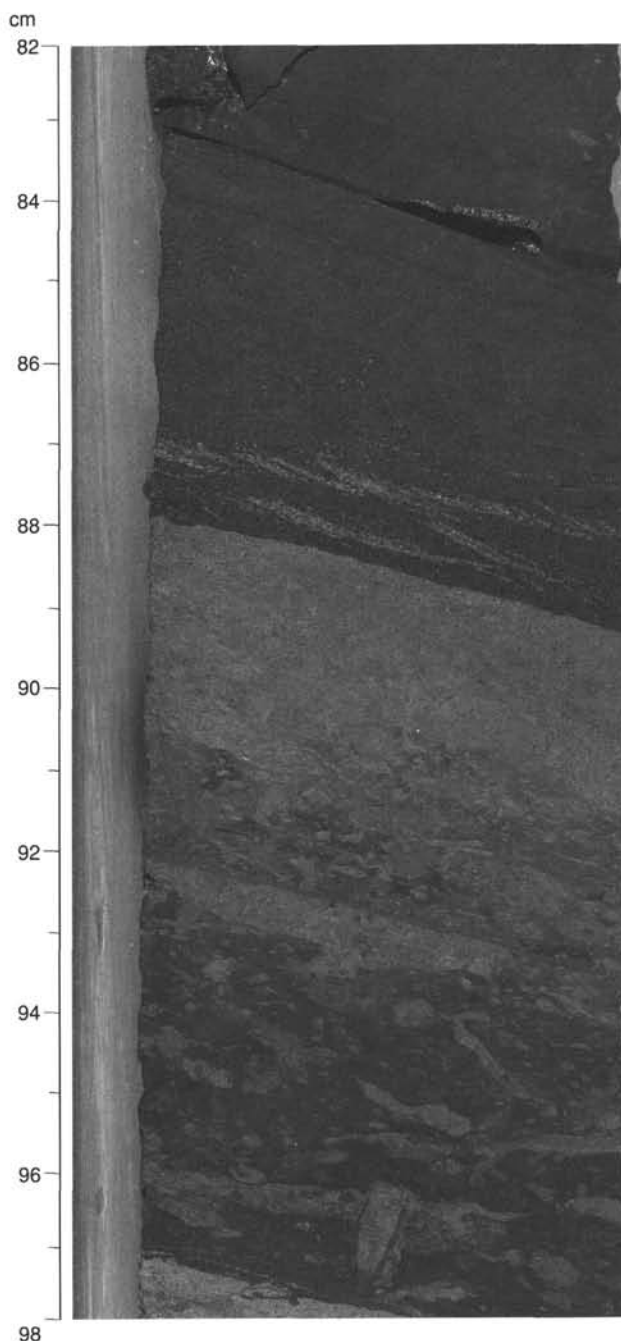


Figure 18. Interval 134-833B-62R-4, 82–98 cm, shows the sharp basal contact of a black, laminated volcanic siltstone (87.5 cm) over a heavily bioturbated calcareous sedimentary lithology typical of Unit IV.

sharp basal contacts and usually culminate in heavily bioturbated carbonate-rich rocks. These sedimentary rocks and the fining-upward sequences within them are very similar to those of the lower part of Unit IV, except for minor contact metamorphic effects from the intrusion of basaltic magmas.

The contacts between the sedimentary rocks and basalt do not exhibit dramatic changes in the character of either lithology relative to intervals farther from the contact (Fig. 20). The most obvious effect on the sedimentary rock appears to be chloritization (e.g., Core 134-833B-90R). The igneous rocks of this unit are discussed elsewhere (see "Igneous Petrology" section, this chapter).

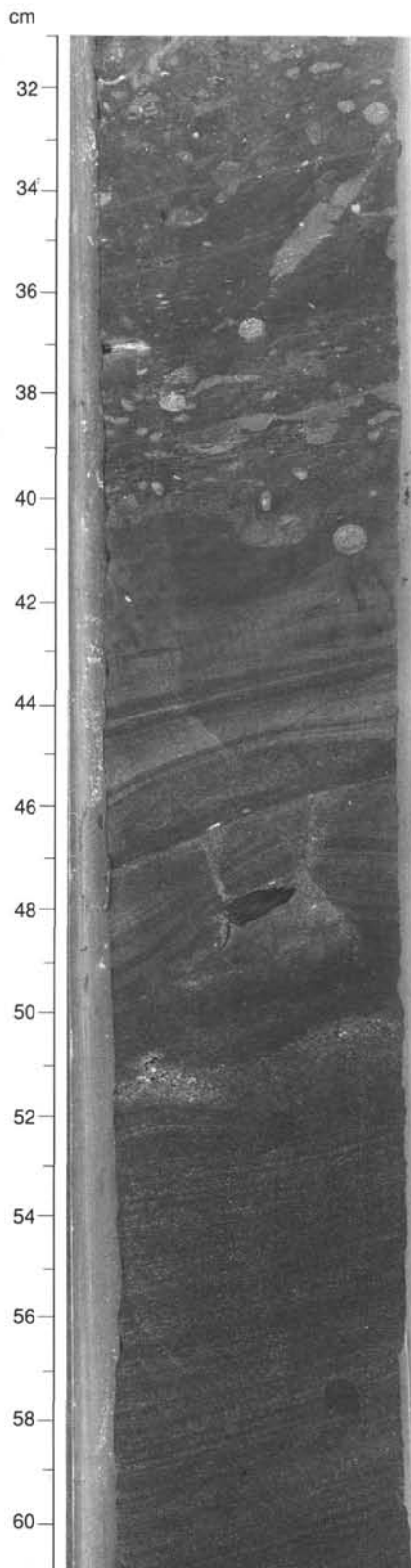


Figure 19. Interval 134-833B-65R-4, 31–61 cm, shows the transition from laminated silty volcanic sandstone to bioturbated calcareous clayey volcanic siltstone typical of the fining upward sequences of Unit IV. The object at 48 cm is a wood fragment.

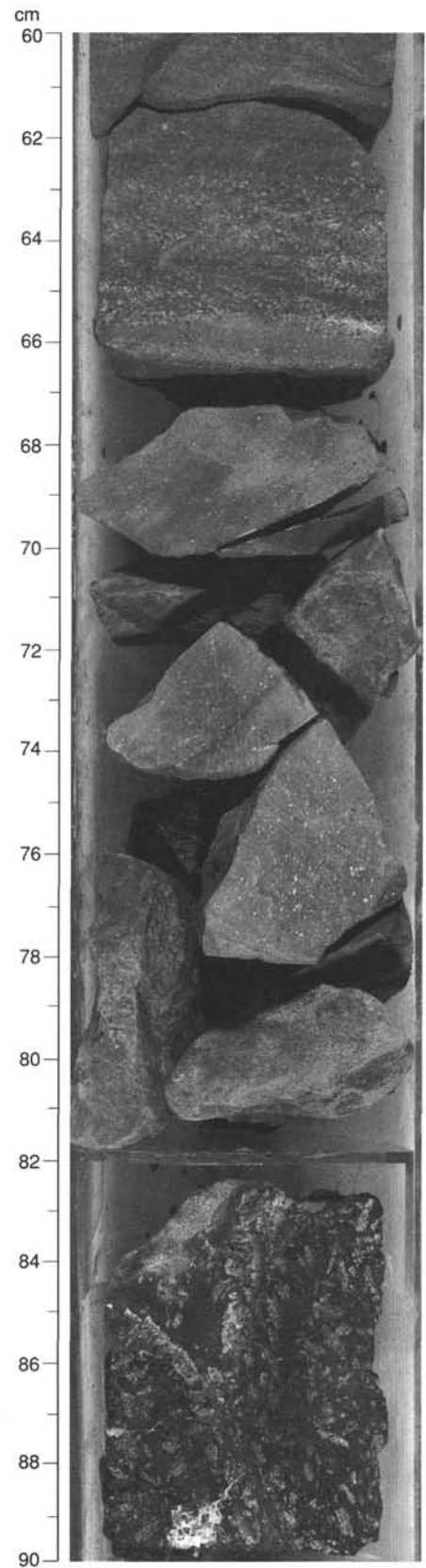


Figure 20. The contact between the sedimentary rocks of Unit IV and the uppermost basaltic sill of Unit V occurs at 830.3 mbsf (Section 134-833B-81R-2, 82 cm). The sedimentary rocks show no obvious signs of deformation and contain only a thin baked zone, which is described elsewhere (see "Igneous Petrology" section, this chapter).

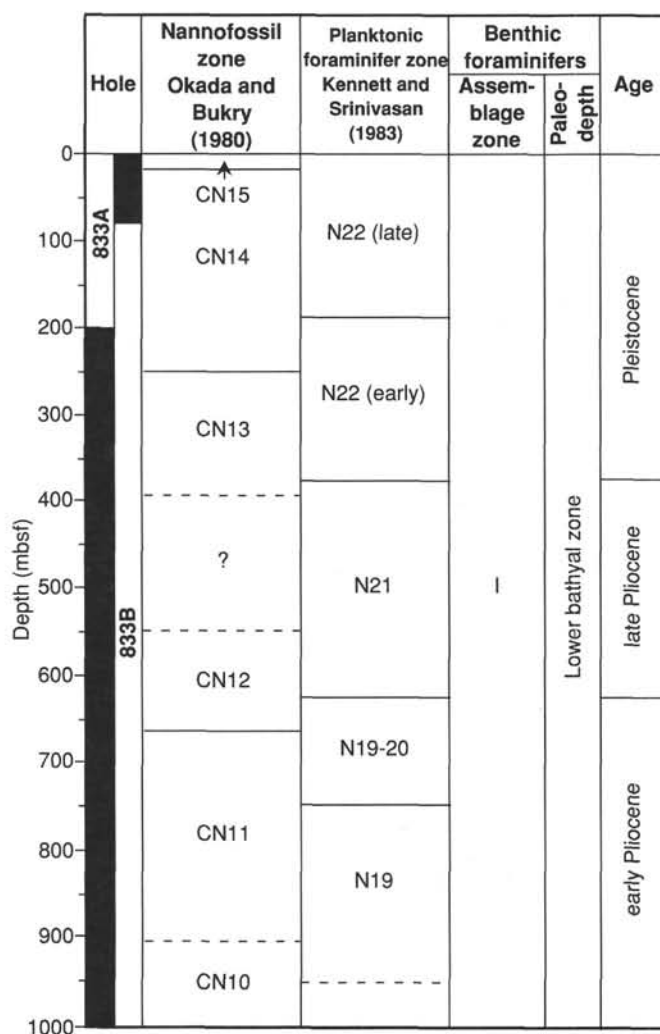


Figure 21. Biostratigraphic summary of Site 833.

BIOSTRATIGRAPHY

Application of foraminiferal and nannofossil biostratigraphy at Site 833 was severely limited by the abundance of volcanic ash, volcanoclastic sediments, turbidites, and slumps. As a result many samples were barren or contained only a few specimens (because of dilution by other components), providing very uncertain ages. In spite of this, planktonic foraminiferal Zones N22 to N19 (Holocene to early Pliocene) have been recognized in the sedimentary succession at Site 833 (Fig. 21). Reworking is common but generally affects only contiguous zones or sedimentary layers.

Calcareous Nannofossils

Pleistocene

Calcareous nannofossils including *Emiliania huxleyi*, *Gephyrocapsa oceanica*, *Gephyrocapsa caribbeanica*, *Helicosphaera kamptneri*, and *Rhabdosphaera claviger* are found in Samples 134-833A-1H-CC through -2H-CC, which are thus placed into Zone CN15. Samples 134-833A-2H-CC to 134-833B-18R-CC contain *H. kamptneri*, *C. leptoporus*, *G. caribbeanica*, small *gephyrocapsids*, *R. claviger*, and *G. oceanica*, indicating that these samples belong to Zone CN14.

Between Sections 134-833B-18R-CC and 134-833B-33R-CC the lack of *G. oceanica* and the relatively low abundances of other *gephyrocapsids* result in the placement of these samples

into Zone CN13. *Pseudoemiliania lacunosa*, *C. leptoporus*, *H. kamptneri*, and *C. doronicoides* dominate the nannofossil assemblage in this interval, their abundances ranging from abundant to rare. The presence of *D. brouweri* in some samples is attributed to reworking since they are often found with discoasters and sphenoliths indicative of the early Pliocene. The age of Samples 134-833B-33R-CC through -52-CC is uncertain because of the paucity of nannofossils.

Pliocene

In the interval from Sections 134-833B-53R-CC through -63R-CC, *D. brouweri* becomes a common constituent of the nannofossil assemblage suggesting that these samples are of late Pliocene age (Zone CN12). *Calcidiscus macintyreii*, *H. kamptneri*, *P. lacunosa*, *Discoaster triradiatus*, and small reticulofenestrids are also present.

Sphenolithus abies, *Sphenolithus neoabies*, *C. macintyreii*, *D. pentaradiatus*, *D. brouweri*, *H. kamptneri*, *Dictyococites*, sp. and small reticulofenestrids comprise the assemblage in Samples 134-833B-64R-CC through -94R-2, 50 cm. The presence of *Sphenolithus abies* and *Sphenolithus neoabies* indicate that these samples are no younger than 3.47 Ma (see Table 1, "Explanatory Notes" chapter, this volume). Although *Reticulofenestra pseudoumbilica* appears only in samples from Cores 134-833B-70R, -89R, and -93R, the interval from Sections 134-833B-64R-CC through -94R-2, 50 cm, is interpreted as being of early Pliocene age.

Planktonic Foraminifers

Late Pleistocene-Holocene

The sediments between the seafloor and 183.5 mbsf (Samples 134-833A-1H-CC to 134-833B-11R-CC) are assigned to the late Pleistocene to Holocene (upper Zone N22) on the basis of the occurrence of *Globorotalia truncatulinoides*, along with *Globorotalia tumida tumida*, *Pulleniatina obliquiloculata*, *Globorotalia crassaformis*, *Globorotalia menardii*, *Globigerinoides conglobatus*, and *Neogloboquadrina dutertrei*, among others. The last appearance datum (LAD) of *Globorotalia tosaensis* was first recorded at 193.1 mbsf (Sample 134-833B-12R-CC), making it possible to distinguish informally the upper from the lower Pleistocene. However, reworking is common in this sequence and may affect the first record of *G. tosaensis*.

Early Pleistocene

The interval between 193.1 and 375.8 mbsf (Samples 134-833B-12R-CC to -31R-CC) is early Pleistocene (early Zone N22) in age, based on the sporadic co-occurrence of *G. tosaensis* s.l. and *G. truncatulinoides*, along with *G. tumida tumida*, *G. conglobatus*, *Sphaeroidinella dehiscens*, *G. crassaformis*, *P. obliquiloculata*, and *Orbulina universa* among others. The lower part of this interval can equally be latest Pliocene because of the diachronous character of the first occurrence of *G. truncatulinoides* (cf. Hills and Thierstein, 1989). Furthermore this interval shows the evolutionary transition between *G. truncatulinoides* and its ancestral form *G. tosaensis*. Such a change is subtle and varies from sample to sample, being readily apparent only by the development of a tiny keel in the last chamber of some adult specimens. Evidence of reworking from lower Pliocene material in this interval is suggested by the occurrence of few to rare specimens of *Dentoglobigerina altispira*, *Globorotalia multicamerata*, *Globigerinoides fistulosus*, and *Sphaeroidinellopsis kochi* in Sample 134-833B-21R-CC.

Late Pliocene

Samples assigned to the late Pliocene (Zone N21) are from the interval between 385.5 and 635.6 mbsf (Samples 134-833B-

32R-CC to -60R-CC). The age is based on the occurrence of *G. tosaensis* and the absence of *G. truncatulinoides*. Some species present in this interval are *G. fistulosus*, *G. tumida tumida*, *G. crassaformis*, *Pulleniatina praecursor*, *S. dehiscens*, *G. conglobatus*, *Globigerinoides extremus*, *Globorotalia multicamerata*, *D. altispira*, and *Sphaeroidinellopsis paenedehiscens*, among others. Abundance varies from rare to common and preservation is poor to moderate.

Early Pliocene

Sediments in the interval between 635.6 and 751.5 mbsf (Samples 134-833B-61R-CC to -72R-CC) are assigned to Zones N19–N20, whereas sediments between 751.5 and 945 mbsf are assigned to Zone N19. These two zones are early Pliocene in age (cf. Kennett and Srinivasan, 1983). Planktonic foraminiferal Zone N20 is indicated by the presence of *G. crassaformis* and the absence of *G. tosaensis*, whereas Zone N19 is indicated by the presence of *S. dehiscens* and the absence of *G. crassaformis*. The following species occur in varying abundance throughout this lower Pliocene sedimentary sequence: *G. tumida tumida*, *Globorotalia tumida flexuosa*, *Pulleniatina praecursor*, *G. conglobatus*, *Globigerinoides extremus*, *Globigerinoides nepenthes*, *Globorotalia multicamerata*, *D. altispira*, *S. paenedehiscens*, *Sphaeroidinellopsis seminulina*, and *Orbulina universa*, among others.

Benthic Foraminifers

Rare benthic foraminifers occur in core-catcher samples examined from Holes 833A and 833B. Preservation is generally moderate to good in the samples from the seafloor to 260.0 mbsf (Sample 134-833B-19R-CC), but becomes poor below this depth. No benthic foraminifers were found in the samples in the intervals 45.2–58.1 mbsf, 69.7–81.1 mbsf, 84.0–103.3 mbsf, 122.6–132.3 mbsf, 151.7–161.3 mbsf, and 180.6–199.5 mbsf in Hole 833A, or in the intervals 135.2–183.5 mbsf, 202.8–222.1 mbsf, 260.0–269.7 mbsf, 288.9–366.2 mbsf, 375.8–616.3 mbsf, 635.6–712.8 mbsf, 722.5–741.9 mbsf, 751.5–760.8 mbsf, and below 770.4 mbsf in Hole 833B.

The assemblages recognized in the upper Cenozoic sequence at Site 833 consist mainly of species such as *Cibicides wuellerstorfi*, *Melonis barleeanus*, *Melonis pacificus*, *Melonis sphaeroides*, *Sphaeroidina bulloides*, *Tosaia hanzawai*, and *Uvigerina proboscidea*. The occurrence of *Melonis sphaeroides* suggests the lower bathyal zone as a possible paleobathymetric setting for the sedimentary sequence of Holes 833A and 833B. Sublittoral species such as *Amphistegina radiata* and *Elphidium crispum* are recognized at 113.0 mbsf (Sample 134-833A-17X-CC), 279.3 mbsf (Sample 134-833B-21R-CC), 288.9 mbsf (Sample 134-833B-22R-CC), 625.9 mbsf (Sample 134-833B-59R-CC), 751.5 mbsf (Sample 134-833B-72R-CC), and 770.4 mbsf (Sample 134-833B-74R-CC). These specimens were derived from the sublittoral zone and transported downslope by turbidity currents.

IGNEOUS PETROLOGY

Three categories of igneous rocks are distinguished at Site 833 in the North Aoba Basin: volcanic ash horizons (0–322 mbsf), clasts in breccias (387–570 mbsf), and basaltic sills (830–1001 mbsf). In each instance the igneous rocks constitute only parts of the depth intervals specified.

Volcanic Ashes

Volcanic ash layers are abundant in lithostratigraphic Unit I of Site 833 (Fig. 22) and are sparse in lithostratigraphic Unit II, becoming very rare below 200 mbsf (see "Lithostratigraphy" section, this chapter). Interbedded

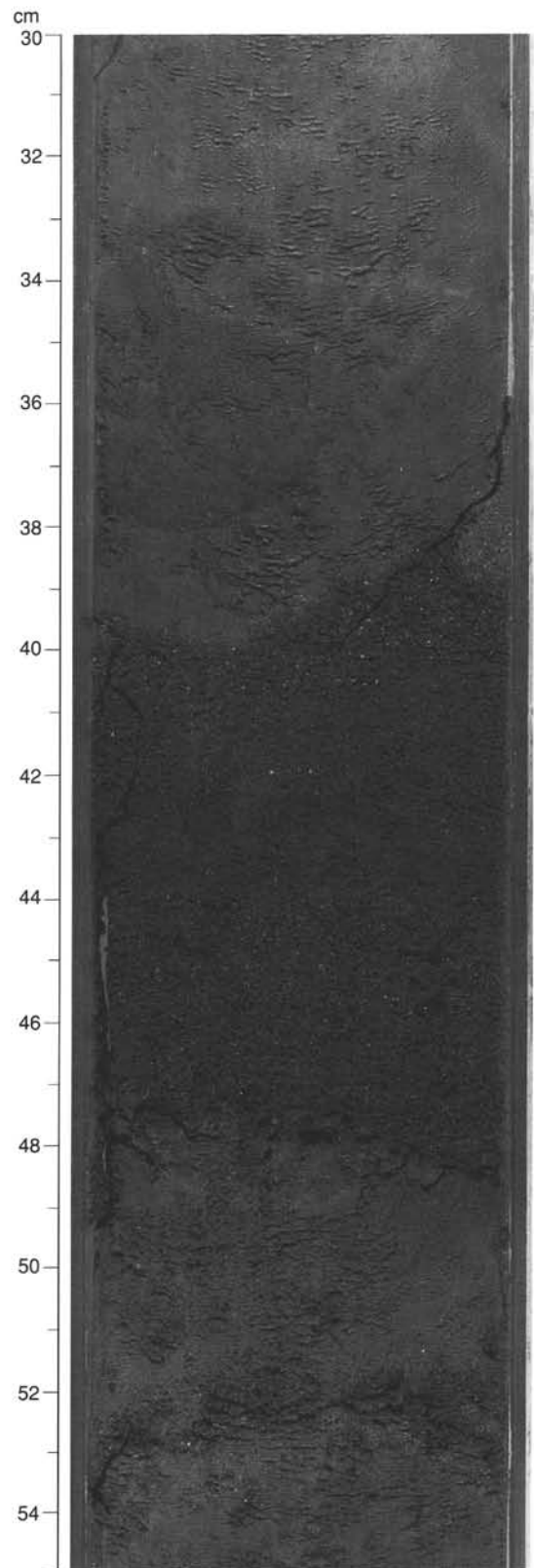


Figure 22. Volcanic ash interbedded with volcanic silt in Unit I (interval 134-833A-1H-6, 30–55 cm).

with clayey volcanic silt, most of the ashes have probably been slightly reworked, judging by the admixture of small quantities of foraminifers, nanfossils, and sponge spicules. A typical example of one of these ash deposits is Sample 134-833A-5H-4, 50–51 cm, from a 5-cm horizon at 37.6 mbsf. It contains volcanic glass (34%), opaque minerals (15%), rock fragments (15%), plagioclase feldspar (10%), clinopyroxene (6%), iron-oxide minerals (5%), clay minerals (3%), chlorite (2%), and calcite (2%), with bioclastic components making up the remaining 8%. The crystal constituents are mostly in the size range 0.1–0.3 mm. In plane-polarized light the glass fragments (0.1–0.2 mm in diameter) vary from colorless to light gray (10YR 7/1) and light brown (7.5YR 6/4). Some of them contain small needles of feldspar and others have irregular opaque inclusions. Many occur as fasciculate clusters and some as clear featureless wedges. In another vitric ash (Sample 134-833A-7H-2, 125–126 cm), the glass (41%) is very pale brown (10YR 7/3 and 7/4), with many of the fragments having the cusped morphology indicative of broken vesicles. This sample is unusual in containing small quantities (<1%) of olivine. Other constituents are opaque minerals (15%), plagioclase (12%), rock fragments (10%), iron-oxide minerals (5%), and chlorite (2%); in addition, there are nanfossils (10%), foraminifers (2%), and undifferentiated calcite (2%).

Sample 134-833B-9H-2, 77–78 cm, is from unconsolidated soupy ash, which is the commonest material between 47 and 81 mbsf. Although it has undoubtedly undergone some remobilization during drilling, it is probably representative of one of the more voluminous volcanic deposits in lithostratigraphic Unit I. It contains glass (45%), opaque minerals (18%), plagioclase feldspar (16%), small rock fragments (10%), clinopyroxene (6%), iron-oxide minerals (3%), and foraminifers (2%). The color of the glass in plane-polarized light varies from light brown (7.5 YR 6/4) to very pale brown (10YR 7/3) and pinkish gray (5YR 7/2). The glass fragments are frequently crowded with stretched or flattened vesicles and some are packed with innumerable filaments, probably very elongate vesicles, arranged in a brush-like form. This sample is also relatively unusual in containing a few crystals of amphibole showing characteristic pleochroism.

Lower down in the sequence (lithostratigraphic Unit II) the incidence of ash layers becomes increasingly sporadic. One such example from 173 mbsf (Sample 134-833B-10R-1, 90–91 cm) is dominated by partially devitrified glass shards (70%), together with plagioclase feldspar (10%), opaque minerals (10%), clinopyroxene (3%), iron-oxide minerals (1%), and foraminifers (5%). Throughout the succession there are also occasional horizons of scattered pumice (e.g., Sample 134-833B-20-R-1, 29–31 cm, from 260.2 mbsf).

At 308–317 mbsf (Core 134-833B-25R), some well-defined black lithified vitric ashes or tuffs are intercalated with calcareous silty claystone; they occur at intervals 134-833B-25R-1, 23–35 cm, and -25R-2, 28–36 cm. Sample 134-833B-25R-1, 29–30, cm contains plagioclase (20%), clinopyroxene (20%), opaque minerals (30%), rock fragments (17%), glass (10%), iron-oxide minerals (2%), and orthopyroxene (1%). Some dark brown but almost certainly reworked ash beds appear a little below this, in the range 318–322 mbsf (e.g., intervals 134-833B-26R-1, 19–44 cm, and -26R-2, 70–89 cm).

Clasts in Breccias

Coarse volcanic sandstones and breccias were encountered at a depth of 375.8 mbsf, marking the top of Unit III. Volcanic clasts (<7 cm in diameter) appear in the breccias from 387 mbsf downward. The clasts are principally pyroxene-phyric basalts or ankaramites. The designation ankaramite is used as

a hand-specimen term for a basaltic lava with conspicuous and dominant pyroxene phenocrysts and has no compositional implications beyond this. Often, plagioclase is also common as phenocrysts in these rocks, but the crystals are much smaller (<1 mm in diameter) and less conspicuous than the pyroxenes (<5 mm in diameter). In Hole 832B, 35 km to the west, the onset of coarse volcanic sandstones and breccias is at a similar depth (385.5 mbsf), with ankaramite again prominent among the clasts.

The volcanoclastic sediments of Hole 833B are black in color (5YR 2.5/1) and vary in grain size from breccias to fine sandstones. From about 500 mbsf downward, zeolites become increasingly abundant in the matrix and fractures, as well as in the vesicles of clasts. The breccias contain basaltic clasts which usually range in size from 1 to 7 cm in diameter. A typical clast is Sample 134-833B-37R-1, 42–43 cm, from 424.6 mbsf, which is a porphyritic basalt with plagioclase (35%), clinopyroxene (15%), and olivine (10%) in a fine-grained matrix composed partly of devitrified glass, together with grains of clinopyroxene, plagioclase, and opaque minerals. Another clast (Sample 134-833B-33R-2, 111–113 cm), comes from 397.8 mbsf and contains abundant phenocrysts of plagioclase (35%; core composition of An_{68} ; 0.2–2 mm in diameter) with subsidiary clinopyroxene (6%; 0.2–2 mm in diameter) and altered olivine (2%; 0.1–1 mm in diameter) in a microcrystalline matrix of plagioclase laths and grains of clinopyroxene and opaque minerals.

Basaltic Sills

At 830.3 mbsf, the top of Unit V, the lower Pliocene calcareous volcanic siltstone is cut by a basaltic sill (Fig. 23). The contact is marked by a zone of discolored (greenish gray 5GY 6/1) and indurated sediment and a series of thin (<1 mm) zeolite-filled fractures. The sill is composed of a highly plagioclase-phyric basalt, which shows subparallel orientation of its feldspar phenocrysts within a few centimeters of the contact. Against the sediment, the sill has a nonvesicular chilled margin, about 5 mm wide. From thin-section examination of the contact zone the chilled margin is revealed as having vitrophyric texture with abundant phenocrysts of plagioclase (30%; 0.5–2 mm in diameter). These feldspar phenocrysts contain small inclusions of opaque minerals and pale brown glass. They usually have euhedral morphology and complex oscillatory zoning with core compositions of An_{60} . Other phenocryst phases are subhedral clinopyroxene (5%; 0.1–1 mm in diameter) and opaque minerals (1%; 0.1–1 mm in diameter). Olivine phenocrysts originally made up about 2% of the rock but they are now mostly altered to chlorite and serpentine. There are small clusters of plagioclase, clinopyroxene, and opaque minerals in the matrix, which is dominated by very pale brown glass (10YR 8/4), becoming greenish gray (5GY 8/1) toward the sediment. Away from the upper contact, phenocryst minerals are similar in type and abundance to those reported for the chilled margin except that olivine is totally pseudomorphed by secondary minerals. In Sample 134-833B-81R-3, piece 8, preliminary determinations of the plagioclase composition are in the range An_{65} – An_{55} . The groundmass is microcrystalline with laths of plagioclase, anhedral clinopyroxene, and opaque minerals. Both the clinopyroxene and the opaque phase often have acicular quench textures. At 852.16 mbsf (interval 134-833B-84R-1, 96–107 cm), calcareous volcanic silt intervenes and the basalt shows another chilled upper margin (<1 cm wide). Farther down (885 mbsf; Section 134-833B-88R-1) a thicker sequence of calcareous volcanic siltstones and bioturbated foraminiferal limestones was drilled: these are similar to the sediments above the basaltic

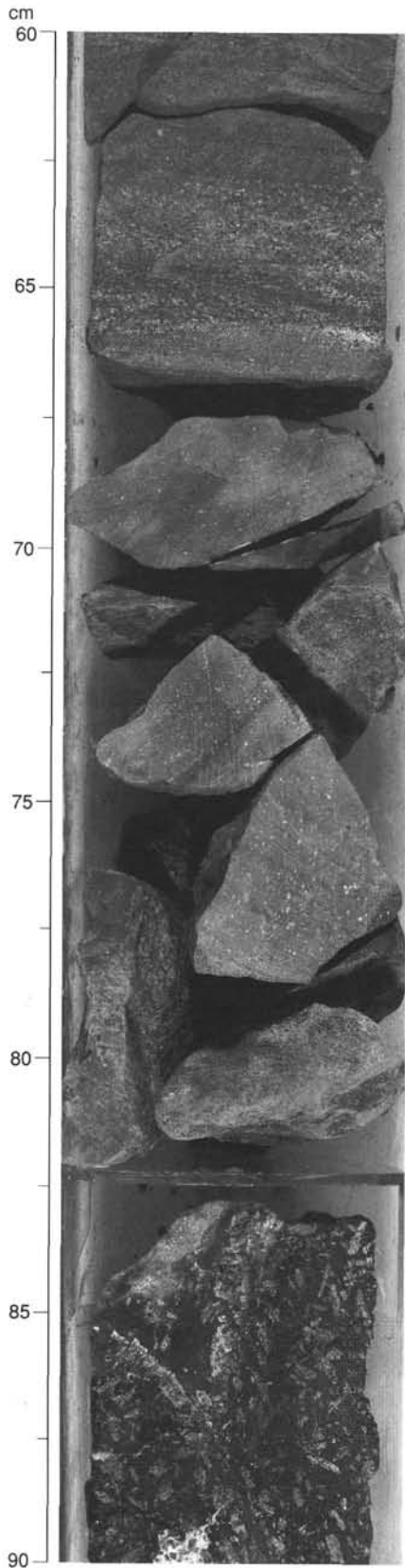


Figure 23. Upper contact of the highly plagioclase-phyric sill with calcareous volcanic silt at 830.3 mbsf in interval 134-833B-81R-2, 60–90 cm.

sill. Basalt was reentered at 886.0 mbsf. In all, seven separate igneous intervals were penetrated, with the intervening sediments ranging in thickness from a few centimeters to 24 meters. Contact relations were established in several but by no means all instances. However, there was sufficient evidence to suggest an intrusive rather than extrusive origin. The only exception may be the basalt from between 943 and 962 mbsf, which is noticeably more vesicular than the rest, but even here there was no sign of the rubbly top usually associated with lavas.

Apart from variations in the immediate vicinity of the chilled margins, the sills tend to remain very uniform over considerable thicknesses. However, there is a gradual but progressive reduction in plagioclase phenocryst content downward through the sequence (e.g., from 30% at 831 mbsf to 15% at 914 mbsf and <10% at 953 mbsf). At the limit of drilling (1001 mbsf), plagioclase phenocrysts make up less than 5% of the total, and in places the rock has developed a medium-grained matrix, making it diabase rather than basalt. Material recovered from the lowermost levels drilled in the sill also appears to be more altered than the rest.

The individual sills might be interpreted as representing a series of separate magmatic injections of slightly different composition and density. However, the apparent compositional continuum suggests a close relationship between the sills at all stratigraphic levels. It therefore seems possible that some preferential concentration of plagioclase had occurred within the magma reservoir prior to its intrusion into the sediments. All or most of the sills may form part of a multiple intrusion that was injected more or less simultaneously along several horizons. Contact relations (e.g., interval 134-833B-84R-1, 100–107 cm) suggest that the sediments were relatively unconsolidated when they were invaded by the magma. Petrographically, the sill rocks are very similar to the plagioclase-phyric basalts described from the Bwatigau Formation of Maewo (Carney, 1986).

IGNEOUS GEOCHEMISTRY

Three categories of igneous rocks were recovered from Holes 833A and 833B (see "Lithostratigraphy" and "Igneous Petrology" sections, this chapter). Six samples were selected for major and trace element analysis by shipboard X-ray fluorescence (see "Explanatory Notes" chapter, this volume) and the results are presented in Table 3. Two of the analyses are of volcanic ashes from lithostratigraphic Unit I (Samples 134-833A-1H-6, 43–45 cm, and 134-833A-4H-3, 8–11 cm), one is a moderately lithified ash or tuff from lithostratigraphic Unit II (Sample 134-833B-25R-1, 27–30 cm), one a basaltic clast from lithostratigraphic Unit III (Sample 134-833B-34R-2, 107–110), and two are from the basalt sills of lithostratigraphic Unit V (Samples 134-833B-81R-3, 98–102 cm, and 134-833B-84R-1, 125–128 cm). Prior to analysis, the two ash samples from lithostratigraphic Unit I were treated with 1N HCl solution in an ultrasonic bath in order to remove organic and inorganic carbonate, but the moderately lithified ash from lithostratigraphic Unit II was analyzed without treatment.

Volcanic Ashes of Lithostratigraphic Unit I

The general similarity of the two volcanic ash samples is apparent from Table 3. They are both of basaltic composition (49.48% and 50.77% SiO₂) with relatively high K₂O (1.47% and 2.18%, respectively) and associated incompatible elements (Ba, Rb, and Sr) compared with mid-ocean ridge basalt (MORB) or most orogenic volcanic rock suites (Jakes and White, 1972). On a K₂O vs. SiO₂ diagram (Taylor et al., 1981), Sample 134-833A-4H-3, 8–11 cm, plots in the high-potassium

Table 3. Major and trace element analyses of volcanic ashes (1–3), basaltic clast (4), and basaltic sill (5, 6) from Site 833.

Sample number	1	2	3	4	5	6
Hole, core, section	833A-1H-6	833A-4H-3	833B-25R-1	833B-34R-2	833B-81R-3	833B-84R-1
Sample interval (cm)	43–45	8–11	27–30	107–110	98–102	125–128
Depth (mbsf)	7.93	31.58	308.47	397.77	831.87	852.45
Major elements (wt%)						
SiO ₂	50.77	49.48	50.54	49.19	52.73	52.31
TiO ₂	0.90	0.81	0.64	0.75	1.05	1.04
Al ₂ O ₃	14.79	13.50	16.22	19.06	17.24	17.47
Fe ₂ O ₃ (t)	11.78	11.92	9.84	9.60	10.50	10.17
MnO	0.21	0.20	0.16	0.16	0.19	0.20
MgO	6.12	8.37	7.45	4.90	2.85	2.82
CaO	9.37	11.50	11.28	11.35	8.90	8.90
Na ₂ O	2.71	2.15	1.70	2.35	3.19	3.11
K ₂ O	2.18	1.47	0.41	0.59	1.88	2.02
P ₂ O ₅	0.24	0.20	0.07	0.10	0.46	0.46
Total	99.05	99.58	98.30	98.03	98.97	98.48
LOI	0.80	0.78	3.65	0.68	0.89	0.90
Mg#	0.51	0.58	0.60	0.50	0.35	0.35
Trace elements (ppm)						
Ti	5366	4826	3837	4466	6265	6235
Nb	3	2	2	2	7	8
Zr	91	58	38	41	130	134
Y	17	14	14	20	32	34
Sr	784	835	401	334	637	660
Rb	37	25	6	7	21	30
Zn	102	91	70	76	102	90
Cu	138	155	107	31	315	331
Ni	55	89	53	35	13	14
Cr	186	359	153	44	5	7
V	340	351	309	370	281	275
Ce	36	24	12	10	50	50
Ba	518	365	92	193	225	228

Note: Fe₂O₃(t) = total iron as Fe₂O₃; LOI = loss on ignition; Mg# = MgO/(MgO + FeO_{total}) mol%.

calc-alkaline field and Sample 134-833A-1H-6, 43–45 cm, falls just within the shoshonitic field (Fig. 24). The samples lie on the potassic trend defined by the islands of the Central Chain of the New Hebrides Island Arc (data from Gorton, 1977; Dupuy et al., 1982; Bardsell et al., 1982; Marcelot et al., 1983; Briquieu, 1984) and the ashes of Site 832. The latter show a broader range of differentiation and a spread of compositions into less potassic varieties, but this may simply reflect the larger number of samples analyzed from Site 832. Of the two ashes, the sample from lower in the sequence (Sample 134-833A-4H-3, 8–11 cm) has significantly higher MgO (8.37%) compared with Sample 134-833A-1H-6, 43–45 cm (6.12%). The more magnesian sample also has higher concentrations of the compatible trace elements Ni and Cr and lower concentrations of incompatible elements. The differences between the two ashes are explicable in terms of crystal fractionation, with the stratigraphically higher sample being slightly more evolved. The MORB-normalized trace element patterns (Pearce, 1983) for the two samples (Fig. 25) are subparallel to each other, also suggesting a relationship by fractional crystallization. The patterns closely resemble those for Site 832 in respect of the degree of enrichment in large ion lithophile (LIL) elements and the negative Nb anomalies. The only significant difference is that the Site 833 ashes have lower concentrations of Zr. High Zr contents in the Site 832 ashes were taken to indicate an origin from the island of Santa Maria (see "Igneous Geochemistry" section, "Site 832" chapter, this volume).

Volcanic Ash of Lithostratigraphic Unit II

The lithified ash, or tuff, from lithostratigraphic Unit II (Sample 134-833B-25R-1, 27–30 cm) has a high loss on igni-

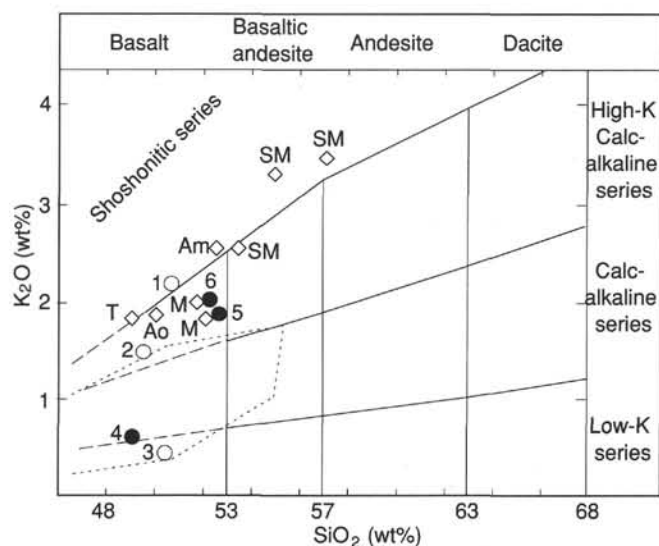


Figure 24. K₂O-SiO₂ diagram for volcanic ashes (1, 2, and 3), basaltic clast (4), and basaltic sill (5 and 6) recovered from Site 833, North Aoba Basin. Numbers refer to samples in Table 3. Dotted line encloses compositions of lavas from several islands of the Central Chain of the New Hebrides Island Arc (data from Gorton 1977; Dupuy et al., 1982; Bardsell et al., 1982; Marcelot et al., 1983; Briquieu, 1984; and Macfarlane et al., 1988). Diamonds refer to more alkali-rich magmas erupted at Tongoa (T), Aoba (Ao), Ambrym (Am), Maewo (M), and Santa Maria (SM) islands. Field boundaries from Taylor et al. (1981).

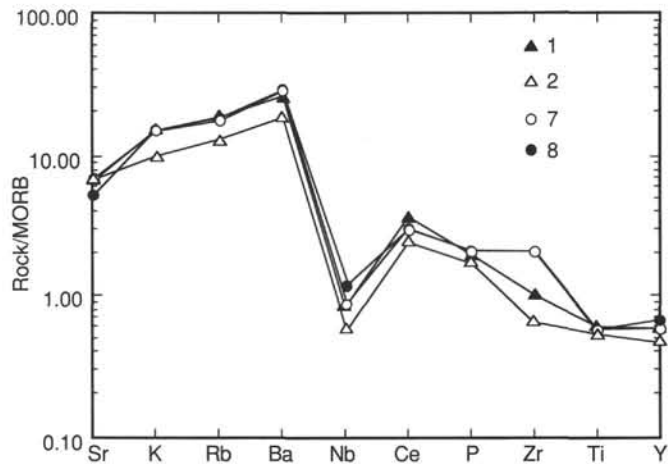


Figure 25. MORB-normalized trace element patterns for volcanic ashes of lithostratigraphic Unit I, Site 833 (1 and 2; see Table 3) compared with those for two ashes from Site 832 (7 = Sample 134-832A-2H-5, 82–87 cm, and 8 = Sample 134-832A-7H-1, 26–28 cm). Normalizing values in this and subsequent figures from Pearce (1983).

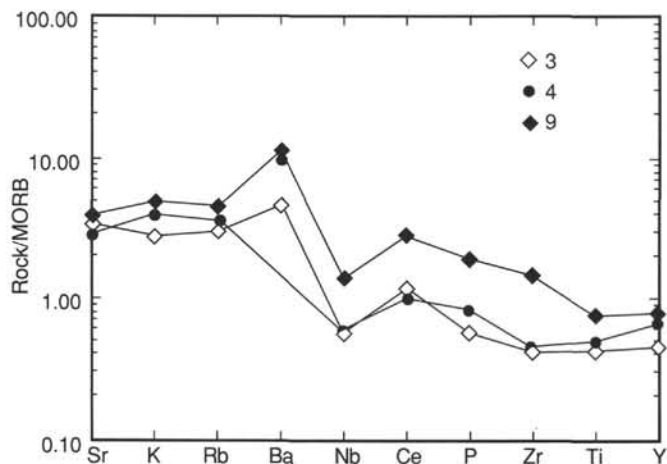


Figure 26. MORB-normalized trace element patterns for tuff (3) and clast (4) from Site 833 compared with that of a clast from Site 832 (9).

tion (3.65%) and may deviate somewhat from its original magmatic composition. However, the analysis is of a relatively undifferentiated basaltic rock (SiO_2 50.54% and MgO 7.45%) with distinctly different trace element characteristics from the ashes of lithostratigraphic Unit I. It has only 0.41% K_2O and on the K_2O vs. SiO_2 classification scheme (Taylor et al., 1981) plots in the field of the low-potassium tholeiite series (Fig. 24). The island-arc tholeiite affinity of this sample is further substantiated by its MORB-normalized trace element pattern (Fig. 26), which shows a marked suppression of LIL elements in comparison with the ashes of lithostratigraphic Unit I.

Basaltic Clast from Lithostratigraphic Unit III

Sample 134-833B-34R-2, 107–110 cm, is a basalt clast from the volcanic breccia at 397.77 mbsf. It has the lowest SiO_2 content (49.19%) of the rocks analyzed from Site 833, the highest Al_2O_3 concentration (19.06%), and is moderately differentiated (MgO 4.90% and Mg number 0.50). On the K_2O vs. SiO_2 plot (Fig. 24) it falls just inside the calc-alkaline field, bordering on that of the low-potassium series. On the MORB-

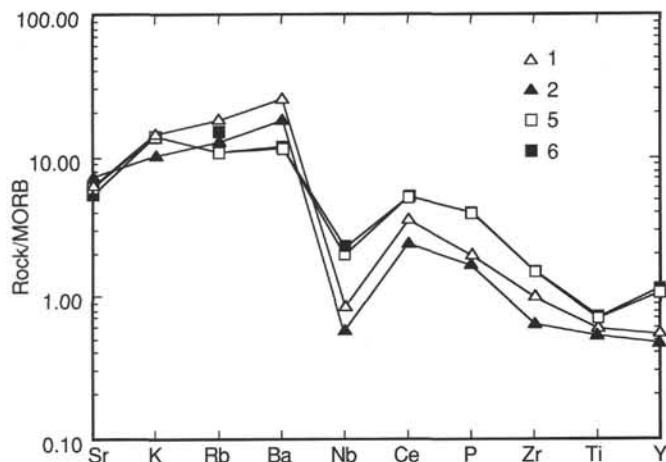


Figure 27. MORB-normalized trace element patterns for samples from the basaltic sill (5 and 6) compared with those for two ashes (1 and 2) from Site 833. Numbers refer to samples in Table 3.

normalized trace element diagram (Fig. 26) it approximates to the pattern of the ash from lithostratigraphic Unit II, apart from having a higher content of Ba (193 parts per million, or ppm, compared with 92 ppm in Sample 134-833B-25R-1, 27–30 cm, from lithostratigraphic Unit II).

Basaltic Sills of Lithostratigraphic Unit V

The two samples chosen for analysis come from the highly plagioclase-phyric upper part of the intrusion (831.87 and 852.45 mbsf) and are similar in chemical composition. They are differentiated basaltic rocks with 52%–53% SiO_2 and only 2.8% MgO . Fe_2O_3 exceeds 10% and the Mg number is consequently low (0.35), suggesting tholeiitic characteristics in terms of iron-enrichment. However, on the K_2O vs. SiO_2 classification scheme (Taylor et al., 1981) the two samples plot in the field of the high-potassium calc-alkaline series (Fig. 24). The MORB-normalized trace element patterns show the typical subduction-related signature of enriched LIL elements combined with negative Nb anomalies and slightly depleted Ti values (Fig. 27).

Conclusions

Despite the limited number of chemical analyses from Site 833, the compositions extend across the entire spectrum of subduction-related volcanic rocks from island-arc tholeiites to high-potassium calc-alkaline and shoshonitic series. This confirms and extends the compositional range encountered at Site 832, where more evolved types were also found. Data from the two drilling sites in the North Aoba Basin generally suggest an upward progression from magmatic rocks of island-arc tholeiite affinity to increasingly potassic volcanics at the top of the succession. However, a range of compositions has apparently been available during much of the evolution of this region (Gorton, 1977; Dupuy et al., 1982; Bardsell et al., 1982; Marcelot et al., 1983; Briquet, 1984).

The basaltic sills in the lowest part of Hole 833B (830–1001 mbsf) are high-potassium calc-alkaline rocks. Because of their intrusive nature the only constraint on the timing of their emplacement is that they are of lower Pliocene age or younger. They may be related to the high-potassium calc-alkaline lavas and dolerites of Maewo Island (Fig. 24), which are described as being of upper Miocene to lower Pliocene age (Macfarlane et al., 1988). Alternatively, they may be intrusive counterparts of the younger potassic lavas of the Central Chain of the New Hebrides Island Arc.

Table 4. Pore-fluid chemistry, Site 833.

Core, section, interval (cm)	Depth (mbsf)	pH	Salinity (%)	Sodium (mM)	Chloride (mM)	Potassium (mM)	Magnesium (mM)	Calcium (mM)	Sulfate (mM)	Alkalinity (mM)	Phosphate (μ M)	Ammonia (μ M)	Silica (μ M)
134-833A-													
1H-3, 145-150	4.5	8.0	34.0	568	488	12.0	39.7	4.3	8.4	14.0	51.3	651	404
3H-3, 145-150	23.5	7.8	35.0	596	506	11.7	35.5	2.6	0.0	19.9	55.2	1645	391
6H-1, 145-150	40.7	8.1	35.0	603	503	11.9	34.3	3.0	0.6	16.9	41.1	1794	307
8H-1, 145-150	55.5	8.0	36.0	613	507	12.1	31.8	3.0	0.0	14.4	30.0	1596	399
10H-4, 145-150	68.9		36.0	617	508	12.2	29.8	3.5	0.0		20.8	1690	366
13H-1, 145-150	79.5	8.1	36.0	620	518	14.2	29.1	4.8	0.7	8.8	18.8	1491	319
16H-2, 140-150	95.6	8.2	36.3	636	533	14.9	24.1	7.4	1.1	2.7	3.3	1600	307
21X-2, 140-150	144.9	8.2	40.0	688	512	12.9	25.9	15.6	3.3	1.1	1.9	1466	292
23X-2, 0-10	162.8	7.8	41.0	702	534	14.6	35.0	22.1	5.1	1.6	1.9	1273	370
26X-1, 92-102	191.2	7.9	44.0	726	521	14.2	35.5	43.1	7.2	0.9	1.9	1223	378
134-833B-													
5R-2, 90-101	118.2	8.0	37.8	660	522	14.7	21.3	14.9	2.4	1.0	0.8	1364	310
16R-1, 140-150	223.5	7.8	46.3	761	500	12.6	35.1	88.7	10.3	0.5	0.6	855	464
18R-1, 141-150	242.3	7.8	48.0	771	485	11.7	31.7	109.6	11.9	0.4	0.4	741	443
20R-1, 140-150	261.4	7.6	50.0	830	483	10.7	30.7	135.7	12.3	0.1	0.4	667	498
22R-2, 0-10	280.8	7.9	58.2	884	419	8.5	11.5	227.9	14.6	0.3	0.4	469	334
25R-1, 95-105	309.2	8.0	65.0	956	329	5.2	1.6	316.7	14.4	0.4	12.0	231	387
27R-1, 136-150	328.9	8.0	70.0	1014	284	3.2	0.7	373.5	13.1	0.3	0.6	43	378
29R-1, 117-131	348.1	8.4	72.0	1042	237	3.6	0.0	399.5	13.9	0.5	0.4	48	414
31R-2, 135-150	369.1	8.0	72.0	1015	242	2.5	0.0	389.0	13.3	0.3	0.6	48	382
33R-1, 112-125	386.3	8.5	69.5	988	228	1.5	0.0	381.0	12.2	0.4	0.4	0	85
38R-4, 135-150	439.3		81.5	1131	187	0.7		491.6	12.7				
46R-3, 135-150	494.5	8.6	88.3	1241	197	0.7	0.0	548.5	12.0	0.5	0.4	0	160
55R-4, 10-30	583.8		71.0	960	163	0.4		407.6	10.4				
60R-5, 0-18	631.4		65.0	908	150	0.8		385.2	5.4				
63R-2, 0-15	656.4	8.0	60.0	851	166	1.3	8.1	349.4	6.2	0.2	0.4	0	173
66R-4, 0-15	688.3		59.0	828	168	0.8	4.4	336.9	5.6		0.4	0	137
69R-2, 0-15	713.7		57.0	805	186	0.7		299.3	6.0				
74R-2, 130-150	763.6		57.5	719	276	1.3		213.3	7.3				130

Note: Values in bold type were measured by atomic absorption spectroscopy.

SEDIMENT AND FLUID GEOCHEMISTRY

The objectives for measuring pore-fluid chemistry at Site 833 were similar to the objectives for Site 832: to quantify the extent of diagenetic reactions in volcanogenic sediments and to determine if the pore-fluid chemistry is affected by flow of meteoric water from the surrounding islands. Large changes in solute concentrations were observed at Site 832 and thus solute concentrations were measured at Site 833 in order to determine if such diagenesis is common throughout the Aoba Basin. As at Site 832, an additional geochemical objective was to quantify the volume of organic matter buried with the sediment in order to assess the hydrocarbon potential of the basin.

Results

A total of 28 fluid samples were collected from whole-round sections of cores at the two holes drilled at Site 833 (Table 4). Seven samples were obtained with the APC and three samples were obtained with the XCB at Hole 833A; the remaining samples were collected by RCB at Hole 833B. As usual, the parts of the samples that had been contaminated with drilling mud were removed prior to squeezing (see "Explanatory Notes" chapter, this volume). The degree of contamination is difficult to determine. Although sulfate concentrations increase in the deepest samples, other solute concentrations indicate that this sulfate is not the result of contamination. One sample (Table 5) was soft and friable and exhibited a chemical composition that indicates it was contaminated by the drilling fluid. Its chemistry is thus not reported in Table 4. Five other samples yielded no fluid (Table 5) although they were squeezed for several hours. These samples were hard, well cemented, and of low porosity.

Samples were spaced approximately 20 m apart, except within hard, well-lithified units and through zones with limited core recovery. Such units occur between ~390 and 630 mbsf and thus only three fluid samples were obtained between these depths. The deepest sample of fluid was taken from rocks located at 763.6 mbsf; another sample was at depth of 896.1 mbsf but squeezing yielded no fluid (Table 5). This dry sample was taken in order to test whether water is trapped during compaction of sediments below the sills at that depth (see "Lithostratigraphy" section, this chapter).

Chloride and Salinity

The chloride concentration and salinity gradients exhibit similar profiles (Fig. 28). Both constituents increase to maxima at 494.5 mbsf; the chloride concentration reaches a value of 1241 mM (~2.2 times seawater concentrations) and the salinity reaches a value of 88.3‰. The profiles are smooth except for two minor perturbations, one at 242.3 mbsf, below which the concentration gradients are slightly steeper, and the other at 348.1 mbsf, where the gradients exhibit slight max-

Table 5. Samples collected but not analyzed, Site 833.

Core, section, interval (cm)	Depth (mbsf)	Problem
134-833B-		
14R-3, 140-150	207.2	Contaminated
36R-3, 0-15	417.5	No fluid
52R-6, 0-18	555.7	No fluid
58R-1, 123-143	607.9	No fluid
76R-4, 120-137	785.2	No fluid
89R-1, 130-150	896.1	No fluid

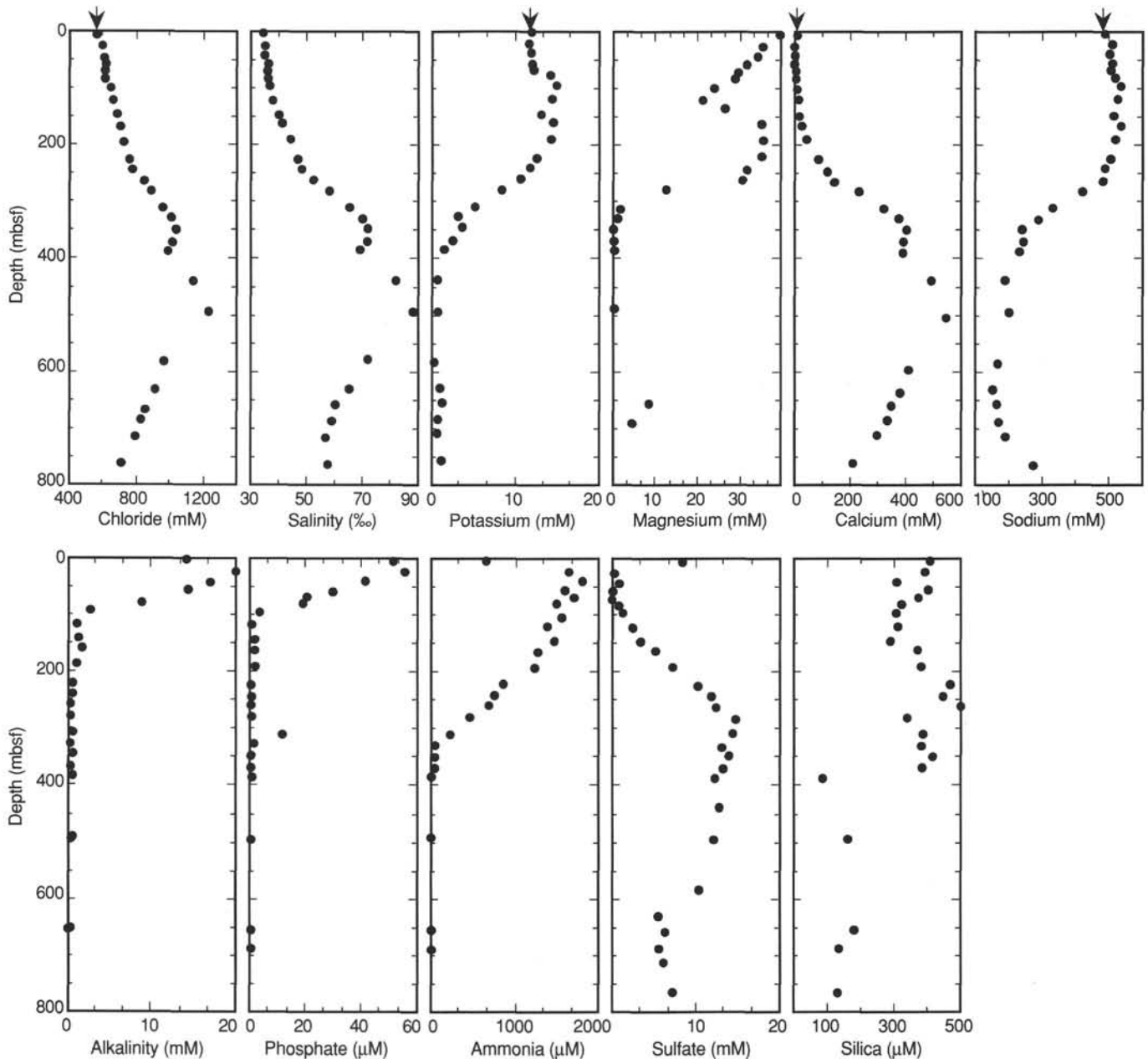


Figure 28. Pore-fluid gradients, Site 833. The arrows indicate seawater concentrations.

ima. Both the chloride concentration and salinity decrease with depth below the maxima at 494.5 mbsf.

Sodium, Potassium, Calcium, and Magnesium

The concentration gradients of sodium, potassium, calcium and magnesium differ above and below ~200 mbsf (Fig. 28). Above this depth, the magnesium concentration exhibits a sharp minimum of 21.3 mM at 118.2 mbsf (Fig. 29). The sodium and potassium concentrations are variable between the sediment-water interface and ~200 mbsf but both concentrations increase steeply at 79.5 mbsf. The calcium concentration decreases to a minimum of 2.6 mM at 23.5 mbsf and then increases rapidly to 43.1 mM at 191.2 mbsf.

Below ~200 mbsf, however, the concentrations differ greatly from seawater values. The sodium concentration decreases to 150 mM (~30% of seawater concentration) at 631.4

mbsf, the potassium concentration decreases to 0.41 mM (~4% of seawater concentration) at 583.8 mbsf, the calcium concentration increases to an extraordinarily high value of 548.5 mM (~52 times seawater concentration) at 494.5 mbsf, and no measurable magnesium exists in the samples between 348.1 and 494.5 mbsf. Although the depths of these maxima and minima do not correlate precisely, all but the deepest (631.4 mbsf) correspond to the location of a volcanic sandstone and sed-lithic breccia (see "Lithostratigraphy" section, this chapter, and Core Description Forms near the back of this volume). Below the extreme values, each concentration exhibits unique characteristics. The potassium concentration remains low to the deepest sample, whereas the calcium concentration decreases sharply and the sodium concentration increases slightly. Several samples were not measured for their magnesium concentration because of the large fluid

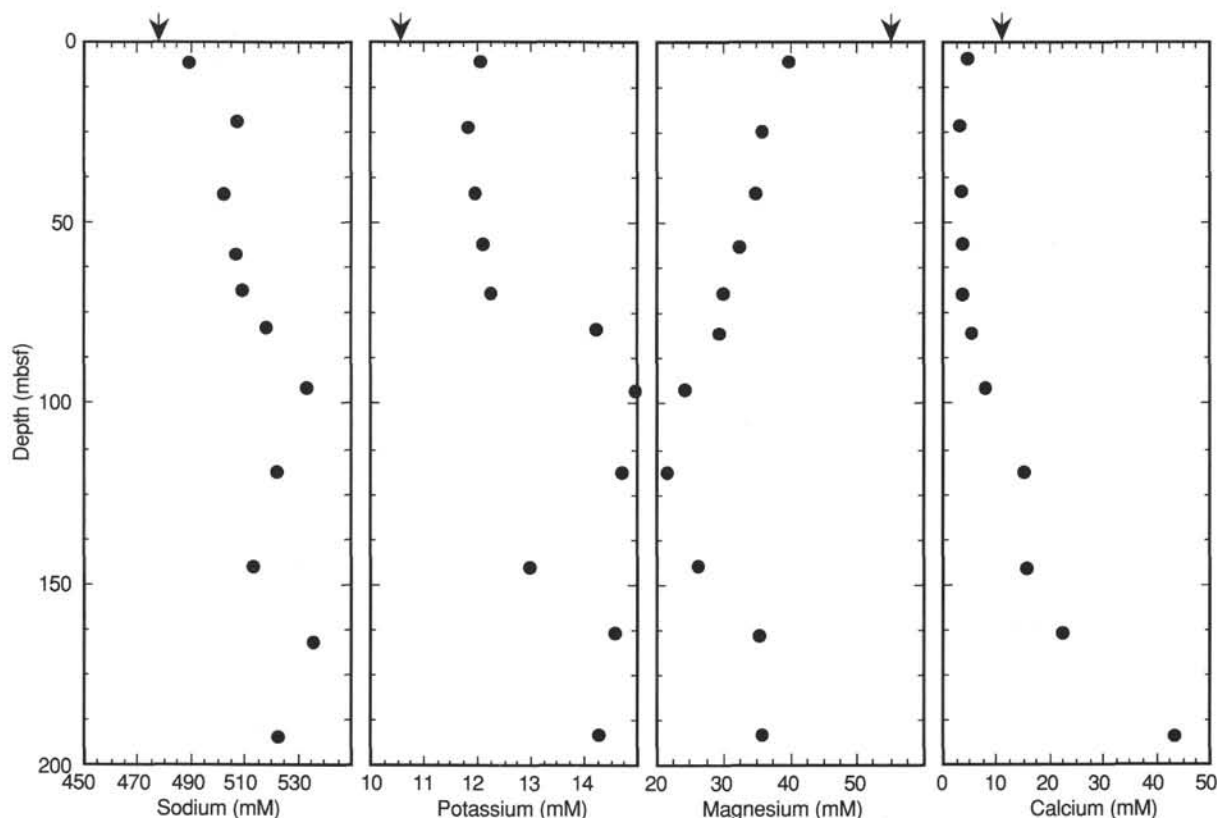


Figure 29. Sodium, potassium, magnesium, and calcium concentrations in samples between 0 and 200 mbsf plotted vs. depth. The arrows indicate seawater concentrations.

volumes needed for the analysis (Gieskes and Gamo, in press), but the two deepest samples contain small but measurable concentrations of magnesium.

Alkalinity, Phosphate, Ammonia, Sulfate, Methane, and Silica

The profiles of alkalinity, phosphate, ammonia, and methane exhibit shallow maxima between 23 and 40 mbsf (Figs. 28 and 30). The alkalinity, phosphate, and methane concentrations decrease to near-zero values at ~100 mbsf, but the ammonia concentration continues to decrease until ~300 mbsf. The concentration maxima of these solutes are lower than those observed at Site 832 and occur at a shallower depth. The concentrations of the sample closest to the sediment-water interface is greater than those measured in comparable samples at Site 832. These observations suggest that the sediment-water interface may not have been recovered at this site.

The shallowest sample contains only 8.4 mM sulfate; sulfate is completely reduced by 23.5 mbsf (Fig. 28). These low sulfate concentrations support the belief that the sediment-water interface may not have been sampled. The sulfate concentration remains low until 95.6 mbsf, below which it increases steeply to a maximum of 14.6 mM at 280.8 mbsf.

The silica concentration is variable throughout the site, but is significantly higher above 369.1 mbsf (292 to 498 μM) than below (85 to 173 μM). The silica concentration does not correlate to extreme concentrations of any other solute, but the depths that exhibit lower concentration values correspond to the volcanic sandstone and sed-lithic unit.

Sediment Carbon Contents

All of the carbon data are reported in Table 6. The CaCO_3 contents are plotted against depth in the "Lithostratigraphy"

section (this chapter) and the organic carbon contents are plotted vs. depth in Figure 31. Every sample measured contains <0.5% organic carbon.

Discussion

Similar to the results from Site 832, the principal control of the solute concentrations at Site 833 appears to be diagenetic reaction. The types of reactions may be the same at the two sites—in particular, the bacterially mediated diagenesis of organic matter (e.g., Claypool and Kaplan, 1974) and the diagenesis of volcanogenic material (e.g., Gieskes, 1981; Lawrence and Gieskes, 1981). The extent of alteration, however, differs between the two sites: pore-water analyses indicate less diagenesis of organic matter and more diagenesis of volcanogenic material at Site 833 than at Site 832. The concentration of sedimentary organic carbon is not significantly lower at Site 833 (Fig. 31). The lower alkalinity and lower concentrations of phosphate, ammonia, and methane therefore might result from greater diffusional loss of the regenerated solutes because of lower sediment accumulation rates at Site 833.

The concentration of calcium in samples taken from sub-bottom depths shallower than 100 mbsf, which is consistent with the precipitation of authigenic carbonate or phosphate minerals, as observed at shallow depths at Site 832. No such authigenic minerals were observed in the shallow cores from Site 833, however, which suggests that little mineralization is taking place. The calcium concentration minimum is slightly greater than at Site 832, implying that less mineralization may occur at Site 833, possibly because of the lower alkalinity and phosphate concentrations. The magnesium concentration is much lower at Site 833; diagenesis of the ash layers may have decreased the magnesium concentration. This diagenesis

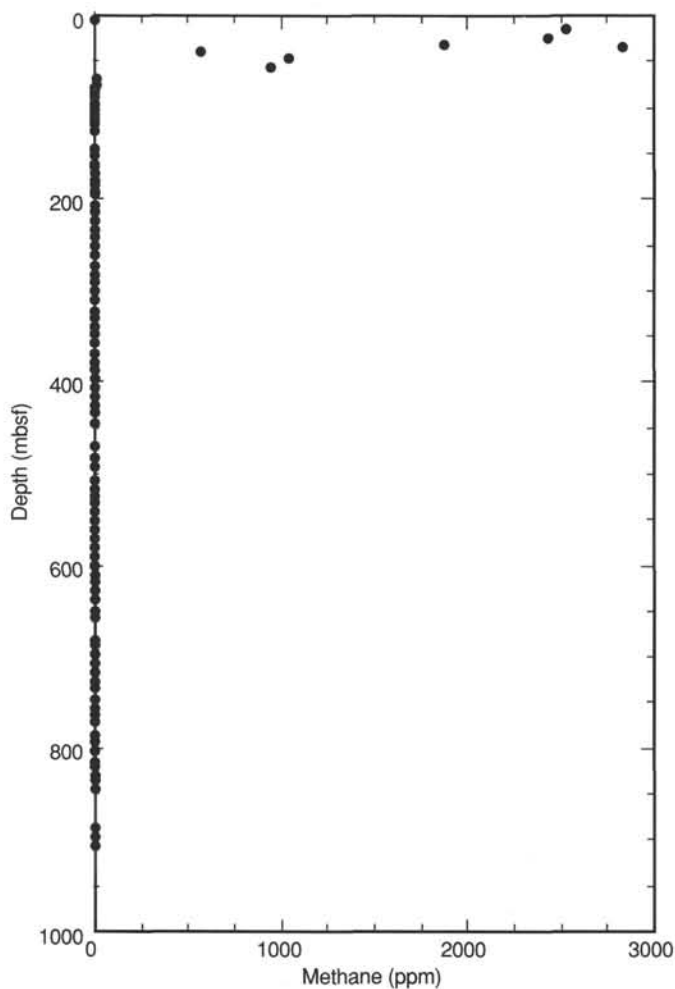


Figure 30. Methane concentrations in the headspace samples.

would provide a source of calcium to the pore fluids and would keep the concentration higher than at Site 832 regardless of the carbonate or phosphate mineralization.

Diagenesis of volcanogenic material apparently causes the greatest changes in the solute concentrations on the basis of the correspondence between the depth of the volcanic sandstone/sed-lithic breccia and the extreme maximum and minimum values of calcium, sodium, potassium, and chloride concentrations (Fig. 28). The volcanic sandstone and sed-lithic breccia are well cemented, apparently with a zeolite cement (see "Lithostratigraphy" section, this chapter), which presumably is the sink for the sodium and potassium. The chloride concentration may increase because of incorporation of water into the hydrated zeolite minerals, although this process would require ~55% of the available pore water to be removed by mineralization in order to increase the chloride concentrations to 2.2 times seawater concentrations.

If significant volumes of water are removed through mineralization, other solute concentrations, in addition to chloride, will also increase. This process must account in part for the high calcium values. Removal of 55% of available water will increase calcium concentrations to only 23.1 mM, assuming that the original fluid contained seawater calcium concentrations. The observed maximum calcium concentration of 548.5 mM (Table 4), however, implies that large amounts of calcium are introduced into the pore fluids, possibly from leaching from the volcanogenic material. A similar process

was proposed for Site 832 but the maximum calcium concentration is ~2 times greater at Site 833 than at Site 832.

Summary

Pore-fluid composition appears to be controlled primarily by diagenetic reactions at Site 833—in particular, by the alteration of volcanogenic material, diagenesis of organic matter, and precipitation of authigenic carbonate and phosphate minerals. The pore-fluid chemistry reflects the low organic carbon contents of the Pliocene to Pleistocene sediment in the Aoba Basin. This sediment probably contains insufficient organic matter to be important for hydrocarbon source material, but the carbon content of the older sediments has not yet been evaluated. Perhaps the most significant finding at Site 833 is the recognition of the extreme diagenetic alteration of volcanogenic material, a result of the large volume of volcanic sediments that have collected in the Aoba Basin and have been undiluted by other solid phases, such as organic sediments (organic matter and diatom tests) as observed in Peru forearc sediments (Suess, von Huene, et al., 1988), or the continental detritus contained in the Barbados forearc sediments (Masclé, Moore, et al., 1988).

STRUCTURAL STUDIES

Deformational structures observed at Site 833 result from small- to large-scale slumping, normal microfaulting, and strike-slip to reverse faulting. In comparison with Site 832, Site 833 is characterized by few large slumps and by the presence of strike-slip and reverse faulting. Structural features observed in Hole 833B (77–1001 mbsf) are illustrated in Figure 32. Attitude of the bedding planes and distribution of deformational structure types allow us to distinguish four structural units (A through D) that are described below from the top to the base of the hole. Boundaries between these structural units are poorly defined because they are never outlined by tectonic features. These structural units correspond to lithostratigraphic units (see "Lithostratigraphy" section, this chapter).

Structural Unit A ranges from 0 to about 376 mbsf (from the top of Core 134-833A-1H to the top of Core 134-833B-32R). Lithologically, it includes volcanic silts and ash layers of lithostratigraphic Unit I and calcareous siltstones and claystones of lithostratigraphic Unit II. Structural Unit A is primarily characterized by horizontal to flat-dipping bedding surfaces and few deformational structures. However, almost vertical or steeply inclined beds bounded above and below by subhorizontal layers at 34 mbsf (the interval from Sections 134-833A-5H-2, 120 cm, to 134-833A-5H-3, 45 cm) and several horizons between 250 and 300 mbsf (from the top of Core 134-833B-19R to the bottom of Core 134-833B-24R) are interpreted as slump-induced (Fig. 33). Thin horizons of folded layers result from convoluted bedding. Arrays of vertical tension gashes were observed near 160 mbsf in the upper part of Unit A (intervals 134-833B-9R-2, 55–60 cm, and 134-833B-10R-1, 134–140 cm). Steeply dipping or vertical microfaults with small normal displacement (a few millimeters to 1 cm) are noted at 254 mbsf (interval 134-833B-19R-3, 90–100 cm), 282 mbsf (interval 134-833B-22R-2, 90–95 cm). Abundant normal microfaulting occurs at the base of this unit (Core 134-833B-31R). Reverse microfaults associated with left-lateral strike-slip motion were also observed in this core (interval 134-833B-31R-3, 80–85 cm). From 203 to 207 mbsf a zone of highly tectonically altered(?) siltstones with slightly inclined scaly fabric occurs, probably indicating a zone of tectonic movement at this level.

Structural Unit B ranges from 376 to 616 mbsf (from the top of Core 134-833B-32R to the top of Core 134-833B-59R). This

unit mainly corresponds to lithostratigraphic Unit III, which consists of black volcanic sandstone and fine basaltic breccia. Bedding is often difficult to observe in this unit, which is also characterized by few structural features. Several horizons between 570 and 615 mbsf (from the top of Core 134-833B-54R to the bottom of Core 134-833B-58R), where the bedding attitude varies frequently, are interpreted to be the result of slumping. Normal faults, sometimes occurring as conjugated pairs, have been observed from 550 to 590 mbsf. The faults in interval 134-833B-55R-1, 60–70 cm (Fig. 34), can be divided into two conjugate sets: one set dips steeply (80° to vertical) and shows dip-slip motion whereas the other set dips gently (30° – 45°), showing a normal sense of movement. When bedding is restored to horizontal, both sets of faults represent a normal displacement and dip steeply in the opposite direction. These structures indicate that the siltstones of structural Unit B were affected by normal faulting prior to tilting.

Structural Unit C ranges from 616 to 830 mbsf (from the top of Core 134-833B-59R to Section 134-833B-81R-2, 80 cm). It corresponds to lithostratigraphic Unit IV, which consists of black volcanic sandstones and siltstones interbedded with calcareous fine siltstones and claystones. The bedding planes dip more or less constantly at 10° to 20° except where local slumps occur. This structural unit is characterized by frequent vein structures (Figs. 35 and 36) and abundant normal faults with very well-developed slickensides and calcite fibers (Fig. 37). Normal faults are most abundant between 635 and 700 mbsf and between 760 and 785 mbsf (Fig. 32). The sense of motion could be determined on almost every fault plane. In addition to these normal faults, some left-lateral strike-slip faults occur (Fig. 36; intervals 134-833B-65R-5, 27–36 cm, 134-833B-74R-2, 60–75 cm, 134-833B-75R-2, 85–100, and 134-833B-80R-2, 20–30 cm). These faults often overprint the older normal faults with steeply inclined slickensides.

Structural Unit D ranges from 830 to 1001 mbsf (from Section 134-833B-81R-2, 80 cm, to the bottom of Hole 833B) and corresponds to lithostratigraphic Unit V, which is composed of basaltic sills interstratified with layers of sedimentary rocks. In this unit, bedding planes are observed only in the two intervals of calcareous volcanic siltstones interstratified with the lavas (from Sections 134-833B-88R-1, 0 cm, to 134-833B-90R-4, 110 cm, and from Sections 134-833B-93R-2, 0 cm, to 134-833B-94R-2, 90 cm). Bedding dips 10° to 30° . This unit is characterized by the occurrence of several reverse and strike-slip faults (Fig. 32). Slickensides can be observed on fault planes that cross-cut the lava. Mostly the reverse component of the sense of motion is associated with a strike-slip component. When the sense of motion along strike-slip faults can be determined unequivocally, it is left-lateral.

PALEOMAGNETISM

The natural remanent magnetization (NRM) and the magnetization after AF demagnetization using a peak-field intensity of 10 mT were measured in all undisturbed archive halves of APC and RCB cores at 5-cm intervals using the cryogenic magnetometer. A pilot set of 133 discrete samples (19 samples from Hole 833A and 113 samples from Hole 833B) was progressively demagnetized using the Schonstedt AF demagnetizer and measured with the Molspin spinner magnetometer. Magnetic susceptibility of all cores from Holes 833A and 833B was measured on the multisensor track at 2.5-cm intervals prior to splitting. Cores 134-833A-2H to -14H were oriented using the multishot orientation technique.

Paleomagnetic Results at Hole 833A

Like their counterparts at Site 832, sediments recovered at Hole 833A are interbedded un lithified volcanic ashes and

sandy to clayey volcanic silts (lithostratigraphic Unit I). Remanent magnetizations in Cores 134-833A-1H to -8H (0 to 58.1 mbsf), after AF demagnetization of archive halves to 10 mT, are of normal polarity (Fig. 38) consistent with deposition during the Brunhes Chron. The observed scatter in inclination and declination is best explained by incomplete removal of a strong drilling-induced component of magnetization and by drilling disturbance. Intensities of remanent magnetization of Pleistocene sediments after demagnetization at 10 mT are about 0.1 to 0.3 A/m, very similar to intensities of the Pleistocene sediments observed at Site 832. Characteristic magnetizations of discrete samples of the Pleistocene sediments (Fig. 39) were easily identified from the orthogonal demagnetization diagrams and the secondary magnetization is generally removed by demagnetization at 20 mT. Sediments were disturbed and recovery rate was poor from 58.1 to 199.5 mbsf (Cores 134-833A-9H to -26X), but the inclinations of discrete samples from these cores show no evidence for reversed polarity, suggesting that these sediments were deposited within the Brunhes Chron.

Paleomagnetic Results at Hole 833B

Five lithostratigraphic units have been described at Site 833 (see "Lithostratigraphy" section, this chapter). Paleomagnetic results will be discussed according to lithostratigraphic units.

Paleomagnetic data after demagnetization at 10 mT from 77.4 to 375.8 mbsf (Cores 134-833B-1R through -31R, lithostratigraphic Unit II) are summarized in Figure 40. The inclinations of Cores 134-833B-1R to -13R are all negative, indicating normal polarity from 77.4 to about 202.8 mbsf. Several intervals of positive inclination are found below a depth of 210 mbsf (from Core 134-833B-15R through -31R). Progressive AF demagnetization of discrete samples from this interval clearly demonstrates that both polarities are recorded in Unit II (Fig. 41). The change in the sign of the inclination at about 212 mbsf (between Core 134-833B-14R and -15R) is tentatively interpreted as the transition from the Brunhes to the Matuyama Chron.

Lithostratigraphic Unit III (Cores 134-833B-32R to -54R, 375.8–577.7 mbsf) is mostly composed of volcanic sandstone. The inclination observed after demagnetization of the archive half sections at 10 mT is predominantly negative (Fig. 42). Lithostratigraphic Unit IV (Cores 134-833B-55R to -81R, 577.7–834.0 mbsf) is composed of interbedded calcareous silty claystone, sandy volcanic siltstone, volcanic sandstone, and mixed sedimentary rocks. Negative inclinations were observed in archive-half sections from the upper part of Unit IV down to about 660.8 mbsf (Core 134-833B-63R), where there is evidence for a reversed polarity (Fig. 43). AF demagnetization of 54 discrete samples from these cores displayed quite different magnetic behavior from that of the overlying units. In many of the discrete samples analyzed (demagnetized in peak fields up to 100 mT), secondary viscous components are removed, and stable characteristic magnetizations that indicate either normal or reversed polarity are isolated (Fig. 44). In other samples, however, stepwise AF demagnetization reveals complicated demagnetization behavior (Fig. 45). As shown in Figure 45, the demagnetization diagrams from some samples curve and miss the origin of the vector plots, indicating incomplete removal of secondary components. This behavior may result from postdepositional disturbances such as slumping, sliding, bioturbation, or compaction.

The stratigraphically lowest unit, lithostratigraphic Unit V (Cores 134-833B-82R to -99R, 834.0–1001.1 mbsf), consists of fine-grained siltstone, claystone, and interbedded basaltic

Table 6. Sediment carbon contents, Site 833.

Core, section, interval (cm)	Depth (mbsf)	Total carbon (wt%)	Inorganic carbon (wt%)	TOC (wt%)	CaCO ₃ (wt%)
134-833A-					
1H-2, 130-133	2.8		2.54		21.2
1H-4, 130-133	5.8	1.59	1.37	0.22	11.4
1H-6, 130-133	8.8		2.07		17.2
2H-2, 110-113	12.1		0.98		8.2
2H-4, 110-113	15.1	1.60	1.37	0.23	11.4
2H-6, 110-113	18.1		1.98		16.5
3H-2, 87-88	21.4		0.26		2.2
3H-4, 77-87	24.3	1.81	1.69	0.12	14.1
3H-6, 7-8	26.6		0.41		3.4
4H-2, 81-82	30.8	0.47	0.39	0.08	3.2
5H-1, 20-23	32.8		1.00		8.3
5H-2, 20-23	34.3	0.52	0.38	0.14	3.2
5H-5, 27-30	38.9		0.12		1.0
6H-1, 108-111	40.3		1.22		10.2
6H-4, 107-110	44.8	0.29	0.23	0.06	1.9
7H-2, 96-98	47.7		1.15		9.6
7H-4, 45-47	50.2	0.88	0.78	0.10	6.5
8H-1, 130-133	55.3		0.58		4.8
8H-3, 87-90	57.8	0.41	0.34	0.07	2.8
9H-3, 80-83	61.9		0.24		2.0
10H-1, 117-120	64.1		1.31		10.9
10H-4, 140-143	68.8	0.34	0.30	0.04	2.5
11H-2, 72-75	71.9	0.28	0.24	0.04	2.0
11H-5, 10-13	75.8		0.02		0.2
12H-1, 43-44	76.4	0.57	0.37	0.20	3.1
13H-1, 132-135	79.3		0.13		1.1
13H-3, 90-92	81.9	0.04	0.03	0.01	0.2
15X-CC, 10-13	84.1	0.65	0.41	0.24	3.4
16X-1, 17-20	93.9	3.13	2.78	0.35	23.2
16X-3, 17-20	96.7		1.21		10.1
17X-CC, 5-7	103.4		1.13		9.4
18X-CC, 11-13	113.1	1.58	1.36	0.22	11.3
21X-1, 27-30	142.3	0.90	0.73	0.17	6.1
21X-2, 127-130	144.8		1.08		9.0
22X-CC, 2-4	151.7		0.41		3.4
23X-1, 37-39	161.7	2.71	2.45	0.26	20.4
24X-1, 33-35	171.2	2.23	1.83	0.40	15.2
25X-CC, 43-45	181.0	3.13	2.76	0.37	23.0
26X-2, 42-44	191.7	2.06	1.81	0.25	15.1
134-833B-					
1R-1, 18-21	77.6	0.28	0.21	0.07	1.7
1R-2, 49-52	79.4		1.17		9.7
2R-1, 23-26	87.1		0.28		2.3
2R-3, 35-38	90.3	3.20	2.99	0.21	24.9
3R-1, 23-26	96.8	2.58	2.30	0.28	19.2
4R-1, 9-11	106.3		1.22		10.2
4R-2, 136-138	109.1	0.54			
5R-1, 10-13	115.9		0.48		4.0
5R-3, 1-4	118.3	2.31	2.12	0.19	17.7
6R-1, 9-11	125.6	1.18	1.01	0.17	8.4
7R-CC, 6-8	135.3	1.28	1.13	0.15	9.4
8R-1, 90-92	145.7	1.88	1.71	0.17	14.2
9R-2, 72-74	156.7	2.18	1.81	0.37	15.1
10R-1, 103-105	165.1	0.96	0.87	0.09	7.2
11R-1, 127-128	175.1	1.14	1.02	0.12	8.5
12R-2, 132-134	186.3	2.35	2.18	0.17	18.2
13R-2, 100-103	195.6	2.07	1.90	0.17	15.8
14R-1, 108-110	203.9		1.76		14.7
14R-4, 55-57	207.4	1.74	1.40	0.34	11.7
15R-1, 29-31	212.7	1.52	1.21	0.31	10.1
16R-1, 137-140	223.5		0.97		8.1
16R-3, 47-49	225.6	1.38	1.29	0.09	10.7
17R-1, 40-42	232.1		1.63		13.6
17R-2, 133-135	234.5	0.39	0.35	0.04	2.9
18R-1, 10-13	241.0		0.43		3.6
18R-2, 103-106	243.4	5.25	4.80	0.45	40.0
19R-2, 127-129	253.3		3.01		25.1
19R-4, 125-127	256.3	2.37	1.91	0.46	15.9
20R-1, 137-139	261.4		2.25		18.7
20R-3, 122-124	264.2	2.46	2.24	0.22	18.7
21R-1, 135-138	271.1		3.88		32.3
21R-3, 135-138	274.1		4.28		35.7
22R-2, 84-86	281.6		5.78		48.1
22R-4, 57-59	284.4		4.02		33.5

Table 6 (continued).

Core, section, interval (cm)	Depth (mbsf)	Total carbon (wt%)	Inorganic carbon (wt%)	TOC (wt%)	CaCO ₃ (wt%)
23R-1, 39-42	289.3		4.38		36.5
23R-3, 30-33	292.2	5.03	4.73	0.30	39.4
24R-1, 137-140	300.0	2.49	2.27	0.22	18.9
25R-1, 25-27	308.5		0.12		1.0
25R-3, 26-28	311.0	3.63	3.33	0.30	27.7
26R-2, 76-78	320.2		0.34		2.8
26R-4, 72-74	323.1	4.77	4.39	0.38	36.6
27R-2, 135-137	330.4		0.53		4.4
27R-3, 23-25	330.7	2.68	2.47	0.21	20.6
28R-2, 73-75	339.4	1.43	1.30	0.13	10.8
29R-2, 88-90	349.1	1.61	1.45	0.16	12.1
30R-1, 36-38	356.9	0.88	0.77	0.11	6.4
31R-2, 100-102	368.7	4.12	3.79	0.33	31.6
31R-CC, 7-10	371.4		1.71		14.2
32R-1, 126-128	377.1		4.85		40.4
32R-3, 85-87	379.3	0.50	0.46	0.04	3.8
33R-2, 48-49	387.2	0.64	0.55	0.09	4.6
34R-1, 111-113	396.3		0.13		1.1
34R-2, 111-113	397.8	0.05	0.04	0.01	0.3
35R-2, 125-127	407.7		0.10		0.8
35R-4, 93-95	410.3	0.08	0.06	0.02	0.5
36R-2, 70-73	416.6		0.04		0.3
36R-4, 51-53	419.4	0.04	0.04	0.00	0.3
37R-2, 61-641	426.3	0.50	0.46	0.04	3.8
38R-2, 145-147	436.8		0.45		3.7
38R-4, 130-132	439.6	0.33	0.31	0.02	2.6
38R-6, 140-142	442.7		0.22		1.8
39R-1, 124-127	444.4		0.20		1.7
39R-3, 120-130	447.4		1.81		15.1
39R-5, 130-132	450.4	0.12	0.12	0.00	1.0
45R-2, 86-88	483.5	0.19	0.19	0.00	1.6
46R-1, 124-127	491.5		1.11		9.2
46R-3, 120-123	494.3	2.14	2.01	0.13	16.7
46R-5, 70-73	496.8		0.09		0.7
47R-2, 128-130	502.8		0.06		0.5
47R-4, 38-40	504.8	0.63	0.61	0.02	5.1
47R-7, 20-22	508.6		0.33		2.7
48R-2, 145-148	512.5		0.06		0.5
48R-4, 70-73	514.8	0.06	0.07	0.00	0.6
48R-6, 90-93	518.0		1.01		8.4
49R-2, 131-133	522.1		0.06		0.5
49R-4, 142-145	525.2	0.05	0.06	0.00	0.5
49R-6, 81-83	527.4		0.60		5.0
50R-2, 110-113	531.5		0.22		1.8
50R-4, 100-103	534.4	0.08	0.08	0.00	0.7
51R-2, 133-135	541.4		0.08		0.7
51R-4, 100-102	544.1	0.07	0.07	0.00	0.6
51R-6, 27-29	546.4		0.06		0.5
50R-2, 140-142	551.1	0.07	0.07	0.00	0.6
52R-3, 140-142	552.6		0.08		0.7
52R-5, 140-142	555.6		0.12		1.0
53R-1, 138-140	559.3		0.07		0.6
53R-3, 138-140	562.3	0.07	0.07	0.00	0.6
53R-6, 80-82	566.2		0.08		0.7
54R-2, 132-134	570.6		0.07		0.6
54R-4, 138-140	573.7	0.19	0.18	0.01	1.5
54R-6, 131-133	576.6		0.09		0.7
55R-2, 138-140	580.6		0.25		2.1
55R-4, 140-142	583.6	2.13	1.93	0.20	16.1
56R-1, 142-144	588.8		2.68		22.3
56R-4, 140-142	593.2	0.15	0.13	0.02	1.1
57R-1, 100-102	598.0		0.41		3.4
57R-3, 12-14	600.1	0.16	0.13	0.03	1.1
58R-1, 120-123	607.9		0.06		0.5
58R-3, 129-131	610.9	0.56	0.49	0.07	4.1
58R-5, 68-71	613.1		0.47		3.9
59R-2, 106-108	618.8		0.35		2.9
59R-4, 37-39	621.0	2.11	1.96	0.15	16.3
59R-6, 15-18	623.2		3.09		25.7
60R-2, 115-118	628.3		1.93		16.1
60R-4, 113-116	631.2	3.39	3.15	0.24	26.2
60R-6, 41-44	633.3		0.60		5.0
61R-1, 43-46	636.0		2.63		21.9
61R-3, 117-119	639.6	6.98	6.55	0.43	54.6
61R-5, 127-129	642.5		1.93		16.1
62R-2, 121-124	647.8		4.28		35.7
62R-4, 144-147	650.9	2.20	2.07	0.13	17.2

Table 6 (continued).

Core, section, interval (cm)	Depth (mbsf)	Total carbon (wt%)	Inorganic carbon (wt%)	TOC (wt%)	CaCO ₃ (wt%)
63R-2, 144-146	657.9		0.47		3.9
63R-5, 142-144	662.1		2.42		20.2
64R-1, 140-142	666.0		4.18		34.8
64R-3, 137-139	668.9	0.63	0.57	0.06	4.7
64R-5, 138-140	671.9		1.70		14.2
64R-7, 30-32	673.7		2.56		21.3
65R-1, 56-58	674.8		2.54		21.2
65R-3, 55-57	677.7	0.50	0.46	0.04	3.8
65R-5, 55-57	680.5		1.00		8.3
66R-2, 70-72	686.0		0.16		1.3
66R-4, 97-99	689.3	0.96	0.84	0.12	7.0
66R-6, 97-99	692.1		0.40		3.3
67R-1, 41-43	693.9		3.55		29.6
67R-2, 91-93	695.9	0.56	0.50	0.06	4.2
67R-3, 41-43	696.9		0.25		2.1
67R-5, 41-43	699.9		1.74		14.5
68R-2, 134-136	705.9		1.26		10.5
68R-4, 136-138	709.0	1.17	1.05	0.12	8.7
69R-1, 66-68	713.5		4.84		40.3
69R-3, 61-63	715.8	1.97	1.81	0.16	15.1
69R-5, 63-65	718.8		2.31		19.2
69R-7, 62-64	721.8		2.06		17.2
70R-1, 61-63	723.1		3.41		28.4
70R-3, 71-73	726.2	0.26	0.26	0.00	2.2
70R-6, 43-45	730.4		1.50		12.5
71R-1, 130-131	733.5		3.69		30.7
71R-3, 2-4	735.2	2.17	1.94	0.23	16.2
71R-6, 17-20	739.9		0.95		7.9
72R-1, 140-143	743.3		0.80		6.7
72R-3, 138-141	746.3	1.60	1.45	0.15	12.1
72R-5, 104-107	748.9		0.15		1.2
72R-7, 18-21	751.1		0.49		4.1
73R-2, 120-122	754.2		1.20		10.0
73R-4, 106-108	757.1	1.49	1.37	0.12	11.4
74R-4, 81-83	766.1	2.56	2.33	0.23	19.4
74R-6, 18-21	768.5		6.45		53.7
75R-3, 69-72	774.0	1.95	2.00		16.7
75R-5, 88-90	777.1		3.11		25.9
76R-2, 80-83	782.0		3.67		30.6
76R-4, 96-99	785.2	3.40	3.12	0.28	26.0
76R-7, 55-57	789.1		4.99		41.6
77R-2, 135-138	792.2		2.30		19.2
77R-4, 144-148	795.1	4.72	4.36	0.36	36.3
78R-1, 139-142	800.4		5.87		48.9
78R-3, 145-148	803.4	2.55	2.35	0.20	19.6
79R-2, 14-17	809.1		2.66		22.2
79R-3, 140-143	811.9	5.34	4.94	0.40	41.2
79R-7, 40-43	816.9		7.62		63.5
80R-2, 140-142	821.2		1.50		12.5
80R-4, 140-142	824.0		5.19		43.2
80R-6, 140-142	826.9		5.75		47.9
81R-1, 71-73	828.7		2.99		24.9
81R-3, 59-62	831.5	0.00	0.03		0.2
82R-1, 87-89	834.9		0.04		0.3
82R-3, 31-33	837.3	0.00	0.03		0.2
83R-2, 134-137	846.8	0.00	0.03		0.2
84R-1, 100-103	852.2	0.58	0.53	0.05	4.4
85R-1, 107-110	857.3		0.06		0.5
85R-3, 128-130	860.3	0.03	0.08		0.7
86R-2, 90-93	868.3		0.04		0.3
86R-4, 22-25	870.5	0.03	0.09		0.7
87R-1, 77-80	876.2	0.00	0.05		0.4
88R-1, 27-30	885.5		0.04		0.3
88R-1, 120-130	886.4		1.93		16.1
88R-2, 40-43	887.1	1.05	0.95	0.10	7.9
89R-1, 116-118	896.0		7.00		58.3
89R-3, 140-143	899.1	1.16	1.08	0.08	9.0
89R-5, 30-33	901.0		2.04		17.0
90R-4, 95-98	910.0	3.20	3.09	0.11	25.7
90R-5, 131-133	911.6		0.03		0.2
91R-1, 131-133	915.5		0.02		0.2
91R-4, 120-123	919.7	0.00	0.03	0.00	0.2
93R-4, 70-73	938.0	2.02			
94R-2, 3-6	944.8	5.32			

Note: TOC = total organic carbon.

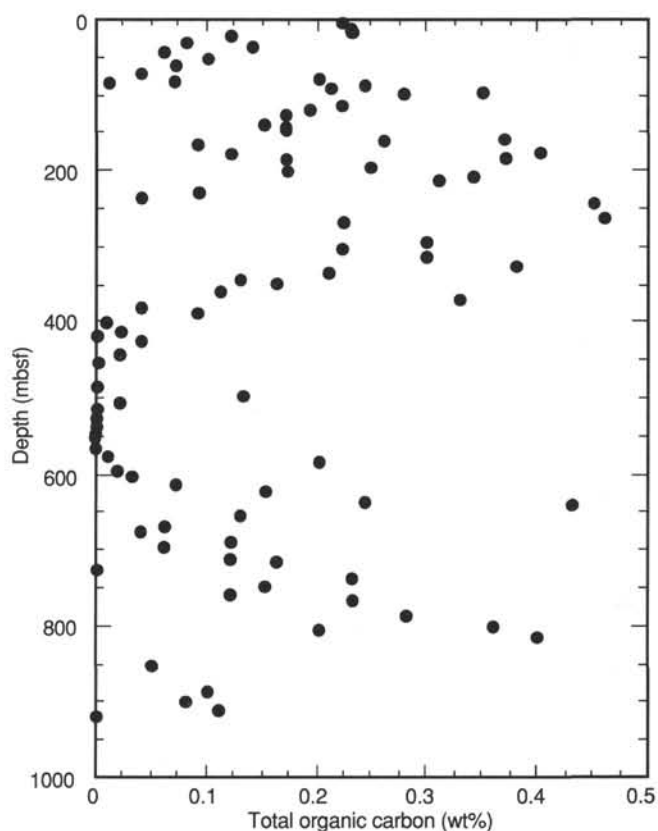


Figure 31. Total organic carbon content of sediments at Site 833 plotted vs. depth.

sills, all of which exhibited complex magnetic behavior. Sediments from Unit V have the same lithology and exhibit magnetic properties similar to those from Unit IV, above the sills. The NRM intensities of the sills are significantly higher than those of the interbedded sediments (up to 100 A/m), as are magnetic susceptibilities (Fig. 46). However, this apparently strong NRM is very soft magnetically, as indicated by the sharp decrease in magnetic intensity during the initial steps of AF demagnetization (Fig. 47A). The median destructive fields (MDFs) for these basaltic sills is generally lower than 10 mT. AF demagnetization of discrete samples from the sills indicates several types of demagnetization behavior. The most unstable samples show evidence of strong secondary overprints characterized by steep negative inclinations that are probably drilling-induced (Fig. 47B). Some samples that are stable during AF demagnetization exhibit shallow positive inclinations whereas other stable samples exhibit shallow negative inclinations.

Magnetostratigraphy

The first polarity reversal was found at a depth of 212 mbsf in Core 134-833B-15R (see Fig. 40). Below this depth to about 375 mbsf, the inclinations of discrete samples from Cores 134-833B-16R to -31R are dominantly positive, thus the interval may correspond to a period of predominantly reversed polarity (Matuyama Chron). Preliminary biostratigraphic evidence suggests that sediments around a depth of about 212 mbsf may be approximately 0.6 m.y. old. Thus, the first magnetic polarity shift from normal to reversed observed between Cores 134-833B-13R and -15R may represent the Brunhes/Matuyama boundary (~0.7 Ma).

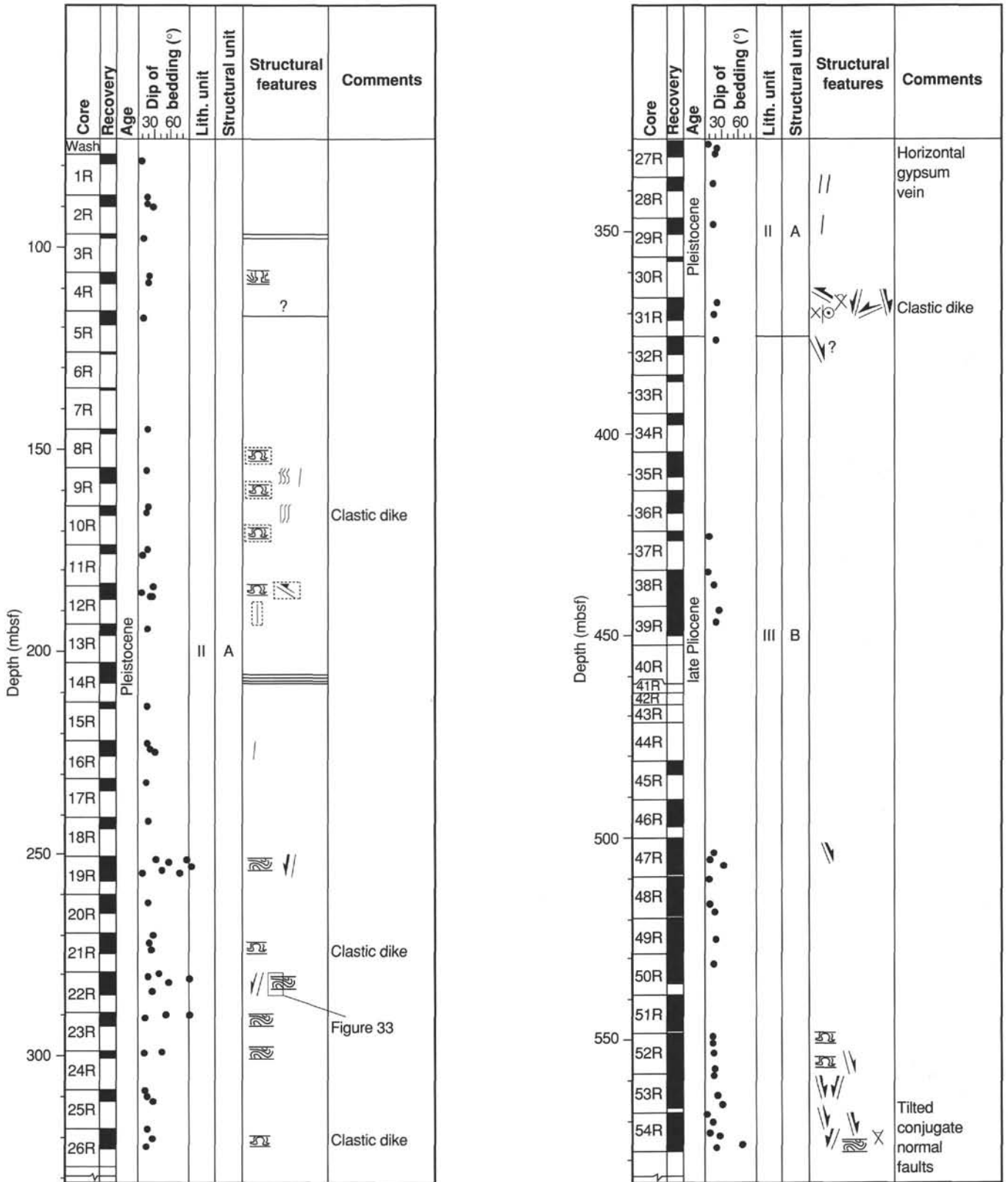


Figure 32. Structural log of Hole 833B. Hole 833A (0–216 mbsf) is not shown; however, structures observed in this hole below 80 mbsf are represented within dashed-line rectangles.

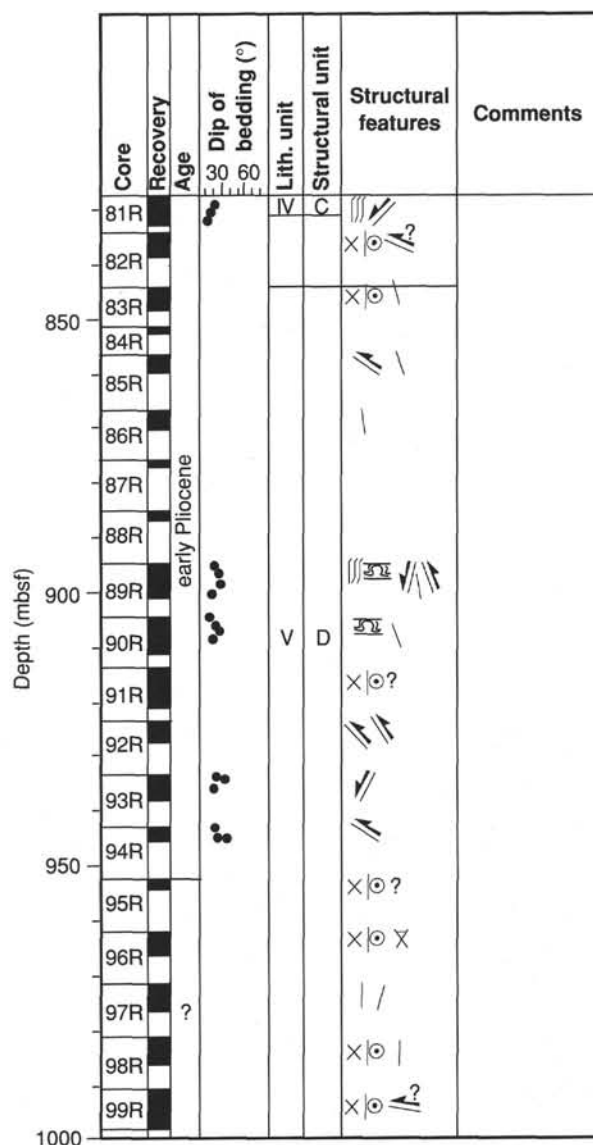
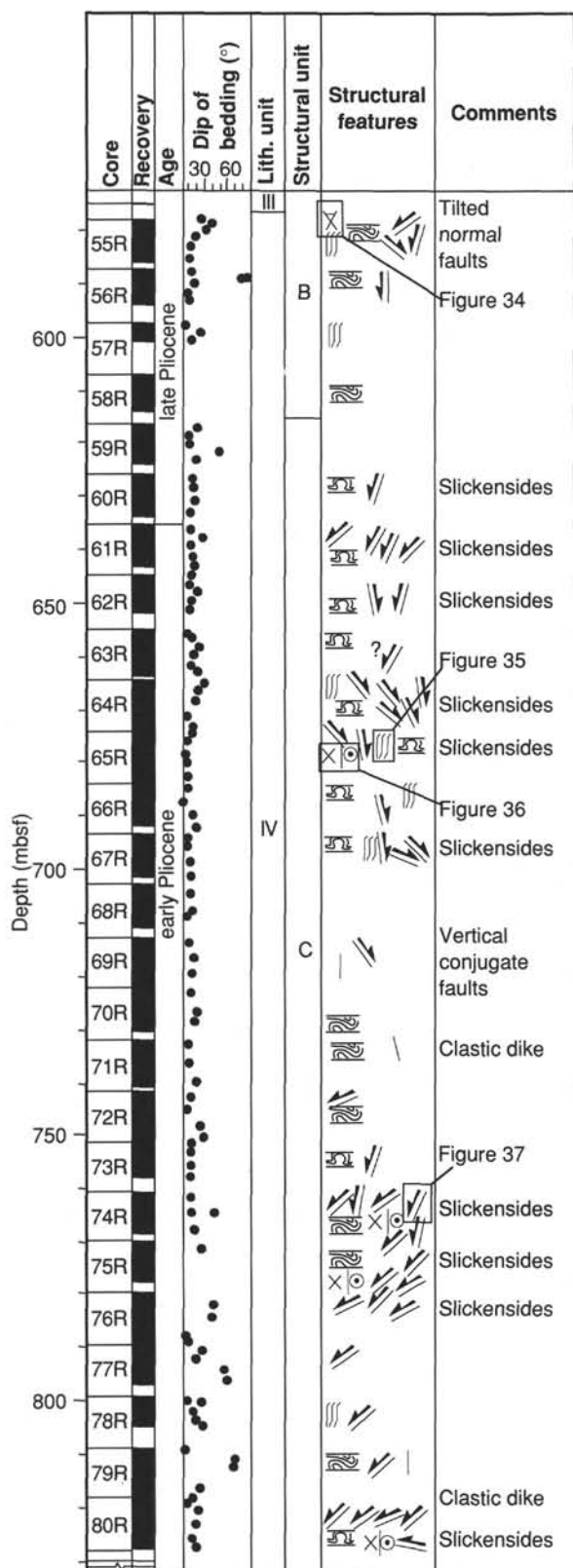


Figure 32 (continued).

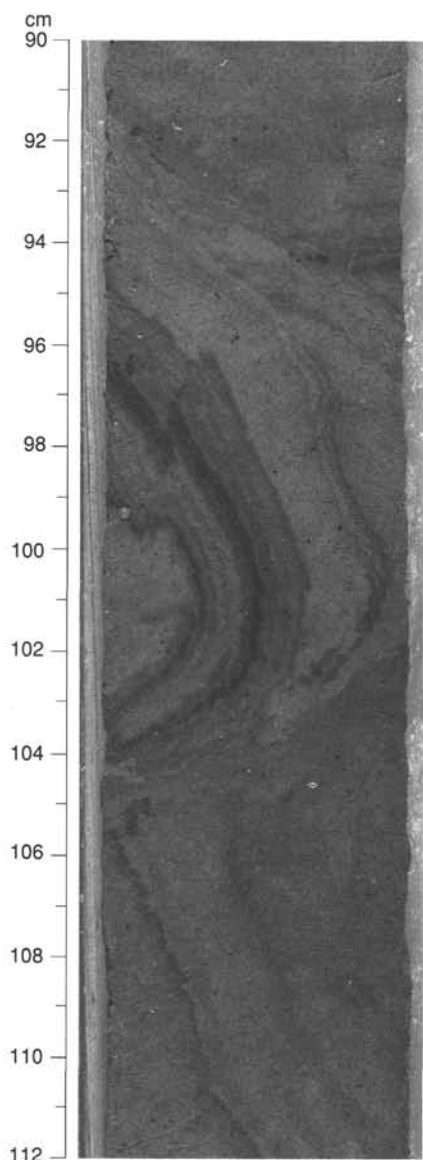


Figure 33. Photograph of a slump fold observed in interval 134-833B-22R-2, 90–112 cm. The location is indicated in Figure 32.

Although both cryogenic magnetometer measurements and preliminary AF demagnetizations of discrete samples suggest that a sequence of polarity reversals is recorded in Hole 833B, more detailed studies of discrete samples may provide a more reliable correlation with the geomagnetic reversal time scale. More accurate biostratigraphic markers are also needed to constrain further interpretation of the paleomagnetic data.

Magnetic Susceptibility

Figure 46 shows the downhole profile of the magnetic susceptibility of sediments and igneous rocks recovered at Site 833. In general, the magnetic susceptibility values correspond well with lithological variations observed in cores recovered from Site 833. Within the top 100 m, the susceptibility of the unlithified volcanic ashes and silt of lithostratigraphic Unit I is relatively high (0.01 to 0.02 SI, with peaks up to 0.04 SI). The magnetic susceptibility of the siltstone and claystone that constitute lithostratigraphic Unit II is generally less than 0.01 SI, whereas that of the volcanic sandstone of

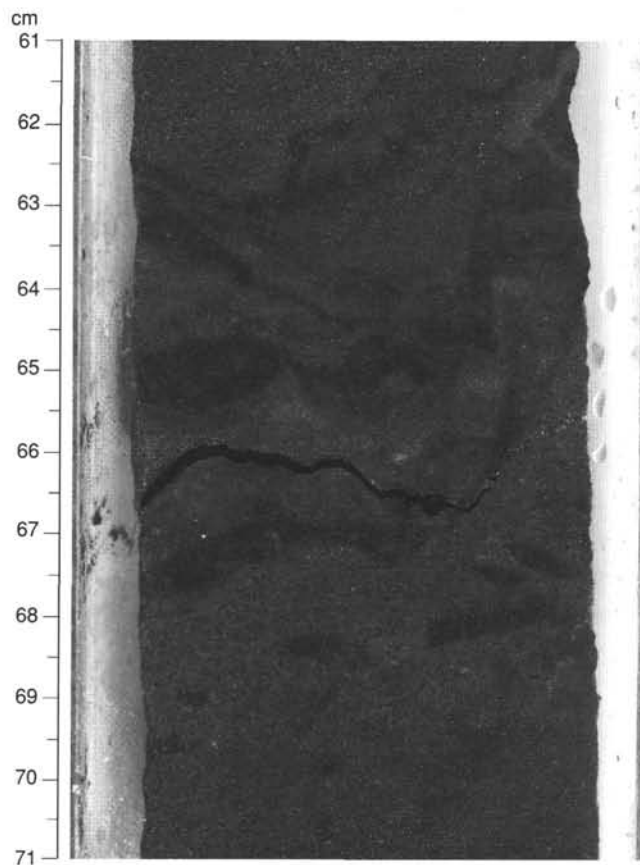


Figure 34. Photograph of tilted conjugate normal faults observed in interval 134-833B-55R-1, 61–71 cm. The location is indicated in Figure 32.

lithostratigraphic Unit III has a mean value between 0.01 and 0.02 SI. From 400 to 430 mbsf and from 550 to 575 mbsf, the basaltic breccia of lithostratigraphic Unit IV is characterized by higher magnetic susceptibilities, typically greater than 0.02 SI. The sedimentary rocks of lithostratigraphic Unit V are easily distinguished by their lower magnetic susceptibilities, typically less than 0.02 SI. Susceptibilities of the interbedded basaltic sills are much higher, up to 0.09 SI, reflecting the fresh condition of the sill and implying the presence of multidomain magnetite.

SEDIMENT ACCUMULATION RATES

Sediment accumulation rates were estimated from an age vs. depth plot for the upper 751.5 mbsf of Holes 833A and 833B (Fig. 48). Rates could not be calculated for the sediments below 751.5 mbsf because of the absence of reliable chronostratigraphic events. The curve is based on four well-defined planktonic foraminiferal chronostratigraphic events (first and last occurrences) as outlined in Table 7. Absolute ages follow the Cenozoic time scale cited in the "Explanatory Notes" chapter (this volume).

The lower Pliocene to Holocene sediment accumulation rates at Site 833 exhibit alternating high and low rates. Sedimentation rates for the early Pliocene (97 m/m.y.) and early Pleistocene (148 m/m.y.) show markedly reduced deposition, compared to exceptionally high accumulation rates during the upper Pliocene interval (313 m/m.y.) and the upper Pleistocene to Holocene (322 m/m.y.) (Fig. 48).

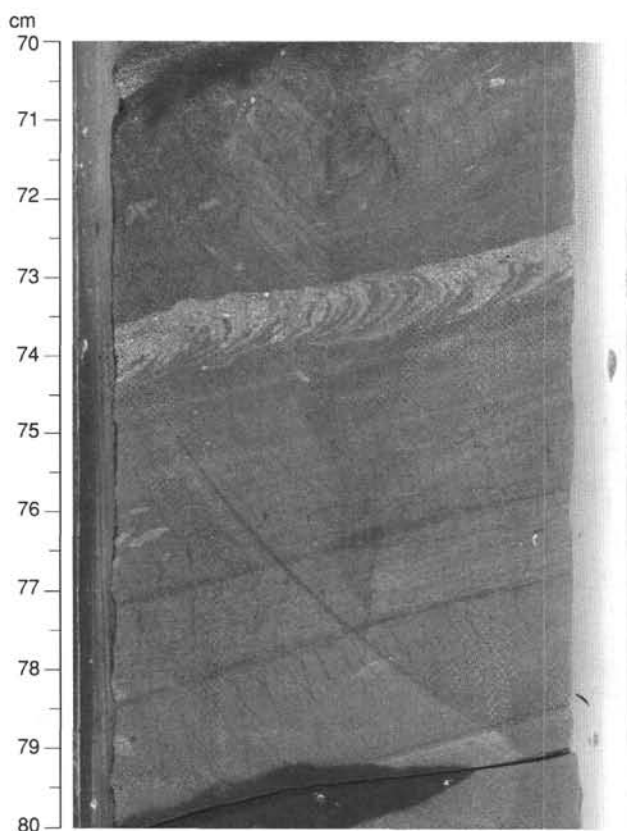


Figure 35. Photograph of an array of sigmoidal tension gashes observed in interval 134-833B-65R-3, 70–80 cm. The location is indicated in Figure 32.

PHYSICAL PROPERTIES

Measurements of index properties, Hamilton Frame sonic velocities, compressional wave (*P*-wave) velocities, and thermal conductivity were completed on sediments and rocks recovered at Site 833. Full APC cores from Hole 833A were measured with the gamma-ray attenuation porosity evaluator (GRAPE) and the *P*-wave logger on the multisensor track. Undrained shear-strength measurements were completed on APC cores from Hole 833A. All measurements were performed in accordance with the procedures described in the "Physical Properties" section of the "Explanatory Notes" chapter (this volume).

Index Properties

The patterns of variation in index properties at Site 833 are more readily understood if they are compared with lithostratigraphy; so, as at previous sites, we will organize our discussion of index properties by lithostratigraphic unit (see "Lithostratigraphy" section, this chapter, for detailed descriptions of the units). Index properties values are listed in Table 8; the variation of index properties as a function of depth below seafloor is illustrated in Figure 49. Bulk density trends often mirror those of porosity and water content; therefore, bulk density and porosity are plotted against depth along with the lithostratigraphic units in Figure 50. A number of special, 2-min GRAPE measurements were performed on lithified cores below 375 mbsf. These data are shown in Figure 51. At Site 833, porosity ranges from 4.5% to 85.2%, water content ranges from 1.6% to 95.0%, and bulk density ranges from 1.57 to 3.16 Mg/m³.

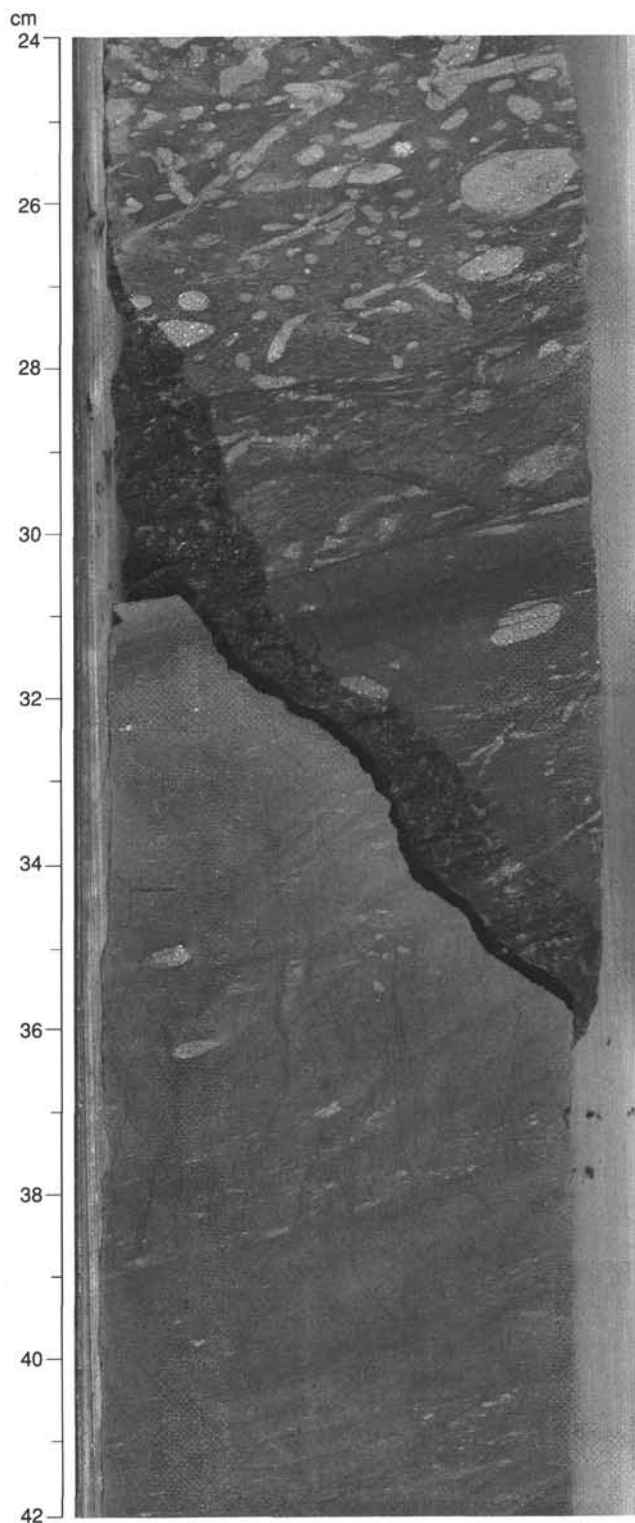


Figure 36. Photograph of an array of sigmoidal tension gashes and a strike-slip fault observed in interval 134-833B-65R-5, 24–42 cm. The location is indicated in Figure 32.

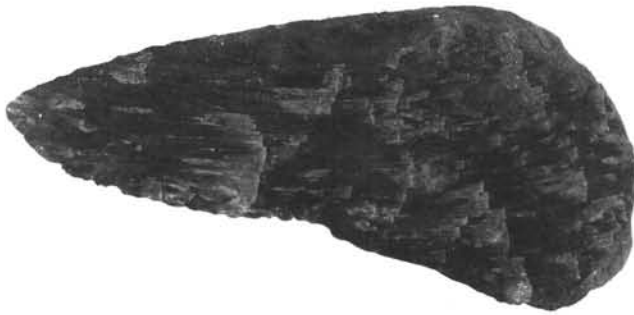


Figure 37. Photograph of a fault surface with slickensides indicating a normal sense of movement along the fault. The structure was observed in interval 134-833B-74R-6, 0–10 cm. The location is indicated in Figure 32.

Lithostratigraphic Unit I (0–84.0 mbsf in Hole 833A) consists of unlithified volcanic silts and clays interbedded with ash layers. In this unit, porosity and water content decrease steadily from values of 68% and 75%, respectively, near the seafloor to a porosity of 55% and a water content of 43% at 84 mbsf. Bulk density increases from 1.62 Mg/m³ at the seafloor to 1.87 Mg/m³ at 84 mbsf (Table 8 and Fig. 49). The lack of variations in index properties suggest a much lesser degree of underconsolidation in the silty volcanic sediments of lithostratigraphic Unit I than in the rapidly deposited sediments at Site 832.

In the mixed sedimentary rocks of lithostratigraphic Unit II (84.0–199.5 mbsf in Hole 833A and 77.4–375.8 mbsf in Hole 833B), porosity ranges 63% at 93.9 mbsf to 46% at 371 mbsf, water content declines from 57% at 93.8 mbsf to 29% at 371 mbsf, and bulk density remains constant between 1.8 Mg/m³ and 2.0 Mg/m³ (Table 8 and Fig. 49).

Pliocene volcanic sandstones and basaltic breccia comprise lithostratigraphic Unit III (375.8–577.8 mbsf in Hole 833B). Porosity and water content decrease sharply from values of 56% and 46%, respectively, at 377 mbsf to a porosity of 34% and a water content of 17% at 379 mbsf. Bulk density increases concomitantly in only 2 m from 1.83 Mg/m³ at 377 mbsf to 2.34 Mg/m³ at 379 mbsf (Table 8; Figs. 49 and 51). The sudden changes in these index properties over only a few meters are correlated with the lithologic change to sandstone and breccia in Unit III.

Lithostratigraphic Unit IV (577.8–830.3 mbsf in Hole 833B) is predominantly foraminiferal sandy volcanic siltstone. In this unit, porosity, water content, and bulk density range from 22% to 85%, 10% to 46%, and 1.92 to 3.12 Mg/m³, respectively. Bulk density decreases from 2.44 Mg/m³ at 576 mbsf to 2.05 Mg/m³ at 815 mbsf (Table 8; Figs. 49 and 51). The variations in these index properties probably result from the variation in lithology between interbedded siltstones, calcareous silty claystones, and mixed sedimentary rocks.

Sills of plagioclase-phyric basalt (see “Igneous Petrology” section, this chapter), interbedded with carbonate-rich volcanic sands, silts, and clays, characterize lithostratigraphic Unit V (830.3–1001.1 mbsf). In the sediment layers, porosity and water content range from 18% to 46% and 8% to 31%, respectively. Bulk density ranges from 2.02 to 2.52 Mg/m³ (Table 8; Figs. 49 and 51). In the basalt, porosity and water content decrease sharply to values of less than 10%, while bulk density generally decreases from 2.90 Mg/m³ at 835 mbsf to 2.68 Mg/m³ at the bottom of the hole (Table 8; Figs. 49 and 51).

Sonic Velocity

Sonic velocities measured in the P-wave logger and the Hamilton Frame from Hole 833A generally agree well with each other (Table 9; Fig. 49). Only Hamilton Frame measure-

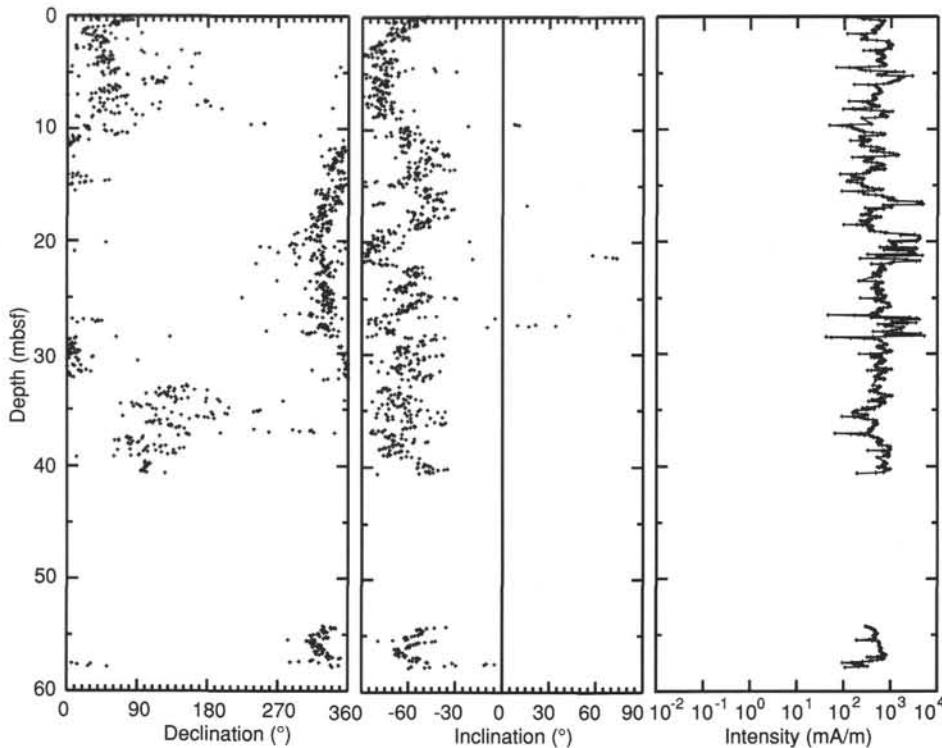


Figure 38. Depth plot of stable magnetization (after AF demagnetization at 10 mT and declination correction) for cores in Hole 833A. Note that Core 134-833A-1H was not oriented. Declinations for Core 134-833A-5H remain anomalous after orientation correction.

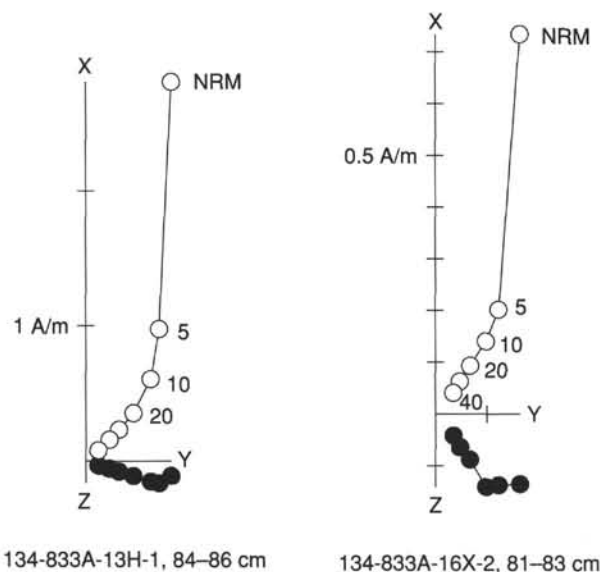


Figure 39. Representative orthogonal demagnetization plots of discrete samples from APC and XCB cores in Hole 833A. Open circles represent vector endpoints projected onto the vertical plane; solid circles represent endpoints projected onto the horizontal plane. NRM = natural remanent magnetization.

ments were obtained for Hole 833B. Because Hamilton Frame data exist for both holes, only these data are discussed here. At Site 833, velocities range from 1535 to 5909 m/s, and vertical and horizontal velocities are isotropic.

In the unlithified silts and clays of lithostratigraphic Unit I (0–84.0 mbsf in Hole 833A), sonic velocity averages about 1570 m/s. Velocities increase very slowly to 2621 m/s at 357 mbsf in the carbonate-rich sedimentary rocks of lithostratigraphic Unit II (84.0–199.5 mbsf in Hole 833A and 77.4–375.8 mbsf in Hole 833B). Sonic velocities in the volcanic sandstones and basaltic breccia of lithostratigraphic Unit III (375.8–577.8 mbsf in Hole 833B) increase sharply, ranging from 3000 to 5909 m/s. These data correlate with a sharp increase in bulk density and decreased porosity and water content in this unit. Velocities decrease to 2300–3000 m/s in the volcanic siltstone of lithostratigraphic Unit IV (577.8–830.3 mbsf in Hole 833B). Velocities range from 2449 to 3915 m/s in the volcanic sands, silts, and clays to more than 4300 m/s in the plagioclase-phyric basalt of lithostratigraphic Unit V (830.3–1001.1 mbsf).

Shear Strength

Undrained shear-strength tests were performed only on the APC cores of lithostratigraphic Unit I in Hole 833A (0–84 mbsf); all other cores were too stiff and lithified to measure. Sediment shear-strength values are low and show a generally steady trend with depth, although the measurements vary (Table 10; Fig. 52). The low and variable values probably result from the wet, unconsolidated ash layers in lithostratigraphic Unit I. Shear strengths in Subunit IB (40.0–84.0 mbsf) are lower than in Subunit IA (0–40.0 mbsf) because of the numerous interbeds of fine vitric ash in Subunit IB.

Thermal Conductivity

At Site 833, thermal conductivity could only be determined to a depth of 191 mbsf. No measurements could be made below that depth because of lithification. Thermal conductivity values in lithostratigraphic Units I to II range from 0.8 to

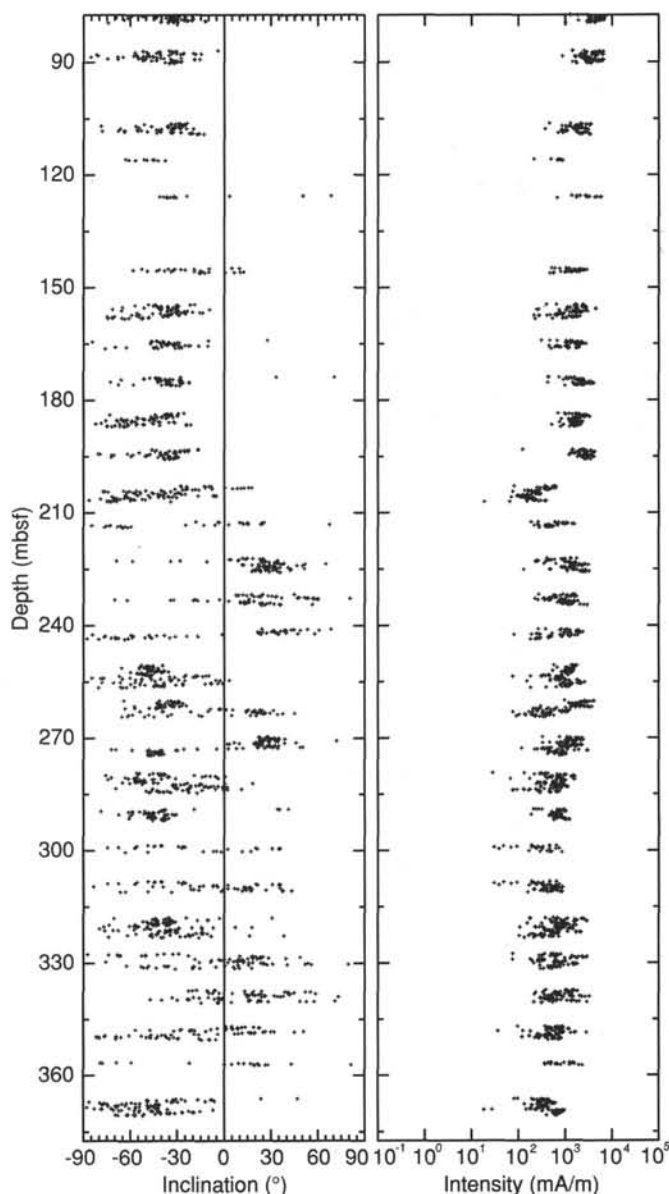


Figure 40. Variation of inclination and intensity (after AF demagnetization at 10 mT) with depth in Hole 833B, lithostratigraphic Unit II (from 75 to 370.5 mbsf).

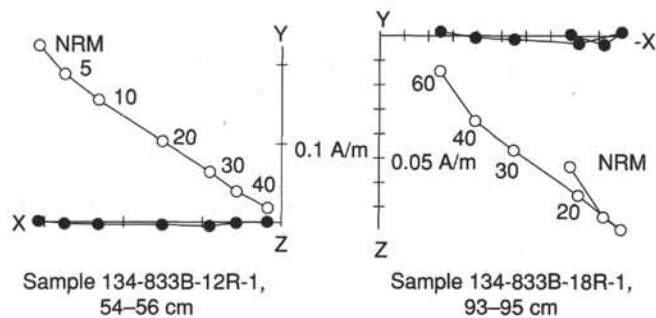


Figure 41. Representative orthogonal demagnetization plots of discrete samples from lithostratigraphic Unit II. Open circles represent vector endpoints projected onto the vertical plane; solid circles represent endpoints projected onto the horizontal plane. NRM = natural remanent magnetization.

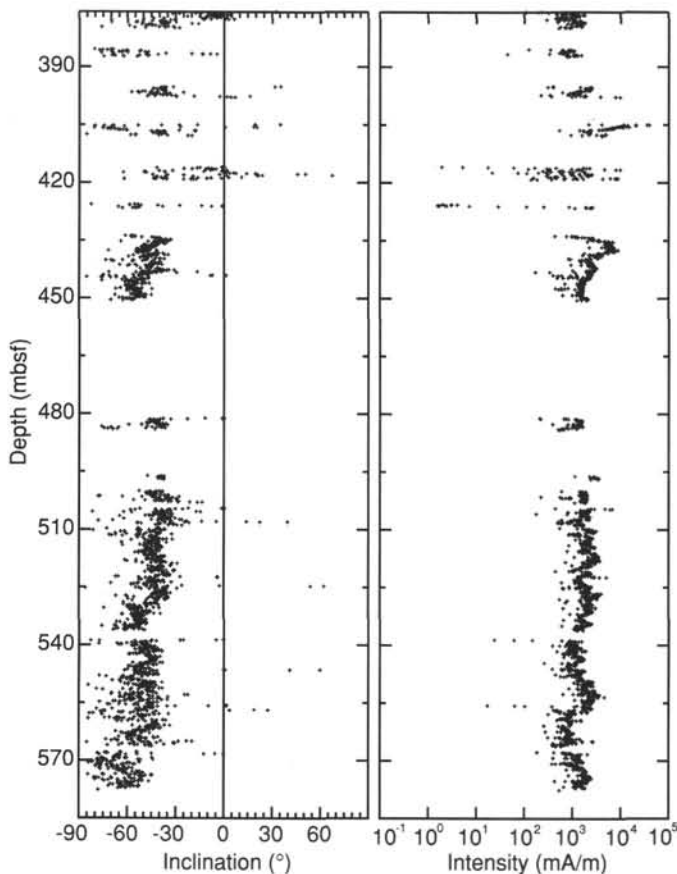


Figure 42. Variation of inclination and intensity (after AF demagnetization at 10 mT) with depth in Hole 833B, lithostratigraphic Unit III (from 375 to 577 mbsf).

nearly $2.0 \text{ W}/(\text{m} \cdot \text{K})$ (Table 11). Thermal conductivity increases from $0.89 \text{ W}/(\text{m} \cdot \text{K})$ at the seafloor to $1.96 \text{ W}/(\text{m} \cdot \text{K})$ in the clayey volcanic silt interbedded with fine vitric ash at the base of lithostratigraphic Unit I (0–84 mbsf, Fig. 53). Wide variations in the thermal conductivity values are probably due to the wet silt/ash interbeds in Unit I.

Summary

In general, physical properties correspond to lithostratigraphic units at Site 833. Unlike Site 832, physical properties do not remain constant to significant depths. They display a normal pattern of decreased porosity and increased density from 0 to 84 mbsf. This is probably a result of the location of Site 833 on the flank of the Aoba Basin, away from the depocenter at Site 832. Physical properties exhibit a distinct correlation between index properties and velocities, particularly in lithostratigraphic Units III (375.8–577.8 mbsf) and V (830–1000 mbsf), which are zones of low porosity and water content, and high bulk density and sonic velocity (Fig. 49). The transition at 375.8 mbsf from Pleistocene siltstones with ash layers to more well-cemented Pliocene sandstones and basaltic breccias is very obvious in the physical properties data.

DOWNHOLE MEASUREMENTS

Logging Operations

Well logging operations for Hole 833B consisted of six logging runs. Logging operations started on 12 December 1990, at 1510 local time (L) and ended on 14 December 1990 at 0430 L. The wiper trip before the logging showed that there

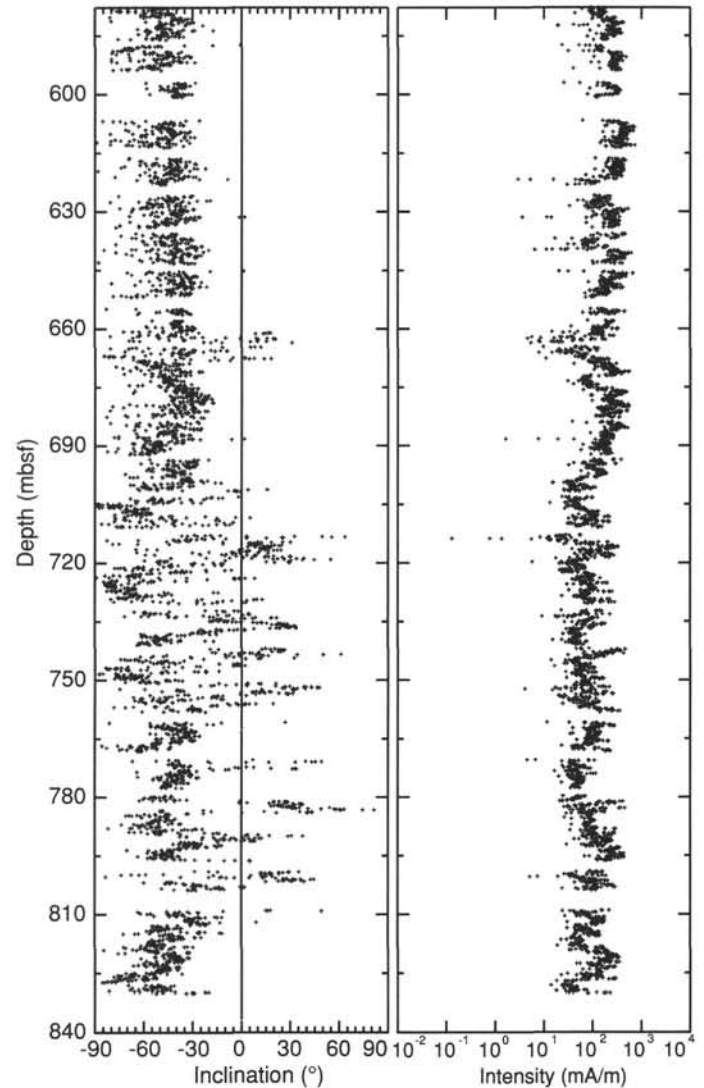


Figure 43. Variation of inclination and intensity (after AF demagnetization at 10 mT) with depth in Hole 833B, lithostratigraphic Unit IV (from 577 to 830 mbsf).

were several intervals shallower than 221 mbsf where hole problems could be expected. The end of the drill pipe was set to 250 mbsf to avoid these problem areas.

Run 1

The first logging run consisted of the seismic stratigraphy combination along with the temperature logging tool. The tools used in this string were the natural gamma-ray tool (NGT), sonic digital tool (SDT), hostile environment lithodensity tool (HLDT), dual induction tool (DIT-E), and the LDGO temperature tool (TLT). The tool string touched down at 887 mbsf in the sediments between the upper and middle sills of lithostratigraphic Unit V and the hole was logged up to the drill pipe at 250 mbsf. The drill pipe became stuck at the end of this run.

Run 2

The second run was done after the drill pipe was freed and two stands of pipe removed from the drill string. The tool string for this run consisted of the formation microscanner (FMS), NGT, and TLT. The hole was blocked by a bridge at 275 mbsf and the logging run was aborted. We then worked

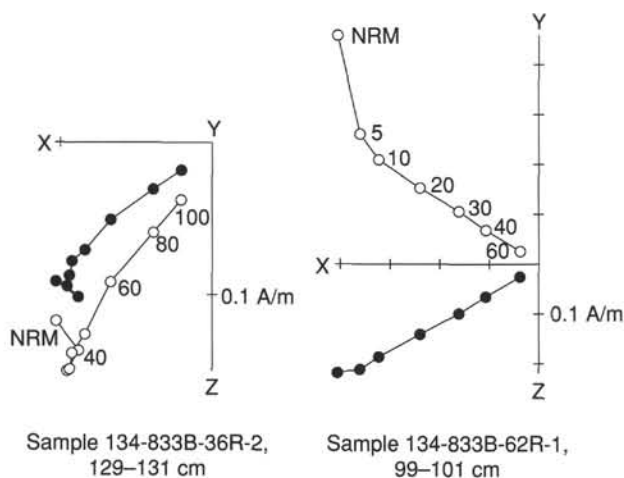


Figure 44. Representative orthogonal demagnetization plots of samples from lithostratigraphic Units III and IV that show stable characteristic magnetizations. Open circles represent vector endpoints projected onto the vertical plane; solid circles represent endpoints projected onto the horizontal plane.

the drill string and circulated it in the drill hole to remove the bridge and checked the condition of the hole.

Run 3

The third run also used the FMS, NGT, and TLT tools. This run was abandoned when further bridges were encountered at a depth of 307 mbsf. A full wiper trip through the hole was done after the tool string was taken out of the drill pipe. Hole problems were encountered down to about 510 mbsf, so the end of the drill pipe was set at 540 mbsf after the wiper trip.

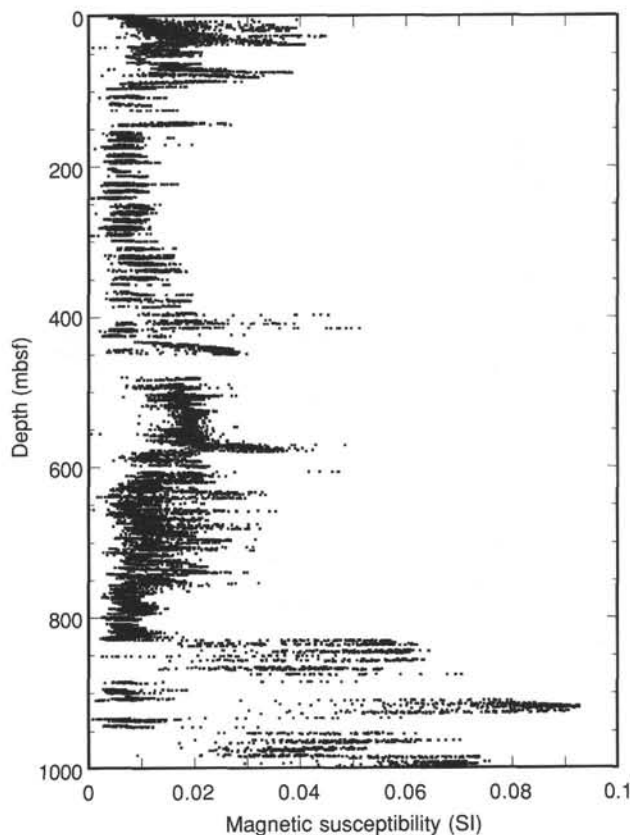


Figure 46. Plot of the magnetic susceptibility as a function of depth below seafloor at Site 833.

Run 4

The fourth run once more tried the FMS, NGT, and TLT tool string. The hole was clear and the tool string touched down at 934 mbsf, between the second and third sills within lithostratigraphic Unit V. The main logging pass was from 934 to 557 mbsf. A short repeat pass was done between 774 and 621 mbsf.

Run 5

The fifth logging run used the geochemical combination tool string, consisting of the NGT, composite neutron tool (CNT), aluminum clay tool (ACT), gamma spectroscopy tool (GST), and TLT. This tool string touched down at 885 mbsf, between the upper and middle sills of lithostratigraphic Unit V. The hole was logged up to the end of the drill pipe at 557 mbsf. A short section of hole from 450 to 408 mbsf was logged through the pipe. This interval had 0% core recovery. There was adequate core recovery for the rest of the hole, so the decision was made to save time for another logging run by not logging the entire interval from 557 to 0 mbsf through the pipe.

Run 6

The final logging run used the magnetometer tool. This tool touched bottom at 866 mbsf. The logging run up to the end of the drill pipe showed that the tool was too sensitive for the conditions in the hole. It was not able to lock onto the magnetic field and track it for more than a few meters at a time.

Results and Interpretation

Well-log data are presented along with summary coring and recovery data in the Log Summary at the end of this chapter.

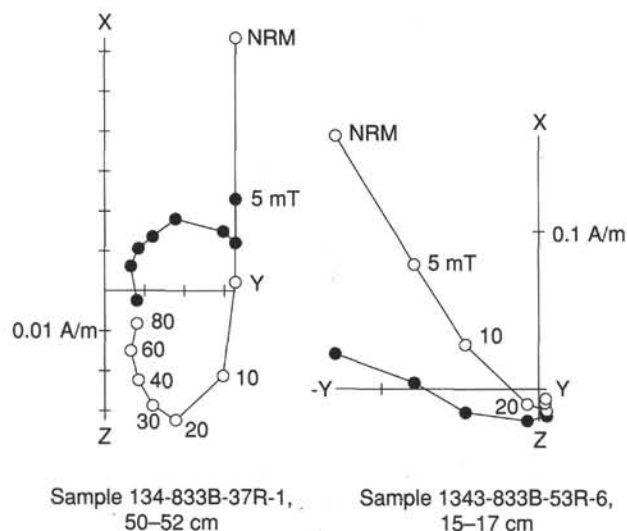


Figure 45. Representative orthogonal demagnetization plots of samples from lithostratigraphic Units III and IV that missed the origin of the vector plots. Open circles represent vector endpoints projected onto the vertical plane; solid circles represent endpoints projected onto the horizontal plane.

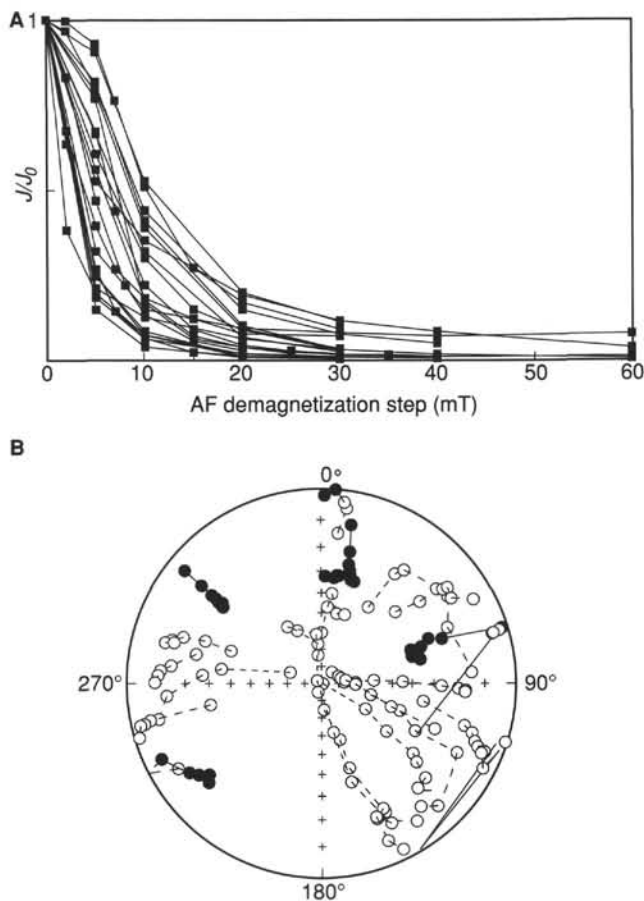


Figure 47. A. Variation of the normalized intensity of magnetization vs. the alternating field value. J/J_0 is the ratio of magnetic intensity (J) after demagnetization at a particular step to the NORM intensity (J_0). B. Stereographic projections of AF demagnetization path of discrete samples from the volcanic sills of Unit V. The NRM of several samples corresponds to steep negative inclination. Open circles are projections in the upper hemisphere; solid circles are projections in the lower hemisphere.

Selected log data from the FMS log are presented in Figure 54. The processed FMS data are provided on microfiche at the back of this volume.

As a result of the hole stability problems discussed above, the well-log data begins in lithostratigraphic Subunit IIC. Lithostratigraphic Unit II consists of calcareous siltstones and claystones that are highly bioturbated with little volcanic ash and sand. Volcanic tuffs increase in Subunit IID. Unit II is clearly distinguished from Unit III in the resistivity, velocity, and bulk density logs. These all show sharp increases from 373 to 382 mbsf in the upper part of Unit III. The gamma-ray logs show a major peak from 266 to 270 mbsf, with a corresponding peak in uranium, thorium, and potassium abundances. This is the most prominent feature in these logs at this site, but nothing unusual was found in the recovered cores. The only possible conclusion is that the sediments responsible for gamma-ray peaks were completely missed due to partial core recovery. The gamma-ray values generally decrease downhole with no characteristic marking the Unit II/Unit III boundary. This decrease downhole is due to a decrease in potassium and thorium while uranium remains relatively constant.

Lithostratigraphic Unit III (375.8–577.8 mbsf) consists of black volcanic sand and fine-grained basaltic breccia with a low carbonate content. The gamma-ray logs are generally low

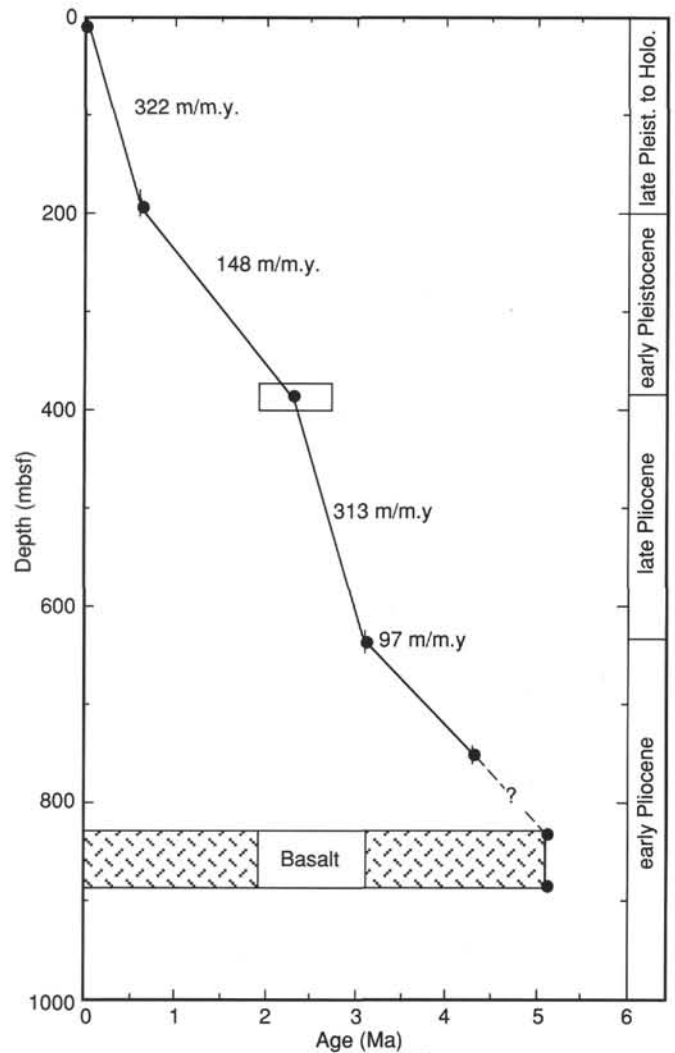


Figure 48. Sedimentation rates for the upper 751.5 mbsf of Holes 833A and 833B. The error bars and rectangle show distances between defining core-catcher samples and age of first appearance datum of *G. truncatulinoides*.

in this unit but show a number of zones from a few meters to a few tens of meters of higher or lower values. Most of these zones correspond to variations in potassium and thorium, as in lithostratigraphic Unit II. Sonic velocity, resistivity, and bulk density, while all remaining at much higher values than in Unit II, also show characteristic coherent intervals of a few meters to tens of meters in thickness. The caliper shows that the hole is generally smooth and is significantly smaller in diameter in Unit VII than it is in Unit II.

Lithostratigraphic Unit IV (577.8–830.3 mbsf) consists of black volcanic sandstones and siltstones interbedded with

Table 7. Early Pliocene to Holocene chronostratigraphic events of Site 833.

Datum levels	Interval	Age (Ma)
LAD <i>Globorotalia tosaensis</i>	Top to Section 134-833B-11R-CC	0–0.6
FAD <i>Globorotalia truncatulinoides</i>	Sections 134-833B-11R-CC to -32R-CC	0.6–1.9
FAD <i>Globorotalia tosaensis</i>	Sections 134-833B-32R-CC to -60R-CC	1.9–3.1
FAD <i>Globorotalia crassaformis</i>	Sections 134-833B-60R-CC to -72R-CC	3.1–4.3

Note: FAD = first appearance datum; LAD = last appearance datum.

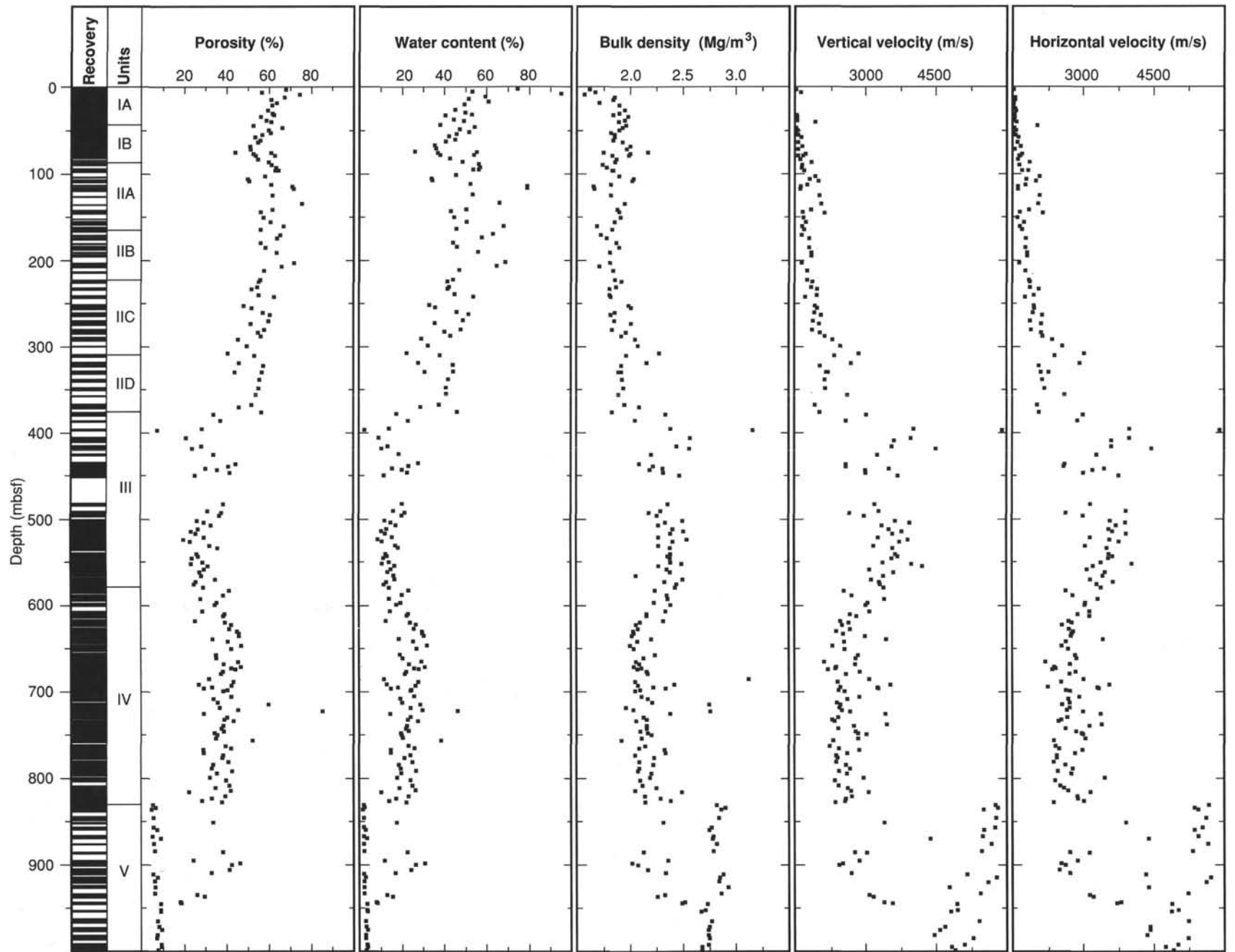


Figure 49. Porosity, water content, bulk density, and vertical and horizontal velocities vs. depth below seafloor at Site 833. Data from both Holes 833A and 833B are plotted on this graph.

Table 8. Index properties data, Site 833.

Sample (cm)	Depth (mbsf)	Unit	Wet-bulk density (Mg/m ³)	Dry-bulk density (Mg/m ³)	Grain density (Mg/m ³)	Porosity		Water content	
						Wet (%)	Dry (%)	Wet (%)	Dry (%)
134-833A-									
1H-2, 130	2.80	IA	1.62	0.93	2.64	67.7	66.0	42.7	74.5
1H-4, 130	5.80	IA	1.67	1.09	2.31	56.4	54.7	34.7	53.0
1H-6, 130	8.80	IA	1.57	0.80	2.75	74.5	72.1	48.7	95.0
2H-2, 110	12.10	IA	1.85	1.16	2.96	67.2	63.4	37.2	59.3
2H-4, 110	15.10	IA	1.84	1.22	2.80	60.8	58.6	33.9	51.2
2H-6, 110	18.10	IA	1.71	1.07	2.68	63.3	61.7	37.8	60.9
3H-2, 87	21.37	IA	1.90	1.27	2.18	61.2	51.5	33.0	49.3
3H-6, 87	27.37	IA	1.95	1.35	2.94	59.2	56.7	31.1	45.0
4H-2, 81	30.81	IA	1.90	1.26	2.92	61.6	58.9	33.3	49.9
5H-1, 20	32.80	IA	1.84	1.20	2.80	62.0	59.3	34.5	52.8
5H-2, 20	34.30	IA	1.98	1.41	2.92	55.8	53.9	28.9	40.6
5H-5, 27	38.87	IA	1.95	1.35	2.93	58.6	56.3	30.8	44.5
6H-1, 107	40.27	IA	1.89	1.27	2.81	60.9	57.7	33.0	49.1
6H-4, 107	44.77	IB	1.96	1.42	2.73	52.6	50.5	27.5	38.0
7H-2, 96	47.66	IB	1.93	1.25	3.43	66.1	64.7	35.2	54.3
7H-4, 45	50.15	IB	1.90	1.29	2.32	59.7	52.0	32.1	47.3
7H-6, 32	53.02	IB	1.82	1.20	2.70	60.4	57.9	34.1	51.6
8H-1, 130	55.30	IB	1.85	1.27	2.72	56.5	55.0	31.3	45.7
8H-3, 87	57.87	IB	1.85	1.30	2.62	53.4	52.2	29.6	42.1
9H-3, 80	61.90	IB	1.84	1.27	2.70	55.7	54.5	31.0	45.0
10H-1, 117	64.07	IB	1.93	1.37	2.82	54.6	53.1	28.9	40.7
10H-4, 140	68.80	IB	2.00	1.48	2.90	51.0	50.2	26.1	35.4
11H-2, 72	71.92	IB	1.97	1.45	2.79	51.1	49.8	26.5	36.1
11H-5, 10	75.80	IB	2.17	1.72	2.98	43.9	43.4	20.7	26.1
12H-1, 40	76.40	IB	1.75	1.13	2.71	60.9	59.6	35.6	55.3
13H-1, 132	79.32	IB	1.99	1.44	2.87	53.6	51.9	27.6	38.1
15X-CC, 10	84.10	IIA	1.87	1.31	2.70	54.7	53.2	29.9	42.7
16X-1, 18	93.88	IIA	1.78	1.14	1.15	63.1	40.5	36.2	56.8
16X-3, 4	96.74	IIA	1.84	1.20	2.80	62.7	59.7	34.9	53.6
17X-CC, 5	103.35	IIA	1.90	1.31	2.75	58.0	55.3	31.3	45.5
18X-CC, 11	113.11	IIA	1.82	1.19	2.77	60.8	58.8	34.3	52.1
21X-1, 27	142.27	IIA	1.88	1.25	2.85	61.5	58.6	33.5	50.3
21X-2, 127	144.77	IIA	1.90	1.33	2.74	55.8	53.8	30.1	43.0
22X-CC, 2	151.72	IIA	1.91	1.32	2.85	57.3	55.6	30.8	44.6
23X-1, 35	161.65	IIA	1.69	1.00	2.67	66.6	64.2	40.5	67.9
24X-1, 33	171.23	IIB	1.72	1.06	2.69	65.0	62.6	38.6	62.9
25X-CC, 43	181.03	IIB	1.87	1.30	2.72	55.9	54.2	30.6	44.1
26X-2, 42	192.22	IIB	1.81	1.16	2.76	63.3	60.3	35.8	55.8
134-833B-									
1R-1, 18	77.58	IIA	2.00	1.46	2.81	52.6	50.5	26.9	36.9
1R-2, 50	79.40	IIA	1.83	1.19	2.83	62.6	60.1	35.0	53.9
2R-1, 23	87.13	IIA	1.86	1.26	2.84	59.5	57.7	32.7	48.5
2R-3, 35	90.25	IIA	1.74	1.11	2.57	61.0	58.7	36.0	56.2
3R-1, 23	96.83	IIA	1.83	1.17	2.76	64.3	60.5	36.0	56.3
4R-1, 10	106.30	IIA	2.03	1.52	2.77	49.9	48.0	25.2	33.8
4R-2, 137	109.07	IIA	2.02	1.50	2.81	50.4	48.7	25.6	34.4
5R-1, 10	115.90	IIA	1.65	0.92	2.87	70.9	69.2	44.1	79.0
5R-3, 2	118.82	IIA	1.66	0.93	2.84	71.6	69.0	44.2	79.1
6R-1, 10	125.60	IIA	1.82	1.19	2.76	61.6	59.2	34.7	53.2
7R-CC, 6	135.26	IIA	1.95	1.17	2.38	75.4	60.8	39.7	65.9
9R-2, 72	156.72	IIA	1.85	1.23	2.70	60.4	57.3	33.5	50.4
10R-1, 104	165.14	IIB	1.83	1.26	2.66	56.1	54.5	31.4	45.7
11R-1, 124	175.04	IIB	1.78	1.13	2.79	63.6	61.4	36.6	57.7
12R-2, 131	186.31	IIB	1.90	1.30	2.77	58.1	55.5	31.4	45.8
14R-1, 108	203.88	IIB	1.81	1.07	2.73	71.8	65.0	40.8	68.8
14R-4, 55	207.85	IIB	1.71	1.04	2.64	65.7	62.8	39.3	64.7
15R-1, 29	212.69	IIB	1.84	1.25	2.63	57.5	55.0	32.0	47.1
16R-1, 137	223.47	IIC	1.86	1.29	2.62	55.7	53.4	30.7	44.2
16R-3, 47	225.57	IIC	1.92	1.36	2.60	55.0	51.6	29.4	41.6
17R-1, 40	232.10	IIC	1.87	1.32	2.68	54.5	52.8	29.8	42.4
17R-2, 132	234.52	IIC	1.81	1.27	2.49	51.9	50.6	29.5	41.8
18R-1, 10	241.00	IIC	1.81	1.25	2.54	55.0	53.1	31.1	45.2
18R-2, 102	242.92	IIC	1.82	1.19	2.75	62.2	59.4	35.0	53.8
19R-2, 127	253.27	IIC	1.99	1.50	2.68	48.1	46.5	24.8	32.9
19R-4, 127	256.27	IIC	2.01	1.48	2.76	51.9	49.5	26.5	36.0
20R-1, 137	261.37	IIC	1.86	1.28	2.72	57.1	55.1	31.4	45.8
20R-3, 122	264.22	IIC	1.82	1.20	2.67	60.3	57.6	34.0	51.4
21R-1, 135	271.05	IIC	1.85	1.24	2.81	59.5	57.6	32.9	49.0
21R-3, 135	274.05	IIC	2.01	1.48	2.74	51.4	48.9	26.2	35.5
22R-2, 85	281.65	IIC	1.83	1.24	2.62	57.7	55.2	32.3	47.7
22R-4, 57	284.37	IIC	1.96	1.40	2.76	54.9	52.3	28.7	40.2
23R-1, 39	289.29	IIC	1.92	1.34	2.74	56.2	53.7	30.1	43.0

Table 8 (continued).

Sample (cm)	Depth (mbsf)	Unit	Wet-bulk density (Mg/m ³)	Dry-bulk density (Mg/m ³)	Grain density (Mg/m ³)	Porosity		Water content	
						Wet (%)	Dry (%)	Wet (%)	Dry (%)
23R-3, 30	292.20	IIC	2.05	1.59	2.68	45.4	43.6	22.7	29.3
24R-1, 137	299.97	IIC	2.08	1.57	2.69	49.7	46.3	24.5	32.5
25R-1, 25	308.45	IID	2.28	1.87	2.83	40.7	38.4	18.3	22.3
25R-3, 25	311.45	IID	1.97	1.43	2.76	53.1	50.9	27.6	38.1
26R-2, 76	320.16	IID	2.16	1.69	2.67	46.1	42.4	21.8	27.9
26R-4, 71	323.11	IID	1.92	1.33	2.74	57.3	54.3	30.6	44.0
27R-2, 135	330.35	IID	1.89	1.31	2.69	56.6	54.1	30.8	44.4
27R-3, 23	330.74	IID	1.92	1.46	2.90	44.1	46.8	23.6	30.8
28R-2, 72	338.42	IID	1.93	1.36	2.72	55.5	52.9	29.5	41.9
29R-2, 88	349.09	IID	1.94	1.38	2.70	55.0	52.1	29.0	40.9
30R-1, 36	356.86	IID	1.89	1.34	2.49	53.7	50.1	29.1	41.0
31R-2, 100	368.70	IID	1.95	1.42	2.67	51.9	49.6	27.3	37.5
31R-CC, 7	371.36	IID	2.09	1.62	2.73	45.9	43.7	22.4	28.9
32R-1, 126	377.06	III	1.83	1.25	2.53	56.4	53.6	31.6	46.2
32R-3, 85	379.33	III	2.34	1.99	2.68	33.9	31.5	14.9	17.4
33R-2, 47	387.47	III	2.05	1.66	2.56	37.2	36.6	18.6	22.9
34R-1, 111	396.31	III	2.39	2.10	2.52	28.3	25.5	12.1	13.8
34R-2, 111	397.81	III	3.16	3.08	3.11	7.6	7.2	2.5	2.5
35R-2, 125	407.65	III	2.57	2.36	2.76	20.9	19.8	8.3	9.1
36R-2, 70	416.60	III	2.44	2.15	2.66	28.1	26.0	11.8	13.4
36R-4, 50	419.40	III	2.56	2.32	2.73	23.7	21.9	9.5	10.5
37R-2, 62	426.32	III	2.20	1.85	2.58	33.8	32.3	15.8	18.7
38R-2, 145	436.75	III	2.09	1.63	2.64	44.5	42.0	21.8	27.9
38R-4, 130	439.60	III	2.22	1.80	2.78	40.9	38.9	18.9	23.3
38R-6, 140	442.70	III	2.31	2.00	2.63	30.1	28.5	13.4	15.4
39R-1, 125	444.45	III	2.19	1.82	2.58	35.6	33.7	16.7	20.0
39R-3, 120	447.40	III	2.32	1.89	2.92	41.6	39.4	18.4	22.6
39R-5, 120	450.40	III	2.47	2.21	2.60	25.1	22.9	10.4	11.6
45R-2, 86	483.46	III	2.36	1.97	2.51	38.4	33.1	16.7	20.0
46R-1, 124	491.54	III	2.29	1.98	2.53	31.0	28.6	13.8	16.1
46R-3, 120	494.34	III	2.18	1.80	2.62	37.6	35.5	17.6	21.4
46R-5, 70	496.81	III	2.26	1.89	2.52	36.7	33.1	16.6	20.0
47R-2, 127	502.77	III	2.50	2.23	2.64	26.2	23.8	10.7	12.0
47R-4, 37	504.87	III	2.34	2.03	2.62	29.6	27.8	13.0	14.9
47R-7, 20	508.60	III	2.27	1.94	2.60	32.8	30.8	14.8	17.3
48R-2, 145	512.51	III	2.41	2.13	2.55	26.7	24.4	11.4	12.8
48R-4, 70	514.76	III	2.51	2.27	2.61	23.5	21.4	9.6	10.6
48R-6, 90	517.96	III	2.39	2.13	2.59	25.6	23.9	11.0	12.3
49R-2, 132	522.12	III	2.27	1.97	2.43	29.6	27.0	13.3	15.4
49R-4, 142	525.22	III	2.54	2.33	2.64	19.9	18.5	8.0	8.7
49R-6, 82	527.62	III	2.41	2.17	2.61	22.9	21.7	9.8	10.8
50R-2, 110	531.50	III	2.27	1.94	2.49	32.1	29.4	14.5	17.0
50R-4, 100	534.40	III	2.38	2.01	2.52	36.0	31.3	15.5	18.3
51R-2, 133	541.43	III	2.39	2.12	2.50	26.0	23.5	11.1	12.5
51R-4, 103	544.13	III	2.36	2.08	2.48	26.8	24.3	11.6	13.2
51R-6, 27	546.37	III	2.38	2.14	2.55	24.0	22.4	10.3	11.5
52R-2, 140	551.10	III	2.39	2.09	2.57	28.9	26.4	12.4	14.1
52R-3, 139	552.59	III	2.49	2.25	2.62	23.4	21.6	9.6	10.7
52R-5, 140	555.60	III	2.27	1.95	3.37	31.4	35.4	14.2	16.5
53R-1, 138	559.28	III	2.35	2.05	2.62	29.5	27.6	12.8	14.7
53R-3, 138	562.28	III	2.38	2.11	2.54	27.3	24.9	11.7	13.3
53R-6, 80	566.21	III	2.06	1.77	2.21	28.1	26.1	14.0	16.2
54R-2, 131	570.61	III	2.50	2.14	2.48	34.7	28.8	14.2	16.6
54R-4, 138	573.68	III	2.33	2.07	2.49	25.5	23.6	11.2	12.6
54R-6, 140	576.70	III	2.44	2.18	2.55	24.8	22.6	10.4	11.6
55R-2, 138	580.58	IV	2.43	2.13	2.70	29.0	27.0	12.2	13.9
55R-4, 140	583.59	IV	2.24	1.82	2.56	41.2	36.9	18.8	23.2
56R-1, 142	588.82	IV	2.35	1.95	2.54	38.4	33.5	16.8	20.1
56R-4, 140	593.23	IV	2.36	2.07	2.58	27.9	25.9	12.1	13.8
57R-1, 101	598.01	IV	2.23	1.86	2.61	35.4	33.3	16.3	19.5
57R-3, 11	600.11	IV	2.39	2.03	2.81	34.6	32.6	14.8	17.4
58R-1, 120	607.90	IV	2.34	2.05	2.63	28.8	27.2	12.6	14.4
58R-3, 127	610.97	IV	2.16	1.76	2.68	39.1	37.5	18.6	22.8
58R-5, 67	613.37	IV	2.16	1.76	2.63	38.6	36.7	18.3	22.4
59R-2, 105	618.85	IV	2.32	2.06	2.54	25.1	23.8	11.1	12.5
59R-4, 37	621.17	IV	2.10	1.70	2.58	39.3	37.7	19.2	23.7
59R-6, 15	623.95	IV	2.06	1.63	2.55	42.3	40.1	21.0	26.6
60R-2, 115	628.55	IV	2.08	1.65	2.63	41.3	39.8	20.4	25.6
60R-4, 113	631.53	IV	2.03	1.56	2.63	45.1	43.4	22.8	29.6
60R-6, 41	633.81	IV	2.04	1.58	2.62	45.8	43.5	23.0	29.8
61R-1, 42	636.02	IV	2.02	1.55	2.59	46.0	43.7	23.3	30.5
61R-3, 117	639.75	IV	2.20	1.85	2.59	33.4	32.0	15.6	18.4
61R-5, 127	642.85	IV	2.07	1.65	2.57	40.8	39.0	20.2	25.3
62R-2, 121	647.91	IV	2.00	1.51	2.59	47.1	44.9	24.2	31.9

Table 8 (continued).

Sample (cm)	Depth (mbsf)	Unit	Wet-bulk density (Mg/m ³)	Dry-bulk density (Mg/m ³)	Grain density (Mg/m ³)	Porosity		Water content	
						Wet (%)	Dry (%)	Wet (%)	Dry (%)
62R-4, 144	650.88	IV	2.04	1.61	2.47	42.2	39.5	21.2	26.9
63R-2, 145	657.85	IV	2.24	1.88	2.66	35.0	33.2	16.0	19.0
63R-5, 142	662.13	IV	2.13	1.77	2.47	35.3	33.1	16.9	20.4
64R-1, 140	666.00	IV	2.06	1.59	2.63	45.5	43.1	22.6	29.2
64R-3, 137	668.94	IV	2.09	1.69	2.56	38.7	37.1	19.0	23.4
64R-5, 137	671.94	IV	2.04	1.56	2.66	46.9	44.7	23.6	30.8
64R-7, 30	673.72	IV	2.11	1.67	2.58	42.3	39.6	20.6	25.9
65R-1, 55	674.75	IV	2.07	1.62	2.64	44.2	42.2	21.9	28.0
65R-3, 55	677.65	IV	2.16	1.77	2.62	38.2	36.3	18.1	22.1
65R-5, 55	680.49	IV	2.17	1.79	2.51	37.3	34.6	17.6	21.4
66R-2, 70	685.99	IV	3.12	2.80	3.63	31.7	29.3	10.4	11.6
66R-4, 97	689.26	IV	2.05	1.60	2.54	43.4	41.0	21.7	27.8
66R-6, 97	692.13	IV	2.42	2.14	2.70	27.0	25.5	11.4	12.9
67R-1, 40	693.90	IV	2.08	1.64	2.61	42.4	40.5	20.9	26.4
67R-2, 90	695.90	IV	2.22	1.88	2.54	33.3	31.2	15.4	18.2
67R-3, 40	696.90	IV	2.34	2.04	2.62	29.2	27.5	12.8	14.7
67R-4, 90	698.90	IV	2.10	1.69	2.54	40.3	37.9	19.6	24.4
67R-5, 40	699.90	IV	2.05	1.65	2.48	38.6	36.9	19.3	23.9
68R-2, 134	705.94	IV	2.11	1.68	2.58	42.2	39.5	20.4	25.7
68R-4, 136	708.96	IV	2.17	1.82	2.51	34.0	32.1	16.0	19.1
69R-1, 65	713.45	IV	2.21	1.84	2.61	36.0	34.0	16.7	20.0
69R-3, 60	715.80	IV	2.75	2.14	2.62	59.7	42.4	22.2	28.6
69R-5, 63	718.83	IV	1.96	1.58	2.62	36.9	38.1	19.3	23.9
69R-7, 62	721.82	IV	2.03	1.57	2.58	45.4	43.1	22.9	29.7
70R-1, 61	723.11	IV	2.76	1.89	2.56	85.2	53.9	31.6	46.3
70R-3, 70	726.20	IV	2.38	2.08	2.58	29.3	26.8	12.6	14.5
70R-6, 43	730.43	IV	2.13	1.72	2.57	40.1	37.7	19.3	23.9
71R-1, 130	733.50	IV	2.16	1.76	2.66	39.0	37.3	18.5	22.7
71R-3, 1	735.21	IV	2.06	1.62	2.60	43.3	41.3	21.5	27.4
71R-6, 17	739.88	IV	2.16	1.77	2.55	38.6	36.0	18.3	22.4
72R-1, 140	743.30	IV	2.16	1.77	2.63	37.7	36.1	17.9	21.8
72R-3, 137	746.27	IV	2.10	1.70	2.58	38.8	37.3	18.9	23.3
72R-5, 103	748.93	IV	2.17	1.82	2.51	34.4	32.3	16.2	19.3
72R-7, 20	751.10	IV	2.20	1.83	2.60	35.6	33.7	16.6	19.9
73R-2, 120	754.20	IV	2.11	1.75	2.48	35.1	33.4	17.0	20.5
73R-4, 107	757.07	IV	1.92	1.39	2.55	52.1	49.2	27.8	38.4
74R-2, 127	763.57	IV	2.15	1.75	2.67	39.6	37.9	18.8	23.2
74R-4, 80	766.10	IV	2.09	1.66	2.62	42.2	40.2	20.7	26.0
74R-6, 20	768.50	IV	2.33	2.03	2.67	29.1	27.8	12.8	14.7
75R-1, 60	771.00	IV	2.34	2.04	2.70	29.3	28.1	12.8	14.7
75R-3, 70	774.10	IV	2.05	1.66	2.48	38.6	36.9	19.3	23.9
75R-5, 87	777.27	IV	2.23	1.84	2.68	38.0	35.9	17.5	21.2
76R-2, 80	782.00	IV	2.09	1.68	2.64	40.9	39.4	20.0	25.0
76R-4, 96	785.16	IV	2.22	1.87	2.63	33.6	32.3	15.6	18.4
76R-7, 55	789.05	IV	2.09	1.75	2.34	33.0	30.9	16.2	19.4
77R-2, 135	792.15	IV	2.08	1.64	2.62	42.7	40.7	21.0	26.6
77R-4, 145	795.25	IV	2.20	1.84	2.63	35.4	33.8	16.5	19.7

finer-grained, more calcareous sandstones, siltstones, and claystones. Unit IV is the first unit to be covered by all the logs: geophysical, geochemical (Log Summary), and FMS (Fig. 54 and back-pocket microfiche). The transition from Unit III to Unit IV is marked by generally lower resistivities which show a layering on a smaller vertical scale. The average resistivity decreases with increasing depth in this unit and shows little variation in the depth range 765–830 mbsf at the base of the unit. Velocity behaves similarly to resistivity, with a slight decrease in Unit IV and it tracks the small-scale behavior of resistivity remarkably well. The bulk density also drops slightly from Unit III to Unit IV, but it shows little variability within Unit IV. The gamma-ray logs increase with depth within Unit IV and have much more small-scale variability than in Unit III. The caliper shows that the hole is becoming somewhat larger and somewhat more rough compared to Unit III, especially at the base of the unit. Aluminum content drops from 8% Al₂O₃ at the top of Unit IV to 4% at the base, changing values in a couple of stepwise transitions at 623 and 760 mbsf. The geochemical yields also show steps in level at about those depth but no

large trends within the unit. Calcium increases slightly downhole and iron decreases slightly through the unit. More detailed analyses await the final processed geochemical data, which will be presented in the Leg 134 *Scientific Results* volume.

The lowermost unit drilled, lithostratigraphic Unit V (830.3–1001.1 mbsf) consists of basaltic sills intruded into sediments similar to those of Unit IV. There is little evidence of structural deformation and only minor contact metamorphism associated with the sills. The contact of Unit V is quite dramatic in most of the logs. The hole diameter decreases abruptly and the cross-section becomes circular rather than highly elliptical. The gamma-ray values increase dramatically as a result of increased potassium and thorium content. Resistivity increases and shows the interbedded sediments between the sills. Decreases in resistivity at 835 and 842 mbsf suggest possible additional instances of interbedded sediments. The uppermost sill exists nominally from 830.3 to 851.9 mbsf, but there are occasional thin sediment layers seen throughout the sills in Unit V. These were tentatively but not definitely classified as sediments that have fallen into the

Table 8 (continued).

Sample (cm)	Depth (mbsf)	Unit	Wet-bulk density (Mg/m ³)	Dry-bulk density (Mg/m ³)	Grain density (Mg/m ³)	Porosity		Water content	
						Wet (%)	Dry (%)	Wet (%)	Dry (%)
78R-1, 140	800.40	IV	2.19	1.86	2.55	32.2	30.8	15.0	17.7
78R-3, 145	803.45	IV	2.10	1.70	2.63	39.9	38.4	19.4	24.1
79R-2, 15	810.35	IV	2.12	1.70	2.66	41.3	39.5	19.9	24.9
79R-3, 140	813.10	IV	2.25	1.89	2.70	34.8	33.3	15.8	18.8
79R-5, 145	814.92	IV	2.05	1.62	2.50	41.9	39.4	20.9	26.4
79R-7, 40	816.87	IV	2.49	2.26	3.54	22.3	26.1	9.2	10.1
80R-2, 140	821.20	IV	2.14	1.74	2.57	39.2	36.9	18.8	23.1
80R-4, 140	824.20	IV	2.29	1.96	2.66	32.9	31.1	14.7	17.2
80R-6, 140	827.20	IV	2.39	2.10	2.76	28.5	27.4	12.2	13.9
81R-1, 71	828.71	IV	2.15	1.76	2.68	37.9	36.7	18.1	22.0
81R-3, 59	831.59	V	2.82	2.77	2.77	5.3	5.1	1.9	2.0
82R-1, 88	834.88	V	2.90	2.83	2.84	6.6	6.3	2.3	2.4
82R-3, 30	837.30	V	2.86	2.81	2.82	4.5	4.3	1.6	1.6
83R-2, 133	846.93	V	2.84	2.78	2.78	5.4	5.2	2.0	2.0
84R-1, 100	852.20	V	2.32	1.97	2.78	33.7	32.4	14.9	17.5
85R-1, 107	857.27	V	2.77	2.72	2.73	5.4	5.1	2.0	2.0
85R-3, 128	860.31	V	2.75	2.67	2.71	7.4	7.0	2.8	2.8
86R-2, 90	868.30	V	2.79	2.73	2.75	5.0	4.9	1.9	1.9
86R-4, 22	870.51	V	2.78	2.68	2.84	9.0	8.8	3.3	3.4
87R-1, 77	876.17	V	2.82	2.76	2.77	5.8	5.5	2.1	2.1
88R-1, 27	885.47	V	2.79	2.73	3.45	6.2	7.3	2.3	2.3
88R-1, 120	886.40	V	2.13	1.74	2.58	38.2	36.4	18.4	22.5
89R-1, 115	895.95	V	2.36	2.11	2.65	24.3	23.5	10.5	11.8
89R-3, 140	899.20	V	2.02	1.54	2.60	46.3	44.1	23.6	30.8
89R-5, 30	901.10	V	2.08	1.65	2.56	42.4	40.0	20.9	26.4
90R-2, 5	906.05	V	2.17	1.75	2.62	41.4	38.5	19.5	24.3
90R-4, 94	909.94	V	2.34	2.00	2.72	32.8	31.0	14.4	16.8
90R-5, 130	911.80	V	2.88	2.82	2.87	5.3	5.1	1.9	1.9
91R-1, 131	915.51	V	2.85	2.77	2.79	7.6	7.2	2.7	2.8
91R-4, 120	919.71	V	2.84	2.77	2.82	6.1	5.9	2.2	2.3
92R-2, 118	926.60	V	2.93	2.87	2.87	6.3	6.0	2.2	2.3
93R-1, 47	934.07	V	2.86	2.80	2.84	6.2	5.9	2.2	2.3
93R-2, 145	936.55	V	2.33	2.07	2.63	26.0	25.0	11.4	12.9
93R-4, 70	938.80	V	2.26	1.95	2.53	29.5	27.8	13.4	15.4
94R-1, 37	943.67	V	2.52	2.34	2.68	18.1	17.3	7.4	7.9
94R-2, 4	944.84	V	2.49	2.30	2.69	18.7	18.1	7.7	8.3
94R-2, 100	945.80	V	2.73	2.64	2.73	9.0	8.6	3.4	3.5
95R-1, 30	953.20	V	2.71	2.61	2.71	9.0	8.6	3.4	3.5
95R-2, 47	954.88	V	2.67	2.58	2.70	9.0	8.7	3.5	3.6
96R-2, 145	965.55	V	2.77	2.70	2.74	7.5	7.2	2.8	2.9
97R-1, 9	972.29	V	2.75	2.67	2.80	8.0	7.8	3.0	3.1
97R-3, 42	975.56	V	2.74	2.65	2.73	9.4	8.9	3.5	3.6
98R-1, 23	982.13	V	2.74	2.67	2.77	7.3	7.1	2.7	2.8
98R-3, 107	985.97	V	2.75	2.68	2.68	7.0	6.6	2.6	2.7
99R-1, 144	992.94	V	2.74	2.65	2.73	9.1	8.6	3.4	3.5
99R-4, 20	996.20	V	2.68	2.58	2.75	9.2	9.0	3.5	3.6
99R-6, 82	999.82	V	2.68	2.60	2.73	7.8	7.6	3.0	3.1

lower parts of the hole (see "Lithostratigraphy" and "Igneous Petrology" sections, this chapter).

The sonic velocity and bulk density logs also show dramatic increases in lithostratigraphic Unit V and considerable complexity within the sills. This supports the suggestion that not all of the sills have been "separated out" in the lithologic description. The length of the geochemical tool string and the need to do an *in-situ* calibration at low logging speed, which irradiates the hole, resulted in very little geochemical log data from Unit V. The total magnetic field log from the FMS tool string (Fig. 54) shows a surprisingly complicated field in the uppermost sills (830–890 mbsf). It should be possible to take the magnetic property measurements done on the recovered cores from the sills and this log to model the boundaries and thicknesses of the different sills. These results will be presented in the *Scientific Results* volume.

Heat Flow

Five runs of the water sampler temperature probe (WSTP) temperature tool were performed at Site 833. Although all

runs appeared to be successful, two of these resulted in temperatures that are hard to interpret.

Run 4H in Hole 833A (28.5 mbsf) is shown in Figure 55 and its reduction to equilibrium temperature is shown in Figure 56. Run 9H in Hole 833A (58.0 mbsf; Fig. 57) is clearly disturbed while it is in the sediment, but the disturbance seems to vary about a cooling curve. The reduction to equilibrium temperature is given in Figure 58; the equilibrium value is only accurate to $\pm 0.5^\circ\text{C}$. Run 19X in Hole 833A at 122.6 mbsf is shown in Figure 59 and the reduction to equilibrium is shown in Figure 60. This appears to be a good value, but the equilibrium temperature is only slightly higher than that of the previous run from a depth that is over 60 m higher in the hole. The reduction to equilibrium of run 24X in Hole 833A (Fig. 61) at 170.9 mbsf is illustrated in Figure 62. The equilibrium temperature for this run is generally consistent with the gradient established by the first two runs and the water temperature at the seafloor, in contrast to run 19X. The final run, 27X in Hole 833A (Fig. 63), was done at 199.5 mbsf, and its reduction to equilibrium is given in Figure 64. The equilib-

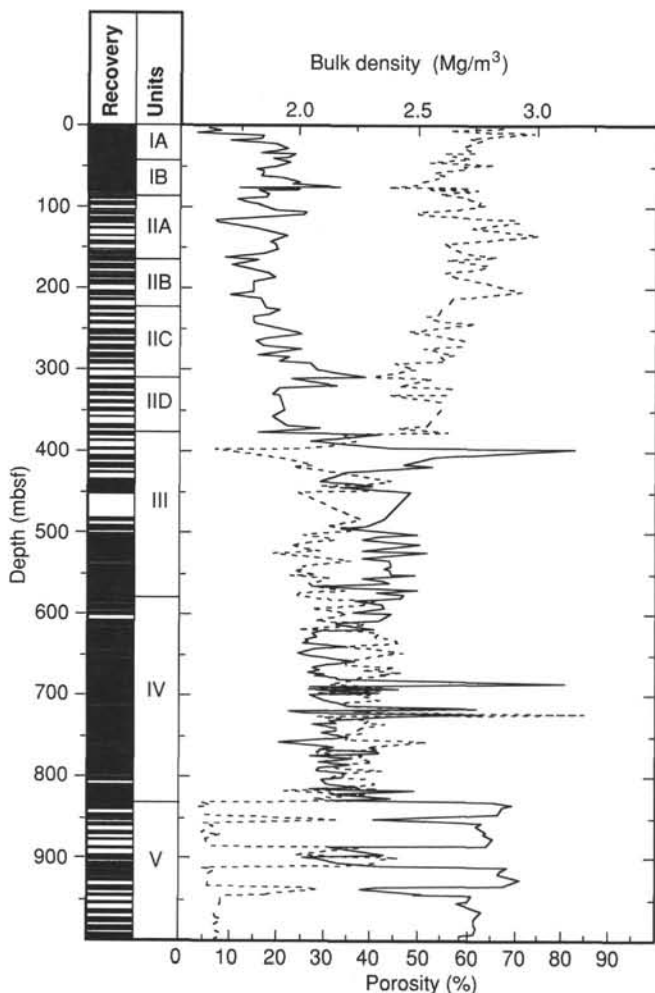


Figure 50. Bulk density (solid line) and porosity (dashed line) vs. depth and lithologic units at Site 833.

rium temperature for this run is actually less than that of run 24X. It is not clear what the exact causes are of the lower than expected temperatures in runs 19X and 27X, but one possibility would be that some sedimentary fill accumulated in the bottom of the hole between the withdrawal of the last core and the insertion of the temperature probe. This sediment would then not have enough time to equilibrate to *in-situ* temperatures. Measurement errors that give higher than expected temperatures are more difficult to explain than those that give lower than expected temperatures (at least in deep-water sites with low bottom-water temperatures).

The seafloor water temperature value and the three “normal” temperature measurements are plotted vs. integrated thermal resistivity in Figure 65. The surficial heat flow that is derived from the regression is 72.2 mW/m², which is significantly higher than the other intra-arc basin value at Site 832. One reason for the difference in the values could be the thinner sediments at this site (see “Background and Objectives” section, this chapter) which would result in a lower-magnitude sedimentation effect. Thermal refraction across the sediment basin, as heat is refracted around the thicker, low thermal conductivity sediments, could also produce the results observed. A final reason could be closer proximity of Site 833 to the volcanic activity at Mere Lava Island, similar to the increase in heat flow near New Georgia seen in the New

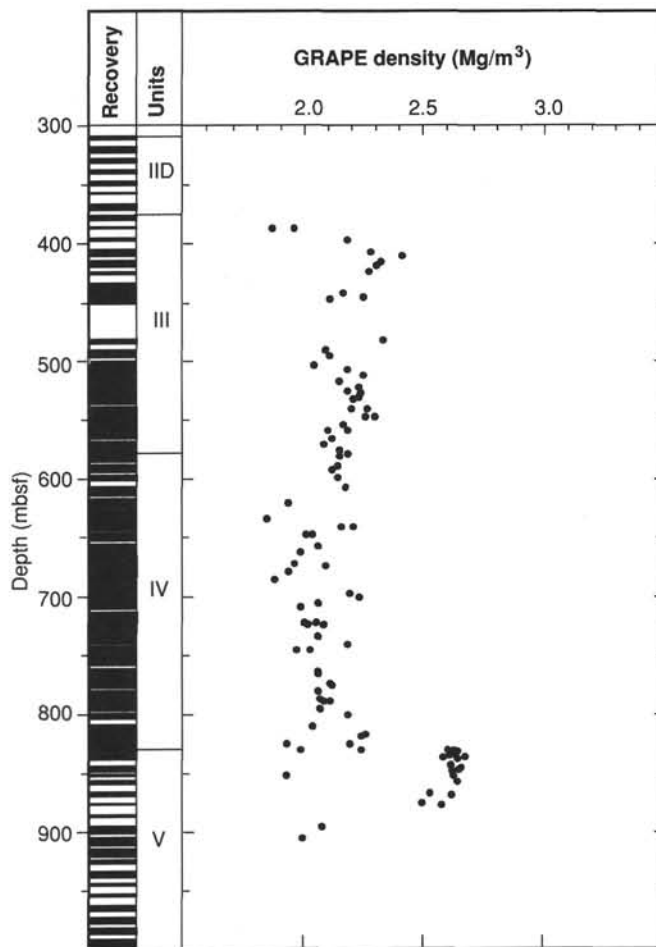


Figure 51. Two-minute GRAPE density vs. depth for Site 833.

Georgia Sound in the Solomon Islands (Hobart and Weissel, 1987).

SUMMARY AND CONCLUSIONS

Site 833 is located 14°52.56'S, 167°52.78'E, in a water depth of 2629 mbsl. This site is located on the lower northwestern flank of Maewo Island or the lower east-central flank of the North Aoba Basin (NAB), approximately 24 km northwest of the northern tip of Maewo Island and about 72 km southeast of the active volcanic island of Santa Maria. The NAB is one of two intra-arc basins that lies between the uplifted blocks that form the Western and Eastern Belts of islands in the central New Hebrides Island Arc (see “Introduction” chapter, this volume). The NAB is furthered constrained physiographically to the north and south by the volcanic islands of Santa Maria and Aoba, which are part of the active volcanic Central Chain of the New Hebrides Island Arc (Vanuatu). Major objectives in drilling at this site were to determine the timing of basin formation, timing of the d’Entrecasteaux Zone collision, origin of magmatic constituents, and the role that subduction polarity reversal may have had in the formation of the central New Hebrides Island Arc. Cross-basin correlations between Sites 832 and 833 were made along with stratigraphical correlations with island geology.

A seismic reflection survey was conducted to connect the two sites (Sites 832 and 833) for lithostratigraphic correlation. Two holes (Hole 833A and 833B) were drilled at the site. Hole 833A was drilled and cored to a total depth (TD) of 199.5 mbsf and 97.75 m of core were recovered for a recovery rate of

49%. Hole 833B was washed down to about 77.5 mbsf, where it was then drilled and cored for 923.7 m to a TD of 1001.1 mbsf, of which 519.54 m of core were recovered for a recovery rate of 56.2%.

Five lithostratigraphic units were defined from the examination of the cores at Site 833 (Fig. 66). Lithostratigraphic Unit I (0–84.0 mbsf, 84 m thick, in Hole 833A) is composed of upper Pleistocene to Holocene unlithified volcanic silts and clayey silts interbedded with numerous fine- to coarse-grained vitric volcanic ashes and is subdivided into two subunits (Subunits IA and IB). Lithostratigraphic Subunit IA (0–40.8 mbsf, 40.8 m thick, in Hole 833A) is composed of upper Pleistocene to Holocene clayey to sandy volcanic silt interbedded with numerous layers of black fine vitric volcanic ash with some coarse vitric volcanic ash layers. Lithostratigraphic Subunit IB (40.8–84.0 mbsf, 43.2 m thick, in Hole 833A) is composed of upper Pleistocene to Holocene volcanic silts interbedded with relatively thick, coarse beds of vitric volcanic ash layers and clayey volcanic silt; the ashes are coarser-grained, thicker, and more compacted than in Subunit IB.

Lithostratigraphic Unit II (84.0–199.5 mbsf, 115.5 m thick, in Hole 833A; 77.4–375.8 mbsf, 298.4 m thick, in Hole 833B) is composed of an upper Pliocene or lower Pleistocene to upper Pleistocene to Holocene sequence of alternating layers of highly bioturbated clayey nanofossil mixed sedimentary rock interbedded with calcareous clayey volcanic siltstone and clayey volcanic silt; the unit is bioturbated to highly bioturbated with abundant burrows, pellets, and mottling. This unit is subdivided into four subunits (lithostratigraphic Subunits IIA, IIB, IIC, and IID). Lithostratigraphic Subunit IIA (84–162 mbsf, 78 m thick, in Hole 833A; 77.4–164.4 mbsf, 87 m thick, in Hole 833B) is a lower Pleistocene to upper Pleistocene or Holocene clayey nanofossil mixed sedimentary rock that exhibits an abrupt end to the vitric volcanic ashes observed in Subunit IIB, with the carbonate constituents increasing downhole. Lithostratigraphic Subunit IIB (162–199.5 mbsf, 37.5 m thick, in Hole 833A; 164.4–222.1 mbsf, 57.7 m thick, in Hole 833B) is lower Pleistocene to upper Pleistocene or Holocene calcareous clayey volcanic siltstone, sandy volcanic siltstone with foraminifers, nanofossils, and calcareous grains, and vitric sandy volcanic siltstone with clay and foraminifers. Subunit IIB contains more tuff layers than Subunit IIA. Lithostratigraphic Subunit IIC (222.1–308.4 mbsf) is a lower Pleistocene, 86.3-m-thick silty volcanic claystone and clayey volcanic siltstone; it has the same lithology as Subunits IIA and IIB except it contains a few volcanic tuff beds. Lithostratigraphic Subunit IID (308.4–375.8 mbsf) is a lower Pleistocene, 67.4-m-thick highly bioturbated carbonate-rich volcanic sandstone that marks a major increase in the occurrence and thickness of vitric volcanic sandstone.

Lithostratigraphic Unit III (375.8–577.8 mbsf) is a 202-m-thick upper Pliocene to lower(?) Pleistocene coarse-grained volcanic sandstone and fine grained basaltic breccia. Lithostratigraphic Unit IV (577.8–830.3 mbsf) is a 252.5-m-thick, lower Pliocene to upper Pliocene foraminiferal sandy volcanic siltstone, very coarse-grained volcanic sandstone, and mixed sedimentary rock or limestone. It exhibits a distinct increase in carbonate content from the overlying unit. Lithostratigraphic Unit V (830.3–1001.1 mbsf) is a 170.8-m-thick sequence of lower Pliocene interbedded sedimentary rocks consisting of basaltic sills interlayered with calcareous silty volcanic claystone or siltstone and clayey or silty mixed sedimentary rocks.

Three different categories of volcanic rocks were recovered from drilling at Site 833. The first category comprised ashes that were recovered from lithostratigraphic Units I

and II. Ash layers of lithostratigraphic Unit I are unlithified and are basaltic with high K_2O (1.47%–2.18%) and with a potassic trend similar to volcanic rocks of the Central Chain. There is a significant difference in trend from the ashes recovered at Sites 832 and 833 in that the ashes of Site 833 (at nearly equivalent depths to those of Site 832) have little concentration of Zr. High Zr contents of Site 832 were taken to indicate an origin from the island of Santa Maria. In Unit II of Site 833 the ashes appear to have been derived from a relatively undifferentiated basaltic magma with island-arc tholeiite affinity. Chemical analysis of basaltic clasts from a volcanic breccia within lithostratigraphic Unit III shows the rocks to lie just inside the calc-alkaline field on the K_2O vs. SiO_2 plot and to be bordering on the low-potassium series. The basaltic sill rocks of lithostratigraphic Unit V appear from chemical analyses to be differentiated basalts with 52%–53% SiO_2 and only 7.8% MgO . Fe_2O_3 exceeds 10% and the Mg number is 0.35, suggesting tholeiitic character in terms of iron enrichment. However, the K_2O vs. SiO_2 classification for the rock show it to fall into the high-potassium calc-alkaline series.

Despite the limited number of chemical analyses, the chemical compositions of the volcanic rocks of Site 833 extend across the entire spectrum of subduction-related volcanic rocks from island-arc tholeiites to high-potassium calc-alkaline and shoshonitic series. This confirms and extends the compositional range encountered at Site 832, where more evolved types of rocks were also found. Data from the two drilling sites in the NAB generally suggest an upward progression from magmatic rocks of island-arc tholeiite affinity to increasingly potassic volcanic rocks at the top of the succession. The basaltic sills in the lowest part of Hole 833B (830.3–1001.1 mbsf) are high-potassium calc-alkaline rocks. Because of their intrusive nature the only constraint on the timing of their emplacement is that they are of early Pliocene age or younger. They may be related to the high-potassium calc-alkaline lava and dolerites of Maewo Island, which are described as being of late Miocene to early Pliocene age (Macfarlane et al., 1988). Alternatively, they may be intrusive counterparts of the younger potassic lavas of the Central Chain of the New Hebrides Island Arc.

Foraminifers and nanofossils were the best source for age information. However, application of these fauna and flora was severely limited by the abundance of volcanoclastic sediments, turbidites, and slumps that diluted the concentration of fauna and flora. A general age stratification was established and is as follows: Pleistocene between 0 and 375 mbsf; late Pliocene between 375 and 635.6 mbsf; and early Pliocene between 635.6 and 945 mbsf.

Four different structural units were defined for Site 833 based on the deformation that occurred to the sediments resulting from small- to large-scale slumping, normal microfaulting, and strike-slip to reverse faulting. In contrast to Site 832, fewer large-scale slump features were observed at Site 833. Structural Unit A (0–376 mbsf) generally correlates with lithostratigraphic Units I and II and is characterized by horizontal to nondipping beds and few deformation structures, such as slump induced features. Some convoluted beds, folded layers, abundant normal microfaults, and a tectonic zone (203–207 mbsf) with slightly inclined fabric exist, which indicates tectonic movement. Structural Unit B (376–616 mbsf) correlates mainly to lithostratigraphic Unit III and is defined on the basis of little structure and poorly defined bedding, with what structures present consisting of slump features and some fault sets that suggest that the siltstone of the unit were affected by normal faulting prior to tilting. Structural Unit C (616–830 mbsf) correlates to lithostratigraphic Unit IV and is characterized by beds that dip 10° – 20° , sporadic slumps, and

Table 9. Vertical and horizontal velocity data, Site 833.

Sample (cm)	Depth (cm)	Unit	Vertical velocity (m/s)	Wave type ^a	Horizontal velocity (m/s)	Wave type ^a
134-833A-						
1H-2, 130	2.80	IA	1537	C	1535	C
1H-4, 130	5.80	IA	1635	C		
2H-2, 104	12.04	IA			1558	C
2H-2, 110	12.10	IA			1549	S
2H-4, 120	15.20	IA			1561	C
2H-6, 122	18.22	IA			1538	C
3H-2, 130	21.80	IA			1524	C
3H-4, 132	24.82	IA			1558	C
3H-6, 137	27.87	IA			1586	C
4H-2, 128	31.28	IA			1551	C
5H-1, 20	32.80	IA	1540	C	1537	C
5H-2, 20	34.30	IA	1549	C	1555	C
5H-5, 27	38.87	IA	1554	C	1540	S
6H-1, 107	40.27	IA	1936	C	1587	S
6H-4, 107	44.77	IB			2036	S
7H-2, 97	47.67	IB	1532	C	1543	C
7H-4, 45	50.15	IB	1565	C	1585	C
7H-6, 32	53.02	IB	1528	C	1532	C
8H-1, 130	55.30	IB	1571	C	1564	C
8H-3, 87	57.84	IB	1639	C	1629	C
10H-1, 117	64.07	IB	1574	C	1605	S
10H-4, 140	68.80	IB	1661	C	1681	C
11H-2, 72	71.92	IB	1574	C	1554	C
13H-1, 132	79.32	IB	1571	C	1645	C
15X-CC, 10	84.10	IIA	1621	C	1626	C
16X-1, 18	93.88	IIA	1656	S		
16X-3, 4	96.74	IIA			1834	S
17X-CC, 5	103.35	IIA	1940	C	2079	C
18X-CC, 11	113.11	IIA	1764	C	1778	C
21X-1, 27	142.27	IIA	1842	C	1854	C
21X-2, 127	144.77	IIA	1667	C	1665	C
22X-CC, 2	151.72	IIA	1696	C	1618	C
23X-1, 35	161.65	IIA	1666	C	1658	C
24X-1, 33	171.23	IIB	1655	C		
26X-2, 32	191.64	IIB			1814	C
26X-2, 42	191.74	IIB	1855	C		
134-833B-						
1R-1, 18	77.58	IIA	1734	C	1710	C
1R-2, 50	79.40	IIA	1679	C	1674	C
2R-1, 23	87.13	IIA	1862	C	1871	C
2R-3, 35	90.25	IIA	1665	C	1646	C
3R-1, 23	96.83	IIA	1701	C	1710	C
4R-1, 10	106.30	IIA	1813	C	1799	C
4R-2, 137	109.07	IIA	2005	C	2006	C
5R-1, 10	115.90	IIA	1634	C	1625	C
5R-3, 2	118.33	IIA	1622	C	1624	C
6R-1, 10	125.60	IIA	2024	C	2081	C
7R-CC, 6	135.26	IIA	2067	C	2047	C
8R-1, 90	145.70	IIA	2127	C	2144	C
9R-2, 72	156.72	IIA	1738	C	1750	C
10R-1, 104	165.14	IIB	1700	C	1708	C
11R-1, 124	175.04	IIB	1807	C	1790	C
12R-2, 131	186.31	IIB	1807	C	1780	C
13R-2, 100	195.60	IIB	1863	C	1811	C
14R-1, 108	203.88	IIB	1658	C	1647	C
15R-1, 29	212.69	IIB	1762	C	1778	C
16R-1, 137	223.47	IIC	1773	C	1851	C
16R-3, 47	225.57	IIC	1878	C	1876	C
17R-1, 40	232.10	IIC	1852	C	1881	C
17R-2, 132	234.52	IIC	1988	C	2070	C
18R-1, 10	241.00	IIC	1975	C	1967	C
18R-2, 102	243.42	IIC	1733	C	1775	C
19R-2, 127	253.27	IIC	1943	C	1967	C
19R-4, 127	256.27	IIC	1984	C	1970	C
20R-1, 137	261.37	IIC	1920	C	1940	C
20R-3, 122	264.22	IIC	2066	C	2139	C
21R-1, 135	271.05	IIC	1894	C	1882	C
21R-3, 135	274.05	IIC	2025	C	2126	C
22R-2, 85	281.65	IIC	1879	C	1910	C
22R-4, 57	284.37	IIC	2043	C	2123	C
23R-1, 39	289.29	IIC	2147	C	2152	C
23R-3, 30	292.20	IIC	2303	C	2362	C
24R-1, 137	299.97	IIC	2475	C	2575	C

Table 9 (continued).

Sample (cm)	Depth (cm)	Unit	Vertical velocity (m/s)	Wave type ^a	Horizontal velocity (m/s)	Wave type ^a
25R-1, 25	308.45	IID	2871	C	3037	C
25R-3, 25	311.00	IID	2356	C	2406	C
26R-2, 76	320.16	IID	2700	C	2930	C
26R-4, 71	323.11	IID	2046	C	2074	C
27R-2, 135	330.35	IID	2206	C	2274	C
27R-3, 23	330.74	IID	2170	C	2111	C
28R-2, 72	339.42	IID	2146	C	2142	C
29R-2, 88	349.09	IID	2157	C	2184	C
30R-1, 36	356.86	IID	2621	C	2611	C
31R-2, 100	368.70	IID	1938	C	2034	C
32R-1, 126	377.06	III	2038	C	2068	C
32R-3, 85	379.33	III	3028	C	3004	C
33R-2, 47	387.22	III	2595	C	2883	C
34R-1, 111	396.31	III	4026	C	3991	C
34R-2, 111	397.81	III	5909	C	5909	C
35R-2, 125	407.65	III	3967	C	3989	C
35R-4, 92	410.24	III	3610	C	3604	C
36R-2, 70	416.60	III	3563	C	3608	C
36R-4, 50	419.40	III	4504	C	4464	C
37R-2, 62	426.29	III	3256	C	3285	C
38R-2, 145	436.75	III	2591	C	2625	C
38R-4, 130	439.60	III	2589	C	2610	C
38R-6, 140	442.70	III	3506	C	3456	C
39R-1, 124	444.44	III	3013	C	3206	C
39R-3, 120	447.40	III	3021	C	3022	C
39R-5, 120	450.31	III	3691	C	3763	C
45R-2, 86	483.46	III	3204	C	3161	C
46R-1, 124	491.54	III	3286	C	3917	C
46R-3, 120	494.34	III	2668	C	2649	C
46R-5, 70	496.81	III	2987	C	3016	C
47R-2, 127	502.77	III	3648	C	3582	C
47R-4, 37	504.82	III	3950	C	3906	C
47R-7, 20	508.63	III	3361	C	3713	C
48R-2, 145	512.51	III	3515	C	3557	C
48R-4, 70	514.76	III	3778	C	3629	C
48R-6, 90	517.96	III	3588	C	3924	C
49R-2, 132	522.12	III	3282	C	3165	C
49R-4, 142	525.16	III	3903	C	3573	C
49R-6, 82	527.41	III	3732	C	3769	C
50R-2, 110	531.50	III	3186	C	3048	C
50R-4, 100	534.40	III	3591	C	3518	C
51R-2, 133	541.43	III	3644	C	3550	C
51R-4, 100	544.10	III	3695	C	3641	C
51R-6, 27	546.37	III	3564	C	3543	C
52R-2, 140	551.10	III	3385	C	3391	C
52R-3, 139	552.59	III	3984	C	4046	C
52R-5, 140	555.60	III	4217	C	3220	C
53R-1, 138	559.28	III	3096	C	3087	C
53R-3, 138	562.28	III	3606	C	3478	C
53R-6, 80	566.21	III	3389	C	3425	C
54R-2, 131	570.61	III	3129	C	3165	C
54R-4, 138	573.68	III	3306	C	3644	C
54R-6, 140	576.70	III	3322	C	3298	C
55R-2, 138	580.58	IV	3399	C	3389	C
55R-4, 140	583.59	IV	2549	C	2637	C
56R-1, 142	588.82	IV	2715	C	2789	C
56R-4, 140	593.23	IV	3410	C	3322	C
57R-1, 101	598.01	IV	3052	C	3056	C
57R-3, 11	600.08	IV	3017	C	3046	C
58R-1, 120	607.90	IV	3087	C	3135	C
58R-3, 127	610.90	IV	2684	C	2899	C
58R-5, 67	613.09	IV	2819	C	3148	C
59R-2, 105	618.78	IV	2475	C	2705	C
59R-4, 37	620.95	IV	2657	C	2772	C
59R-6, 15	623.23	IV	2514	C	2560	C
60R-2, 115	628.26	IV	2677	C	2711	C
60R-4, 113	631.15	IV	2389	C	2796	C
60R-6, 41	633.33	IV	2537	C	2774	C
61R-1, 42	636.02	IV	2992	C	2749	C
61R-3, 117	639.56	IV	3451	C	3421	C
61R-5, 127	642.52	IV	2547	C	2635	C
62R-2, 121	647.75	IV	2309	C	2547	C
62R-4, 144	650.88	IV	2566	C	2695	C
63R-2, 145	657.85	IV	2852	C	2840	C
63R-5, 142	662.13	IV	2796	C	2865	C
64R-1, 140	666.00	IV	2132	C	2211	C

Table 9 (continued).

Sample (cm)	Depth (cm)	Unit	Vertical velocity (m/s)	Wave type ^a	Horizontal velocity (m/s)	Wave type ^a
64R-3, 137	668.94	IV	2788	C	2722	C
64R-5, 137	671.87	IV	2383	C	2392	C
64R-7, 30	673.72	IV	2367	C	2424	C
65R-1, 55	674.75	IV	2207	C	2358	C
65R-3, 55	677.65	IV	2881	C	2850	C
65R-5, 55	680.49	IV	2593	C	2718	C
66R-2, 70	685.99	IV	3081	C	3016	C
66R-4, 97	689.26	IV	2412	C	2544	C
66R-6, 97	692.13	IV	3537	C	3566	C
67R-2, 40	695.40	IV	2473	C	2253	C
67R-2, 90	695.90	IV	3264	C	3303	C
67R-3, 40	696.90	IV	3277	C	3340	C
67R-4, 90	698.90	IV	2430	C	2643	C
67R-5, 40	699.90	IV	2570	C	2725	C
68R-2, 134	705.94	IV	2875	C	2921	C
68R-4, 136	708.96	IV	2622	C	2685	C
69R-1, 65	713.45	IV	2398	C	2716	C
69R-3, 60	715.80	IV	2469	C	2566	C
69R-5, 63	718.83	IV	2458	C	2718	C
69R-7, 62	721.82	IV	2507	C	2659	C
70R-1, 61	723.11	IV	2687	C	3006	C
70R-3, 70	726.20	IV	3430	C	3373	C
70R-6, 43	730.43	IV	2425	C	2668	C
71R-1, 130	733.50	IV	2297	C	2540	C
71R-3, 1	735.21	IV	2347	C	2483	C
71R-4, 129	738.00	IV	3454	C	3401	C
71R-6, 17	739.88	IV	2765	C	3139	C
72R-1, 140	743.30	IV	2422	C	2634	C
72R-3, 137	746.27	IV	2806	C	2863	C
72R-5, 103	748.93	IV	2856	C	2980	C
72R-6, 20	749.60	IV	3028	C	3001	C
73R-2, 120	754.20	IV	2854	C	3051	C
73R-4, 107	757.08	IV	2320	C	2386	C
74R-2, 127	763.57	IV	2248	C	2422	C
74R-4, 80	766.10	IV	2445	C	2503	C
74R-6, 20	768.48	IV	2873	C	2995	C
75R-1, 60	771.00	IV	2624	C	2839	C
75R-3, 70	774.00	IV	2387	C	2457	C
75R-5, 87	777.10	IV	2415	C	2452	C
76R-2, 80	782.00	IV	2394	C	2387	C
76R-4, 96	785.16	IV	2593	C	2628	C
76R-7, 55	789.05	IV	2684	C	2787	C
77R-2, 135	792.15	IV	2447	C	2470	C
77R-4, 145	795.13	IV	2617	C	2757	C
78R-1, 140	800.40	IV	2966	C	3463	C
78R-3, 145	803.38	IV	2365	C	2413	C
79R-2, 15	809.12	IV	2437	C	2523	C

Table 9 (continued).

Sample (cm)	Depth (cm)	Unit	Vertical velocity (m/s)	Wave type ^a	Horizontal velocity (m/s)	Wave type ^a
79R-3, 140	811.87	IV	2628	C	2594	C
79R-5, 145	814.92	IV	2702	C	2693	C
79R-7, 40	816.87	IV	3073	C	3159	C
80R-2, 140	821.20	IV	2721	C	2887	C
80R-4, 140	824.01	IV	2601	C	2889	C
80R-6, 140	826.94	IV	2572	C	3026	C
81R-1, 71	828.71	IV	2367	C	2387	C
81R-3, 59	831.48	V	5766	C	5674	C
82R-1, 88	834.88	V	5810	C	5370	C
82R-3, 30	837.30	V	5507	C	5451	C
83R-2, 133	846.81	V	5776	C	5618	C
84R-1, 100	852.20	V	3410	C	3915	C
85R-1, 107	857.27	V	5757	C	5539	C
85R-3, 128	860.31	V	5518	C	5365	C
86R-2, 90	868.30	V	5495	C	5452	C
86R-4, 22	870.51	V	4388	C	4401	C
87R-1, 77	876.17	V	5680	C	5649	C
88R-1, 27	885.47	V	5470	C	5330	C
88R-1, 120	886.40	V	2780	C	2726	C
88R-2, 40	887.10	V	3039	C	3138	C
89R-1, 115	895.95	V	2873	C	2887	C
89R-3, 140	899.10	V	2525	C	2542	C
89R-5, 30	901.00	V	2449	C	2629	C
90R-2, 6	906.06	V			2502	C
90R-4, 95	909.95	V	2712	C	2730	C
90R-5, 131	911.57	V	5165	C	4344	C
91R-1, 131	915.51	V	5791	C	5715	C
91R-5, 120	921.11	V	5601	C	5622	C
92R-2, 118	926.60	V	4791	C	4402	C
93R-1, 47	934.07	V	5450	C	5233	C
93R-2, 145	935.70	V	3082	C	3137	C
93R-4, 70	937.95	V	3180	C	3218	C
94R-1, 37	943.67	V	3399	C	3816	C
94R-2, 4	944.84	V	3572	C	3716	C
94R-2, 100	945.80	V	4942	C	4896	C
95R-1, 30	953.20	V	4953	C	5030	C
95R-2, 47	954.88	V	4810	C	4884	C
96R-2, 145	965.55	V	5416	C	5245	C
97R-1, 9	972.29	V	4685	C	4432	C
97R-3, 42	975.56	V	4576	C	4433	C
98R-1, 23	982.13	V	4464	C	4358	C
98R-3, 111	985.61	V	5276	C	5237	C
99R-1, 144	992.94	V	5096	C	5018	C
99R-4, 20	995.93	V	4818	C	4746	C
99R-6, 82	999.55	V	4902	C	4923	C

^aC = compressional (P-wave) and S = shear (S-wave).

abundant normal faults with very well-developed slickensides and calcite fibers; some faults exhibit left-lateral strike-slip movement. Structural Unit D (830–1001 mbsf) correlates with lithostratigraphic Unit V and is defined on the basis of 10° to 30° dipping beds entrapped by the intruded sill and the presence of several reverse and strike-slip faults.

Pore fluids were analyzed primarily to quantify the extent of diagenetic reactions in the volcanogenic sediments and to determine if the pore fluids are chemically affected by flow of meteoric water. The chemistry of the pore fluids show that intense diagenetic reactions have occurred at Site 833. Particularly significant is the increase to extremely high maxima at 494.5 mbsf of chloride to 1241 mM (~2.2 times seawater concentration) and salinity that reaches values of 88.3%. Calcium increases to an extraordinarily high value of 548.5 mM (~52 times seawater concentration) at 494.5 mbsf. Organic carbon found in all samples was low (<0.5%). Essentially, the pore-fluid chemistry reflects the low organic carbon contents of the Pliocene to Pleistocene sediments in the NAB. This sediment probably contains too little organic matter to be important for hydrocar-

bon source material, but older sediments have not yet been evaluated for their carbon content. Perhaps the most significant result of pore-fluid analyses at Site 833 is the extreme diagenetic alteration of the volcanogenic material. The extreme diagenesis may result partly from the large volumes of volcanic sediments that are trapped in the NAB.

Magnetic susceptibility in the volcanic sandstone at Site 833 is high (0.02 SI) and this nearly normal magnetization may have been acquired during diagenesis and consolidation; viscous magnetization of these rocks appear to be quite strong as well. The interbedded sills at the bottom of Hole 833B also have high magnetic susceptibility (0.04–0.08 SI) and a high intensity (100 A/m) of magnetization. However, this magnetization is very soft and easily removed with low AF magnetization. Results from the most stable samples indicate a shallow positive inclination that may correspond to a reversed polarity.

As with Site 832, physical properties measurements of cores at Site 833 correlate well with the lithostratigraphic units. Values of index properties vs. depth for the upper 375 mbsf show porosity and water content from 50% to 80% and

Table 10. Shear strength data, Hole 833A.

Sample (cm)	Depth (mbsf)	Unit	Undrained shear strength ^a (kPa)
134-833A-			
1H-5, 4	6.04	IA	58.7
1H-7, 4	9.04	IA	49.9
2H-2, 122	12.22	IA	31.5
2H-4, 130	15.30	IA	73.3
2H-6, 90	17.90	IA	68.2
3H-2, 87	21.37	IA	54.3
3H-4, 76	24.26	IA	90.2
3H-6, 87	27.37	IA	73.3
4H-2, 81	30.81	IA	58.7
5H-1, 26	32.86	IA	33.0
5H-2, 26	34.36	IA	18.3
5H-5, 32	38.92	IA	187.0
6H-1, 113	40.34	IA	71.1
6H-4, 113	44.83	IB	5.9
7H-2, 89	47.59	IB	3.7
7H-2, 103	47.73	IB	20.5
7H-4, 40	50.10	IB	7.3
7H-6, 44	53.14	IB	5.1
8H-1, 136	55.36	IB	53.5
8H-3, 84	57.81	IB	15.4
9H-3, 85	61.95	IB	2.2
10H-1, 112	64.02	IB	33.7
10H-1, 123	64.13	IB	10.3
10H-4, 136	68.76	IB	8.1
11H-1, 66	70.36	IB	38.1
11H-5, 16	75.86	IB	12.5
12H-1, 37	76.37	IB	20.5
13H-1, 127	79.27	IB	41.1

^aValues determined by Wykeham-Farrance spring vane-shear apparatus.

low shear strengths. Sediments at Site 833 are slightly drier and less porous than at Site 832. From 200 to 375 mbsf, bulk density increases from 1.60 to 2.00 Mg/m³. At 376 mbsf a distinct sharp decrease in porosity to 20% and a sharp increase in bulk density to 2.50 Mg/m³ occurs and is associated with a lithologic change from Pleistocene volcanic siltstone and calcareous claystone to upper Pliocene coarse volcanic sandstone and basaltic breccia. From 600 to 830 mbsf, porosity increases to 40% or more and bulk density drops to about 2.00 Mg/m³. At 830 mbsf, at the upper contact of the basaltic sill, bulk density increases sharply to 2.82 Mg/m³, with porosity and water content dropping to less than 5%.

Sonic velocities at Site 833 range from 1535 m/s at the seafloor to 2038 m/s at 377 mbsf. From 379 to 600 mbsf, velocities increase sharply to between 3000 and 4500 m/s in volcanic sandstone breccia. They increase sharply again, to above 5000 m/s, in the basaltic sill from 830 to 1000 mbsf.

Because of partial hole collapse and filling problems after drilling ceased, not all of the hole could be logged, and constraints on time prevented us from using the complete complement of logging tools. However, good results were obtained from the geophysical and geochemical tools between 250 and 900 mbsf, with distinct increases in resistivity and velocities taking place between 380 and 430 mbsf, which correlates with volcanic sandstones and breccia at these depths. The contact with the basaltic sill and the overlying sedimentary rocks is easily distinguished in the logs with sharp increases in resistivity, velocities, thorium, and potassium at 830 mbsf.

Initial interpretations of the drilling data at Site 833 indicate that a thick (nearly 400 m) Pleistocene volcanic sandstone and ash sequence exists. Although not as thick as that found at Site 832 (<600 m), this sequence represents a rapid accumulation of Pleistocene volcanic material, emitted from the active Central Chain volcanoes. The existence of volcanic breccia at about

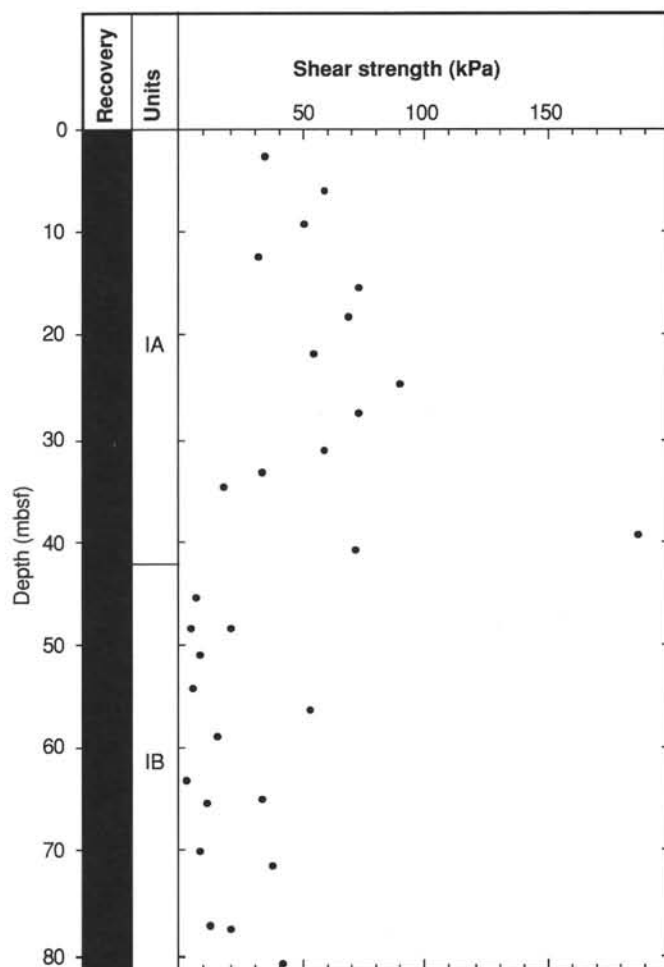


Figure 52. Shear strength vs. depth in Hole 833A.

400–560 mbsf suggests uplift and erosion of volcanic rocks on Maewo Island. A much thicker (>350 m) Pliocene sequence exists at Site 833, compared to only about 70 m recovered at Site 832; however, nearly half of this sequence is composed of basaltic sills that may have been intruded into the Pliocene sedimentary rocks as late as the Pleistocene. Initial evaluation of this sill complex indicates the rocks are highly potassic and share similar petrology with the Central Chain.

REFERENCES

- Bardsell, M., Smith, I.E.M., and Sporli, K. B., 1982. The origin of reversed geochemical zoning in the Northern New Hebrides volcanic arc. *Contrib. Mineral. Petrol.*, 81:148–155.
- Briqueu, L., 1984. Etude du magmatisme associé aux zones de subduction à l'aide de traceurs géochimiques multiples: éléments trace et rapports isotopiques ⁸⁷Sr/⁸⁶Sr et ¹⁴³Nd/¹⁴⁴Nd [Thèse]. Univ. Montpellier, Documents et Travaux du Centre de Géologie et de Géophysique, No. 5.
- Carney, J. N., 1986. *Geology of Maewo*. Regional Rept.—Vanuatu Dept. Geol., Mines, and Rural Water Supplies.
- Chase, T. E., and Seekins, B. A., 1988. Submarine topography of the Vanuatu and southeastern Solomon Islands regions. In Greene, H. G., and Wong, F. L. (Eds.), *Geology and Offshore Resources of Pacific Island Arcs—Vanuatu Region*. Circum-Pac. Council. Energy and Miner. Resour., Earth Sci. Ser., 8:201–224.
- Claypool, G. E., and Kaplan, I. R., 1974. The origin and distribution of methane in marine sediments. In Kaplan, I. R. (Ed.), *Natural Gases in Marine Sediments*: New York (Plenum), 99–139.

- Daniel, J., Gérard, M., Mauffet, A., Boulanger, D., Cautin, B., Collot, J.-Y., Durand, J., Fisher, M., Greene, H. G., Michaux, P., Pelletier, B., Pezzimenti, A., Renard, V., Schaming, M., Tissot, J. D., 1989. Deformation comprehensive d' un bassin intra-arc dans un contexte de collision ride/arc: le bassin d'Aoba, arc des Nouvelles-Hebrides. *C. R. Acad. Sci. Ser. 2*, 308:239-245.
- Dupuy, C., Dostal, J., Marcellot, G., Bougault, H., Joron, J. L., and Treuil, M., 1982. Geochemistry of basalts from central and southern New Hebrides arc: implication for their source rock composition. *Earth Planet. Sci. Lett.*, 60:207-225.
- Gieskes, J., and Gamot, T., in press. Chemical methods for interstitial water analysis on JOIDES Resolution. *ODP Tech. Note*.
- Gieskes, J. M., 1981. Deep-sea drilling interstitial water studies: implications for chemical alteration of the oceanic crust, layers I and II. In Warne, J. E., Douglas, R. G., and Winterer, E. L. (Eds.), *The Deep Sea Drilling Project: A Decade of Progress*. Soc. Econ. Paleontol. Mineral. Spec. Publ., 32:149-167.
- Gorton, M. P., 1977. The geochemistry and origin of Quaternary volcanism in the New Hebrides. *Geochim. Cosmochim. Acta*, 41:1257-1270.
- Hills, S. J., and Thierstein, H. R., 1989. Plio-Pleistocene calcareous plankton biochronology. *Mar. Micropaleontol.*, 14:67-96.
- Hobart, M. A., and Weissel, J. K., 1987. Geothermal surveys in the Solomon Islands—Woodlark Basin Region. In Taylor, B., and Exon, N. F. (Eds.), *Marine Geology, Geophysics, and Geochemistry of the Woodlark Basin—Solomon Islands*. Circum-Pac. Council. Energy and Miner. Resour., Earth Sci. Ser., 7:49-66.
- Jakes, P. and White, A.J.R., 1972. Major and trace element abundances in volcanic rocks of orogenic areas. *Geol. Soc. Am. Bull.*, 83:29-39.
- Kennett, J. P., and Srinivasan, M. S., 1983. *Neogene Planktonic Foraminifera: A Phylogenetic Atlas*. Stroudsburg, PA (Hutchinson Ross).
- Lawrence, J. R., and Gieskes, J. M., 1981. Constraints on water transport and alteration in the oceanic crust from the isotopic composition of pore water. *J. Geophys. Res.*, 86:7924-7934.
- Macfarlane, A., Carney, J. N., Crawford, A. J., and Greene, H. G., 1988. Vanuatu—a review of the onshore geology. In Greene, H. G., and Wong, F. L. (Eds.), *Geology and Offshore Resources of Pacific Island Arcs—Vanuatu Region*. Circum-Pac. Council. Energy and Miner. Resour., Earth Sci. Ser., 8:45-92.
- Marcelot, G., Maury, R. C., and Lefevre, C., 1983. Mineralogy of Erromango lavas (New Hebrides): evidence of an early stage of fractionation in island arc basalts. *Lithos*, 16:135-151.
- Masclé, A., Moore, J. C., et al., 1988. *Proc. ODP, Init. Repts.*, 110: College Station, TX (Ocean Drilling Program).
- Okada, H., and Bukry, D., 1980. Supplementary modification and introduction of code numbers to the low-latitude coccolith biostratigraphic zonation (Bukry, 1973; 1975). *Mar. Micropaleontol.*, 5:321-325.
- Pearce, J. A., 1983. The role of sub-continental lithosphere in magma genesis at destructive plate margins. In Hawkesworth, C. J., and Norry, M. J. (Eds.), *Continental Basalts and Mantle Xenoliths*: Nantwich (Shiva), 230-250.
- Suess, E., von Huene, R., et al., 1988. *Proc. ODP, Init. Repts.*, 112: College Station, TX (Ocean Drilling Program).
- Taylor, S. R., Arculus, R. J., Perfit, M. R., and Johnson, R. W., 1981. Island arc basalts. In *Basaltic Volcanism on the Terrestrial Planets* (Basaltic Volcanism Study Project): New York (Pergamon Press), 193-213.

Ms 134A-113

NOTE: All core description forms ("barrel sheets") and core photographs have been printed on coated paper and bound as Section 4, near the back of this volume, beginning on page 581.

Table 11. Thermal conductivity data, Hole 833A.

Sample (cm)	Depth (mbsf)	Unit	Value (W/[m · K])
134-833A-			
1H-1, 75	0.75	IA	0.8909
1H-3, 75	3.75	IA	0.9289
1H-5, 75	6.75	IA	0.8992
1H-6, 75	8.25	IA	0.9303
2H-2, 75	11.75	IA	0.9719
2H-3, 75	13.25	IA	1.0012
2H-5, 75	16.25	IA	0.9936
2H-6, 75	17.75	IA	0.8833
3H-2, 75	21.25	IA	0.9437
3H-3, 75	22.75	IA	0.9915
3H-5, 75	25.75	IA	0.9473
3H-6, 75	27.25	IA	1.0079
4H-1, 75	29.25	IA	1.0243
4H-2, 75	30.75	IA	1.0807
4H-3, 40	31.90	IA	1.0447
5H-1, 75	33.35	IA	0.8903
5H-2, 75	34.85	IA	1.0512
5H-3, 75	36.35	IA	0.9236
5H-4, 75	37.85	IA	0.9430
6H-1, 75	39.95	IA	0.9272
7H-1, 75	45.95	IB	0.9585
7H-2, 75	47.45	IB	0.9094
7H-4, 50	50.20	IB	0.8452
7H-6, 75	53.45	IB	0.9521
8H-1, 75	54.75	IB	1.5083
8H-2, 75	56.22	IB	0.9298
8H-3, 45	57.42	IB	0.8676
10H-1, 75	63.65	IB	0.8719
10H-5, 45	69.35	IB	1.8304
11H-1, 75	70.45	IB	1.2041
11H-2, 75	71.95	IB	1.2160
11H-3, 75	73.45	IB	1.0387
11H-4, 75	74.95	IB	0.9224
12H-1, 30	76.30	IB	1.2032
13H-1, 75	78.75	IB	1.1253
13H-2, 75	80.25	IB	1.9593
13H-3, 60	81.60	IB	1.1470
16X-1, 75	94.45	IIA	0.9650
16X-2, 75	95.95	IIA	0.9825
21X-1, 75	142.75	IIA	1.1185
21X-2, 40	143.90	IIA	1.0047
21X-3, 35	145.35	IIA	0.9308
23X-1, 59	161.89	IIA	0.9411
23X-2, 25	163.02	IIB	0.8065
26X-1, 50	190.80	IIB	0.8311

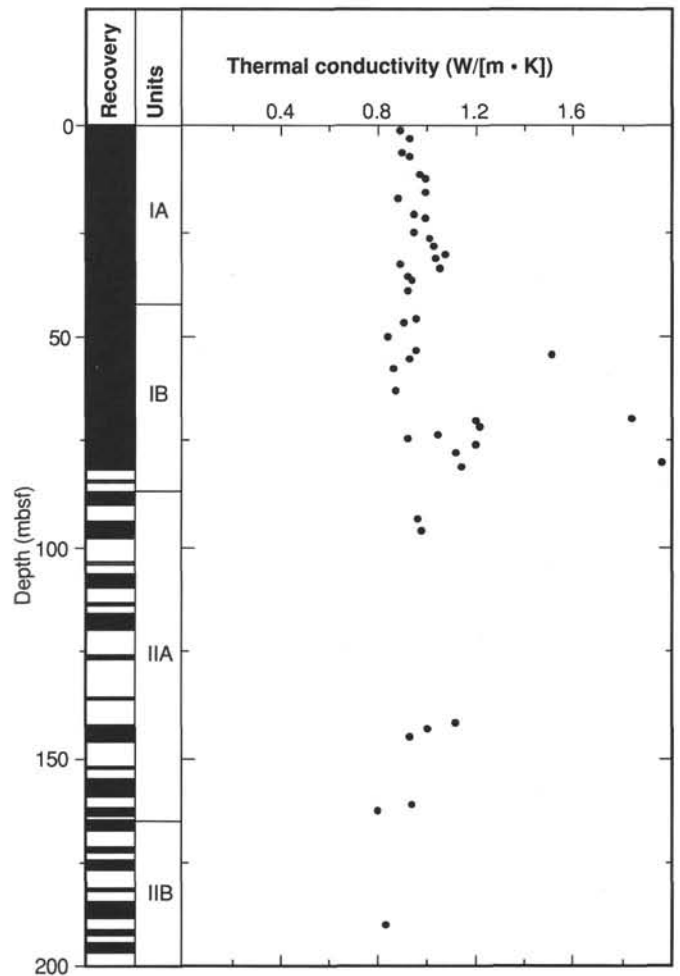


Figure 53. Thermal conductivity vs. depth in Hole 833A.

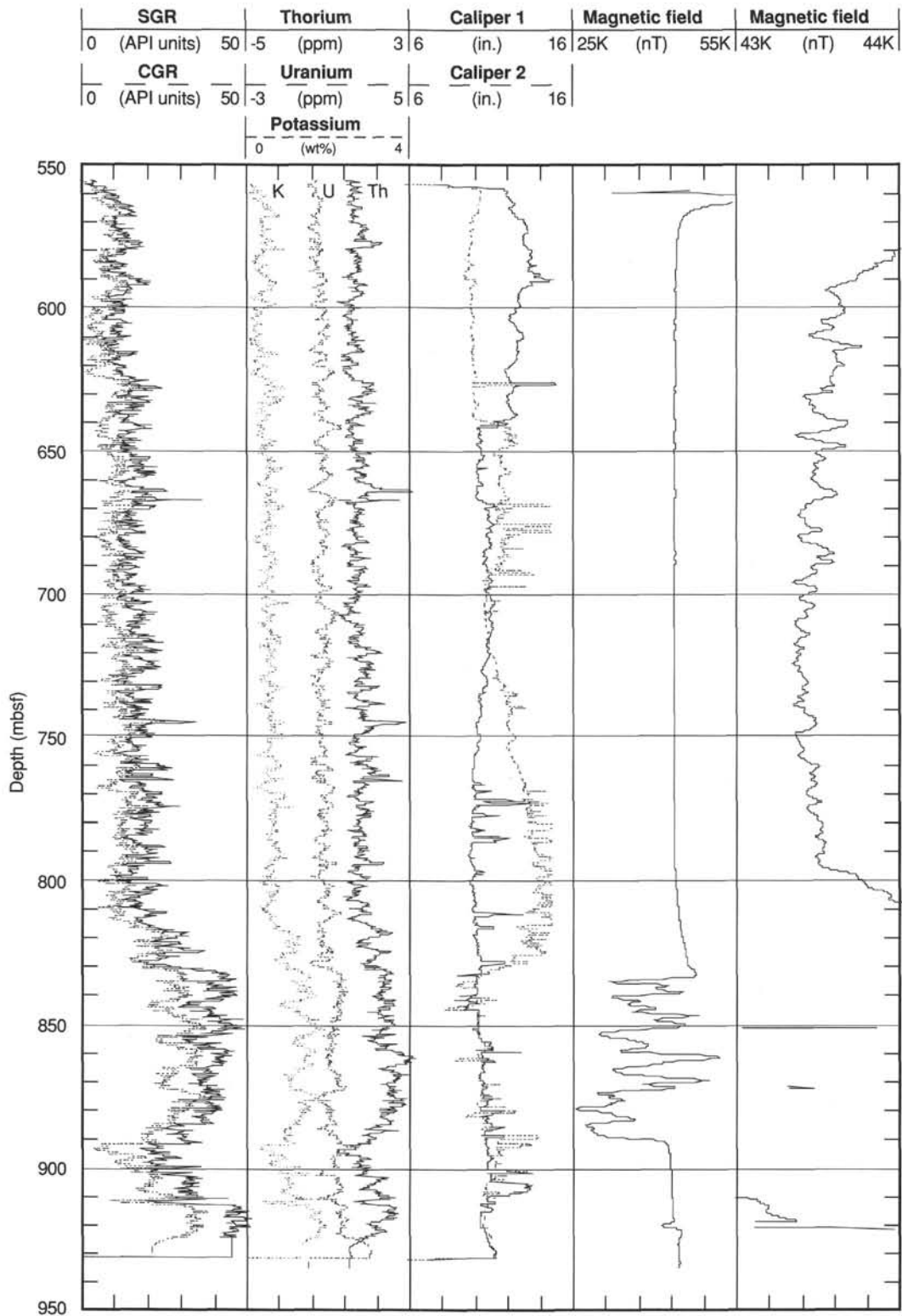


Figure 54. Well-log data recorded using the formation microscanner tool string at Hole 833B from 550 to 950 mbsf. Definitions of the curves and the scales are given on the figure. Abbreviations are: CGR = complete gamma-ray log, SGR = spectral gamma-ray log.

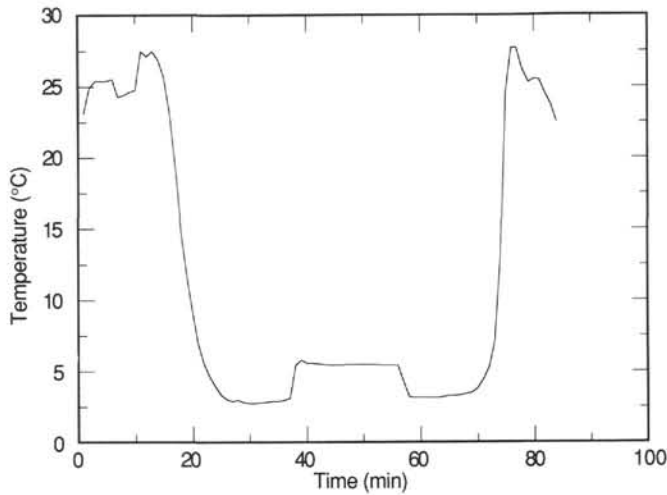


Figure 55. Temperature vs. time for WSTP run 4H in Hole 833A at a depth of 28.5 mbsf.

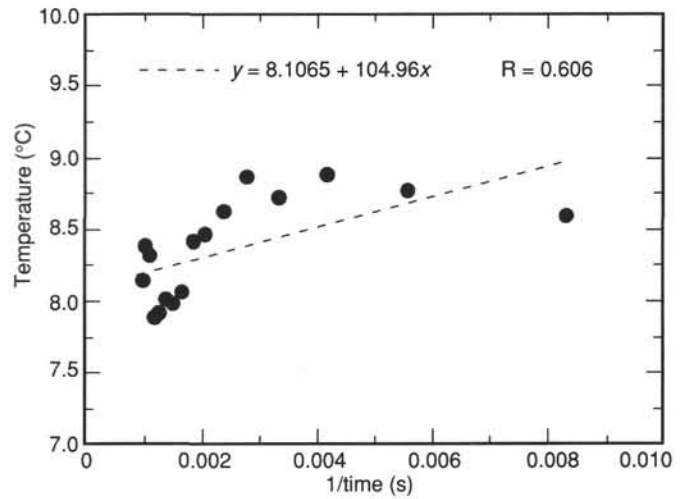


Figure 58. Reduction to equilibrium temperature for WSTP run 9H in Hole 833A. The temperature value at 1/time = 0 is the equilibrium value. The uncertainty in this value caused by the disturbance is at least 0.5°C.

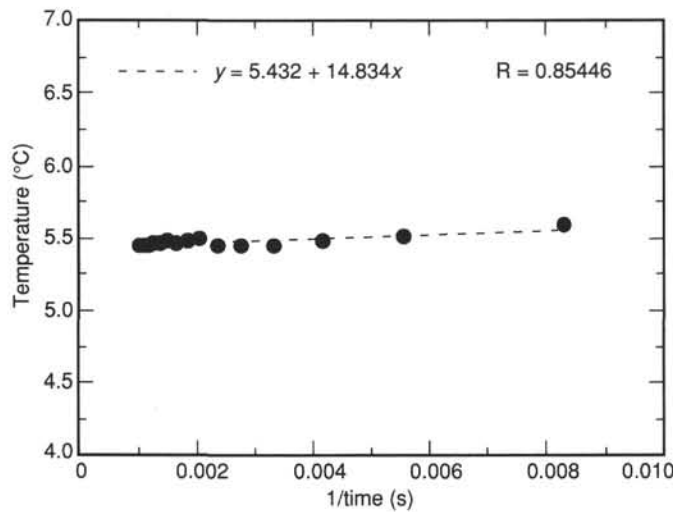


Figure 56. Reduction to equilibrium temperature for water sampler temperature probe WSTP run 4H in Hole 833A. The temperature value at 1/time = 0 is the equilibrium value.

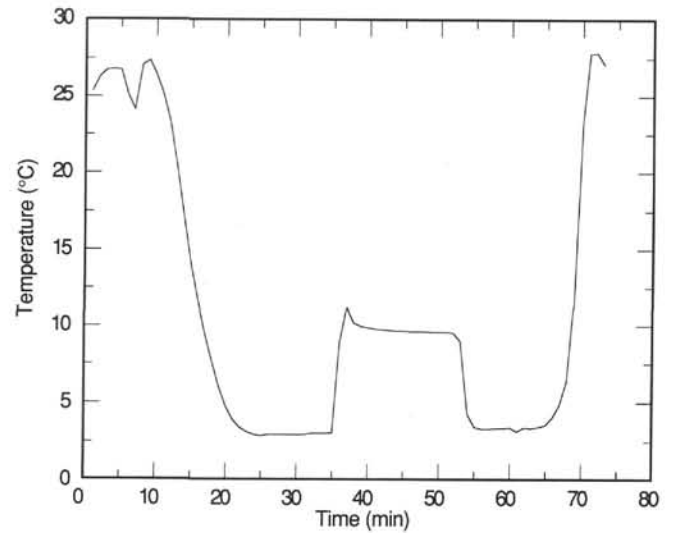


Figure 59. Temperature vs. time for WSTP run 19X in Hole 833A at a depth of 122.6 mbsf.

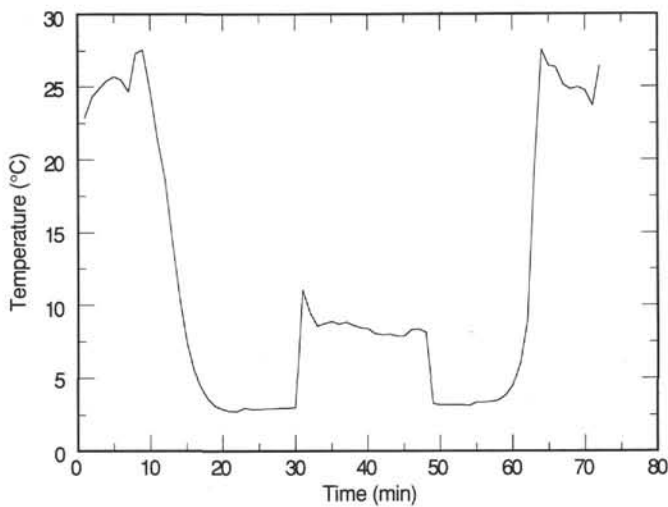


Figure 57. Temperature vs. time for WSTP run 9H in Hole 833A at a depth of 58.0 mbsf. Note the disturbance to the cooling curve while the probe is in the bottom.

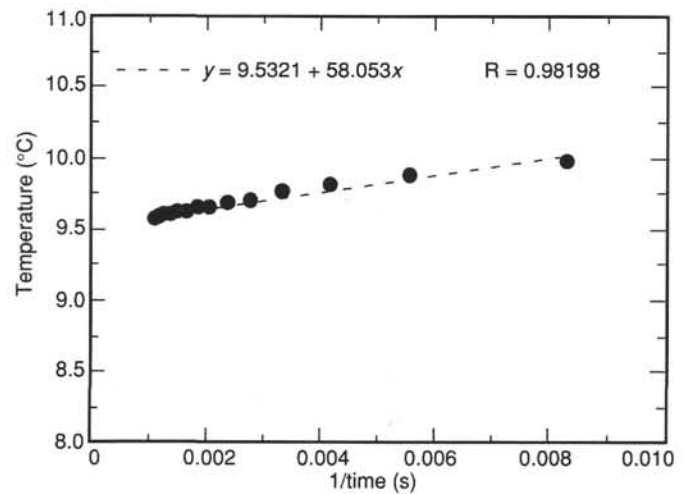


Figure 60. Reduction to equilibrium temperature for WSTP run 19X in Hole 833A. The temperature value at 1/time = 0 is the equilibrium value, which is only slightly higher than that of run 9H, over 60 m higher in the hole.

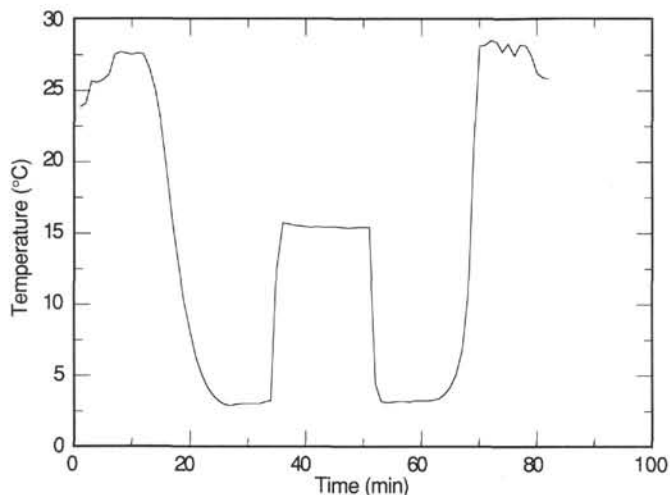


Figure 61. Temperature vs. time for WSTP run 24X in Hole 833A at a depth of 170.9 mbsf.

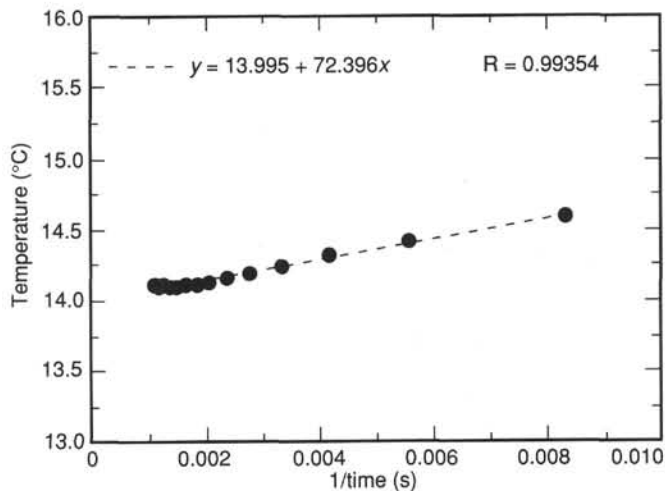


Figure 64. Reduction to equilibrium temperature for WSTP run 27X in Hole 833A. The temperature value at 1/time = 0 is the equilibrium value, which is actually less than the value from run 24X.

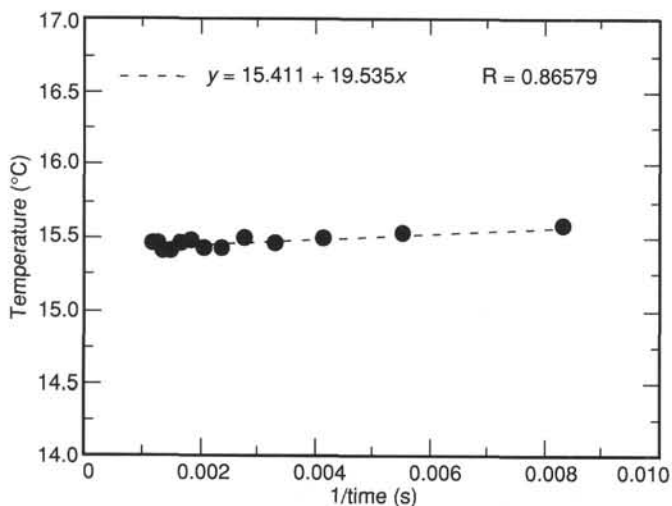


Figure 62. Reduction to equilibrium temperature for WSTP run 24X in Hole 833A. The temperature value at 1/time = 0 is the equilibrium value.

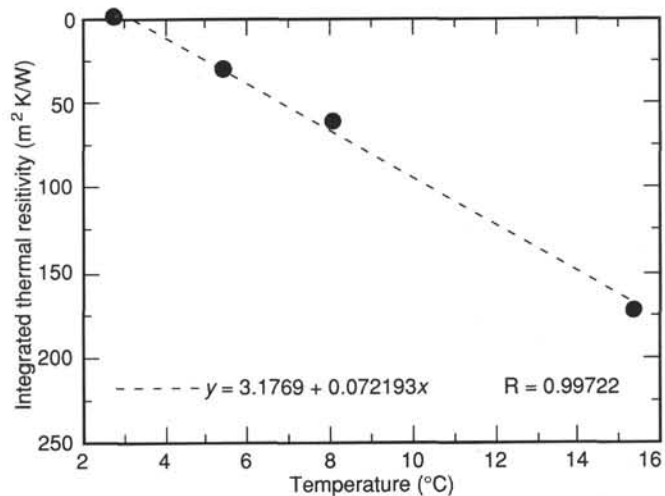


Figure 65. Temperature vs. the depth integral of thermal resistivity. The two "anomalous" temperature points are not plotted. The slope of the linear regression line is the conductive heat flow of 72.2 mW/m².

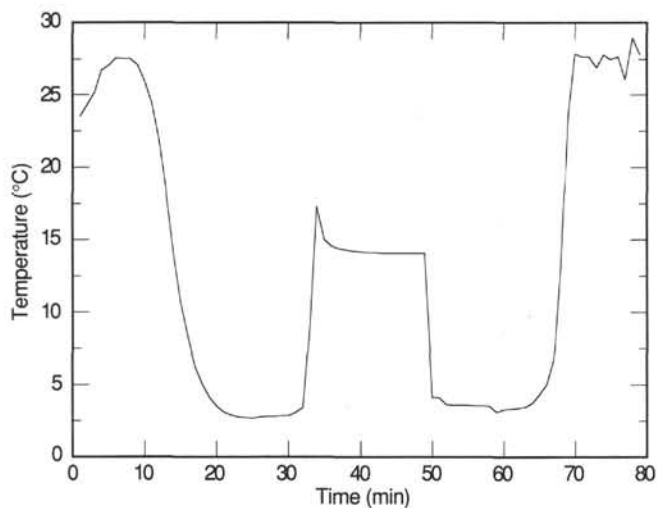


Figure 63. Temperature vs. time for WSTP run 27X in Hole 833A at a depth of 199.5 mbsf.

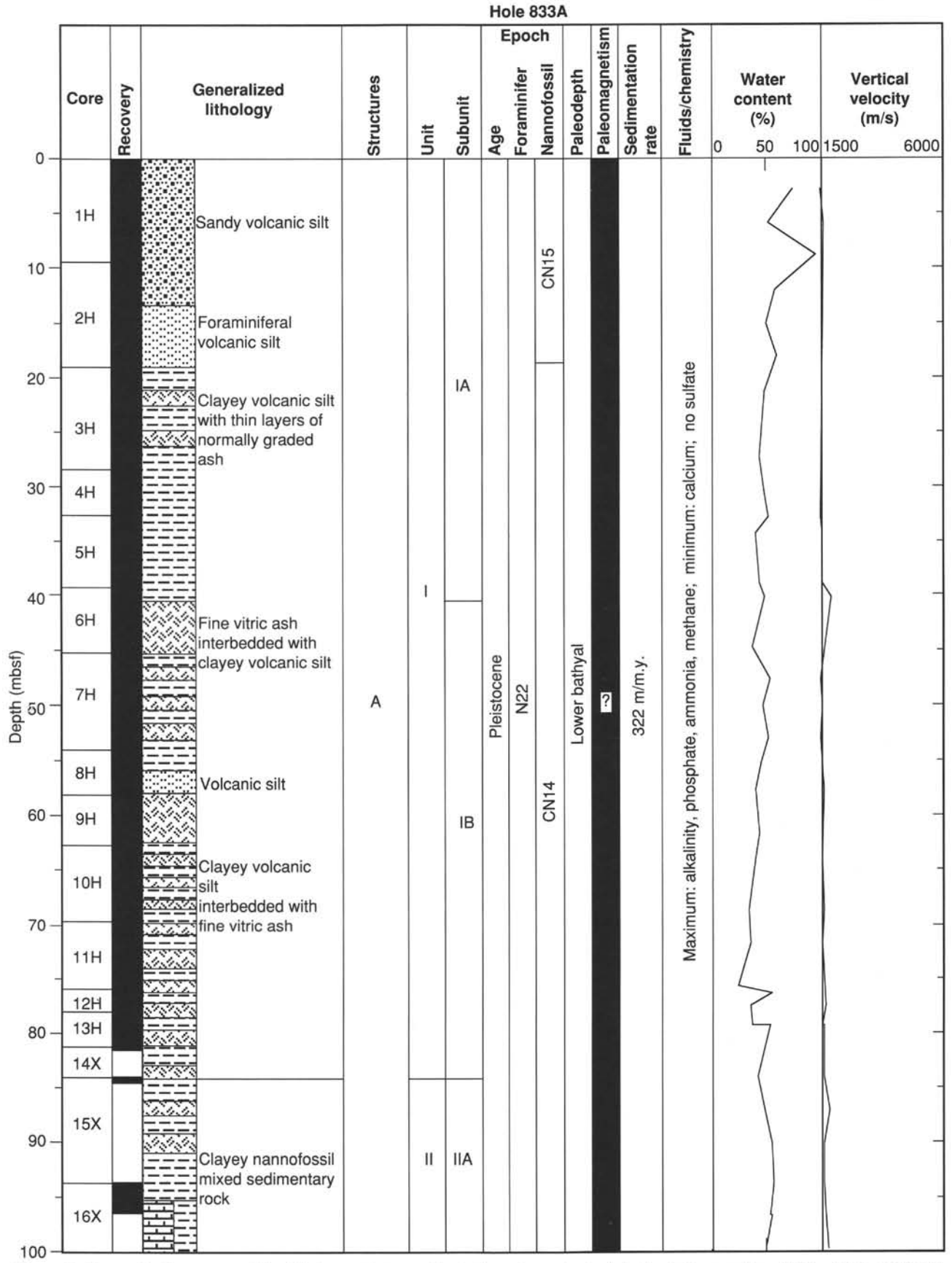


Figure 66. Generalized summary of the lithology, structure, biostratigraphy, and selected physical properties of Holes 833A and 833B. If no data or annotations appear in a particular column, refer to the appropriate section of this chapter for details.

Hole 833A

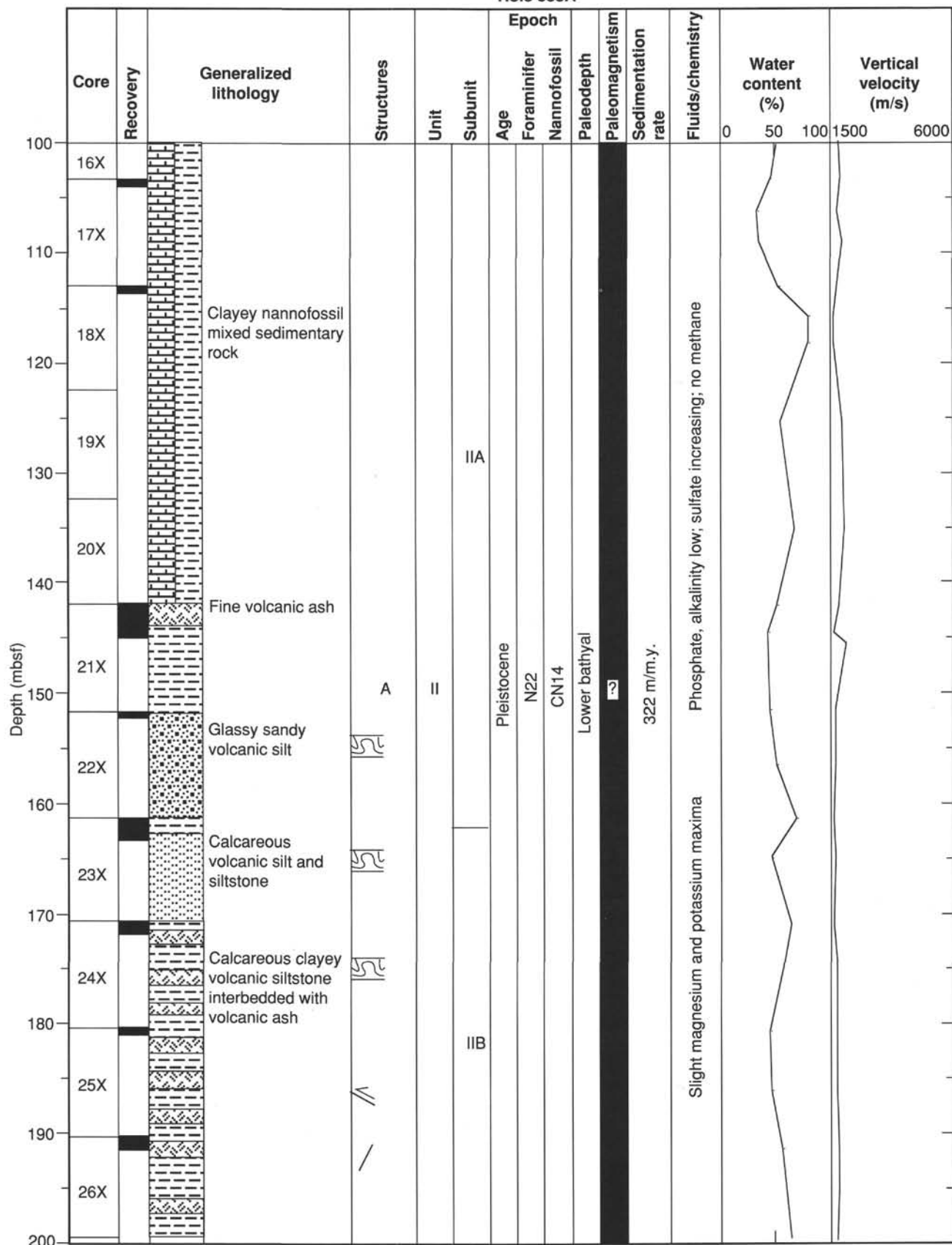


Figure 66 (continued).

Hole 833B

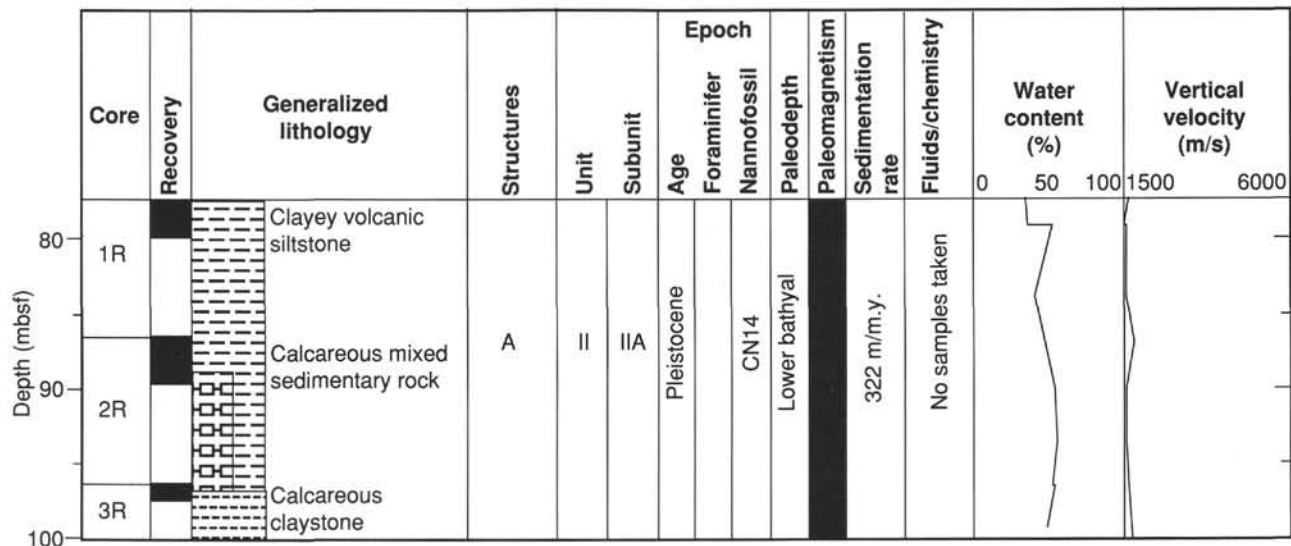


Figure 66 (continued).

Hole 833B

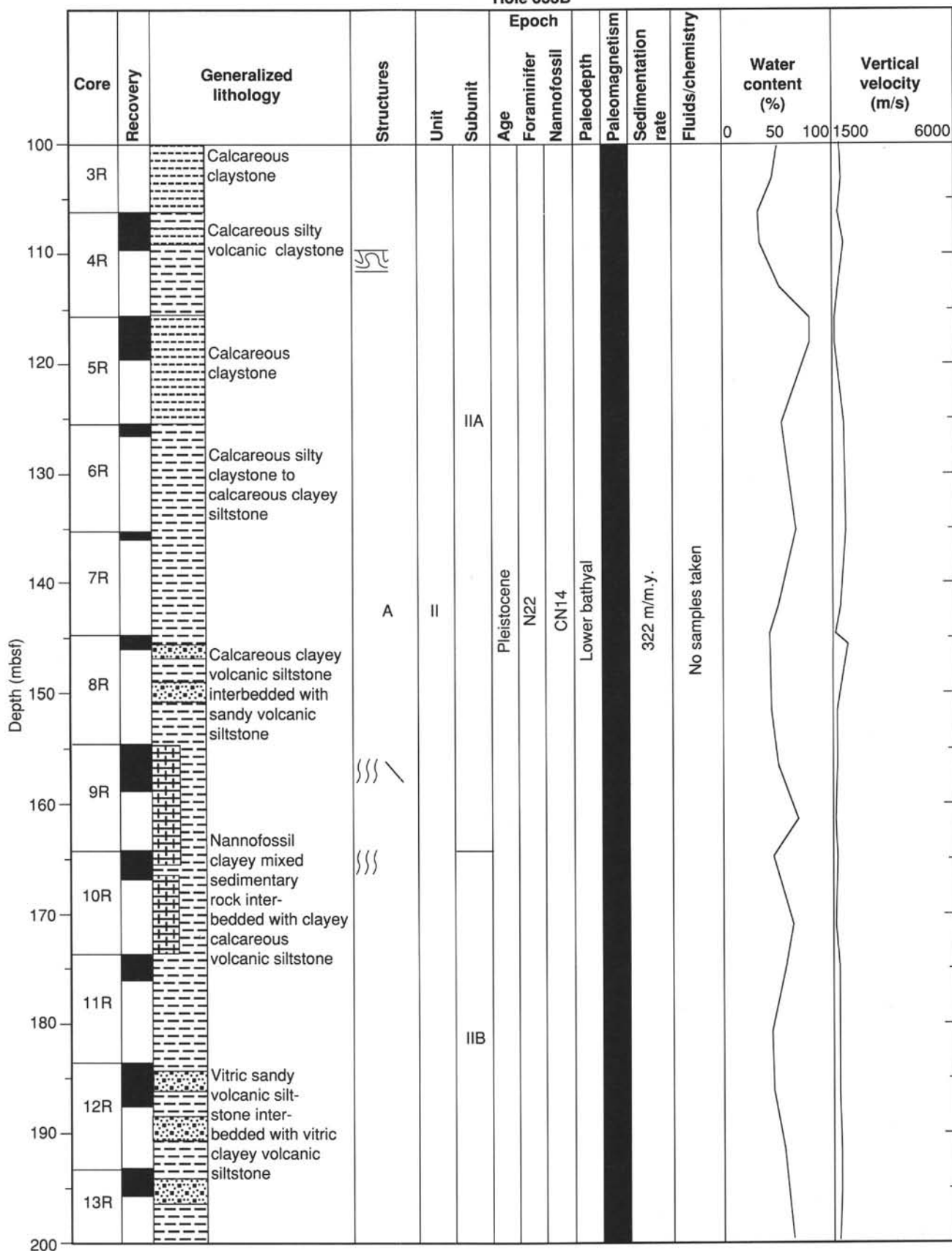


Figure 66 (continued).

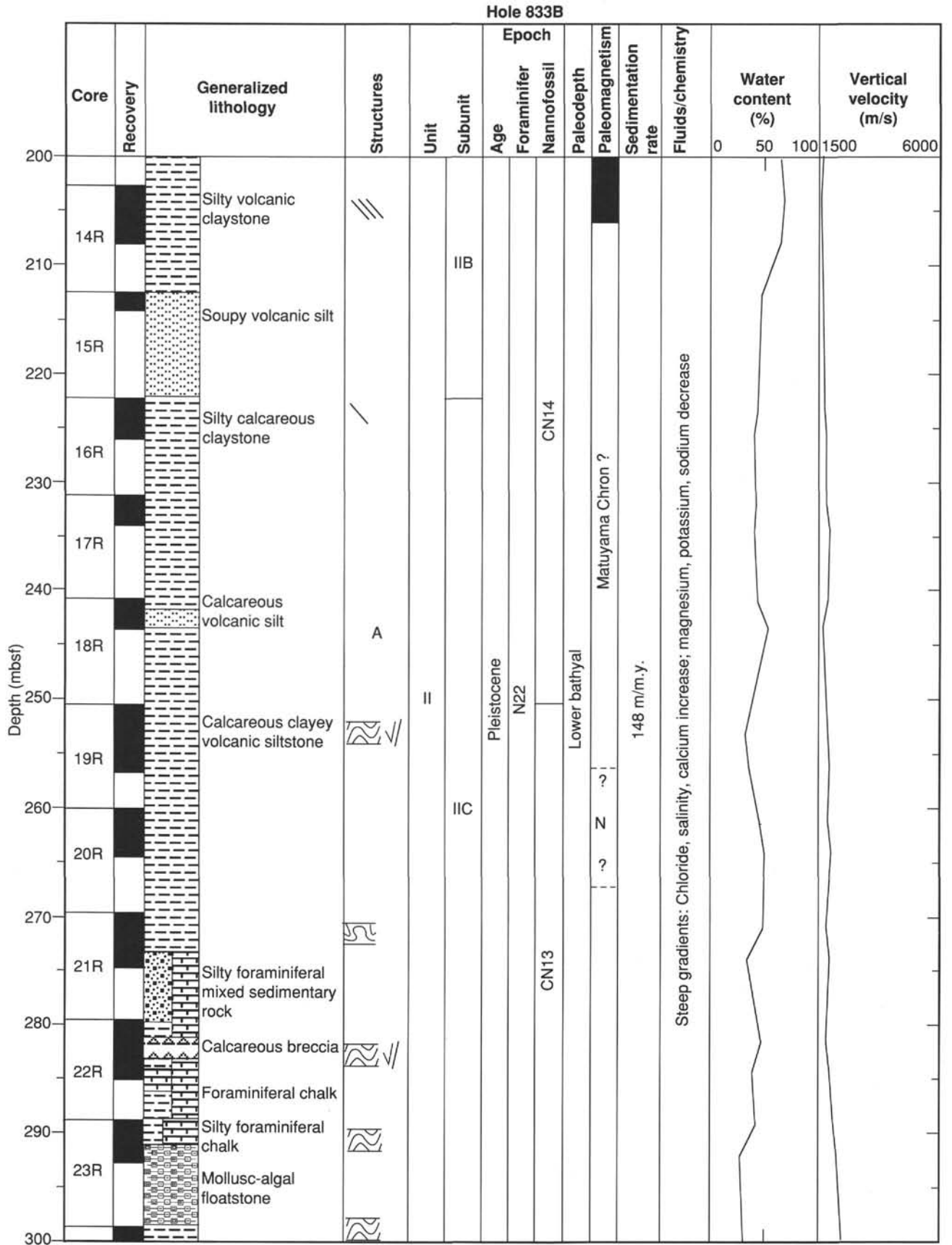


Figure 66 (continued).

Hole 833B

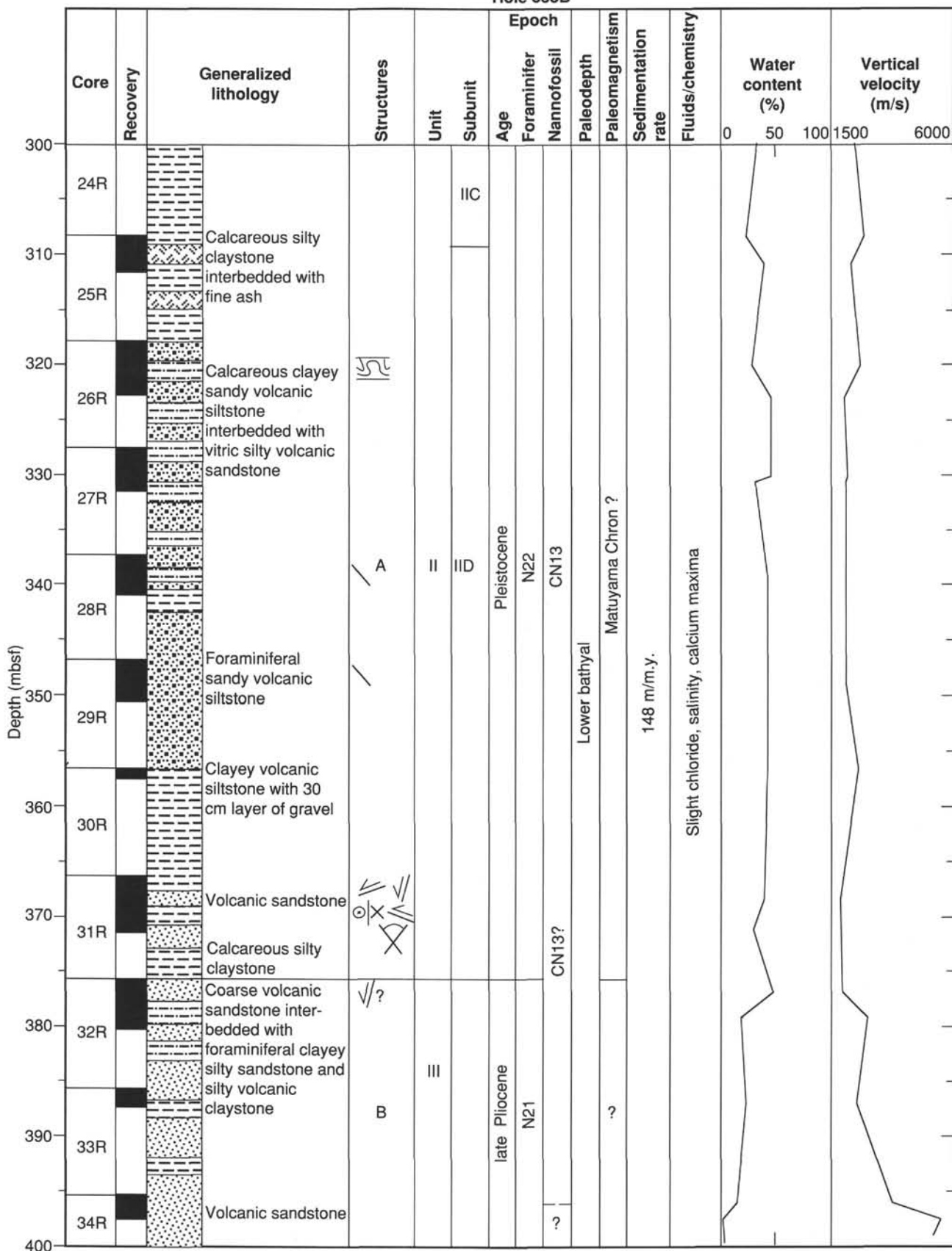


Figure 66 (continued).

Hole 833B

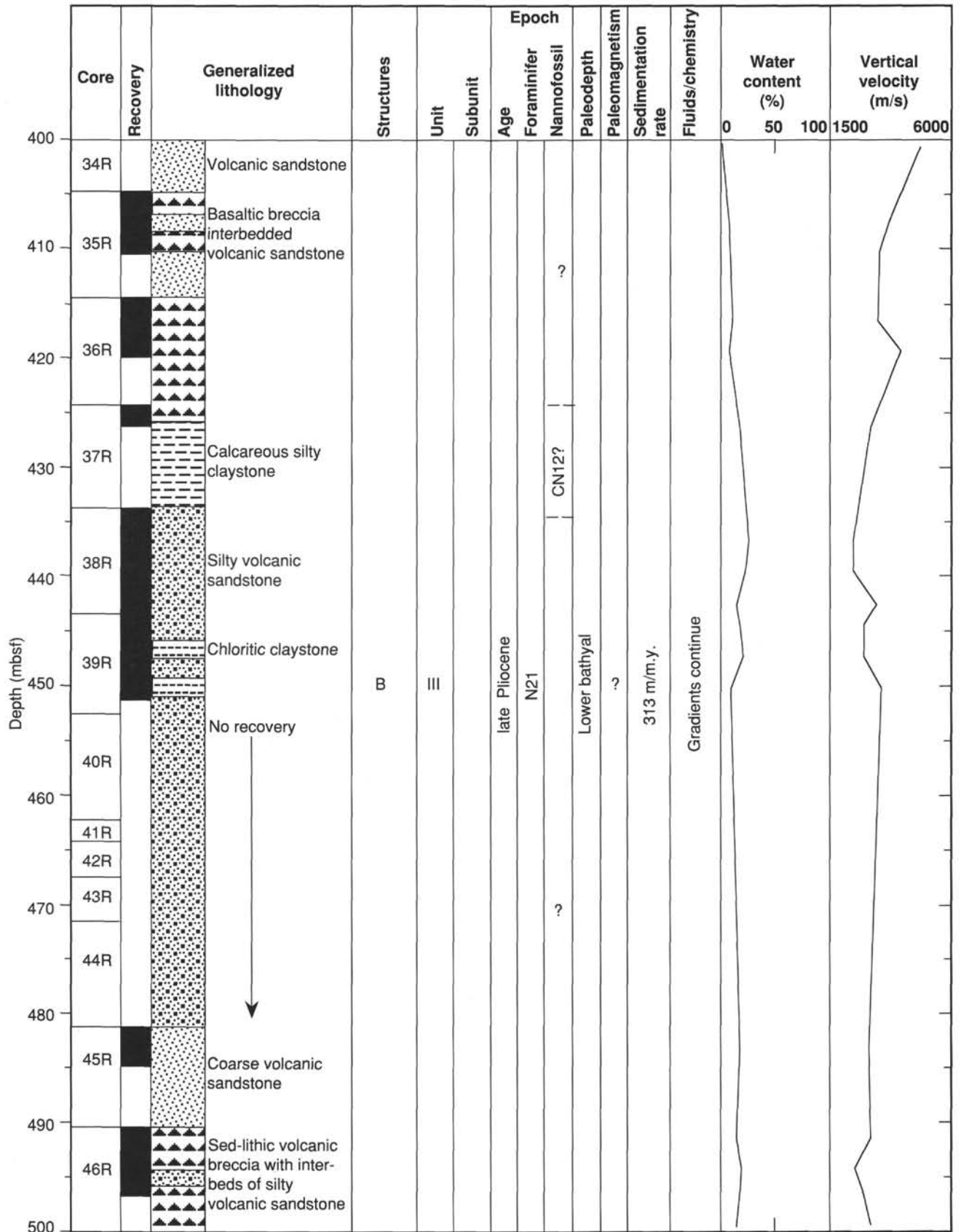


Figure 66 (continued).

Hole 833B

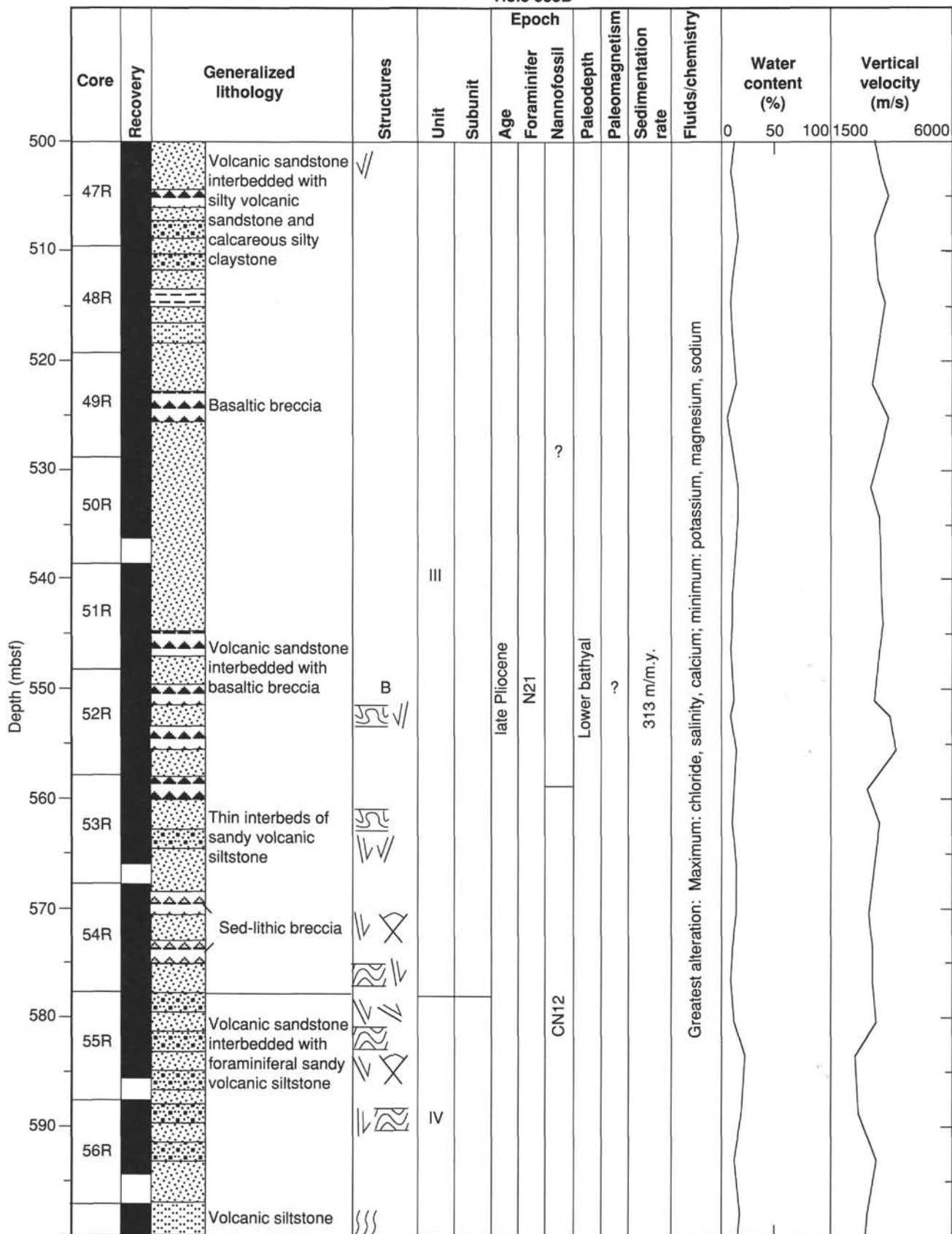


Figure 66 (continued).

Hole 833B

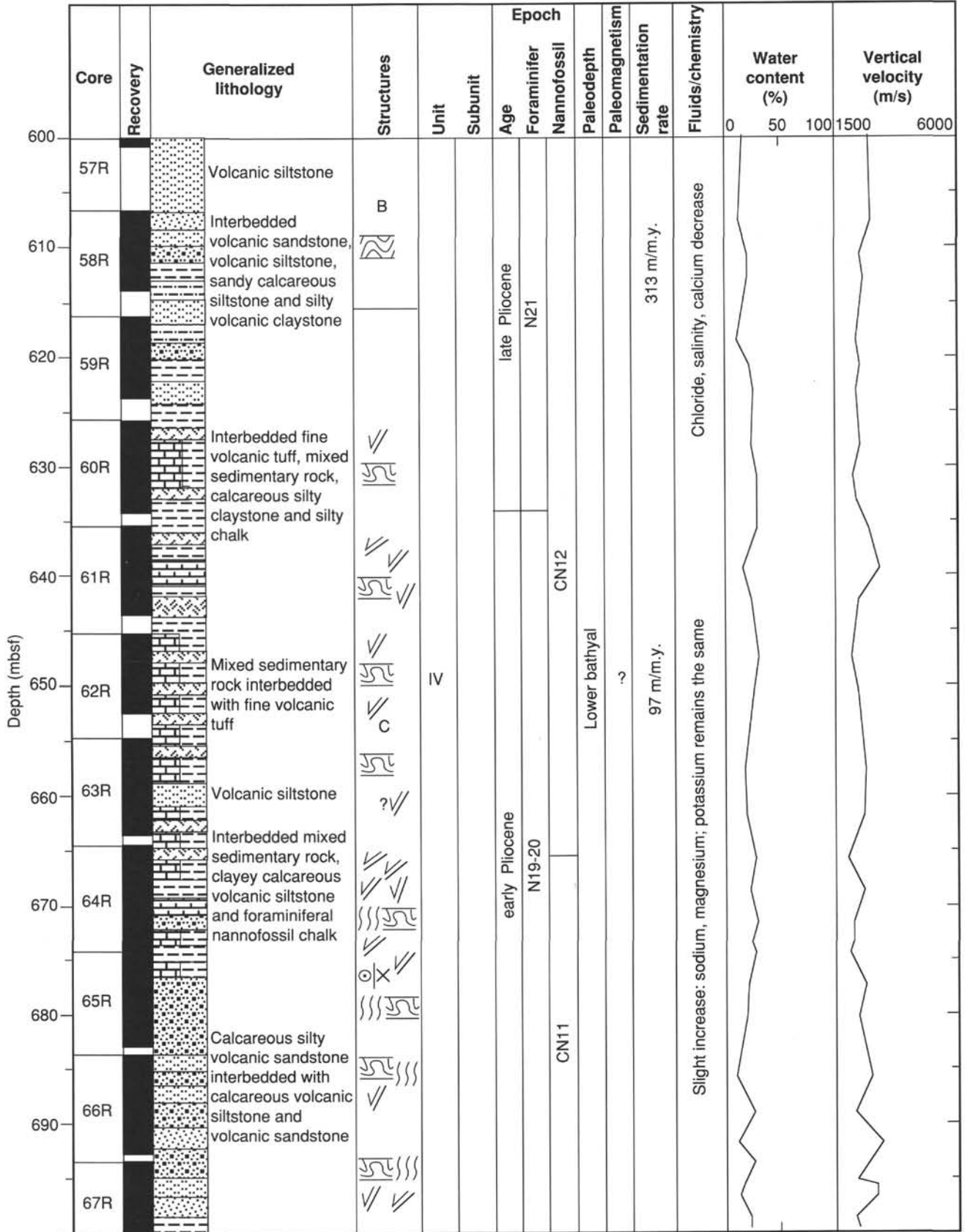


Figure 66 (continued).

Hole 833B

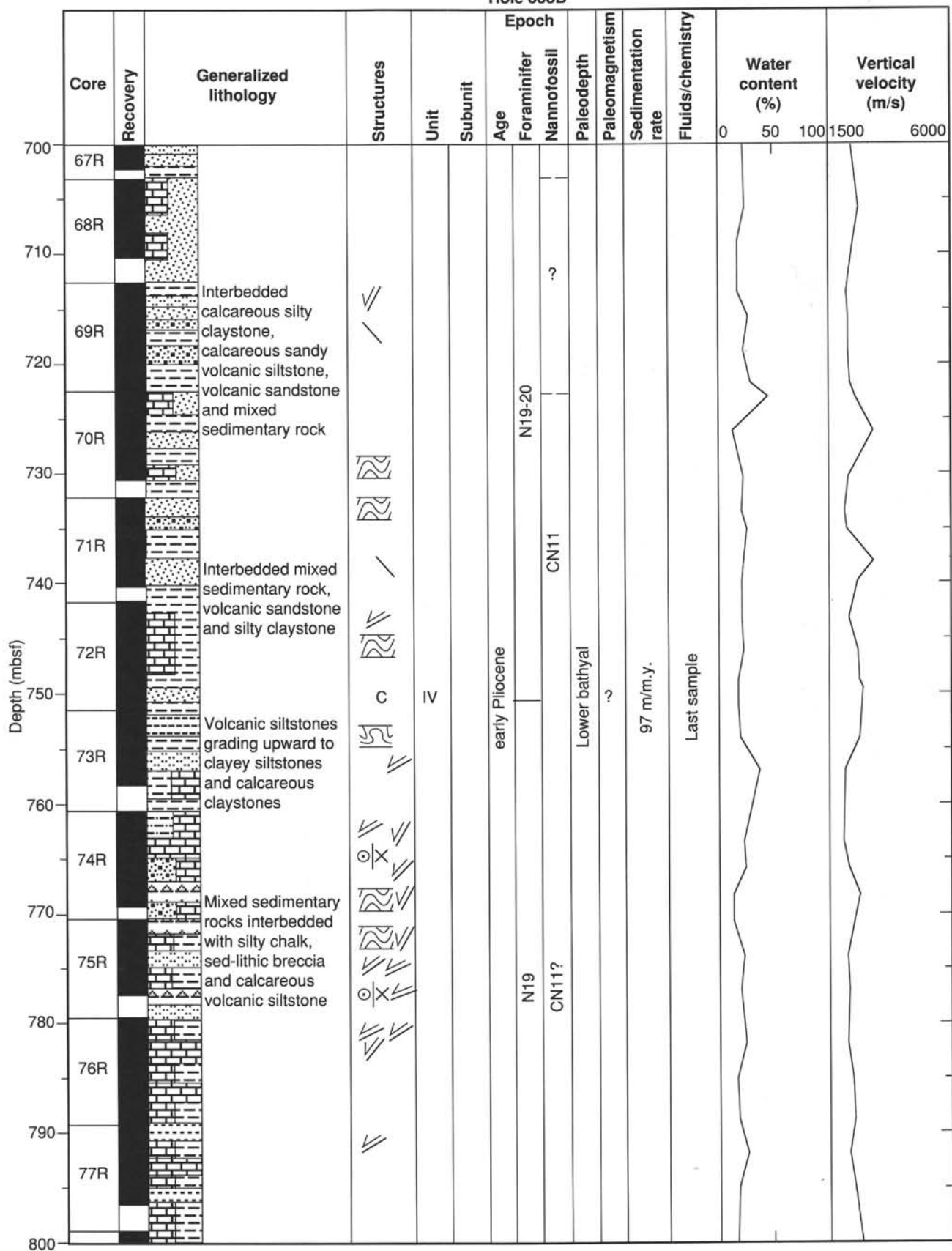


Figure 66 (continued).

Hole 833B

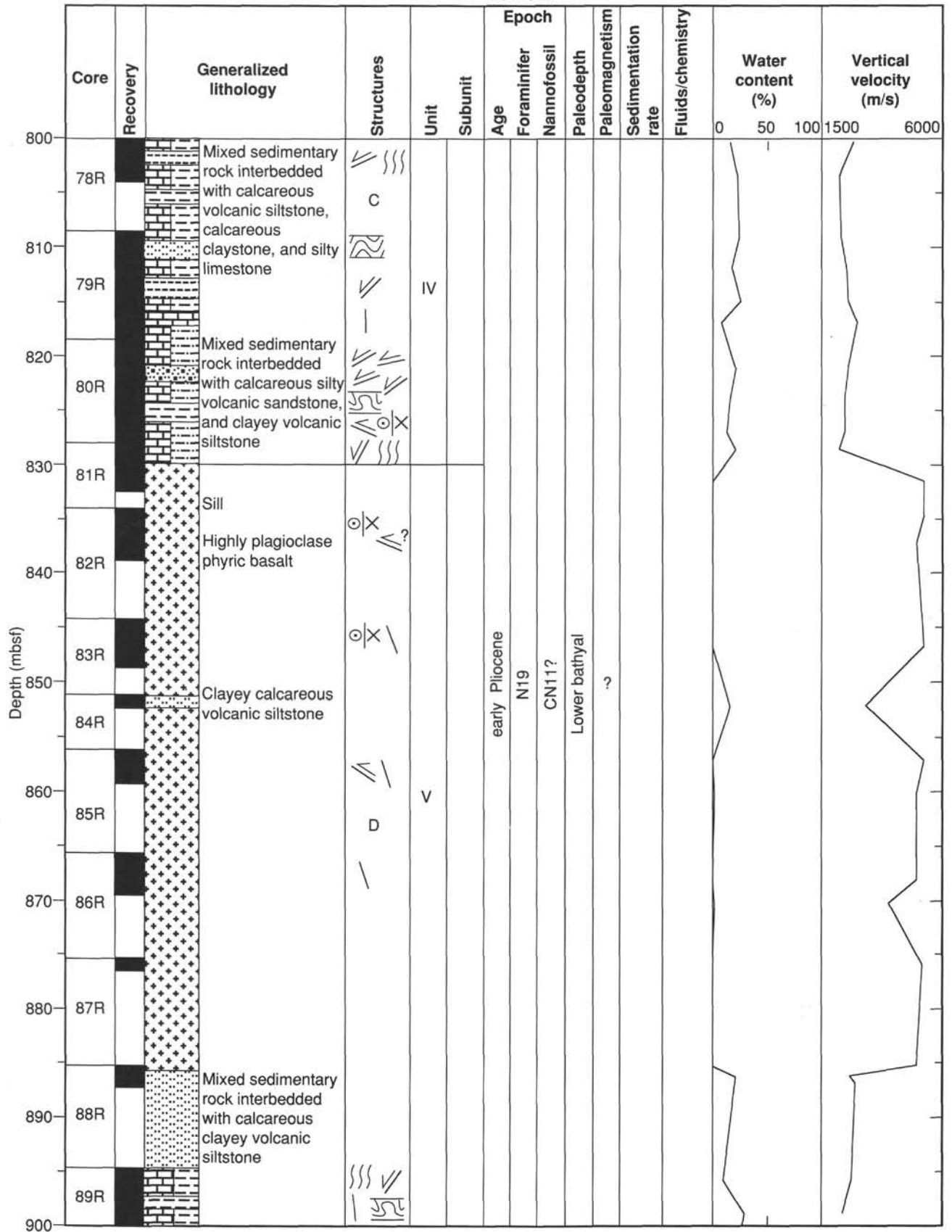


Figure 66 (continued).

Hole 833B

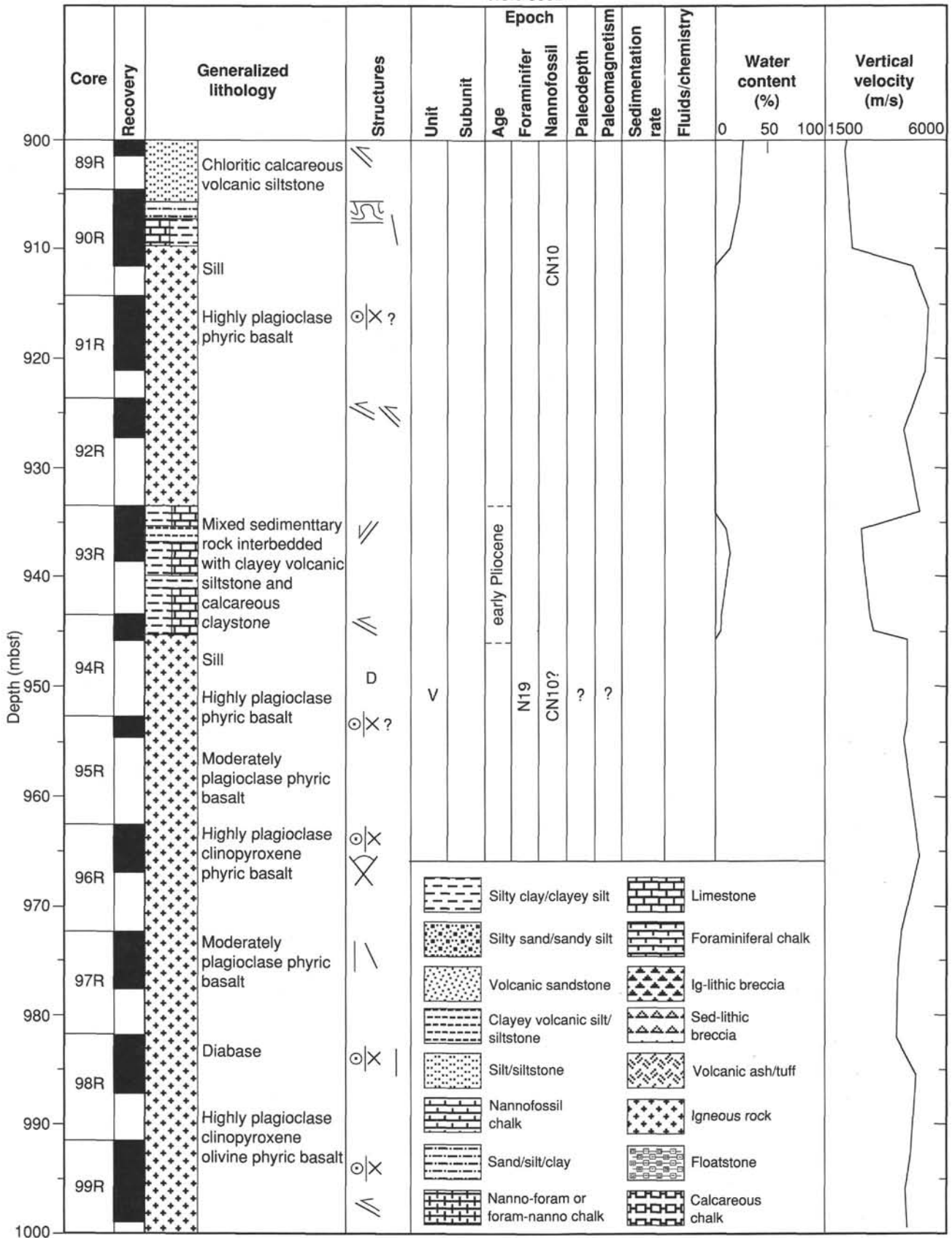
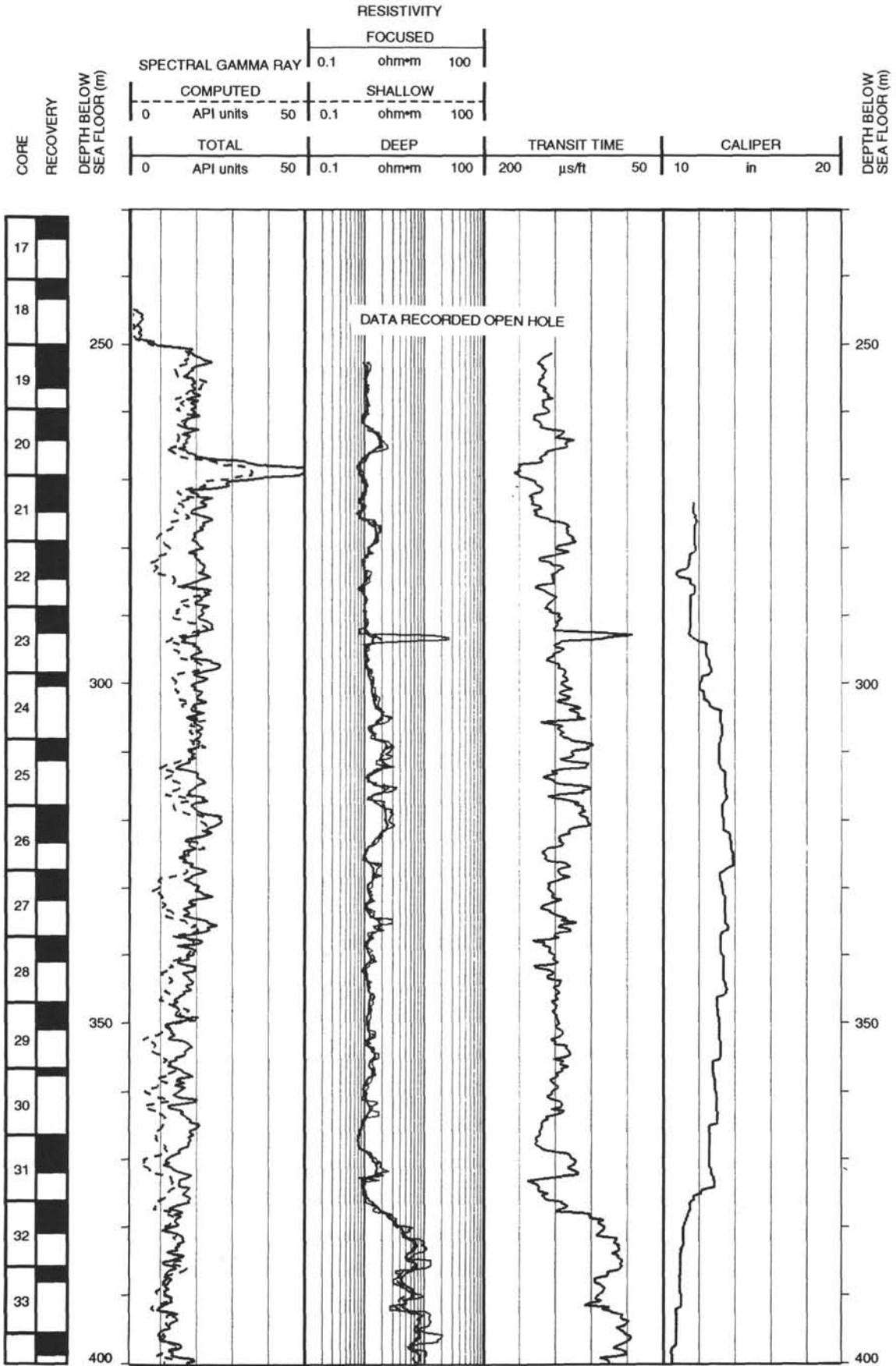
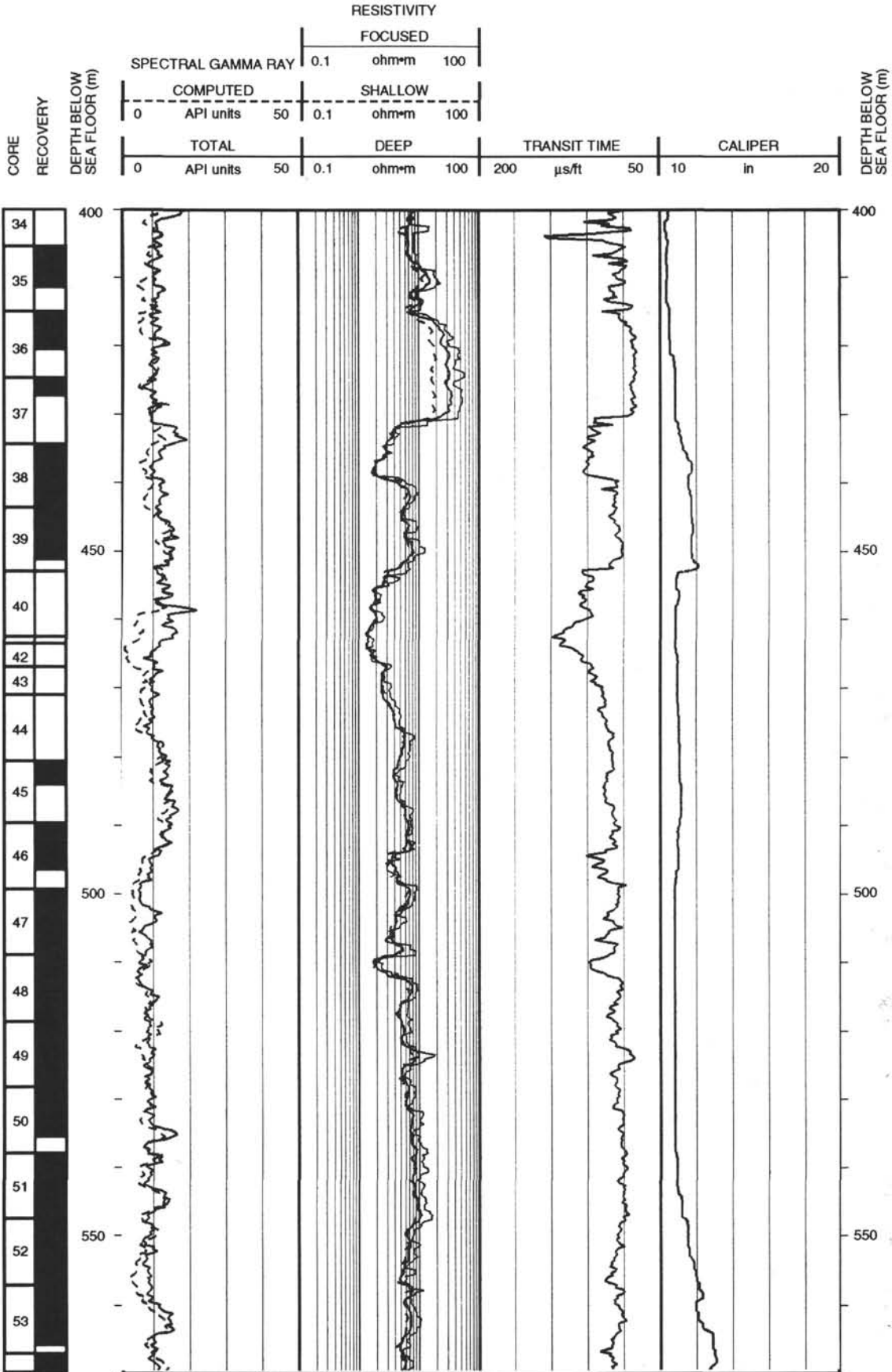


Figure 66 (continued).

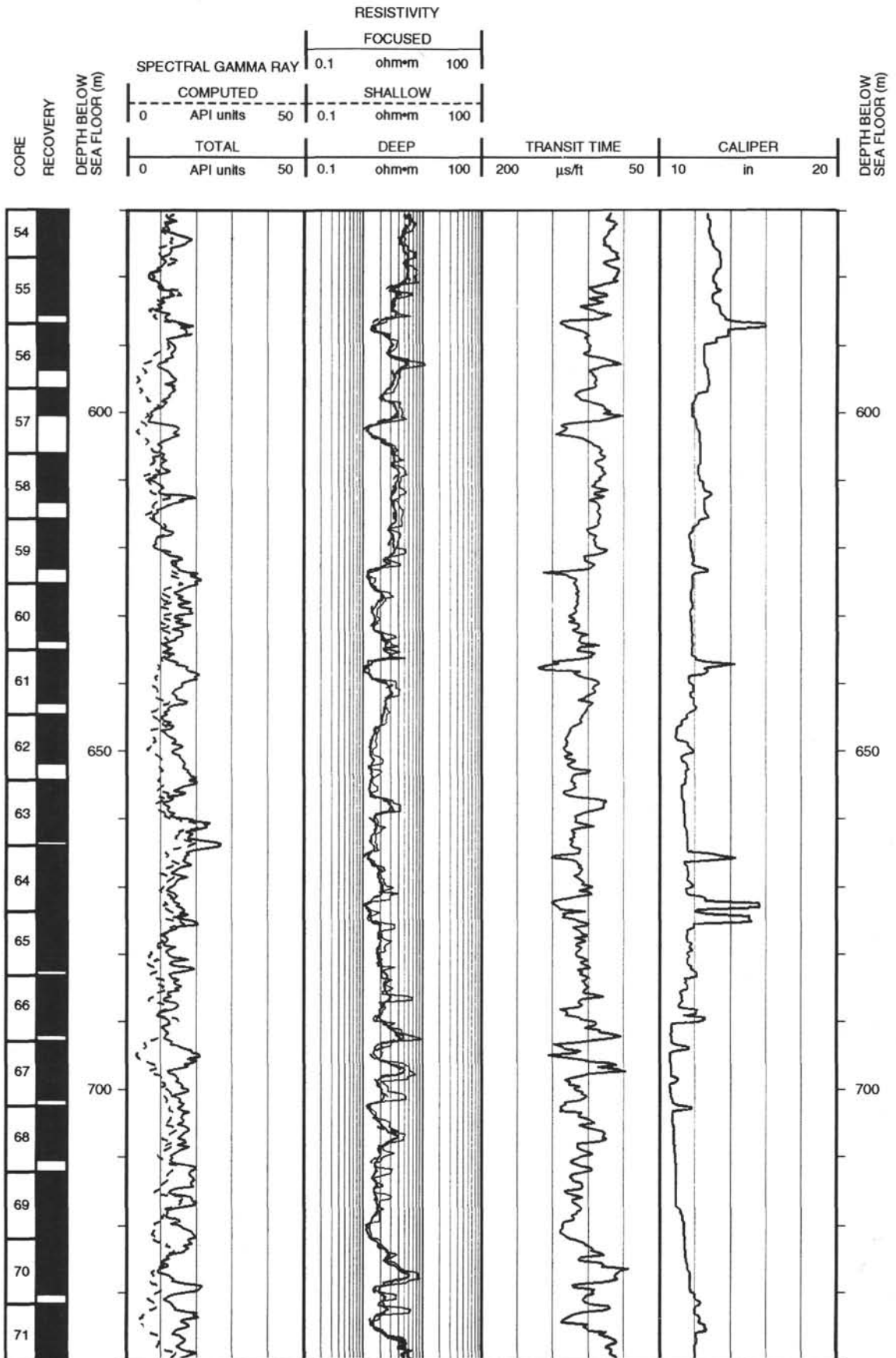
Hole 833B: Resistivity-Sonic-Natural Gamma Ray Log Summary



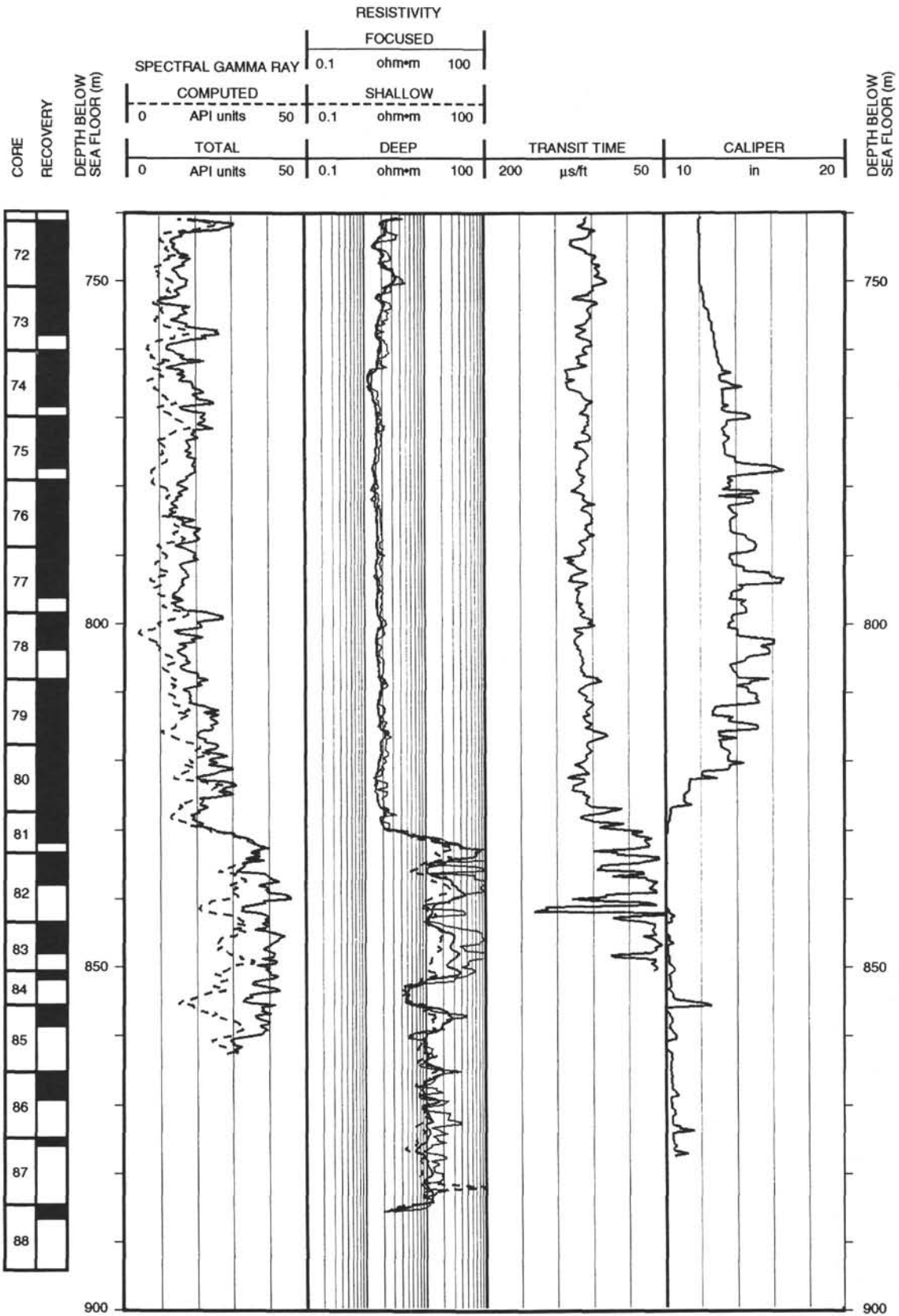
Hole 833B: Resistivity-Sonic-Natural Gamma Ray Log Summary (continued)



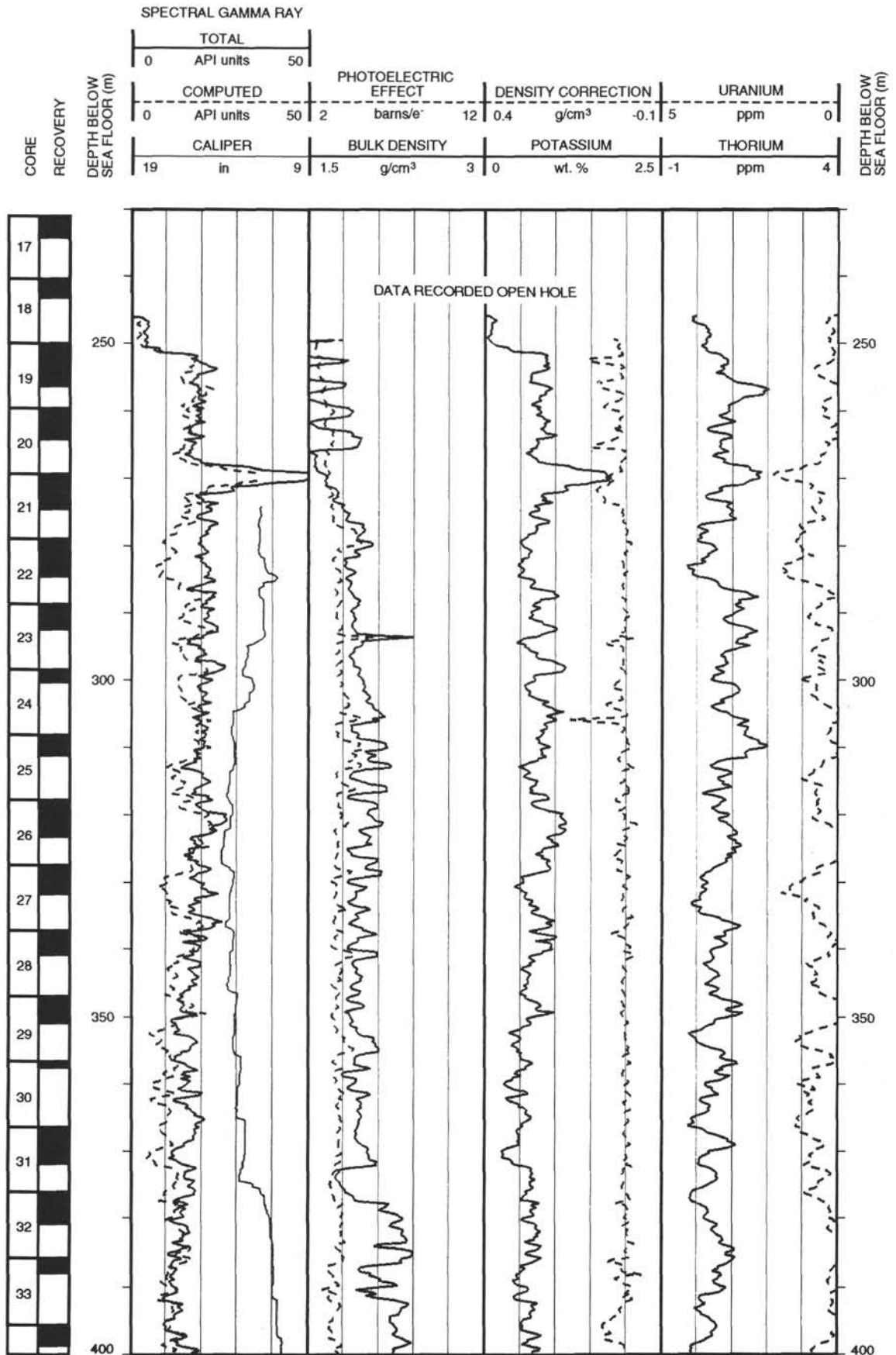
Hole 833B: Resistivity-Sonic-Natural Gamma Ray Log Summary (continued)



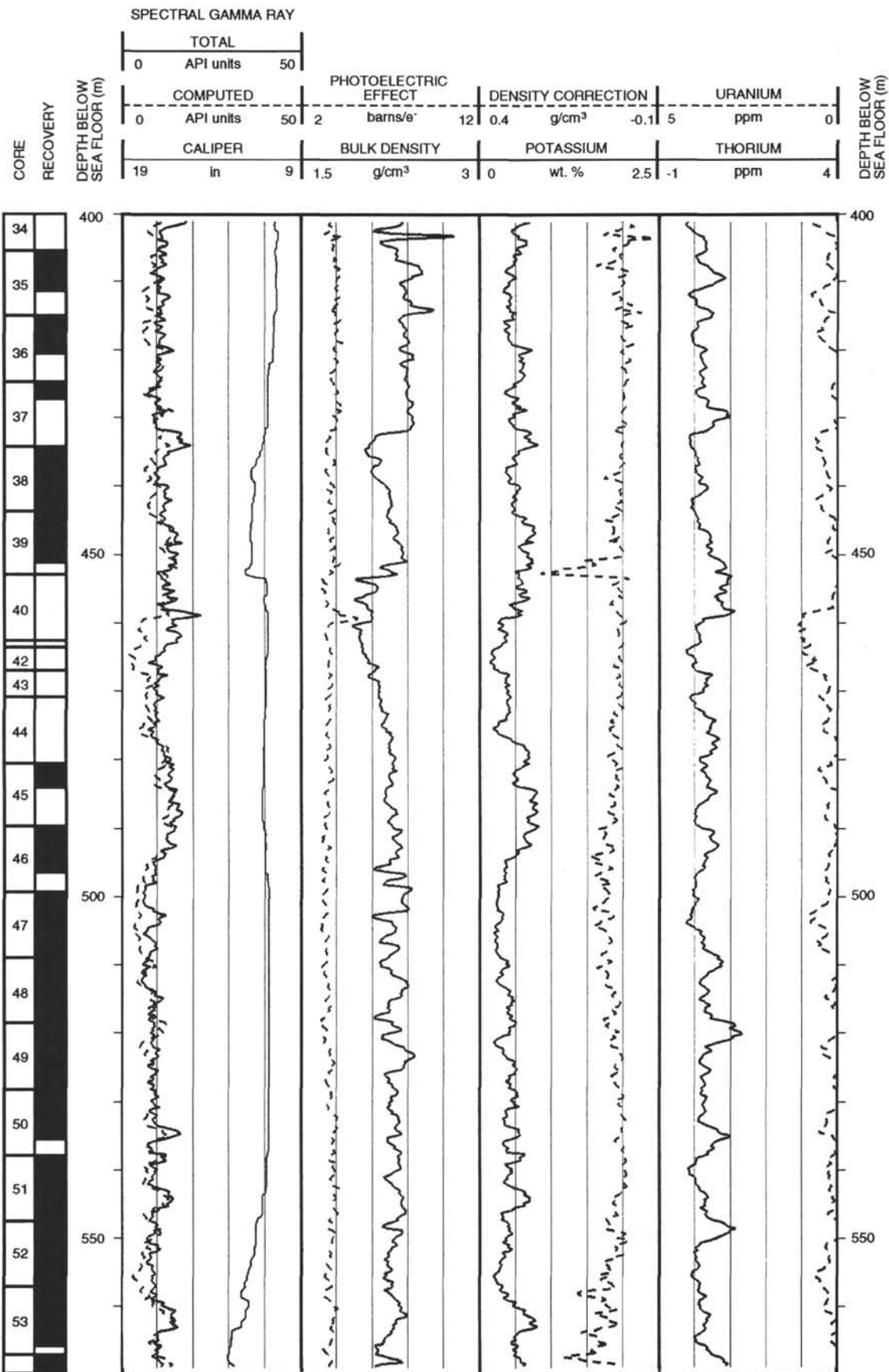
Hole 833B: Resistivity-Sonic-Natural Gamma Ray Log Summary (continued)



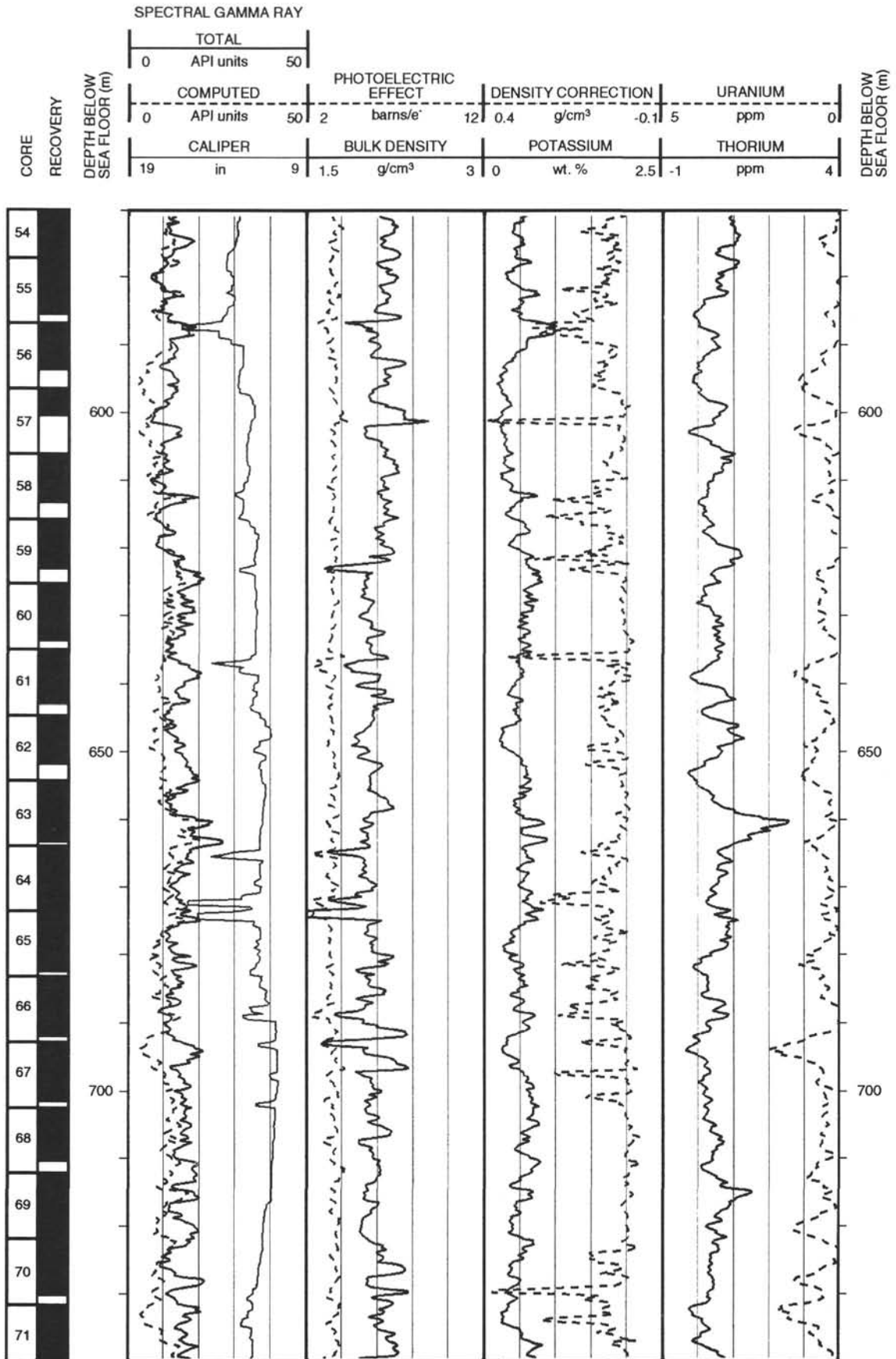
Hole 833B: Density-Natural Gamma Ray Log Summary



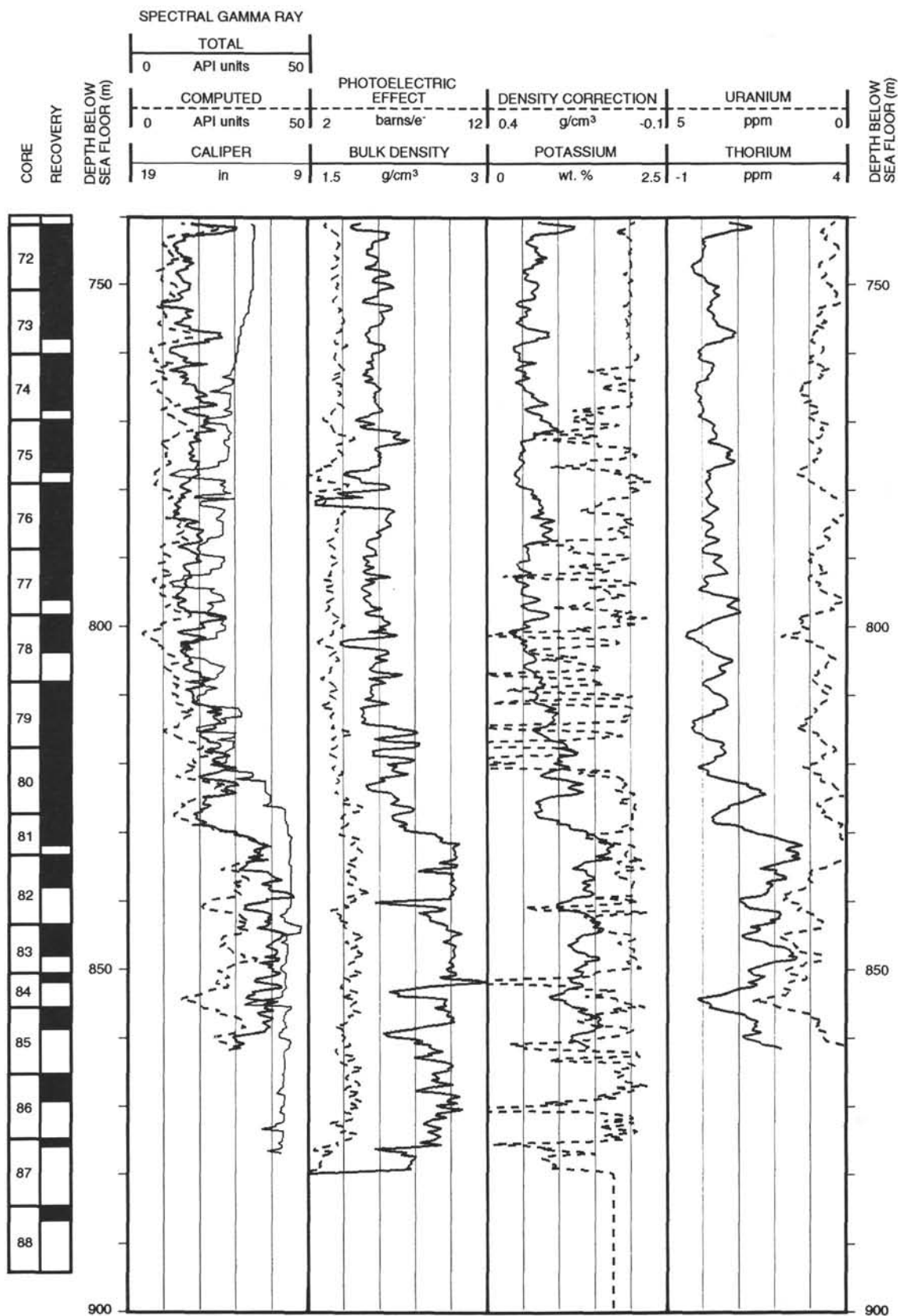
Hole 833B: Density-Natural Gamma Ray Log Summary (continued)



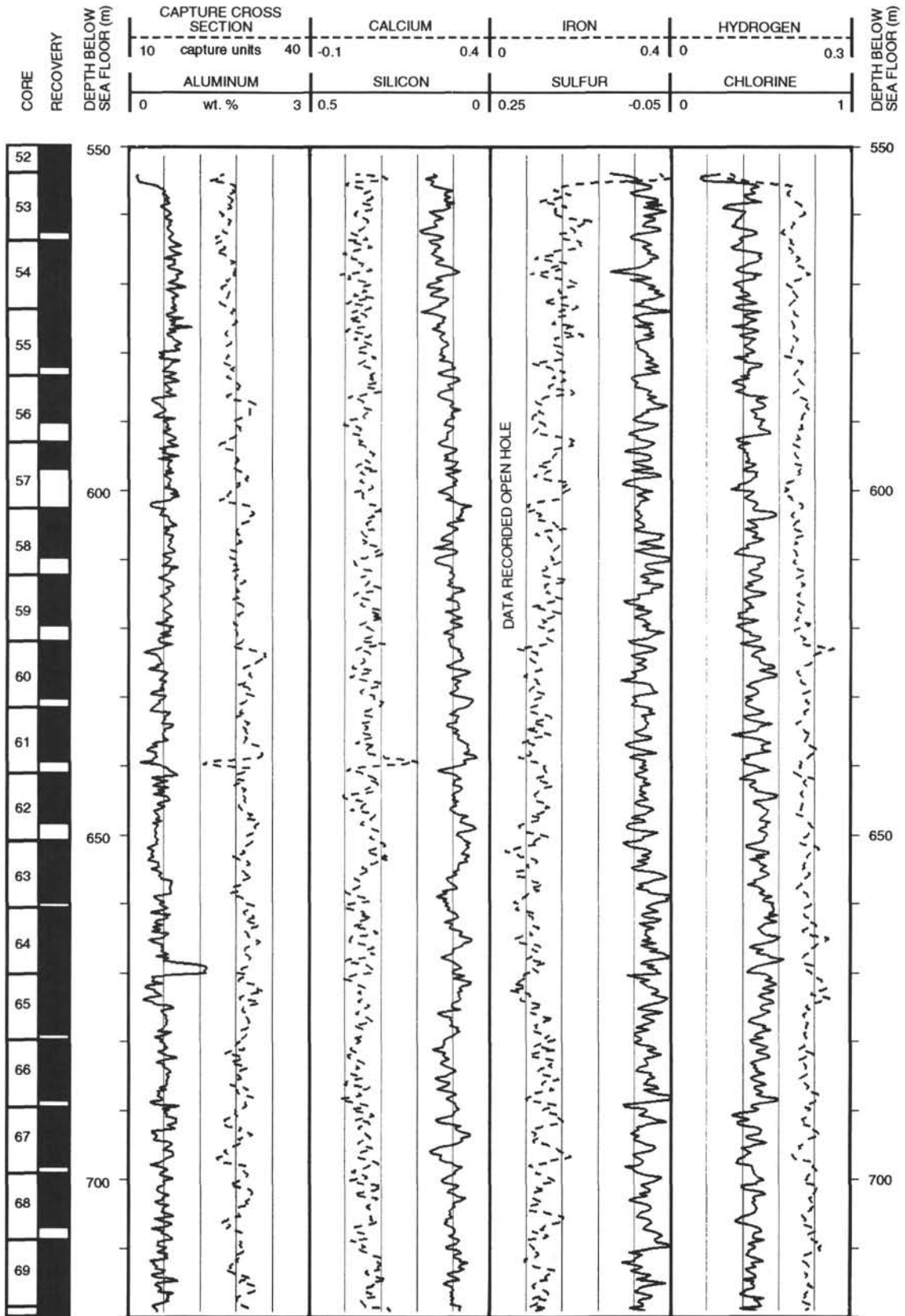
Hole 833B: Density-Natural Gamma Ray Log Summary (continued)



Hole 833B: Density-Natural Gamma Ray Log Summary (continued)



Hole 833B: Geochemical Log Summary



Hole 833B: Geochemical Log Summary (continued)

